AD-A170 973 RADAR CROSS SECTION PREDICTION FOR COATED PERFECT CONDUCTORS WITH ARBITRARY GEOMETRIES(U) AIR FORCE INST OF TECH WRIGHT-PATTERSON AFB OH S W ROGERS 1986 1/3

UNCLASSIFIED AFIT/CI/NR-86-105T F/G 17/9 NL

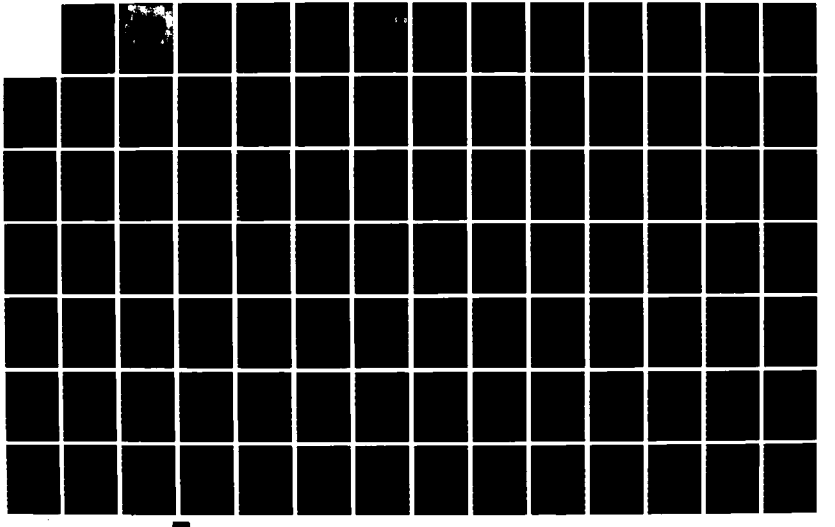

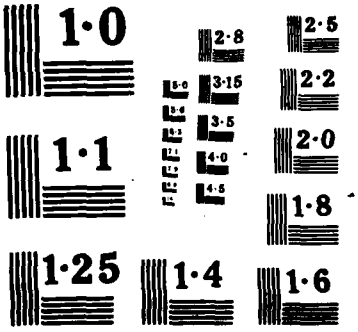
1·0
1·1
1·25
2·8
3·15
3·5
4·0
4·5
1·4
2·5
2·2
2·0
1·8
1·6

SECURITY CLASSIFICATION OF THIS PAGE *(When Data Entered)*

REPORT DOCUMENTATION PAGE		READ INSTRUCTIONS BEFORE COMPLETING FORM
1. REPORT NUMBER AFIT/CI/NR 86-105T	2. GOVT ACCESSION NO.	3. RECIPIENT'S CATALOG NUMBER
4. TITLE *(and Subtitle)* Radar Cross Section Prediction for Coated Perfect Conductors with Arbitrary Geometries		5. TYPE OF REPORT & PERIOD COVERED THESIS/DISSERTATION
		6. PERFORMING ORG. REPORT NUMBER
7. AUTHOR(s) Steven Wayne Rogers		8. CONTRACT OR GRANT NUMBER(s)
9. PERFORMING ORGANIZATION NAME AND ADDRESS AFIT STUDENT AT: Massachusetts Institute of Technology		10. PROGRAM ELEMENT, PROJECT, TASK AREA & WORK UNIT NUMBERS
11. CONTROLLING OFFICE NAME AND ADDRESS AFIT/NR WPAFB OH 45433-6583		12. REPORT DATE 1986
		13. NUMBER OF PAGES 243
14. MONITORING AGENCY NAME & ADDRESS*(if different from Controlling Office)*		15. SECURITY CLASS. *(of this report)* UNCLAS
		15a. DECLASSIFICATION/DOWNGRADING SCHEDULE

16. DISTRIBUTION STATEMENT *(of this Report)*

APPROVED FOR PUBLIC RELEASE; DISTRIBUTION UNLIMITED

17. DISTRIBUTION STATEMENT *(of the abstract entered in Block 20, if different from Report)*

18. SUPPLEMENTARY NOTES

APPROVED FOR PUBLIC RELEASE: IAW AFR 190-1

LYNN E. WOLAVER 6 AUG 86
Dean for Research and
Professional Development
AFIT/NR

19. KEY WORDS *(Continue on reverse side if necessary and identify by block number)*

20. ABSTRACT *(Continue on reverse side if necessary and identify by block number)*

ATTACHED.

DD FORM 1 JAN 73 1473 EDITION OF 1 NOV 65 IS OBSOLETE

SECURITY CLASSIFICATION OF THIS PAGE *(When Data Entered)*

RADAR CROSS SECTION PREDICTION FOR COATED PERFECT CONDUCTORS WITH ARBITRARY GEOMETRIES

by

STEVEN WAYNE ROGERS

Submitted to the Department of Electrical Engineering and Computer Science
of the Massachusetts Institute of Technology
on March 31, 1986 in partial fulfillment of the requirements for the
Degree of Master of Science

ABSTRACT

Radar cross section prediction for coated objects is an important problem with many practical applications. The method of moments is applied to solve the electromagnetic scattering from dielectric/magnetic coated perfect conductors with arbitrary geometries. The governing equations are derived by making use of the equivalence principle and the dyadic formulation of Huygens' principle. Matching boundary conditions then generates a set of integro-differential equations with the equivalent electric and magnetic surface currents as the desired unknowns. Triangular patch modelling is applied to the boundary surfaces. The method of moments with a bi-triangular subdomain basis is used to convert the set of integro-differential equations into a matrix equation which can be solved by matrix inversion for the unknown surface current coefficients. Huygens' principle is again applied to calculate the scattered electric field produced by the equivalent surface currents. Finally, the far-field monostatic radar cross section is calculated from the scattered electric field to perform the radar cross prediction for coated perfect conductors with arbitrary geometries. The governing equations for both completely coated and partially coated perfect conductors are derived. The coatings may have any arbitrary complex permittivity and/or permeability. Radar cross section measurements of various coated and uncoated square aluminum plates also have been made to validate the theoretical predictions. Comparisons between the predicted and measured data are made. The concepts for the generalization to multi-layered coatings also are discussed.

Thesis Supervisor: Dr. Robert Shin
Title: Staff Member, MIT Lincoln Laboratory

RADAR CROSS SECTION PREDICTION FOR COATED PERFECT CONDUCTORS WITH ARBITRARY GEOMETRIES

by

STEVEN WAYNE ROGERS, Capt, USAF

SUBMITTED IN PARTIAL FULFILLMENT
OF THE REQUIREMENTS FOR THE DEGREE OF

MASTER OF SCIENCE
IN ELECTRICAL ENGINEERING AND COMPUTER SCIENCE

at the

MASSACHUSETTS INSTITUTE OF TECHNOLOGY

1986

243 pages

(1)

RADAR CROSS SECTION PREDICTION FOR COATED PERFECT CONDUCTORS WITH ARBITRARY GEOMETRIES

by

STEVEN WAYNE ROGERS

B.S. Chemistry, Ohio State University
(1978)

B.S. Elec. Eng., Air Force Institute of Technology
(1981)

SUBMITTED IN PARTIAL FULFILLMENT
OF THE REQUIREMENTS FOR THE DEGREE OF

MASTER OF SCIENCE
IN ELECTRICAL ENGINEERING AND COMPUTER SCIENCE

at the
MASSACHUSETTS INSTITUTE OF TECHNOLOGY
June 1986

Signature of Author 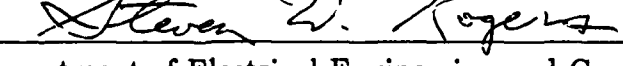
Department of Electrical Engineering and Computer Science
March 29, 1986

Certified by 
Robert T. Shin
Thesis Supervisor

Accepted by _____
Arthur C. Smith
Chairman, Departmental Committee on Graduate Students

RADAR CROSS SECTION PREDICTION FOR COATED PERFECT CONDUCTORS WITH ARBITRARY GEOMETRIES

by

STEVEN WAYNE ROGERS

Submitted to the Department of Electrical Engineering and Computer Science
on March 31, 1986 in partial fulfillment of the requirements for the
Degree of Master of Science

ABSTRACT

Radar cross section prediction for coated objects is an important problem with many practical applications. The method of moments is applied to solve the electromagnetic scattering from dielectric/magnetic coated perfect conductors with arbitrary geometries. The governing equations are derived by making use of the equivalence principle and the dyadic formulation of Huygens' principle. Matching boundary conditions then generates a set of integro-differential equations with the equivalent electric and magnetic surface currents as the desired unknowns. Triangular patch modelling is applied to the boundary surfaces. The method of moments with a bi-triangular subdomain basis is used to convert the set of integro-differential equations into a matrix equation which can be solved by matrix inversion for the unknown surface current coefficients. Huygens' principle is again applied to calculate the scattered electric field produced by the equivalent surface currents. Finally, the far-field monostatic radar cross section is calculated from the scattered electric field to perform the radar cross prediction for coated perfect conductors with arbitrary geometries. The governing equations for both completely coated and partially coated perfect conductors are derived. The coatings may have any arbitrary complex permittivity and/or permeability. Radar cross section measurements of various coated and uncoated square aluminum plates also have been made to validate the theoretical predictions. Comparisons between the predicted and measured data are made. The concepts for the generalization to multi-layered coatings also are discussed.

Thesis Supervisor: Dr. Robert Shin
Title: Staff Member, MIT Lincoln Laboratory

ACKNOWLEDGEMENTS

I gratefully acknowledge the contributions of the following people and organizations without whose support this thesis would have been impossible:

• The taxpayers of the United States of America and the United States Air Force for the opportunity and funding for three college degrees. Only in America!! I'll do my very best to repay this investment.

• Dr. Robert T. Shin for his guidance, understanding, and patient explanations of my numerous questions and concerns.

• Prof. Jin Au Kong for encouraging me to accomplish more than I ever believed possible with the time constraints imposed upon me.

• Dr. David L. Briggs and the staff of Group 45 at the MIT Lincoln Laboratory for their logistics support and office space.

• Mr. Steven Lee of Group 44 at the MIT Lincoln Laboratory for the use of the EFIE series of computer programs, and his advice on their use.

• Mr. Jose Munoz and the staff of the MIT Lincoln Laboratory Group 95 RCS Measurement Facility for their patience and courtesy with my many requests.

• The members of Prof. Kong's research group for their patient attention at my seminars, and their uncomplaining tolerance of my use of so much computer time: Diane Gaylor, Soon Poh, Freeman Lin, Jean-Fu Kiang, Eric Yang, Ann Tulintseff, Richard Kim, Ari Sihvola, Russell Basch, Son Nghiem, Tser-Yuan Brian Yang, Karen Adler, Check Lee, and Michael Tsuk.

• Finally, to my friend and office mate, Maurice Borgeaud, whose kindness and assistance I can never repay.

DEDICATION

To my wife, Beth: without your emotional support, encouragement, patience, understanding, friendship, and love, the landscape of my life would be terribly bleak.

Steve
29 March 1986

"Come with me
On a journey through life,
Be my lady, be my wife,
Share the good times, share the bad,
Share the happy, share the sad,
Always be there, and be true,
And forever I'll love you."

TABLE OF CONTENTS

LIST OF FIGURES

LIST OF TABLES

Chapter 1

INTRODUCTION

1.1 Electromagnetic Scattering

Radar cross section (RCS) prediction is currently an active research area [1-31]. It has been known for nearly 100 years that objects reflect radio waves. But with the increasing use of radar since World War II, the determination of the electromagnetic scattering from an object illuminated by an incident plane wave has generated great practical and academic interest. References [1] through [123] are a small survey of the current literature addressing this research topic, and these references demonstrate the ongoing investigations into electromagnetic scattering.

The ultimate objective in this research area is to develop a general electromagnetic wave scattering model for arbitrary targets. These arbitrary targets could be perfect conductors or penetrable bodies. They could also be perfect conductors coated with dielectric and/or magnetic materials. Further, they could have any geometric shape. As Knott [33] and Senior [25] point out in their respective surveys of RCS prediction techniques, electromagnetic scattering problems fall naturally into three categories according to body size: the low-frequency, resonant, and high-frequency regions. These regions do not refer to the actual frequency used, but to the size of the target with respect to wavelength. When the object is much smaller than the wavelength, all parts of the body are strongly coupled to each other. The electromagnetic scattering depends only slightly on shape and varies with the fourth power of the frequency [33]. Shape details are too small to resolve because the wavelength is too long. When objects are between approximately one and ten wavelengths in size, they lie in the resonance region. All parts of the body interact with each other. Finally, a target larger than approximately ten wavelengths is in the optical region. The scattering mechanisms

are highly localized, and the various target elements typically act independently of one another except for the shadowing of one element by another.

1.2 Theoretical Approaches

Several approaches to the prediction of electromagnetic scattering are apparent from the literature. The approach taken depends on the target size with respect to wavelength, as discussed in the previous paragraph. The high frequency techniques are the asymptotic theories of geometrical optics (GO) [32,33,75,76] and physical optics (PO) [33-36,75,76]. To compensate for deficiencies in the GO theory, an extension has been developed by Keller known as the geometric theory of diffraction (GTD) [33,37-46,75,76]. Similarly, Ufimtsev developed an extension for physical optics known as the physical theory of diffraction (PTD) [33,41,45,47,48,75,76]. These will be discussed in more detail below. The low frequency techniques are the numerical theories of the method of moments (MOM) [33,60-110] and the finite element method [17]. The number of unknown surface current coefficients limits the size of target which can be handled due to computer storage and processing limitations. As computer storage and processing capabilities continue to expand in the future, the upper frequency at which these numerical techniques can be used will increase proportionately. Additionally, hybrid methods [75,76,89-98] have been devised which merge GTD and MOM [75,76,89-92,94] or PTD and MOM [75,76,93]. These approaches are designed to use each technique on the respective regions of a target where that particular technique has its best predictive capability.

1.3 Geometrical Optics

For the calculation of electromagnetic scattering at high frequencies (where the dimensions of the target are large with respect to wavelength) the asymptotic theories have been developed. The oldest and most familiar theory is geometrical optics (GO) which is also known as ray tracing [32,33,75,76]. The basic assumption of GO is that

energy propagates along slender tubes (rays). Since the field components are transverse to the direction of propagation, GO solutions are not valid near discontinuities such as edges. Implicit in this method is the need to find the specular point on the body where the reflection occurs, for it is the principal radii there that govern the spreading of the rays away from the body. If this point is too close to an edge, the assumed field structure no longer satisfies the assumptions of the method. One failure of GO is that it predicts an infinite RCS for a flat or singly curved surface where one or both radii of curvature is infinite. This failure can be overcome by the theory of physical optics.

1.4 Physical Optics

Physical optics (PO) [33-36,75,76] uses a GO approximation of the fields induced on a body surface and integrates the induced fields to obtain the scattered field. The induced surface fields can be approximated for nonconducting as well as conducting surfaces. If the scattering direction varies too much from the specular direction, PO fails by wider margins to yield the correct scattering behavior. Further, the integrals of PO can be evaluated exactly for only a few cases that include flat plates, cylinders, and spherical caps viewed at axial incidence. Targets can be modelled as a grouping of structural features for which PO solutions exist. Thus, PO is restricted to the high frequency region where interactions between major structural features of the target are minimal.

1.5 Geometrical Theory of Diffraction

As mentioned previously, the geometrical theory of diffraction (GTD)[33,37-46,75,76] and the physical theory of diffraction (PTD) [33,41,45,47,48,75,76] were developed by Keller and Ufimtsev, respectively, as extensions to GO and PO. Unlike GO, in which the specular direction is unique, GTD permits diffracted rays to lie along any of the generators of a forward cone whose apex lies at the local point of edge diffraction. The GTD estimates of the field at a point on a diffracted ray depend on the distance

from the edge and upon the local angles of arrival and departure. Using this approach, GTD compensates for edge diffraction whereas GO cannot. As in GO, one need only sum all the rays reaching the point of observation.

Since GTD is a ray tracing technique it suffers from a serious drawback. At the transitions between the shadow regions and the illuminated regions the GTD approximations produce singularities. The uniform theory of diffraction (UTD) [49-51] and the uniform asymptotic theory of diffraction (UAT) [50,52-59] are current attempts to compensate for this error. The uniform theories overcome the transition region singularities at reflection and shadow boundaries. However, at points where an infinite number of rays converge (caustics) all of these high frequency techniques predict infinite fields. Further, none of the high frequency techniques can account for the surface traveling wave phenomenon. This is because these methods treat localized scattering phenomena, while the surface traveling wave involves the entire surface.

1.6 Physical Theory of Diffraction

Analogous to the relation between GTD and GO is the relation between the physical theory of diffraction (PTD) and PO. Ufimtsev recognized that the PO theory was inadequate in many instances, particularly when the scattering direction is far from the specular direction [33]. He postulated the existence of a "nonuniform" (edge) current in addition to the "uniform" (physical optics) surface current. This edge current is designed to compensate for the departure of the target structure from the assumptions implicit in the PO theory. Such departures include shadow boundaries and geometrical discontinuities such as edges. PTD attempts to modify PO when there are surface discontinuities where diffraction becomes important.

1.7 Method of Moments and Finite Element Method

For the calculation of electromagnetic scattering at low frequencies or the resonance region (where the dimensions of the target are on the order of a wavelength)

the numerical theories of the method of moments (MOM)[33,60-110] and the finite element method [17] have been developed. The MOM basically solves the integral form of Maxwell's equations numerically for the surface currents induced on a scatterer by an incident plane wave. The finite element method numerically solves the differential form of Maxwell's equations throughout the region of interest. For both methods the number of unknowns to be calculated limits the size of the target which can be handled due to computer storage and processing limitations. Hence, their designation as low frequency techniques. For more detail on the MOM approach see the next section.

This thesis is an application of the MOM numerical technique to an arbitrary target as defined above. Rao, Wilton, and Glisson [81] have used this approach for perfectly conducting targets with arbitrary geometries. They used triangular patches to construct arbitrary targets. They then defined a set of basis functions [64,81] which, when combined with triangular patch modelling, greatly simplify the equations for the electric surface currents.

Medgyesi-Mitschang, et al [71,73] have applied the MOM to coated perfectly conducting and penetrable targets. However, the targets must be bodies of revolution (BOR) and cannot have arbitrary geometries. Using only BORs provides a great simplification in the equations and computations for the surface currents due to the symmetry of the target.

This thesis is an attempt to lay the theoretical foundation for the prediction of the radar cross section of coated perfect conductors with arbitrary geometries. Chapter 2 briefly discusses the method of moments and its application to coated targets with arbitrary geometries. Chapter 3 provides the problem formulation and the method of solution. A description of the experimental RCS measurements is contained in Chapter 4. Chapter 5 presents the results of the experimental RCS measurements and the theoretical RCS predictions. A comparison of the experimental RCS measurements and the theoretical RCS predictions is also contained in this chapter. Chapter 6 outlines the generalization to multi-layered coatings of the approach used in this thesis to compute the RCS for a single layer of coating. Finally, Chapter 7 contains the conclusions and suggested future efforts.

Chapter 2

METHOD OF MOMENTS

2.1 Introduction

The method of moments (MOM) approach has the advantage that the governing integro-differential equations to which the MOM is applied are exact solutions to the electromagnetic scattering problem. The interactions of all the structural elements of the target are accounted for. Further, since the MOM solves for the induced surface currents explicitly, the MOM has application to near-field (electromagnetic compatability) as well as far-field (RCS) phenomena. Disadvantages include the large number of unknowns to be calculated (n) for most practical problems and the inversion of an $n \times n$ matrix. Alternatively, the n equations in n unknowns may be solved iteratively [28,60,85].

The integral equation formulation for electromagnetic scattering from a target (Huygens' Principle) is exact. The MOM reduces these integro-differential equations to a matrix equation by dividing the target surface into subdomains. The matrix equation represents each subdomain's interaction with every other subdomain. The solution (surface currents and charges) can be found by inverting the interaction matrix and multiplying it by the column vector that is related to the incident field at each surface element. The scattered field is then computed by summing the surface current and charge distributions in a radiation integral. Typically, the integral is for the far-field scattering (RCS), but the field at an arbitrary point in space can be calculated (electromagnetic compatability, near-field RCS, etc.). This feature makes the MOM a very powerful tool with which to conduct detailed investigations of scattering behavior, and the MOM can provide insights into the most critical target element interactions that should be accounted for in the high frequency techniques discussed previously.

2.2 Variations and Alternatives

Several variations and alternatives in the MOM are apparent in the literature. Various approaches to surface modeling of the target have been suggested [99-110], and each has applications to recommend its use. Two of the more popular methods of surface modeling are the wire grid [82,100,103] and the surface patch [81] models. The target is represented as a mesh of wire grids or a patchwork quilt of surface patches. Their popularity stems from the complexity of the targets that can be constructed from these subdomains. If the MOM is applied to the expression for the electric field in Huygens' principle, the method is known as the electric field integral equation (EFIE) formulation. If the MOM is applied to the corresponding magnetic field expression in Huygens' principle, the method is called the magnetic field integral equation (MFIE) formulation. The EFIE formulation [69-73,75,76,78,81,88] can be used for open and closed surfaces. The MFIE formulation [69-73,75,76,78,81,88] can be used only for closed surfaces. However, the EFIE and MFIE will give erroneous results near the internal resonance frequency of a closed structure using the MOM [69-73,81,88]. The combined field integral equation (CFIE) [69-73,75,76,78,81,88] is a linear combination of the EFIE and MFIE which gives valid results near the internal resonance frequency [19,58,67]. Another variation in the MOM is the merger of the MOM with GTD and PTD high frequency techniques, as described in the previous chapter [75,76,89-98].

To predict the electromagnetic scattering from treated perfectly conducting targets the approximate boundary condition (ABC) approach has been developed for use with the MOM. A coated target is one which has a dielectric/magnetic coating. Specific research areas within the ABC numerical theory are the impedance boundary condition (IBC) [111,115,117-122], the resistive boundary condition (RBC) [120-123], and its analog the magnetic boundary condition (MBC) [117-122]. In each of these approaches the coating is approximated by modeling the perfect conductor as an equivalent impedance/resistance.

2.3 Coated Target With Arbitrary Geometry

This thesis is an application of the MOM numerical technique to a coated target with arbitrary geometry as defined in Chapter 1. Rao, Wilton, and Glisson [81] have used this approach for perfectly conducting targets with arbitrary geometries. They used triangular patches to construct arbitrary targets. They then defined a set of basis functions [64,81] which, when combined with triangular patch modelling, greatly simplify the equations for the electric surface currents.

Medgyesi-Mitschang, et al [71,73] have applied the MOM to coated perfectly conducting and penetrable targets. However, the targets must be bodies of revolution (BOR) and cannot have arbitrary geometries. Using only BORs provides a great simplification in the equations and computations for the surface currents due to the symmetry of the target.

Applying the MOM to a three-dimensional coated target will produce three times the number of unknowns to be calculated as compared to a perfectly conducting target. For a perfectly conducting target the electric surface current density is required to calculate the electromagnetic scattering. In the MOM, this electric surface current density is represented by the n basis functions over the n subdomains (triangular patches). For a coated target (perfect conductor) the electric and magnetic surface current densities over the outermost surface are required to calculate the electromagnetic scattering. To calculate these current densities, the electric surface current density on the perfect conductor is also required (magnetic current density equals zero on the perfect conductor). In the MOM, each of these three current densities is represented by n basis functions over the subdomains. Thus, there will be three times the number of unknowns to be calculated as compared to a perfectly conducting target. This increase in the number of unknowns inherently reduces the upper frequency or size of target for which the electromagnetic scattering can be calculated (as compared to a perfectly conducting target) due to the computer limitations discussed previously.

Chapter 3

PROBLEM FORMULATION AND METHOD OF SOLUTION

3.1 Introduction

This thesis problem involves calculating the electromagnetic scattering (radar cross section) from a coated perfect conductor with arbitrary geometry. Figure 3.1 illustrates the problem. An assumed plane wave is incident on the target. Equivalent electric and magnetic surface currents (J_1 and M_1, respectively, in Figure 3.1) on the outer surface of the target are calculated using the method of moments. These calculated equivalent surface currents are then used to compute the scattered electromagnetic field and, ultimately, the monostatic radar cross section (RCS) of the coated target. Figures 3.1 and 3.2 illustrate the problem for a completely coated perfect conductor, and Figure 3.3 is an illustration of the problem for a partially coated perfect conductor. For the partially coated perfect conductor, equivalent electric and magnetic surface currents (J_1 and M_1, respectively, in Figure 3.3) on the outer surface of the coating and an equivalent electric surface current (J_2 in Figure 3.3) on the outer surface of the exposed perfect conductor are calculated using the method of moments. Again, these calculated equivalent surface currents are then used to compute the monostatic RCS of the partially coated target. A detailed derivation of the governing equations for both of these cases is provided in Appendix A.

Throughout this thesis only the monostatic RCS will be computed and discussed. However, the bistatic RCS could have been calculated just as readily. One of the elegances of the method of moments lies in the fact that once the equivalent electric and magnetic surface currents have been calculated, all desired electromagnetic scattering phenomena can be computed. This includes near-field as well as far-field scattering.

For the completely coated perfect conductor shown in Figure 3.1, the target con-

sists of an inner core and an outer core, each of which can be of arbitrary geometrical shape. The inner core of the target is assumed to be a perfectly conducting surface. Surrounding this inner core is a coating which completely encloses the perfect conductor. The coating can have a complex permittivity, ϵ, and/or a complex permeability, μ. The complex permittivity and permeability correspond to dielectric and magnetic materials, respectively, with loss.

For the partially coated perfect conductor shown in Figure 3.3, the target consists of a perfectly conducting object of arbitrary geometrical shape which is partially coated by a material of arbitrary geometrical shape. Again, this material can have a complex permittivity, ϵ, and/or a complex permeability, μ.

The remaining sections of this chapter discuss in greater detail the formulation of the problem and the method chosen to calculate the RCS for coated perfect conductors with arbitrary geometries.

3.2 The Approach

The approach to the solution of this problem is one of using the equivalence principle to replace the target with an equivalent set of electric and magnetic surface currents. The equivalent problem to the target illustrated in Figure 3.1 is shown in Figure 3.2. The region inside the coating is replaced with the equivalent electric surface current, J_1, and the equivalent magnetic surface current, M_1, as shown in the left half of Figure 3.2. The electric and magnetic fields inside the coating are now in the region of no interest and are, therefore, assumed to be identically zero. Since the fields in the region of no interest are zero, the permittivity and permeability are assumed to be that of the surrounding free space, which results in an homogeneous, unbounded medium.

The right half of Figure 3.2 demonstrates the remainder of the equivalence principle. The region outside the coating is replaced by the equivalent electric surface current, J_1', and the equivalent magnetic surface current, M_1'. The perfect conductor is replaced by an equivalent electric surface current, J_2. No equivalent magnetic surface current is required at the surface of the perfect conductor since the boundary condi-

tion at the surface of the perfect conductor requires the tangential electric field, and hence the equivalent magnetic surface current, to equal zero. Now the region of no interest becomes the volume outside the surface of the coating and inside the surface of the perfect conductor. As before, the electric and magnetic fields in the region of no interest are assumed to be zero, and, therefore, the permittivity and permeability of the region of no interest are assumed to be that of the coating. This again results in an unbounded homogeneous medium.

The next step is to satisfy the boundary conditions. At the surface of the coating, the tangential electric field is continuous and the tangential magnetic field is continuous. At the surface of the perfect conductor, the tangential electric field is zero and the tangential magnetic field is equal to the induced electric surface current, J_2. Now, the total fields outside the coating equal the incident fields plus the scattered fields. The scattered fields can be expressed in terms of J_1 and M_1 using Huygens' principle [128]:

$$\overline{E}_s(\bar{r}) = \oint_{S'} dS' \left\{ i\omega\mu \overline{\overline{G}}(\bar{r},\bar{r}') \cdot [\hat{n} \times \overline{H}(\bar{r}')] + \nabla \times \overline{\overline{G}}(\bar{r},\bar{r}') \cdot [\hat{n} \times \overline{E}(\bar{r}')] \right\} \tag{3.1}$$

and

$$\overline{H}_s(\bar{r}) = \oint_{S'} dS' \left\{ -i\omega\epsilon \overline{\overline{G}}(\bar{r},\bar{r}') \cdot [\hat{n} \times \overline{E}(\bar{r}')] + \nabla \times \overline{\overline{G}}(\bar{r},\bar{r}') \cdot [\hat{n} \times \overline{H}(\bar{r}')] \right\} \tag{3.2}$$

where $[\hat{n} \times \overline{H}(\bar{r}')] = \overline{J}$ and $[\hat{n} \times \overline{E}(\bar{r}')] = -\overline{M}$. The above expressions are the dyadic formulation of Huygens' principle, and $\overline{\overline{G}}$ is the dyadic Green's function which is defined in Appendix A. S' is the surface of the scatterer. Further, the fields inside the coating can be expressed in terms of J_1', M_1', and J_2 using Huygens' principle. Satisfying the boundary conditions yields a set of integro-differential equations (see Appendix A) in terms of the incident electric and magnetic fields and the unknown electric and magnetic surface currents.

The method of moments is now applied to the set of integro-differential equations which express the boundary conditions. This results in a matrix equation of the form

$\overline{V} = \overline{\overline{Z}} \cdot \overline{I}$. For more detail, see Appendix A. $\overline{V}$ represents the incident electric and magnetic field excitation vector at the boundary surfaces. $\overline{I}$ represents the unknown electric and magnetic surface current coefficients. $\overline{\overline{Z}}$ represents the interaction matrix for all the triangular patches used to model the surfaces (see Section 3.3). The unknown surface current coefficients, $\overline{I}$, can now be obtained by inverting the Z-matrix and multiplying the excitation vector, $\overline{V}$, by this inverted Z-matrix, $\overline{\overline{Z}}^{-1}$: $\overline{I} = \overline{\overline{Z}}^{-1} \cdot \overline{V}$.

Once the unknown surface current coefficients are computed, it is desired to compute the scattered electric field, $\overline{E}_s$, and, ultimately, the monostatic RCS, σ. The surface current coefficients are used with the appropriate basis functions and substituted into Huygens' principle to compute the scattered electric field. For the completely coated perfect conductor, only the surface current coefficients for the coating are required to compute the scattered electric field. The target has now been replaced with an equivalent set of electric and magnetic surface currents as shown in the left side of Figure 3.2. The far-field approximation to Huygens' principle is made:

$$\overline{E}_s(\bar{r}) = i\omega\mu_0\{\hat{\theta}(R_{1\theta} + R_{2\phi}) + \hat{\phi}(R_{1\phi} - R_{2\theta})\} \tag{3.3}$$

where

$$\overline{R}_1 \simeq \frac{e^{ik_0 r}}{4\pi r} \int_{S_1'} dS_1' \, \overline{J}_1(\bar{r}') e^{-i\bar{k}_0 \cdot \bar{r}'} \tag{3.4}$$

and

$$\overline{R}_2 \simeq \sqrt{\frac{\epsilon_0}{\mu_0}} \frac{e^{ik_0 r}}{4\pi r} \int_{S_1'} dS_1' \, \overline{M}_1(\bar{r}') e^{-i\bar{k}_0 \cdot \bar{r}'} \tag{3.5}$$

in the radiation zone. After the scattered electric field is computed in the backscatter direction, the monostatic RCS, σ, is calculated using the following formula:

$$\sigma = \lim_{r \to \infty} 4\pi r^2 \left| \frac{\overline{E}_s}{\overline{E}_{inc}} \right|^2 \tag{3.6}$$

Finally, the monostatic RCS in decibels referenced to 1 square meter (dBsm) is computed as

$$\sigma_{\mathrm{dBsm}} = 10\log_{10}\left(\frac{\sigma}{1\,\mathrm{m}^2}\right) \tag{3.7}$$

To handle the case of a partially coated perfect conductor, the only modification to the approach outlined above which is required is to replace the target with three equivalent surface currents instead of the two used previously. The coated portion of the target is replaced with an equivalent set of electric and magnetic surface currents, (J_1 and M_1, respectively, over surface S_1 in Figure 3.3), and the exposed perfect conductor is replaced with an equivalent electric surface current, (J_2 over surface S_2 in Figure 3.3). The scattered field then becomes

$$\overline{E}_s(\bar{r}) = i\omega\mu_0\left\{\hat{\theta}(R_{3\theta} + R_{4\phi}) + \hat{\phi}(R_{3\phi} - R_{4\theta})\right\} \tag{3.8}$$

where

$$\overline{R}_3 \simeq \frac{e^{ik_0 r}}{4\pi r}\left\{\int_{S_1'} dS_1'\,\overline{J}_1(\bar{r}')e^{-i\bar{k}_0\cdot\bar{r}'} + \int_{S_2'} dS_2'\,\overline{J}_2(\bar{r}')e^{-i\bar{k}_0\cdot\bar{r}'}\right\} \tag{3.9}$$

and

$$\overline{R}_4 \simeq \sqrt{\frac{\epsilon_0}{\mu_0}}\,\frac{e^{ik_0 r}}{4\pi r}\int_{S_1'} dS_1'\,\overline{M}_1(\bar{r}')e^{-i\bar{k}_0\cdot\bar{r}'} \tag{3.10}$$

in the radiation zone. The monostatic RCS is then computed using equations (3.6) and (3.7), as before.

3.3 Surface Modeling

To model the arbitrary geometry of the surfaces of the coating and perfect conductor, the triangular patch model of Rao, Wilton, and Glisson [81] is used. The motivation and justification for this triangular patch model is provided in Reference [81]. For the purposes of this thesis, the motivation for using triangular patch modeling is that almost any arbitrary geometry (singly and doubly-curved surfaces) can be modelled using triangular subdomains. Figure 3.4 displays a cylinder modelled using triangular subdomains. Further, various coatings or an homogenous coating with

variable thickness over the surface of the perfect conductor can be modelled with the appropriate triangularly patched surfaces. Thus, this triangular patch modelling in conjunction with the basis function over the bi-triangular subdomain used by Rao, Wilton, and Glisson [81], the method of moments, the equivalence principle, Huygens' principle, and the appropriate boundary conditions permit the RCS prediction for coated perfect conductors with arbitrary geometries. The bi-triangular subdomain of the basis function is shown in Figure 3.5, and more detail on the basis function is contained in Appendix A.

3.4 Computer Programs

A flowchart of the computer programs written to implement the procedures described in Section 3.2 is presented in Appendix B. It is not a flowchart of the individual computer programs, but a flowchart to show the progression through the electric field integral equation (EFIE) series of computer programs used to calculate the desired far-field RCS patterns. Appendix B also contains a brief description of the EFIE programs.

Program EFIE1 translates condensed, user-supplied geometry specifications into EFIE usable data. This program automatically breaks the described surface into triangular patches (see Figure 3.4) and does the bookkeeping for such items as coordinates of nodes, which nodes form which edges, which edges form which triangular faces, etc. All of this information is then placed into the output file labelled STORAGE.DAT. The EFIE series of computer programs assume an excitation frequency of 300 megahertz, which gives a free space wavelength of one meter. Thus, all target geometry specifications are normalized to wavelength.

Program EFIE2C calculates the symmetric Z-matrix for the completely coated perfect conductor. The inputs to this program are the STORAGE.DAT file generated by EFIE1 for the perfect conductor, and the CSTORAGE.DAT file (renamed from STORAGE.DAT) generated by EFIE1 for the coating. The output of EFIE2C is a file labelled RESMAT.DAT which contains the Z-matrix. This Z-matrix is discussed

in detail in Appendix A. Since the Z-matrix is symmetric and, therefore, equal to its transpose, only half the Z-matrix is stored in RESMAT.DAT.

Program EFIE2PC calculates the symmetric Z-matrix for the partially coated perfect conductor. The inputs to this program are the STORAGE.DAT file generated by EFIE1 for the coated portion of the perfect conductor, the KSTORAGE.DAT file (renamed from STORAGE.DAT) generated by EFIE1 for the exposed portion of the perfect conductor, and the CSTORAGE.DAT file (renamed from STORAGE.DAT) generated by EFIE1 for the coating. The output of EFIE2C is a file labelled RESMAT.DAT which contains the Z-matrix. This Z-matrix is discussed in detail in Appendix A. Since the Z-matrix is symmetric and, therefore, equal to its transpose, only half the Z-matrix is stored in RESMAT.DAT.

Program EFIE3 inverts the symmetric Z-matrix stored in RESMAT.DAT. The Z-matrix is inverted by the technique of border inversion. The input to EFIE3 is the RESMAT.DAT file. The output of EFIE3 is the inverted Z-matrix, $\overline{\overline{Z}}^{-1}$, which is placed into the RESMAT.DAT file.

Program EFIE5BC computes the scattered electromagnetic field, $\overline{E}_s$, far-field radiation pattern from the equivalent electric, J_1, and magnetic, M_1, surface current distributions of the completely coated perfect conductor. A plane wave is assumed to excite the target, and the equivalent surface currents are computed by multiplying the excitation vector by the inverted Z-matrix. Then, the scattered electric field is calculated only in the backscatter direction for the desired, user-specified angles using equations 3.3 through 3.5. The inputs to EFIE5BC are the inverted Z-matrix, RESMAT.DAT, and the coating geometry data, CSTORAGE.DAT. The output file, SPATTERN.DAT, contains the far-field radiation pattern versus the desired angles.

Program EFIE5PC computes the scattered electromagnetic field, $\overline{E}_s$, far-field radiation pattern from the equivalent electric, $\overline{J}_1$ and $\overline{J}_2$, and magnetic, $\overline{M}_1$, surface current distributions of the partially coated perfect conductor. A plane wave is assumed to excite the target, and the equivalent surface currents are computed by multiplying the excitation vector by the inverted Z-matrix. Then, the scattered electric field is calculated only in the backscatter direction for the desired, user-specified angles us-

ing equations 3.8 through 3.10. The inputs to EFIE5PC are the inverted Z-matrix, RESMAT.DAT, the coating geometry data, CSTORAGE.DAT, and the exposed perfect conductor geometry data, KSTORAGE.DAT. The output file, SPATTERN.DAT, contains the far-field radiation pattern versus the desired angles.

Program EFIE5R calculates the far-field RCS pattern from the scattered electric field pattern. Equations 3.6 and 3.7 are used to compute the monostatic RCS, σ, for each user-specified angle. The input to EFIE5R is the file RPATTERN.DAT (renamed from SPATTERN.DAT). This program is interactive, and the output is available in a variety of forms. The RCS plots versus desired angle can be displayed on a graphics terminal or written into the file HDCOPY.PLT for printing. Further, the file DPATTERN.DAT is created which contains the RCS data versus angle.

Program EFIE5V presents the geometry information in user viewable form. This is an interactive program which will display the geometry created on a graphics terminal or write geometry information into the file HDCOPY.PLT for printing. The input is a file called RESULT.DAT (renamed or copied STORAGE.DAT, KSTORAGE.DAT, or CSTORAGE.DAT file). Figure 3.4 was generated using this program.

The author wrote the EFIE2C and EFIE2PC programs described above, and modified EFIE5B (provided by Group 44 at MIT Lincoln Laboratory) to produce the EFIE5BC and EFIE5PC programs. Additionally, the author modified versions of the EFIE5R and EFIE5V programs to produce the outputs described. The remainder of the programs were generously provided for the author's use by the MIT Lincoln Laboratory.

3.5 Numerical Integration Over Triangular Subdomains

To calculate the elements of the interaction matrix, $\overline{\overline{Z}}$, an integration of several types of functions over each triangular patch is required as shown in Appendix A, equations *A*.106 through *A*.114 and *A*.201 through *A*.216. Since the basis functions used only exist over the bi-triangular subdomains, the integration of these functions is performed over each subdomain. The integration of these functions over the triangular

patches is accomplished numerically using a quadrature technique for surface integration over a triangular surface. Three types of numerical integrations are required:

$$\int_{T_n^{\pm}} d\bar{r}' \frac{e^{ik_0 R_m^{\pm}}}{4\pi R_m^{\pm}} \tag{3.11}$$

and

$$\int_{T_n^{\pm}} d\bar{r}' \bar{\rho}_n^{\pm} \frac{e^{ik_0 R_m^{\pm}}}{4\pi R_m^{\pm}} \tag{3.12}$$

and

$$\int_{T_n^{\pm}} d\bar{r}' \bar{\rho}_n^{\pm} \times (\bar{r}_m^{c\pm} - \bar{r}')(1 - ik_0 R_m^{\pm}) \frac{e^{ik_0 R_m^{\pm}}}{(R_m^{\pm})^3}. \tag{3.13}$$

Appendix C discusses the seven-point numerical integrations used to compute the integrals shown in 3.11, 3.12, and 3.13. Each of these integrals has a singularity which must be considered when the source triangle and the observation triangle are the same triangular patch, $m = n$. The integration of $\int_{T_n^{\pm}} d\bar{r}' \bar{\rho}_n^{\pm} \frac{e^{ik_0 R_m^{\pm}}}{R_m^{\pm}}$ and $\int_{T_n^{\pm}} d\bar{r}' \frac{e^{ik_0 R_m^{\pm}}}{R_m^{\pm}}$ are accomplished in subroutine NINT7 of FORTRAN program EFIE2PC listed in Appendix D, and the integration of $\int_{T_n^{\pm}} d\bar{r}' \bar{\rho}_n^{\pm} \frac{e^{ik_1 R_m^{\pm}}}{R_m^{\pm}}$ and $\int_{T_n^{\pm}} d\bar{r}' \frac{e^{ik_1 R_m^{\pm}}}{R_m^{\pm}}$ are accomplished in subroutine NINT7A of EFIE2PC. The seven-point numerical integration scheme used is discussed in Chapter 3 of Kiang's thesis [124], and will not be repeated here. Further, Kiang's thesis discusses the effects of various triangular patch shapes on the computation of the scattering from perfect conductors. The integration of $\int_{T_n^{\pm}} d\bar{r}' \bar{\rho}_n^{\pm} \times (\bar{r}_m^{c\pm} - \bar{r}')(1 - ik_0 R_m^{\pm}) \frac{e^{ik_0 R_m^{\pm}}}{(R_m^{\pm})^3}$ is accomplished in subroutine NINT7B of FORTRAN program EFIE2PC (Appendix D), and the integration of $\int_{T_n^{\pm}} d\bar{r}' \bar{\rho}_n^{\pm} \times (\bar{r}_m^{c\pm} - \bar{r}')(1 - ik_1 R_m^{\pm}) \frac{e^{ik_1 R_m^{\pm}}}{(R_m^{\pm})^3}$ is accomplished in subroutine NINT7C of EFIE2PC. The seven-point numerical integration over the triangular patches is an adaptation of the numerical quadrature technique discussed in reference [125]. The values used in the quadrature integration can also be found in Abramowitz and Stegun [126] on page 893.

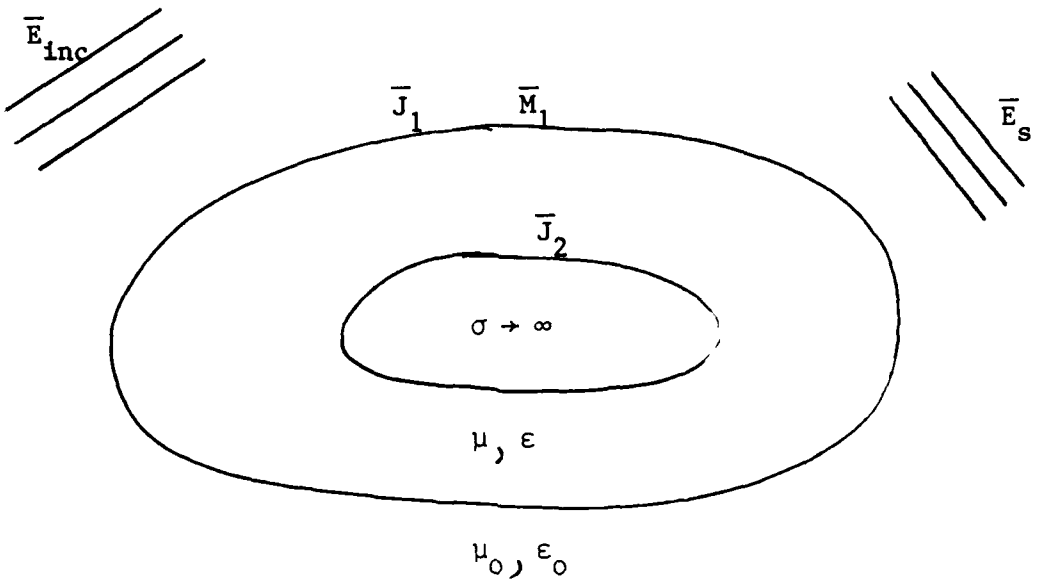

Figure 3.1. The Problem

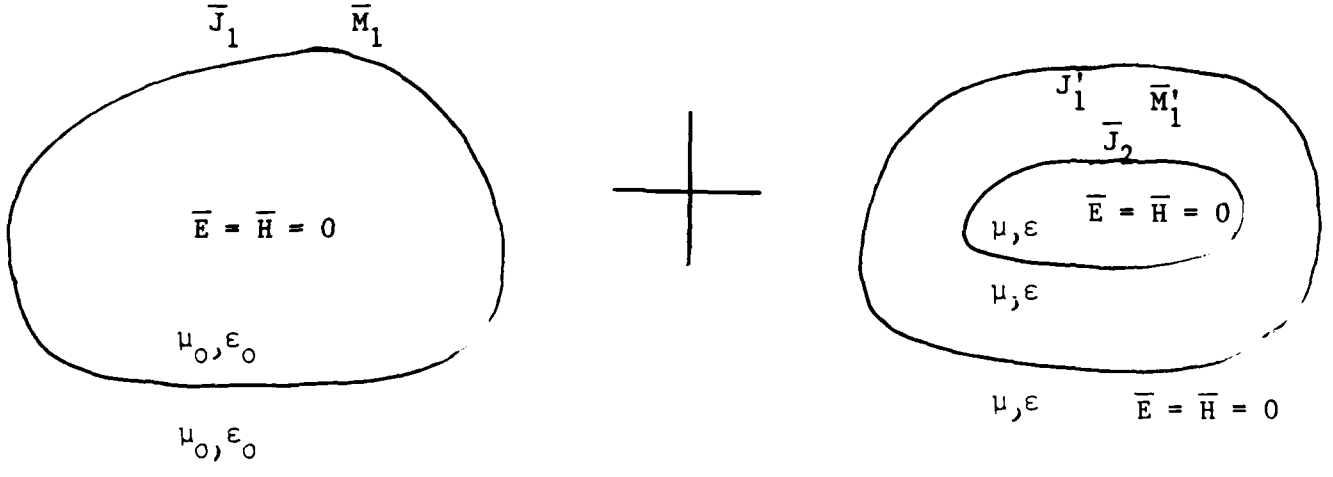

Figure 3.2. Equivalent Problem

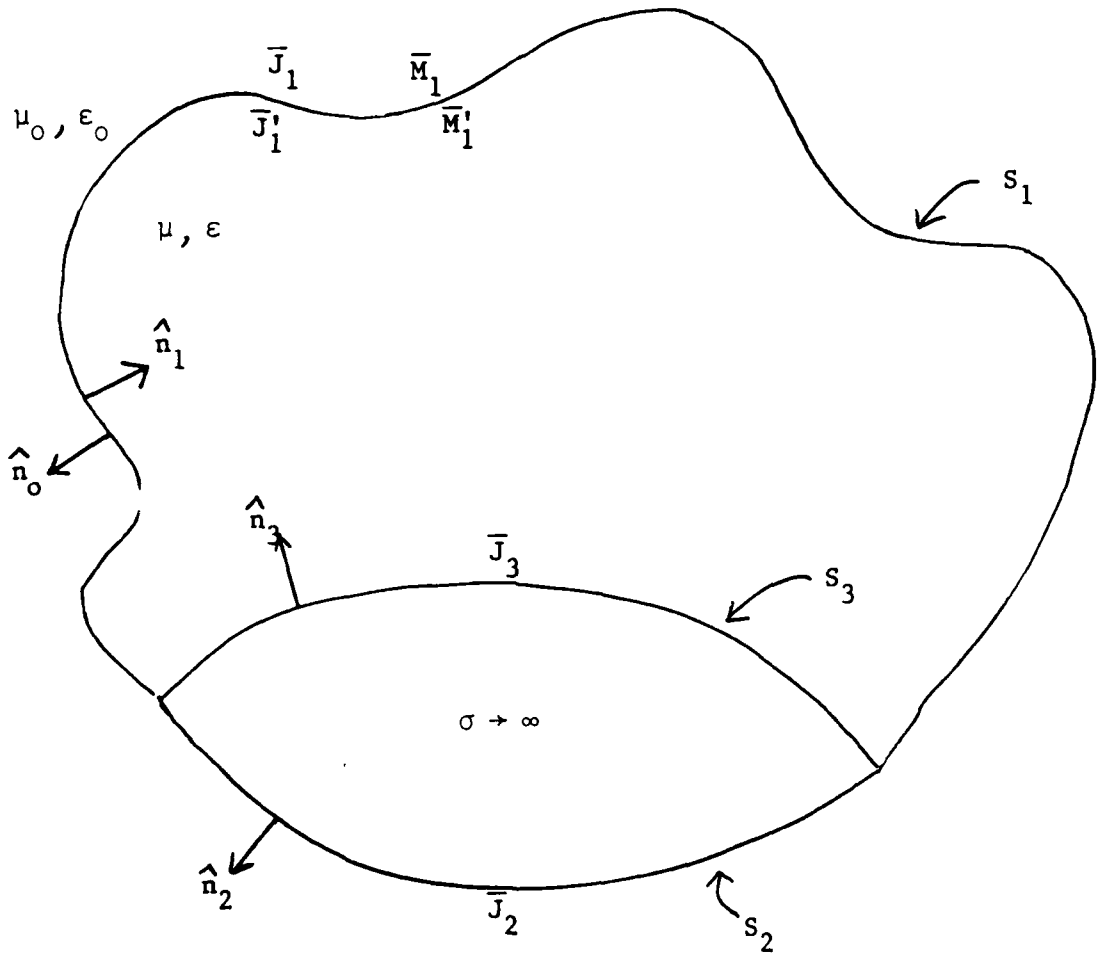

Figure 3.3. Partially Coated Perfect Conductor

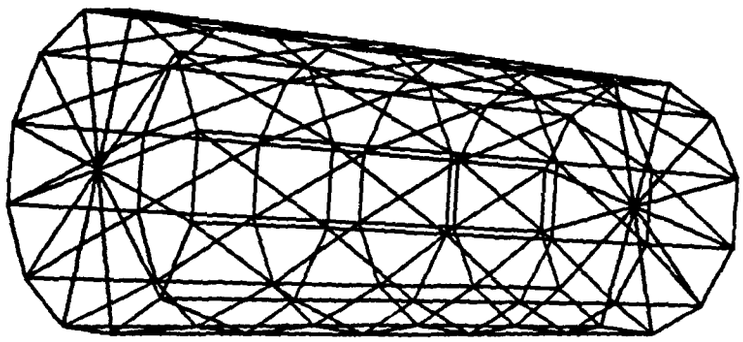

Figure 3.4. Triangular Patch Model of Cylinder

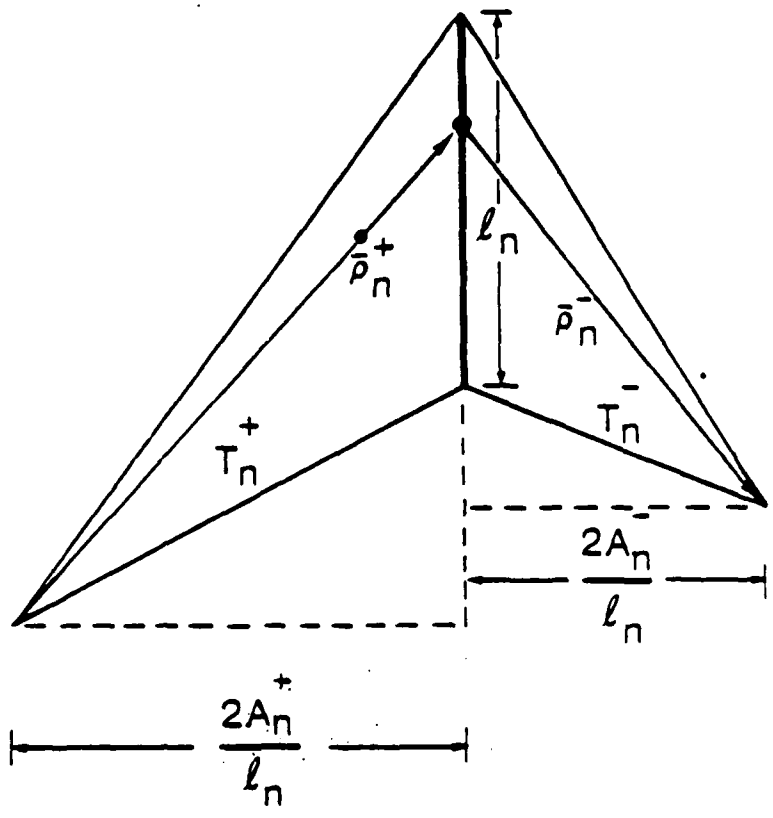

Figure 3.5. Bi-Triangular Subdomain of Basis Function

Chapter 4

EXPERIMENT

4.1 Introduction

Experimental data were collected at the MIT Lincoln Laboratory Group 95 Radar Cross Section (RCS) Measurement Facility. RCS data were collected from square aluminum plates, some coated with radar absorbing material and some without. Section 4.2 presents a brief description of the RCS Measurement Facility, and section 4.3 describes the data which were collected.

4.2 Radar Cross Section Measurement Facility

A block diagram of the MIT Lincoln Laboratory Group 95 RCS Measurement Facility apparatus used to collect the RCS data presented in this thesis is shown in Figure 4.1. The operating frequency of this radar is approximately 2.5 gigahertz (GHz) to 8.0 GHz. As shown in the block diagram, this is a pulsed radar system. The transmitted pulse is approximately 20 nanoseconds in duration, and the received pulse is approximately 40 nanoseconds in duration. The pulse repetition frequency of the radar is seven megahertz. The received pulses are averaged for 40 milliseconds. The quoted noise threshold for this radar is -60dBsm.

A block diagram of the RCS data collection process is shown in Figure 4.2. A styrofoam mount is used to hold the target in the desired position. With the styrofoam mount in position and no target on the mount, a background measurement is performed. The styrofoam mount can be rotated azimuthally 360 degrees in one-half degree increments, if desired. An RCS measurement of the background is taken at the desired angle increments. This background measurement is subtracted from all succes-

sive measurements to arrive at the measured RCS of the target. Next, a calibration sphere is placed on the styrofoam mount. RCS measurements are performed at the desired angle increments to verify the calibration of the radar system. Now, the desired target is placed into the radar chamber. It is positioned on the styrofoam mount so the desired cut will be obtained as the styrofoam mount is rotated azimuthally. Again, RCS measurements are taken at the desired angle increments. Finally, the calibration process is repeated to verify the radar system performance.

4.3 Data Collection

As mentioned in the introduction, RCS data were collected from square aluminum plates, some coated with radar absorbing material and some without. Those plates coated with radar absorbing material were only coated on one side (partially coated perfect conductors). The plates were mounted on styrofoam. The styrofoam mount was then rotated azimuthally 360 degrees in one degree increments, and the RCS measurements were obtained at each of these angles. Table 4.1 lists the data collected, and the RCS plots corresponding to this table can be found in Appendix E.

RCS data were collected from square aluminum plates which were 32 mils (0.032 inches = 0.8128 mm) thick. See Table 4.1. Two sizes of aluminum plates were used. The first size was 10 cm by 10 cm which is one wavelength by one wavelength at a frequency of 3.0 GHz. The second size plate was 15 cm by 15 cm which is three wavelengths by three wavelengths at 6.0 GHz. RCS data were collected at 3.0 GHz and at 6.0 GHz. Two different polarizations of RCS data are shown in Table 4.1 and Appendix E: horizontally transmitted and horizontally received RCS data; and vertically transmitted and vertically received RCS data. The horizontally transmitted and horizontally received RCS data corresponds to the VV entries in Table 4.1 and the SIGMA-VV versus angle RCS plots in Appendix E. This is because the aluminum plate was chosen as the reference, and the aluminum plate was mounted in a vertical position on the styrofoam mount. The styrofoam mount was then rotated azimuthally for the RCS measurements. Therefore, VV corresponds to a vertically polarized electric field

for the incident wave and a vertically polarized electric field for the scattered wave with respect to the edge of the plate. Similarly, the vertically transmitted and vertically received RCS data corresponds to the HH entries in Table 4.1 and the SIGMA-HH versus angle RCS plots in Appendix E. Therefore, HH corresponds to a horizontally polarized electric field for the incident wave and a horizontally polarized electric field for the scattered wave with respect to the edge of the plate. There is no cross-polarization return for the RCS pattern cuts measured due to symmetry.

Three different radar absorbing materials were used to coat the square aluminum plates: Eccosorb FDS, Eccosorb SF 6.0, and Eccosorb FGM 40 (Eccosorb is a registered trademark of the Emerson and Cuming Division of the W. R. Grace and Co.). The three types of coating, along with some of the specifications for each as provided by the manufacturer, are shown in Table 4.2. Eccosorb FDS is a silicone rubber based material which was purchased in one foot by one foot sheets. More information on Eccosorb FDS may be found in Table 4.3 and Technical Bulletin 2-22A and Folder 819-91 from the manufacturer. The information in Table 4.3 was taken from this technical bulletin. Eccosorb SF 6.0 is also a silicone rubber based material which was also purchased in one foot by one foot sheets. It is cut for a resonance frequency of 6.0 GHz. More information on Eccosorb SF 6.0 may be found in Technical Bulletin 8-2-18 from the manufacturer. Finally, Eccosorb FGM 40 is a ferrite loaded silicone based rubber material which was purchased in one foot by one foot sheets. More information on Eccosorb FGM 40 may be found in Technical Bulletin 8-2-23 from the manufacturer. Specifications comparable to those listed in Table 4.3 for Eccosorb FDS were not available in the respective technical bulletins for Eccosorb SF 6.0 and Eccosorb FGM 40.

The radar absorbing materials used were chosen for the frequency at which the RCS data were collected. Since the method of moments is a relatively low frequency technique (dimensions of the object relatively small or comparable to the wavelength of interest), a compromise was made between the size of the aluminum plates used, the frequency of the RCS measurements, and the type of radar absorbing materials used to coat the aluminum plates. Table 4.1 represents the results of the compromise.

Coatings used were Eccosorb radar absorbing material

Square plate targets were mounted on styrofoam

f = radar frequency in gigahertz (GHz)

RCS measurements taken in 1° increments

Radar pulses averaged for 40 milliseconds

Radar pulse repetition frequency (PRF) = 7 megahertz

Radar pulse width: XMIT-20 nanoseconds, RCVR-40 nanoseconds

Plate Size	Coating	f (GHz)	Polarization
10cm × 10cm	None	3.0	hh
10cm × 10cm	None	3.0	vv
10cm × 10cm	FDS	3.0	hh
10cm × 10cm	FDS	3.0	vv
10cm × 10cm	SF 6.0	3.0	hh
10cm × 10cm	SF 6.0	3.0	vv
10cm × 10cm	FGM 40	3.0	hh
10cm × 10cm	FGM 40	3.0	vv
15cm × 15cm	None	3.0	hh
15cm × 15cm	None	3.0	vv
15cm × 15cm	FDS	3.0	hh
15cm × 15cm	FDS	3.0	vv
15cm × 15cm	SF 6.0	3.0	hh
15cm × 15cm	SF 6.0	3.0	vv
15cm × 15cm	FGM 40	3.0	hh
15cm × 15cm	FGM 40	3.0	vv

Table 4.1. Experimental Radar Cross Section Measurements

Coatings used were Eccosorb radar absorbing material

Square plate targets were mounted on styrofoam

f = radar frequency in gigahertz (GHz)

RCS measurements taken in 1° increments

Radar pulses averaged for 40 milliseconds

Radar pulse repetition frequency (PRF) = 7 megahertz

Radar pulse width: XMIT-20 nanoseconds, RCVR-40 nanoseconds

Plate Size	Coating	f (GHz)	Polarization
10cm × 10cm	None	6.0	hh
10cm × 10cm	None	6.0	vv
10cm × 10cm	FDS	6.0	hh
10cm × 10cm	FDS	6.0	vv
10cm × 10cm	SF 6.0	6.0	hh
10cm × 10cm	SF 6.0	6.0	vv
10cm × 10cm	FGM 40	6.0	hh
10cm × 10cm	FGM 40	6.0	vv
15cm × 15cm	None	6.0	hh
15cm × 15cm	None	6.0	vv
15cm × 15cm	FDS	6.0	hh
15cm × 15cm	FDS	6.0	vv
15cm × 15cm	SF 6.0	6.0	hh
15cm × 15cm	SF 6.0	6.0	vv
15cm × 15cm	FGM 40	6.0	hh
15cm × 15cm	FGM 40	6.0	vv

Table 4.1 (cont.). Experimental Radar Cross Section Measurements

Eccosorb radar absorbing material purchased from W. R. Grace Co.

Specifications quoted from literature supplied by manufacturer

Δ = thickness in millimeters

Weight is in (kg/m^2)

Loss = dB/cm at normal incidence ($\theta_{inc} = 0°$)

$\theta_{inc} = 0°$ $f = 3.0$ GHz

Eccosorb	Δ (mm)	Color	Weight	Loss (dB/cm)
FDS	0.762	Black	2.0	-8.6
SF 6.0	2.1844	Gray	7.8	-5.0
FGM 40	1.016	Gray	4.9	-5.0

Table 4.2. Eccosorb Radar Absorbing Material Specifications

Dielectric Properties	$f = 1.2$ GHz	$f = 3.0$ GHz	$f = 8.6$ GHz
Dielectric Constant	13	8.9	7.4
Dielectric Loss Tangent	0.15	0.07	0.15
Magnetic Permeability	2.3	1.7	1.4
Magnetic Loss Tangent	0.41	0.80	0.48
Attenuation (dB/cm)	3	9	16
Relative Impedance Z/Z_0	0.4	0.5	0.5

Table 4.3. Eccosorb FDS Manufacturer Specifications

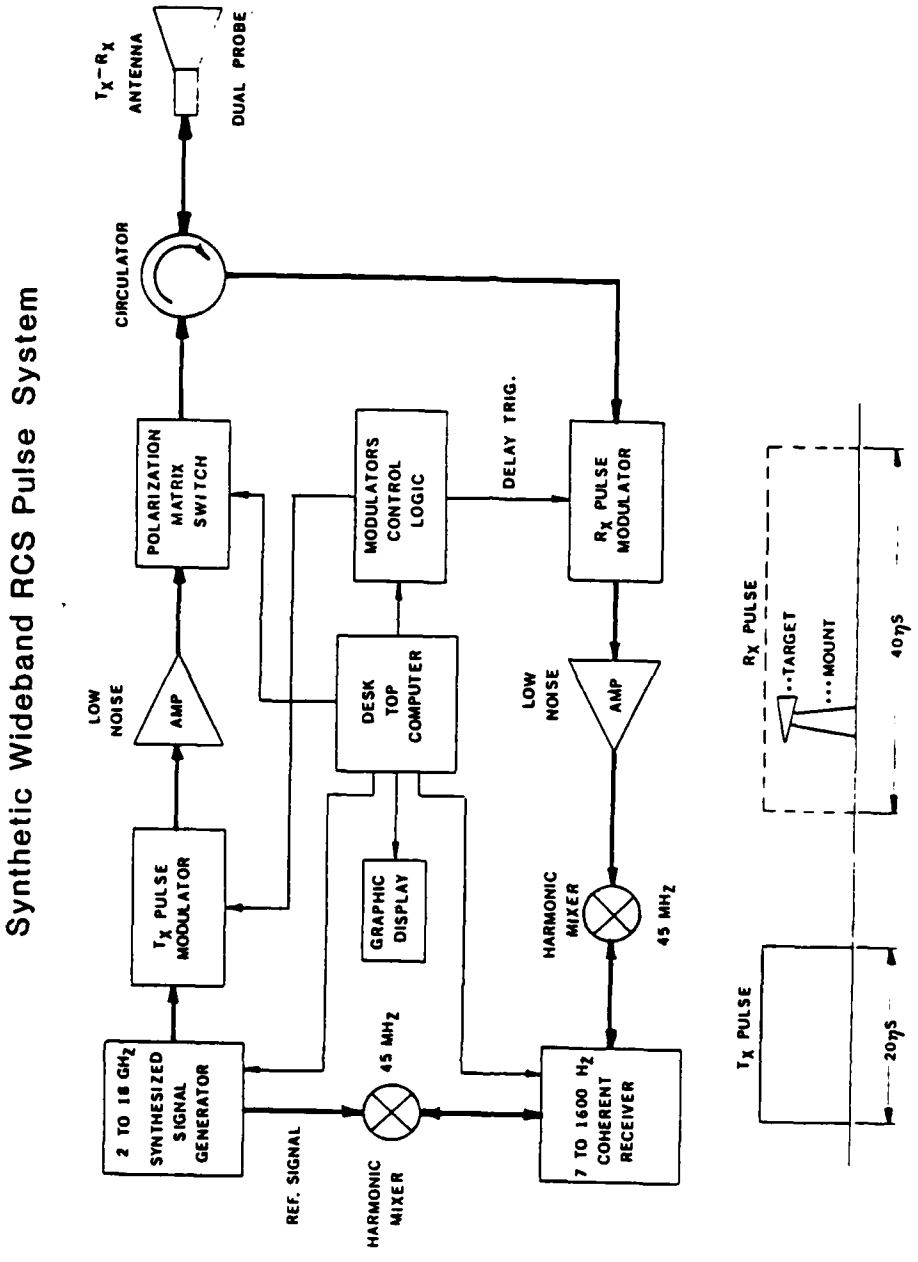

Figure 4.1. Block Diagram of MIT Lincoln Laboratory Group 95 RCS Measurement Facility

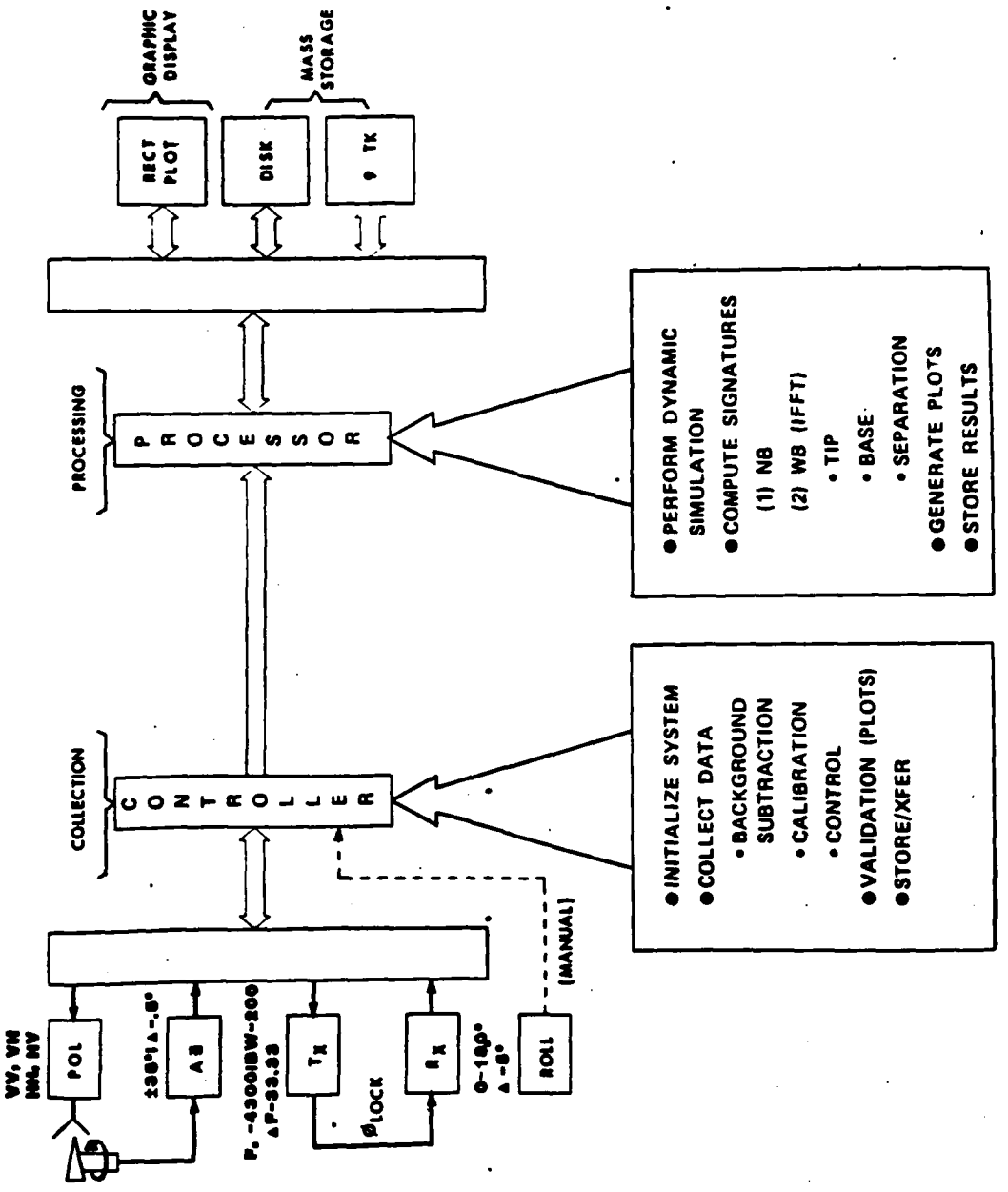

Figure 4.2. Block Diagram of RCS Data Collection Process

Chapter 5

EXPERIMENTAL AND THEORETICAL RESULTS

5.1 Introduction

This chapter contains a discussion of the radar cross section (RCS) data generated at the MIT Lincoln Laboratory Group 95 RCS Measurement Facility and by the EFIE series of computer programs. Section 5.2 describes the experimental RCS data collected at the MIT Lincoln Laboratory Group 95 RCS Measurement Facility as discussed in Chapter 4. Section 5.3 describes the theoretical RCS data generated by the EFIE series of computer programs discussed in Chapter 3. Finally, section 5.4 contains a comparison of the experimental results and the theoretical results. All the RCS plots contained in this thesis are for either partially coated or uncoated square aluminum plates. Appendix E contains copies of all the RCS plots discussed in this thesis.

5.2 Experimental Radar Cross Section Data

The experimental RCS measurements taken at the MIT Lincoln Laboratory Group 95 RCS Measurement Facility are discussed in Chapter 4. Table 4.1 in Chapter 4 provides a list of the RCS measurements taken, and Appendix E contains copies of each of the RCS plots generated from the measured data. Table 5.1 summarizes these experimental RCS plots. As discussed in Chapter 4, the RCS measurements were all performed on square aluminum plates. Some of the RCS measurements were taken on uncoated plates, and some of the RCS measurements were taken on plates which were coated on only one side with an appropriate layer of the Eccosorb radar absorbing material corresponding to the entries in Table 4.1. The RCS was measured

360 degrees around each plate at one degree increments. As mentioned in Chapter 4, the aluminum plates were mounted vertically on a styrofoam mount which was then rotated azimuthally in one degree increments for the RCS measurements.

Figures E.1 through E.16 in Appendix E are the experimental RCS plots corresponding to the entries in Table 4.1. These plots are summarized in Table 5.1. Two orthogonal polarizations are displayed in the same figure. The σ_{hh} polarization is on the top of each figure, and the σ_{vv} polarization is on the bottom of each figure. These polarizations are explained in the next paragraph. Table 5.1 also lists the value of the RCS at normal incidence to the coated side of the plate ($\theta = 0°$) for the σ_{hh} polarization.

All the experimental RCS plots in Appendix E display the RCS in decibels referenced to one square meter (dBsm) on the Y-axis versus angle on the X-axis. The frequency of the RCS measurement is also annotated along the Y-axis of each RCS plot. The σ_{hh} versus angle RCS plots in Appendix E correspond to a horizontally polarized electric field for the incident wave and a horizontally polarized electric field for the scattered wave with respect to the edge of the plate. Similarly, the σ_{vv} versus angle RCS plots in Appendix E correspond to a vertically polarized electric field for the incident wave and a vertically polarized electric field for the scattered wave with respect to the edge of the plate. The angle measurement on the X-axis is in degrees.

The angle displayed on the X-axis in the RCS plots of Appendix E is theta (θ) in the spherical coordinate system. This follows naturally since the aluminum plates were mounted vertically on the styrofoam mount which was then rotated azimuthally. If the plane of the plate is considered the X-Y plane, then the normal to this plane is the Z-axis. Theta (θ) in the spherical coordinate system is measured with respect to the Z-axis. Thus, the amount of rotation of the styrofoam mount corresponds to the angle θ in spherical coordinates. Assuming the edges of the plate are parallel to the imaginary X-axis and Y-axis, the cut obtained is for $\phi = 0°$ as the mount rotates. If the plate is coated on one side, the angle $\theta = 0°$ on the RCS plot corresponds to normal incidence on the side of the plate with the coating. The angles $\theta = \pm 180°$ on the RCS plot correspond to normal incidence on the uncoated side of the plate.

To determine how much the Eccosorb radar absorbing material has decreased the RCS at normal incidence, compare the σ_{hh} entry in Table 5.1 for the plate with no coating to the corresponding entry for the plate with the coating of interest. For example, Table 5.1 shows the σ_{hh} for the 10cm by 10cm uncoated plate at 3.0 GHz is -9.7 dBsm, the first entry in Table 5.1. Compare this to the σ_{hh} value of -13.3 dBsm for the FGM 40 coated square aluminum plate at 3.0 GHz, the fourth entry in Table 5.1. The Eccosorb FGM 40 radar absorbing material decreased the RCS at normal incidence by -3.6 dB at 3.0 GHz for the σ_{hh} polarization.

For the three different types of Eccosorb radar absorbing material measured, Table 5.1 shows the Eccosorb FGM 40 provided the largest RCS reduction at normal incidence to the square aluminum plate at a frequency of 3.0 GHz for the σ_{hh} polarization. This is not true at a radar frequency of 6.0 GHz. The Eccosorb SF 6.0 provides the largest RCS reduction at normal incidence to the plate at 6.0 GHz. The Eccosorb SF 6.0 is tuned to a resonance frequency of 6.0 GHz, and it would be expected to provide the largest RCS reduction at normal incidence at this frequency if the properties of the radar absorbing materials are comparable. Table 5.1 further shows the Eccosorb FDS provided the smallest RCS reduction of all three radar absorbing materials at normal incidence to the plate at 3.0 GHz and 6.0 GHz for the σ_{hh} polarization. This reduction was approximately -1 dB for both plate sizes and both frequencies listed in Table 5.1. This is consistent with the manufacturer's claim that Eccosorb FDS was more effective for surface wave effects than for specular reduction.

By overlaying enlarged versions of Figures E.2, E.6, E.10, and E.14 onto Figures E.1, E.5, E.9, and E.13, respectively, the radar absorbing properties of the Eccosorb FDS material become more apparent. This technique was used to generate Figures 5.1 and 5.2. Figure 5.1 is a composite of the σ_{hh} curves of Figures E.1 and E.2, and Figure 5.2 is a composite of the σ_{hh} curves of Figures E.9 and E.10. Figures 5.1 and 5.2 show that indeed the Eccosorb FDS radar absorbing material is more effective for surface wave effects than for specular reduction. For example, this phenomenom is demonstrated by the fact that for the angles between 0° and ±90°, not inclusive, on Figures 5.1, 5.2, E.2, E.6, E.10, and E.14 the amount of RCS reduction is greater than

the RCS reduction at 0° on these figures. Again, the RCS reduction is determined by comparison with the appropriate uncoated case.

At the angles near ±90° for the σ_{hh} plots in all the figures for the coated plates, the RCS is actually larger than the RCS for the corresponding uncoated plates at the same angles. Figures 5.1 and 5.2 explicitly display this phenomenom. The finite thickness of the coating and the reflection coefficient of the coating might be contributing factors to this effect. For these specific angles, the RCS measurements are being made at the edges of the plates. Since the edges of the coated plates are not covered with radar absorbing material, the exposed edges of the coated plates reflect radar energy in the same manner as the edges of the uncoated plates. However, there is the additional reflection of radar energy from the coating/free space interface due to the impedance mismatch at this boundary. This may account for the increase in RCS at these angles for the coated plates compared to the RCS at these angles for the uncoated plates.

At the angles near ±90° for the σ_{vv} plots in all the figures for the coated plates, the null in the RCS plot is shifted several degrees from the null in the RCS plot for the the corresponding uncoated plates at the same angles. The finite thickness of the coating and the reflection coefficient of the coating might also be contributing factors to this effect. For these specific angles, the RCS measurements are being made at the edges of the plates. Since the coating has a finite thickness at the edges, the edges of the coated plates reflect more radar energy than the edges of the uncoated plates. Further, the reflection coefficient of the coating varies with the angle. This may account for the shift in the null of the RCS plot at these angles for the coated plates compared to the null in the RCS plot at these angles for the uncoated plates.

5.3 Theoretical Radar Cross Section Data

The theoretical RCS data were generated by the EFIE series of FORTRAN computer programs. The EFIE series of computer programs are discussed in Chapter 3. Table 5.2 provides a list of the RCS data computed by this series of programs, and

Appendix E contains copies of each of the RCS plots generated from this computed data. The RCS data were all computed for square perfectly conducting plates. The size of the perfectly conducting plates was 10cm by 10cm for all the computations, and the frequency was always 3.0 GHz. The perfectly conducting plates were coated on only one side with a coating which had the complex relative permittivity (ϵ_R) and complex relative permeability (μ_R) of interest. The RCS was computed 360 degrees around each plate at 109 equally spaced points. Since the method of moments is a relatively low frequency technique (dimensions of the object relatively small with respect to the wavelength of interest), a compromise was made between the size of the plate used, the frequency of the RCS calculations, the magnetic disk storage requirements for the Z-matrix, and the computation time required for the VAX 11/750 to calculate the RCS data. Table 5.2 represents the results of the compromise.

Figures E.17 through E.28 in Appendix E are the theoretical RCS plots generated by the EFIE series of FORTRAN computer programs. These RCS plots are summarized in Table 5.2. Two orthogonal polarizations are displayed in the same figure. The σ_{hh} polarization is on the top of each figure, and the σ_{vv} polarization is on the bottom of each figure. These polarizations are explained in the next paragraph. Table 5.2 also lists the computed value of the RCS at normal incidence to the coated side of the plate ($\theta = 0°$) for the σ_{hh} polarization.

All the theoretical RCS plots in Appendix E display the RCS in decibels referenced to one square meter (dBsm) on the Y-axis versus angle on the X-axis. The frequency of the RCS calculation is also annotated along the Y-axis of each RCS plot. The σ_{hh} versus angle RCS plots in Appendix E correspond to a horizontally polarized electric field for the incident wave and a horizontally polarized electric field for the scattered wave with respect to the edge of the plate. Similarly, the σ_{vv} versus angle RCS plots in Appendix E correspond to a vertically polarized electric field for the incident wave and a vertically polarized electric field for the scattered wave with respect to the edge of the plate. The angle measurement on the X-axis is in degrees.

The angle displayed on the X-axis in the RCS plots of Appendix E is theta (θ) in the spherical coordinate system. If the plane of the plate is considered the X-Y

plane, then the normal to this plane is the Z-axis. Theta (θ) in the spherical coordinate system is measured with respect to the Z-axis. Assuming the edges of the plate are parallel to the X-axis and Y-axis, the cut obtained is for $\phi = 0°$ as θ varies. The plate is coated on only one side, and the angle $\theta = 0°$ on the RCS plot corresponds to normal incidence on the side of the plate with the coating. The angles $\theta = \pm 180°$ on the RCS plot correspond to normal incidence on the uncoated side of the plate.

There are several issues involved in the computation of the RCS data using the EFIE series of computer programs. The first issue is modelling of the partially coated perfect conductor. The second issue is the continuity of surface current between the boundary of the exposed perfect conductor and the coated perfect conductor.

The question of how to model the partially coated perfect conductor is the first issue which arises. Figure 5.3 shows how the partially coated perfect conductor was modelled in this thesis to compute the RCS data for Figures E.17 through E.28. Figure 5.3 shows the perfect conductor is modelled as an infinitely thin plate composed of 128 triangular patches. This figure also shows the coating is modelled as an infinitely thin plate composed of 128 triangular patches. The plate forming the surface of the coating is spaced the distance corresponding to the thickness of the coating away from the plate forming the perfect conductor.

Notice that the surfaces of the coating along the sides which would meet the perfect conductor are not present in Figure 5.3. The coatings used for the experimental measurements are relatively thin, and satisfactory RCS results were obtained from the EFIE computer programs without including the sides of the coating surface. Also, it was found the RCS computation was not improved by the addition of the sides of the coating. Since the coatings were thin, the sides were composed of elongated triangular patches. With the seven-point numerical quadrature integration scheme used to compute the elements of the Z-matrix over the bi-triangular subdomains, the best results are obtained with triangular patches which have sides of relatively the same length [124]. The triangular patches used to model the sides of the coating surface do not meet this criteria. Further, the computation time was decreased by not including the sides of the coating (fewer triangular patches produces a smaller Z-matrix).

The second issue was the continuity of surface current across the boundary between the exposed perfect conductor and the coated perfect conductor. The model of the perfect conductor shown in Figure 5.3 is actually two infinitely thin plates composed of 128 triangular patches. These two plates which form the exposed and coated portions of the perfect conductor, respectively, are modelled as having a separation of zero. However, they are still modelled as two distinct plates. For each plate, the component of current normal to an exposed edge is zero. Therefore, there is no continuity of current between the boundary of the exposed perfect conductor and the coated perfect conductor with the modelling scheme used in this thesis. The only justification for this is that it was much simpler, and it gives satisfactory results. A model of the perfect conductor was tried where the plate forming the exposed perfect conductor was separated from the plate forming the coated perfect conductor by a distance corresponding to the thickness of the aluminum plates (32 mils) used in the experimental measurements. No improvement in the calculated RCS data was noted. Therefore, this added complexity was discarded.

As the first step after developing and debugging the EFIE series of FORTRAN computer programs used to compute the RCS data for Figures E.17 through E.28, it was necessary to verify that the programs gave reasonable results. As described in Chapter 3, the required inputs to the computer programs were the geometry specifications for the partially coated perfect conductor and the complex relative permittivity (ϵ_R) and permeability (μ_R) of the coating. The relative permittivity ($\epsilon_R = 1$) and permeability ($\mu_R = 1$) of free space and a coating thickness of 7.62×10^{-4} meters were used to verify the proper performance of the computer programs. With these inputs, the computer programs would be expected to give RCS data equivalent to that for an uncoated perfect conductor. This was not achieved until the EFIE2PC program was modified.

The required modification to the EFIE2PC computer program involves the approximation of the integration of the weighting function over the bi-triangular subdomain as its value at the centroid of the triangular patch as shown in equation (A.69) of Appendix A. When this approximation was made for all the triangular patches, the EFIE computer programs gave an unsatisfactory match to the experimental measure-

ments for the uncoated 10cm by 10cm square aluminum plate (Figure E.1 of Appendix E). The EFIE2PC computer program was then modified to perform a seven-point numerical quadrature integration over the bi-triangular subdomain instead of making this approximation whenever the distance from the observation triangle to the source triangle was less than the length of any edge of the observation triangle. The results were satisfactory when this modification was incorporated into the EFIE2PC computer program. The first entry in Table 5.2 and Figure E.17 of Appendix E show the calculated RCS results with this modification. These results will be discussed further in the next section.

The computed RCS data for the Eccosorb FDS coated plate are shown in the second entry of Table 5.2 and in Figure E.18 of Appendix E. A value of $\epsilon_R = 8.9 + i0.623$ was used for the complex relative permittivity of the Eccosorb FDS radar absorbing material, and a value of $\mu_R = 1.7 + i1.36$ was used for the complex relative permeability of the Eccosorb FDS radar absorbing material. These values for the complex relative permittivity and permeability are equivalent to the quoted manufacturer specifications in Table 4.3 for the Eccosorb FDS at a frequency of 3.0 GHz.

The computed RCS data for the Eccosorb SF 6.0 coated plate are shown in the third through seventh entries of Table 5.2 and in Figures E.19 through E.23 of Appendix E. Values for the complex permittivity and permeability (or dielectric and magnetic constants and loss tangents) were not available in the manufacturer's literature for the Eccosorb SF 6.0 radar absorbing material. However, a nominal value for the loss at normal incidence of -5 dB at a frequency of 3.0 GHz was quoted. Therefore, the values for the complex relative permittivity and permeability shown in Table 5.2 were chosen.

The values of $\epsilon_R = 8.9 + i0.623$ and $\mu_R = 2.9 + i2.32$ for the complex relative permittivity and permeability, respectively, of the Eccosorb SF 6.0 were chosen in the following manner. The manufacturer's quoted value of a -5 dB loss at normal incidence for a frequency of 3.0 GHz was used. It was assumed this was for an infinite sheet of the radar absorbing material. Ignoring reflection at the free space/coating boundary, a value for the imaginary part of the propagation constant which would give -5 dB of loss was computed according to the following formula:

$$-5 \text{ dB} = 20 \log_{10} e^{-k''z} \tag{5.1}$$

where k'' is the imaginary part of the propagation constant ($k = \omega\sqrt{\mu\epsilon}$), and z is equal to twice the thickness of the Eccosorb SF 6.0 radar absorbing material (the wave travels through the coating, is reflected at the perfect conductor, and travels back through the coating). This value for the imaginary part of the propagation constant easily yields a value for the product of the complex relative permittivity and permeability. Next, since both the Eccosorb SF 6.0 and the FDS materials are based on a silicon rubber compound, it was assumed the same value for the complex relative permittivity of the SF 6.0 as the manufacturer quoted for the FDS radar absorbing material. Thus, the value for the complex relative permeability was fixed. This is how the values for the complex relative permittivity and permeability of the Eccosorb SF 6.0 radar absorbing material quoted above were arrived at.

The values discussed in the previous paragraph for ϵ_R and μ_R of the Eccosorb SF 6.0 coating produced a decrease in the RCS at normal incidence of -5.7 dB, as shown by the first and third entries in Table 5.2. Unfortunately, this was more loss than was measured experimentally (see Table 5.1). Various values for ϵ_R and μ_R were then used to examine the behavior of the EFIE computer programs and to see which values might produce the best fit to the experimental RCS data. This will be discussed further in the next section.

The computed RCS data for the Eccosorb FGM 40 coated plate are shown in the eighth through twelfth entries of Table 5.2 and in Figures E.24 through E.28 of Appendix E. Values for the complex permittivity and permeability (or dielectric and magnetic constants and loss tangents) were also not available in the manufacturer's literature for the Eccosorb FGM 40 radar absorbing material. The values of ϵ_R and μ_R shown in Table 5.2 for the Eccosorb FGM 40 coating were chosen in the same manner as outlined in the previous paragraphs for the Eccosorb SF 6.0 coating.

The values of ϵ_R and μ_R shown in the seventh and twelfth entries of Table 5.2 for the Eccosorb SF 6.0 and FGM 40 coatings, respectively, were chosen in a slightly different manner. The complex relative permittivities and permeabilities listed in these

entries were calculated assuming the coatings have one-half the thickness and twice the loss quoted by the manufacturer's literature for each respective coating. The results will be discussed further in the next section.

5.4 Comparison of Experimental and Theoretical Results

The comparison of the experimental and theoretical results is done in Figures 5.4 through 5.15 at the end of this chapter. These figures are the composites of the theoretical RCS predictions listed in Table 5.2 and the corresponding experimental RCS plots for the same set of conditions. Figures 5.4 through 5.15 display the σ_{hh} versus angle curves for the experimental RCS data (solid line) and the corresponding theoretical RCS predictions (dashed line) generated by the EFIE series of computer programs. These figures were produced by overlaying the experimental RCS plots onto the theoretical RCS predictions.

Verification of the performance of the EFIE series of computer programs is provided by Figure 5.4. The relative permittivity (ϵ_R) and permeability (μ_R) of the coating were set equal to the free space values in the EFIE series of computer programs to generate the theoretical RCS prediction. As discussed in the previous section, the computer programs would be expected to give RCS data equivalent to that for an uncoated perfect conductor for these values of ϵ_R and μ_R. Figure 5.4 is a comparison of the experimental RCS data for an uncoated 10cm by 10cm aluminum plate and the corresponding theoretical RCS prediction. The theoretical results are very close to the experimental data. The first entries in Tables 5.1 and 5.2 show the theoretical RCS at normal incidence to the coated side of the plate is only 0.1 dB below the experimental measurement. This provides confidence in the performance of the EFIE series of computer programs.

Figure 5.5 is a comparison of the experimental and theoretical data for an Eccosorb FDS coated plate. The relative permittivity (ϵ_R) and permeability (μ_R) of the coating were set equal to the values shown in the second entry in Table 5.2 for the EFIE series of computer programs to generate the theoretical RCS prediction. Again,

the theoretical results are very close to the experimental data. The RCS at normal incidence to the coated side of the plate (σ_{hh} in Tables 5.1 and 5.2) is -10.3 dBsm for the theoretical prediction and -10.6 dBsm for the experimental measurement, a 0.3 dB difference. Figure 5.5 also shows the match is almost exact down to approximately -25 dBsm.

Figures 5.6 through 5.10 are the comparisons of the experimental and theoretical data for an Eccosorb SF 6.0 coated plate. Figure 5.8 shows the best fit of the theoretical RCS prediction to the expermental measurement down to approximately -20 dBsm. The relative permittivity (ϵ_R) and permeability (μ_R) of the coating were set equal to the values shown in the third through seventh entries in Table 5.2 for the EFIE series of computer programs to generate the theoretical RCS predictions. As discussed in the previous section, all the values for ϵ_R and μ_R shown in Table 5.2 for the Eccosorb SF 6.0 radar absorbing material were chosen, and they are not the manufacturer's specifications. The different values of ϵ_R and μ_R were chosen to investigate the behavior of the EFIE computer programs, and to see which value gave the closest fit to the experimental data.

The RCS at normal incidence to the coated side of the plate (σ_{hh} in Tables 5.1 and 5.2) is -12.5 dBsm for the experimental measurement (third entry in Table 5.1). The theoretical predictions for the RCS at normal incidence to the coated side of the plate are -15.5, -12.1, -12.4, -12.0, and -11.2 dBsm, respectively, for the third through seventh entries in Table 5.2. The first theoretical prediction is -3.0 dB too low. As discussed in the previous section, the values for ϵ_R and μ_R used to generate this prediction were based on the manufacturer's quoted RCS reduction of a nominal -5 dB at normal incidence. The computed reduction is actually -5.7 dB (the third entry minus the first entry in Table 5.2). The next three RCS predictions in Table 5.2 for the SF 6.0 are relatively close: a difference of +0.4 dB, +0.1 dB, and +0.5 dB, respectively, from the experimental measurement. The last RCS prediction for the SF 6.0 assumed a coating with twice the thickness and one-half the loss to compute the values of ϵ_R and μ_R. This prediction was +1.3 dB too high.

Figures 5.11 through 5.15 are the comparisons of the experimental and theo-

retical data for an Eccosorb FGM 40 coated plate. Figures 5.13 and 5.14 both show a close fit of the theoretical RCS prediction to the expermental measurement down to approximately -20 dBsm. The relative permittivity (ϵ_R) and permeability (μ_R) of the coating were set equal to the values shown in the eighth through twelfth entries in Table 5.2 for the EFIE series of computer programs to generate the theoretical RCS predictions. As discussed in the previous section, all the values for ϵ_R and μ_R shown in Table 5.2 for the Eccosorb FGM 40 radar absorbing material were chosen, and they are not the manufacturer's specifications. The different values of ϵ_R and μ_R were chosen to investigate the behavior of the EFIE computer programs, and to see which value gave the closest fit to the experimental data.

The RCS at normal incidence to the coated side of the plate (σ_{hh} in Tables 5.1 and 5.2) is -13.3 dBsm for the experimental measurement (fourth entry in Table 5.1). The theoretical predictions for the RCS at normal incidence to the coated side of the plate are -12.5, -15.3, -13.0, -13.5, and -12.2 dBsm, respectively, for the eighth through twelfth entries in Table 5.2. The first four RCS predictions in Table 5.2 for the FGM 40 are a difference of +0.8 dB, -2.0 dB, +0.3dB, and -0.2 dB, respectively, from the experimental measurement. The last RCS prediction for the FGM 40 assumed a coating with twice the thickness and one-half the loss to compute the values of ϵ_R and μ_R. This prediction was +1.1 dB too high.

The difference of the theoretical RCS predictions from the experimental RCS measurements is a function of the approximations made in the theoretical model. One approximation to consider is the modelling of the coating. As discussed in the previous section, the surfaces of the coating along the sides which would meet the perfect conductor were not used. This could account for the differences between the theoretical RCS predictions and the experimental RCS measurements near $\pm 90°$ in Figures 5.4 through 5.15. At these angles the contribution of the sides of the coating to the overall RCS could be more important. This issue and others are discussed further in Chapter 7.

Coatings listed are Eccosorb radar absorbing material

Targets are square aluminum plates coated on one side

f = radar frequency in gigahertz (GHz)

RCS measurements made at 360 points from $-180°$ to $180°$

RCS is in decibels referenced to one square meter (dBsm)

σ_{hh} = RCS at normal incidence (0°) to coated side of plate for HH polarization

Plate Size	Coating	Case	f	σ_{hh}	Figure
10cm × 10cm	None	13	3.0	-9.7	E.1
10cm × 10cm	FDS	16	3.0	-10.6	E.2
10cm × 10cm	SF 6.0	15	3.0	-12.5	E.3
10cm × 10cm	FGM 40	14	3.0	-13.3	E.4
10cm × 10cm	None	13B	6.0	-3.4	E.5
10cm × 10cm	FDS	16B	6.0	-4.5	E.6
10cm × 10cm	SF 6.0	15B	6.0	-20.0	E.7
10cm × 10cm	FGM 40	14B	6.0	-15.2	E.8
15cm × 15cm	None	9	3.0	-1.1	E.9
15cm × 15cm	FDS	12	3.0	-2.1	E.10
15cm × 15cm	SF 6.0	11	3.0	-4.4	E.11
15cm × 15cm	FGM 40	10	3.0	-7.0	E.12
15cm × 15cm	None	9B	6.0	4.5	E.13
15cm × 15cm	FDS	12B	6.0	3.3	E.14
15cm × 15cm	SF 6.0	11B	6.0	-13.3	E.15
15cm × 15cm	FGM 40	10B	6.0	-9.4	E.16

Table 5.1. Experimental Radar Cross Section Plots

Coating parameters used correspond to Eccosorb specfications

ϵ_R = complex relative permittivity of coating

μ_R = complex relative permeability of coating

Targets are square plate perfect conductors coated on one side

Radar frequency is 3.0 gigahertz (GHz) for all entries

RCS computations made at 109 points from $-180°$ to $180°$

σ_{hh} = RCS at normal incidence (0°) to coated side of plate
for HH polarization

* permittivity and permeability for these two cases computed assuming coatings have one-half the thickness and twice the loss

Plate Size	Coating	ϵ_R	μ_R	σ_{hh}	Figure
10cm × 10cm	None	(1.0,0.0)	(1.0,0.0)	-9.8	E.17
10cm × 10cm	FDS	(8.9.0.623)	(1.7,1.36)	-10.3	E.18
10cm × 10cm	SF 6.0	(8.9,0.623)	(2.9,2.32)	-15.5	E.19
10cm × 10cm	SF 6.0	(5.0,0.623)	(1.3,0.93)	-12.1	E.20
10cm × 10cm	SF 6.0	(5.0,0.0)	(1.18,1.09)	-12.4	E.21
10cm × 10cm	SF 6.0	(8.9,0.623)	(1.85,0.83)	-12.0	E.22
10cm × 10cm	SF 6.0	(8.9,0.623)	(0.46, 0.21)*	-11.2	E.23
10cm × 10cm	FGM 40	(11.0,0.1)	(4.2,3.8)	-12.5	E.24
10cm × 10cm	FGM 40	(5.0,0.0)	(9.2,8.5)	-15.3	E.25
10cm × 10cm	FGM 40	(8.9,0.623)	(5.5,4.4)	-13.0	E.26
10cm × 10cm	FGM 40	(8.0,0.0)	(5.8,5.4)	-13.5	E.27
10cm × 10cm	FGM 40	(8.9,0.623)	(1.37, 1.1)*	-12.2	E.28

Table 5.2. Theoretical Radar Cross Section Predictions

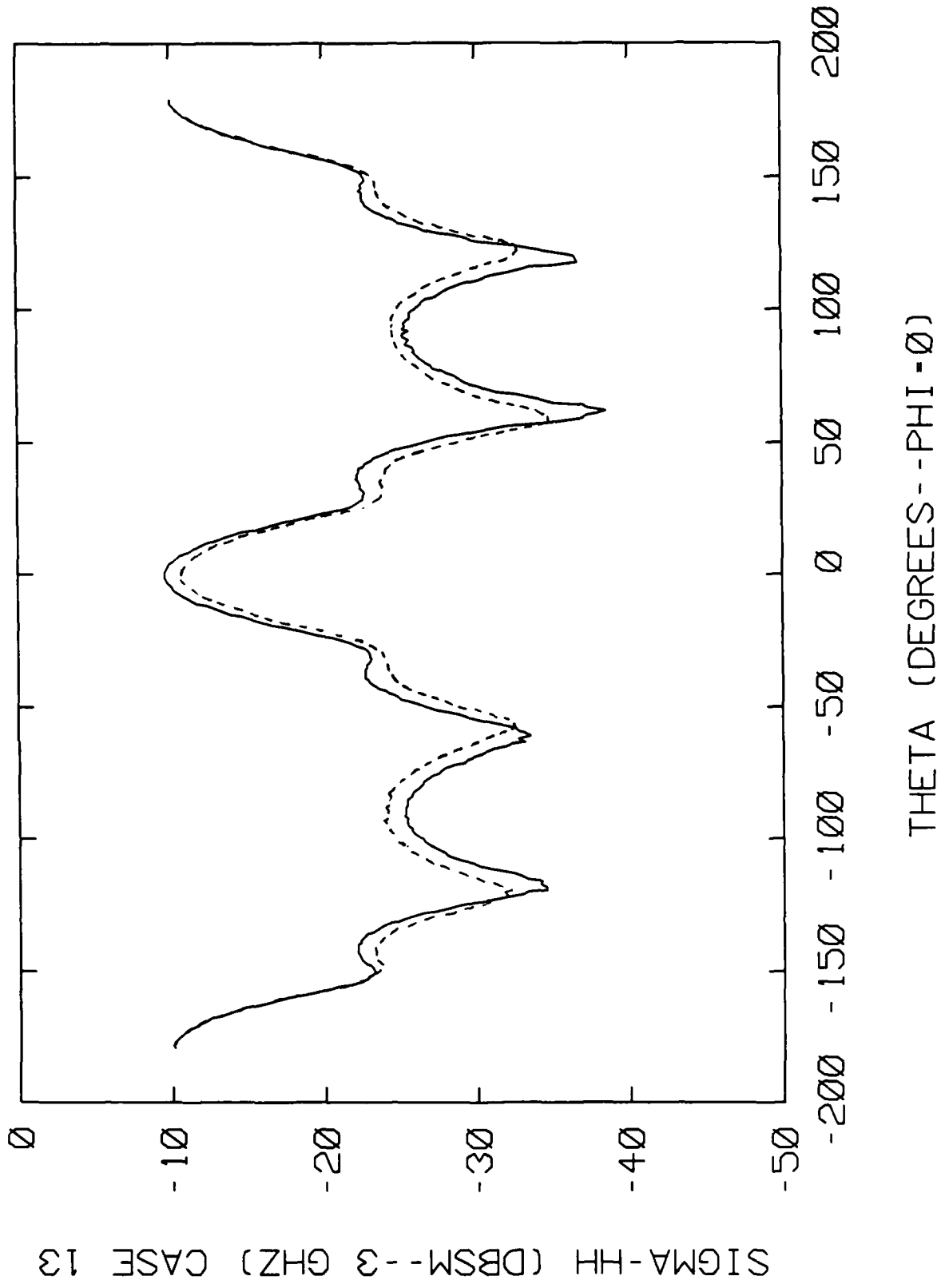

Figure 5.1. Experimental 3.0 GHz RCS for uncoated (solid line) and Eccosorb FDS coated (dashed line) 10cm by 10cm aluminum plate: σ_{hh} versus angle

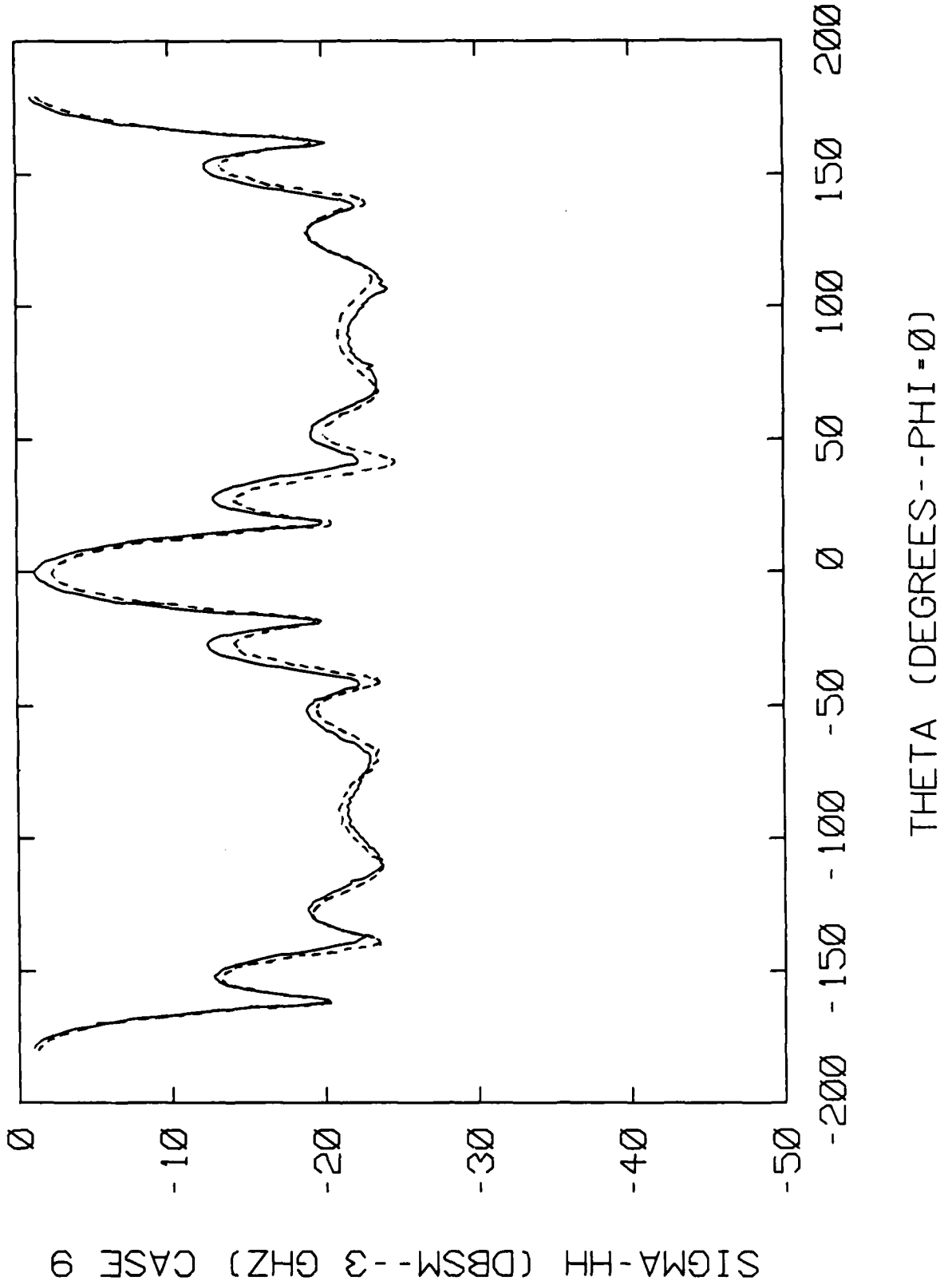

Figure 5.2. Experimental 3.0 GHz RCS for uncoated (solid line) and Eccosorb FDS coated (dashed line) 15cm by 15cm aluminum plate: σ_{hh} versus angle

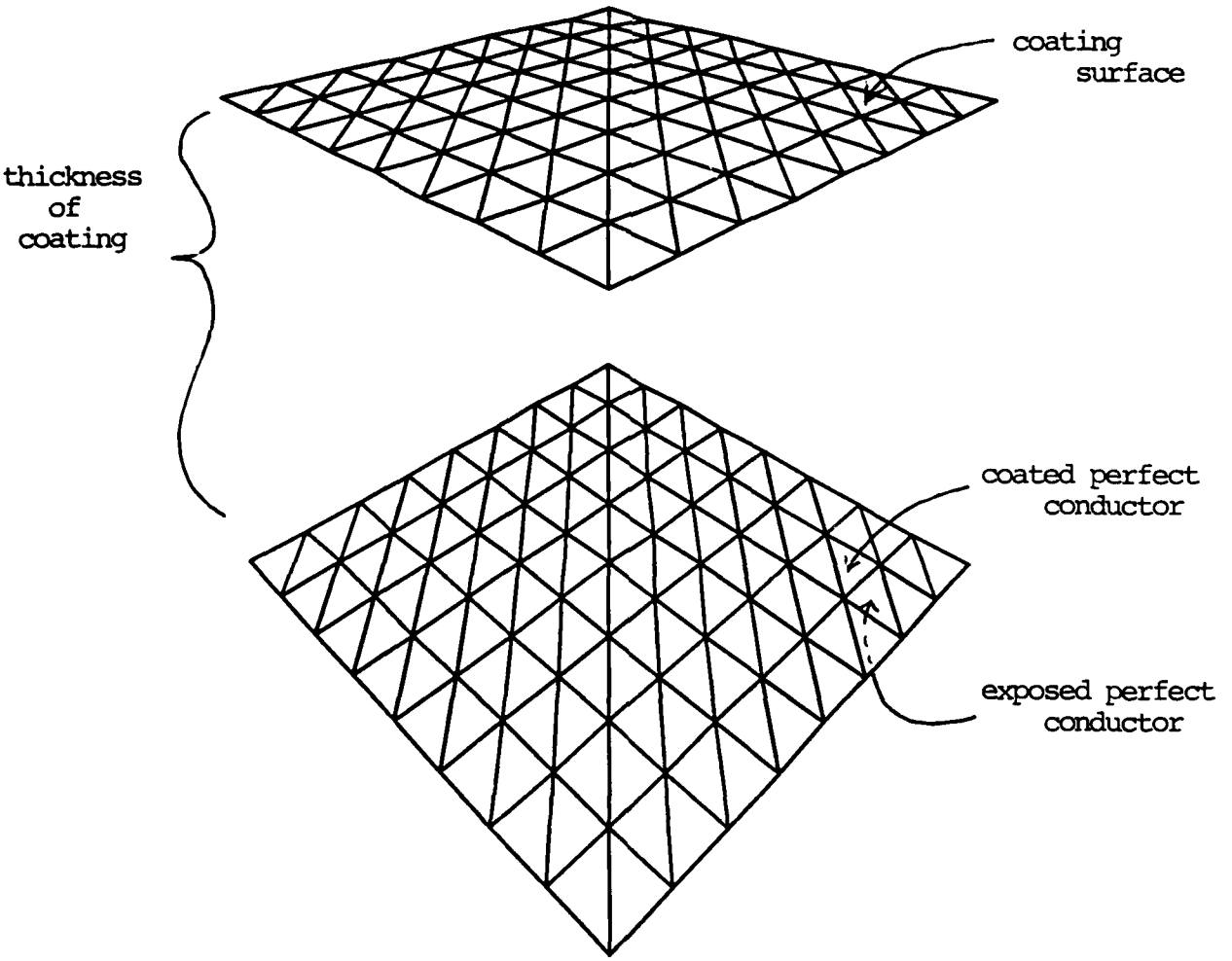

Figure 5.3. Triangular patch model of partially coated perfectly conducting square plate

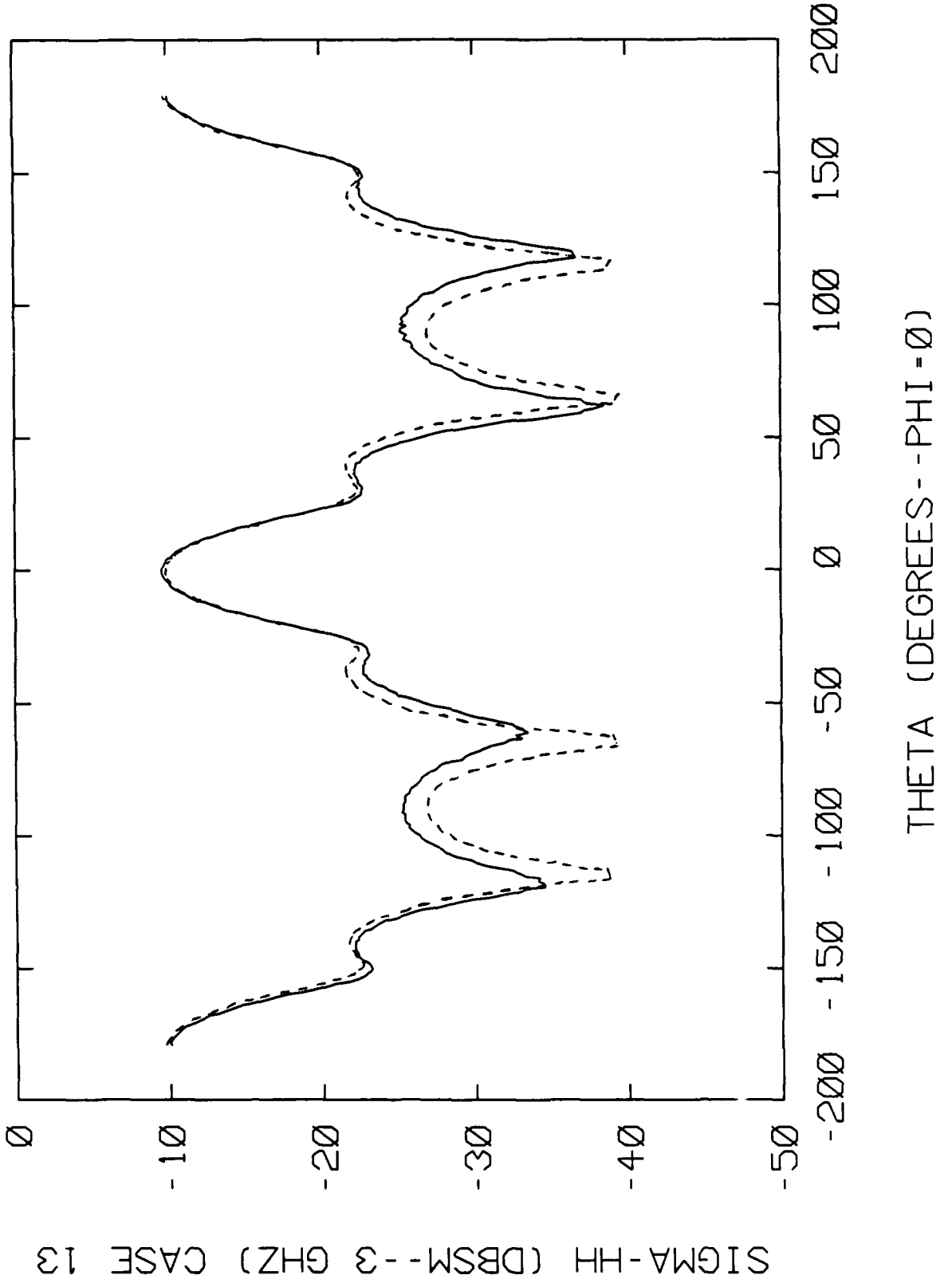

Figure 5.4. Experimental (solid line) and theoretical (dashed line) 3.0 GHz RCS for uncoated 10cm by 10cm aluminum plate: σ_{hh} versus angle

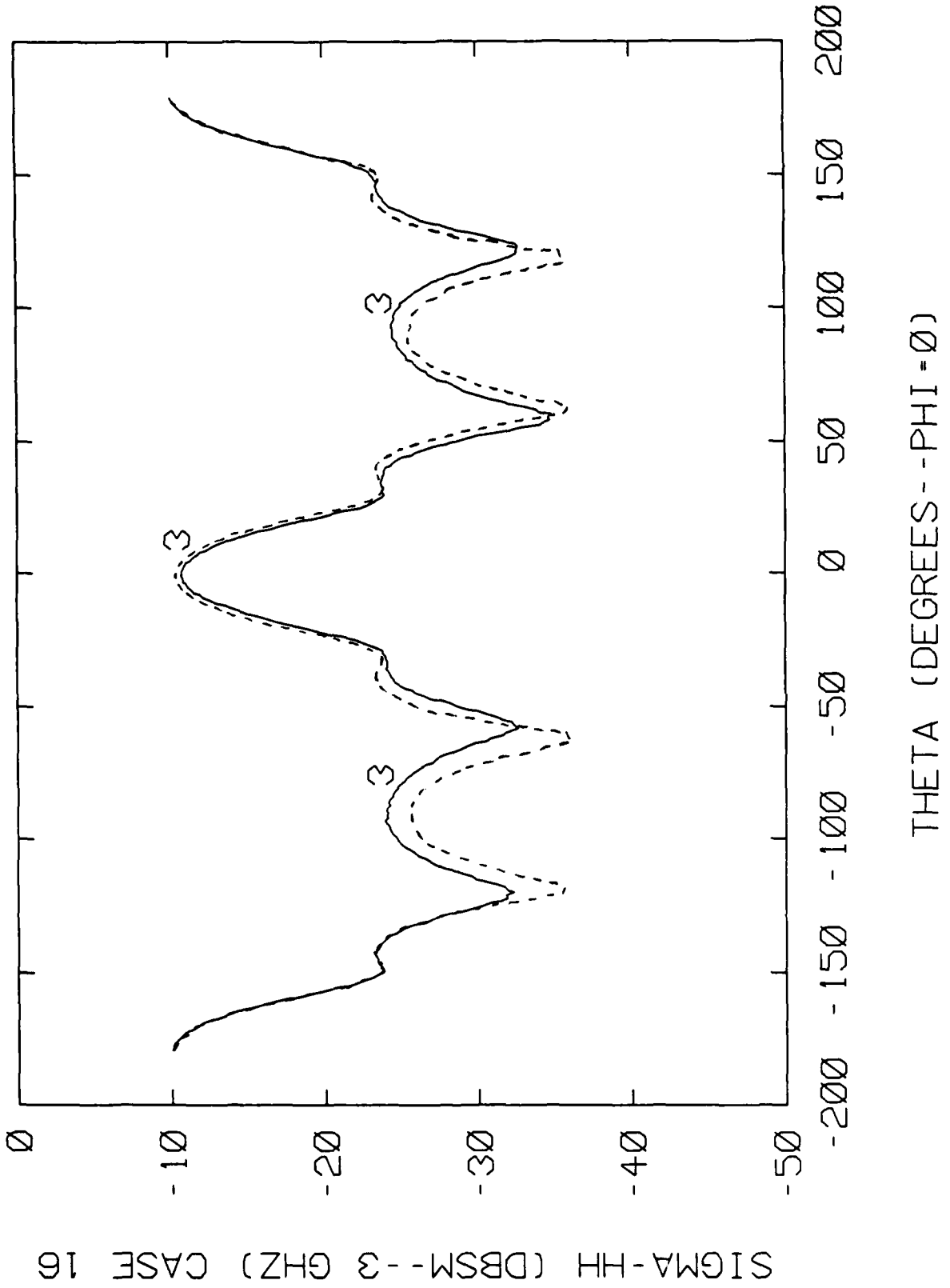

Figure 5.5. Experimental (solid line) and theoretical (dashed line) 3.0 GHz RCS for Eccosorb FDS coated 10cm by 10cm aluminum plate: σ_{hh} versus angle

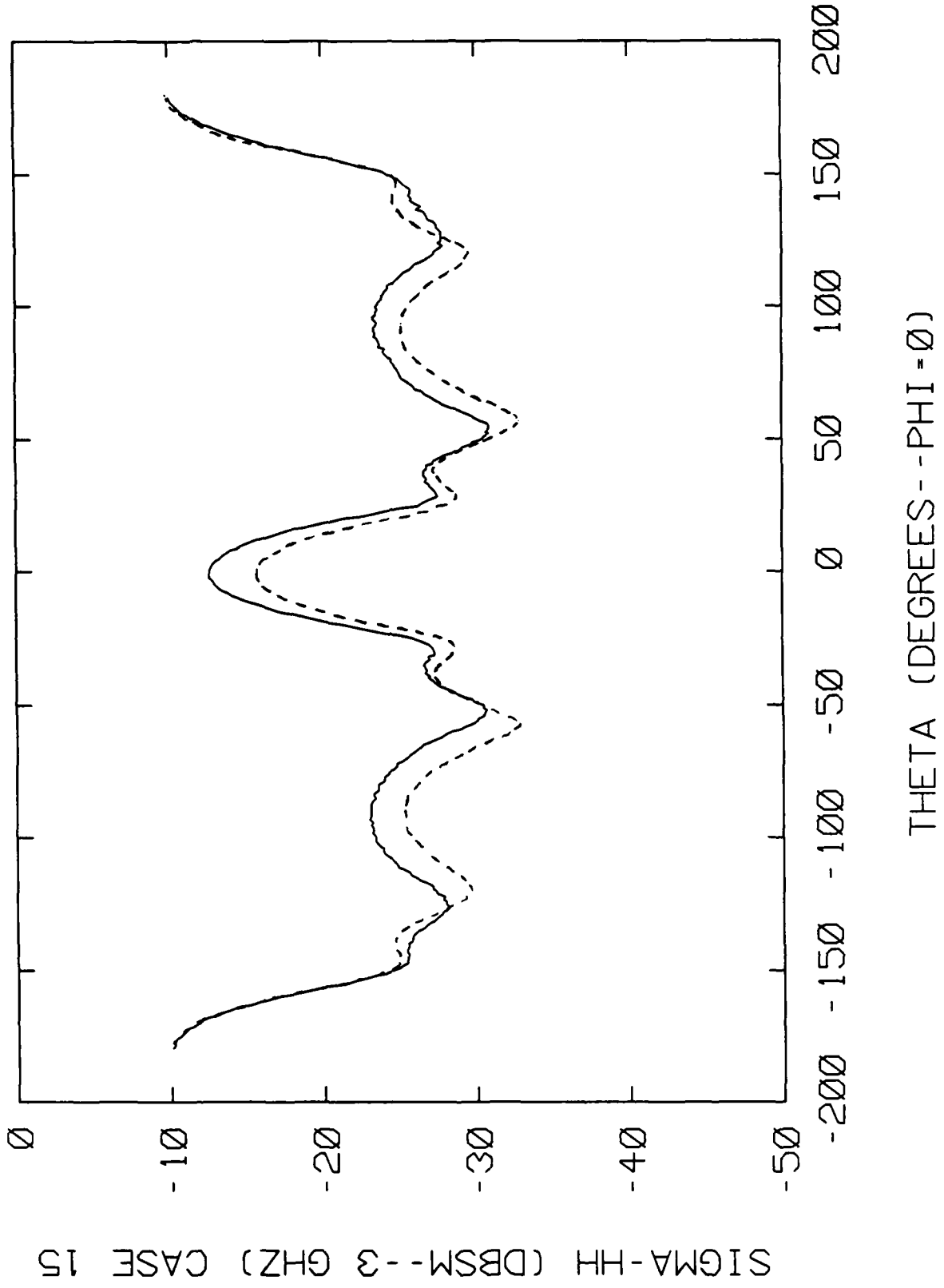

Figure 5.6. Experimental (solid line) and theoretical (dashed line) 3.0 GHz RCS for Eccosorb SF 6.0 coated 10cm by 10cm aluminum plate: σ_{hh} versus angle (1 of 5)

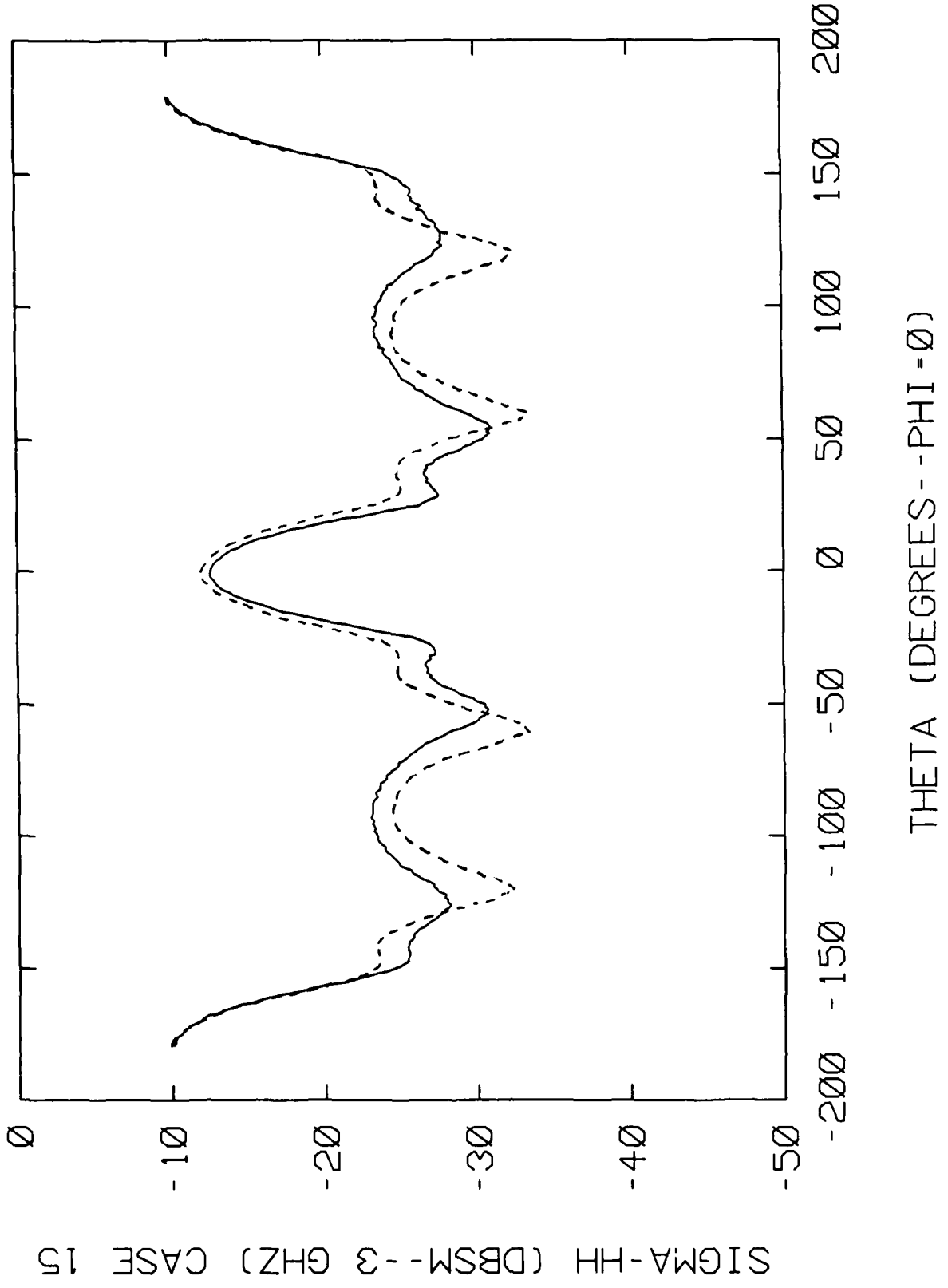

Figure 5.7. Experimental (solid line) and theoretical (dashed line) 3.0 GHz RCS for Eccosorb SF 6.0 coated 10cm by 10cm aluminum plate: σ_{hh} versus angle (2 of 5)

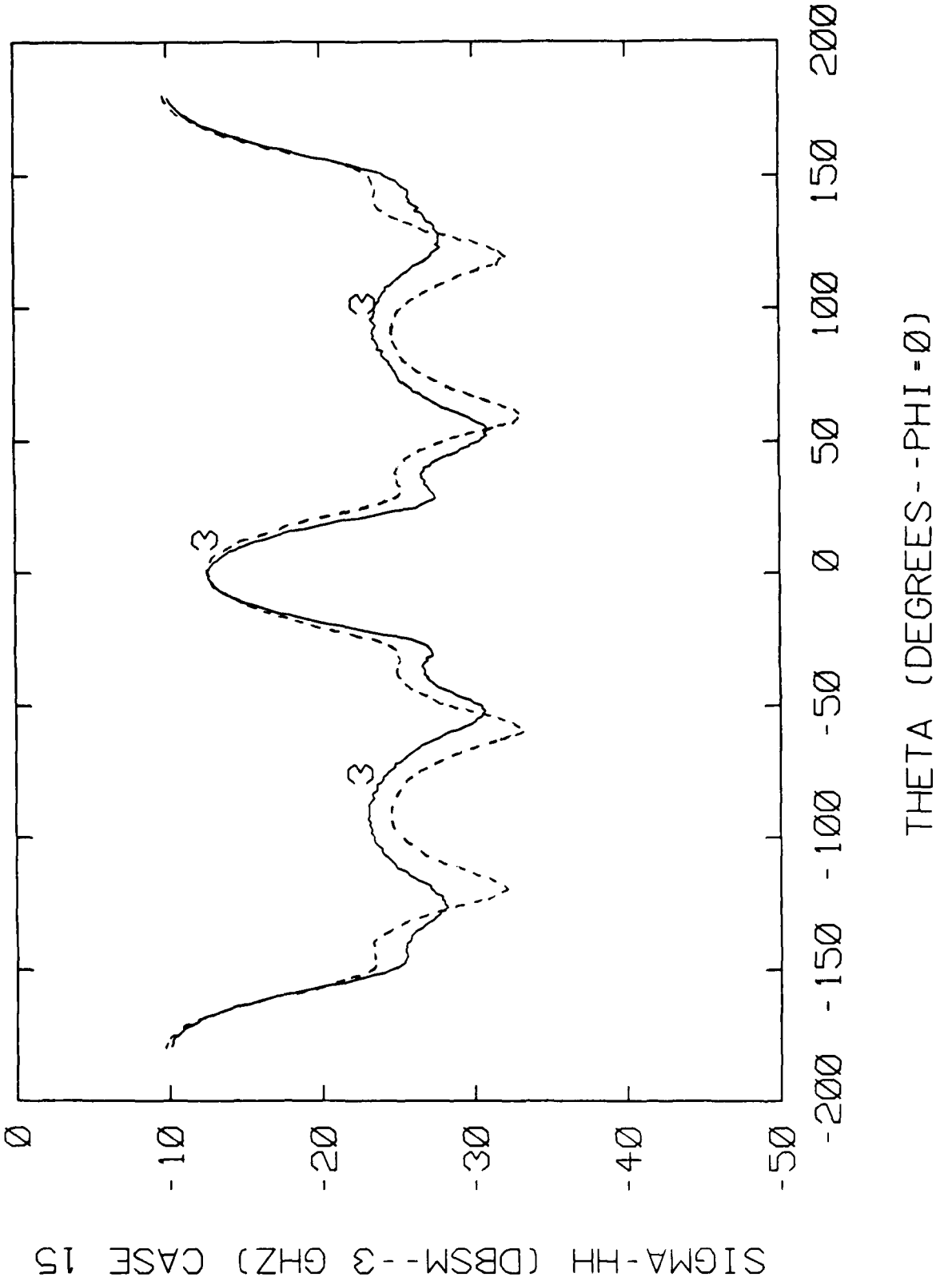

Figure 5.8. Experimental (solid line) and theoretical (dashed line) 3.0 GHz RCS for Eccosorb SF 6.0 coated 10cm by 10cm aluminum plate: σ_{hh} versus angle (3 of 5)

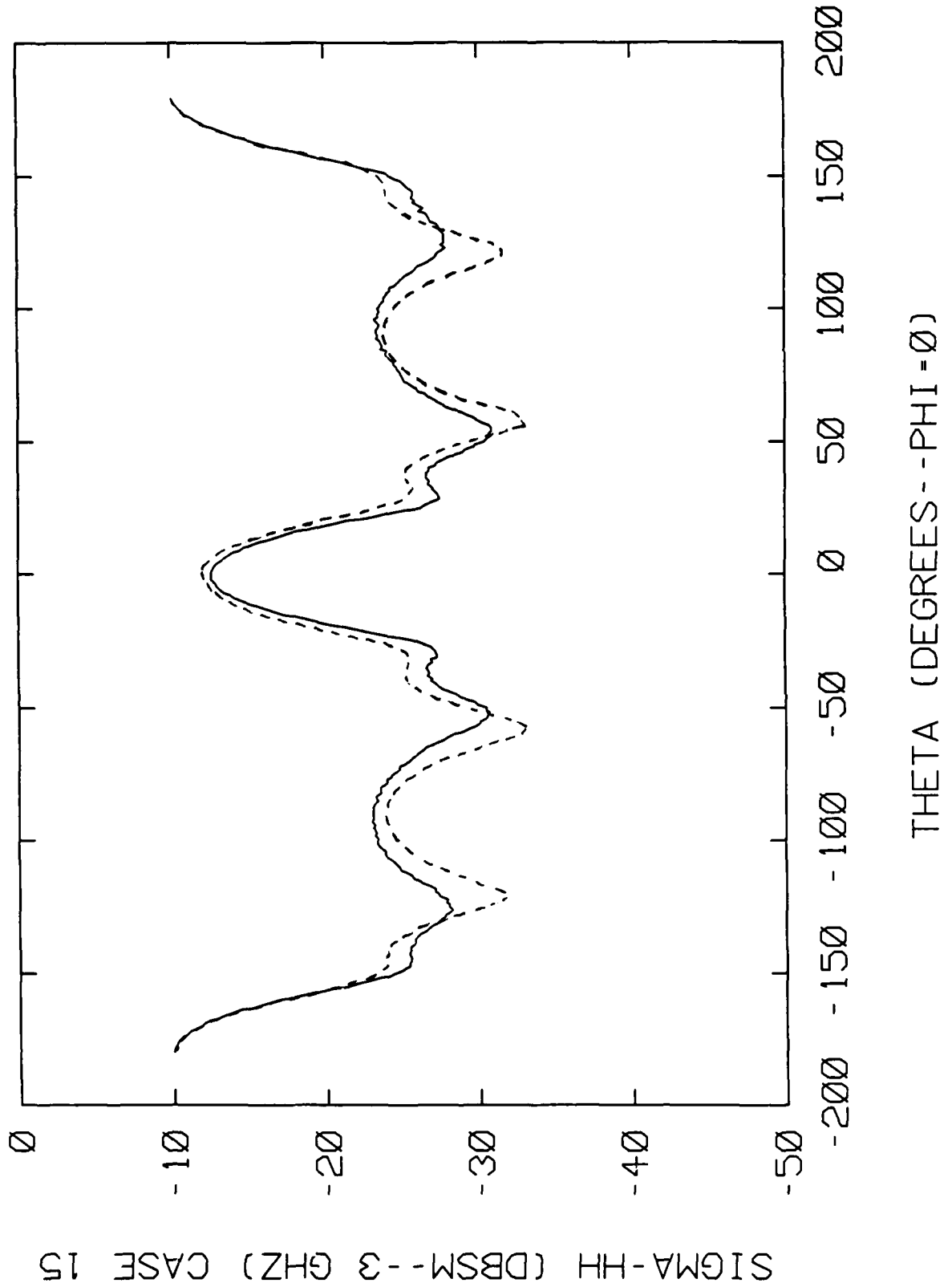

Figure 5.9. Experimental (solid line) and theoretical (dashed line) 3.0 GHz RCS for Eccosorb SF 6.0 coated 10cm by 10cm aluminum plate: σ_{hh} versus angle (4 of 5)

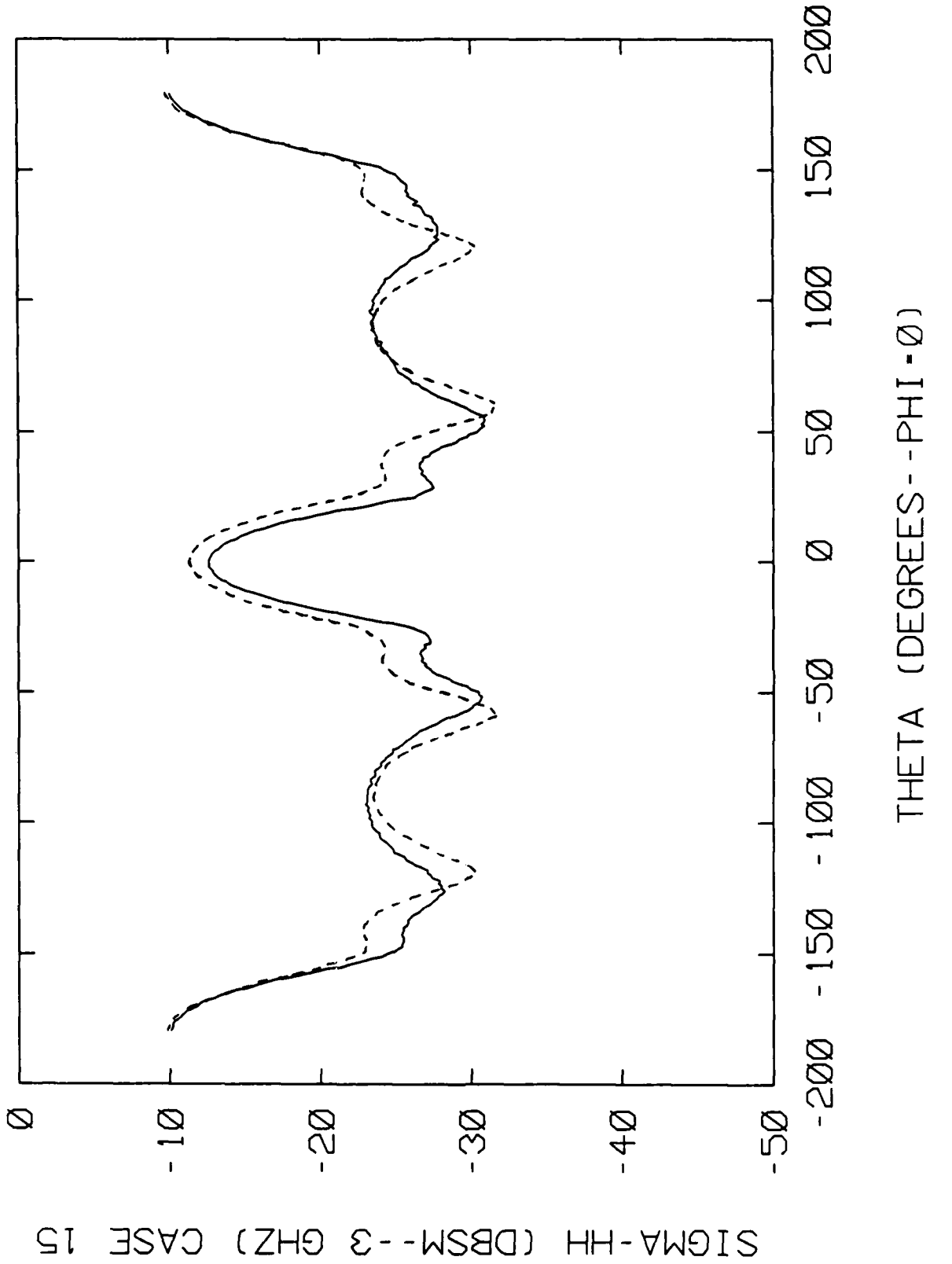

Figure 5.10. Experimental (solid line) and theoretical (dashed line) 3.0 GHz RCS for Eccosorb SF 6.0 coated 10cm by 10cm aluminum plate: σ_{hh} versus angle (5 of 5)

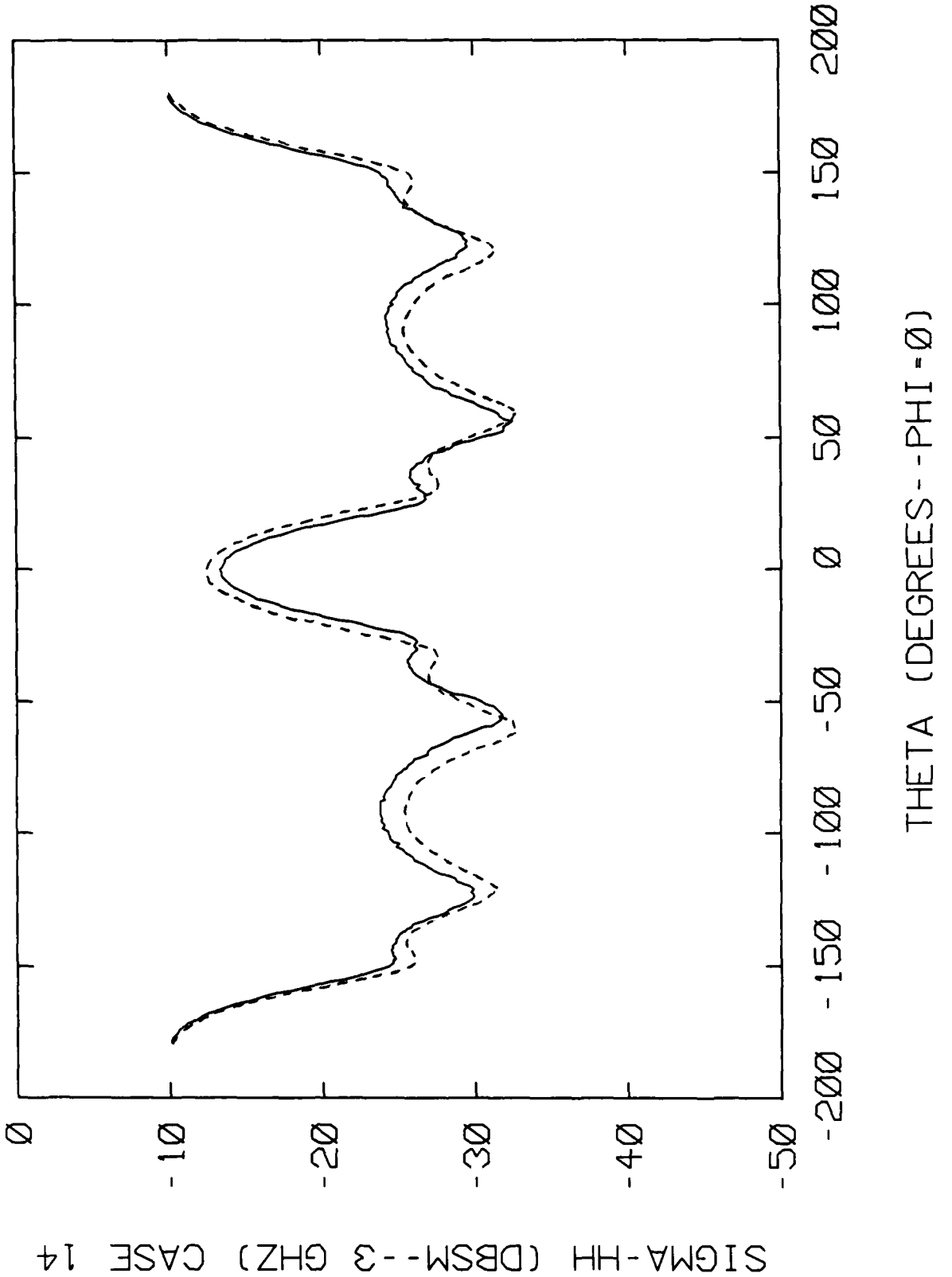

Figure 5.11. Experimental (solid line) and theoretical (dashed line) 3.0 GHz RCS for Eccosorb FGM 40 coated 10cm by 10cm aluminum plate: σ_{hh} versus angle (1 of 5)

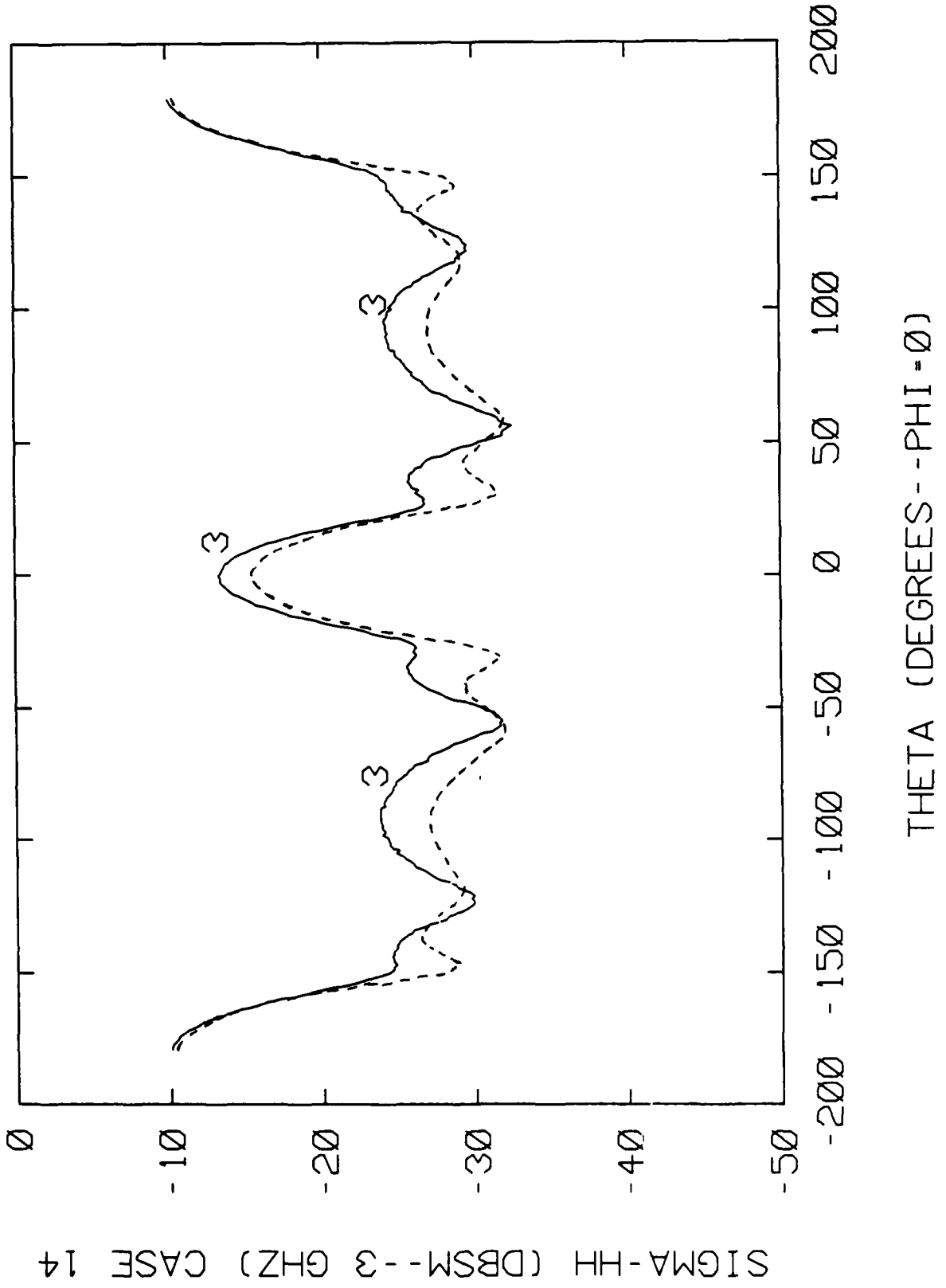

Figure 5.12. Experimental (solid line) and theoretical (dashed line) 3.0 GHz RCS for Eccosorb FGM 40 coated 10cm by 10cm aluminum plate: σ_{hh} versus angle (2 of 5)

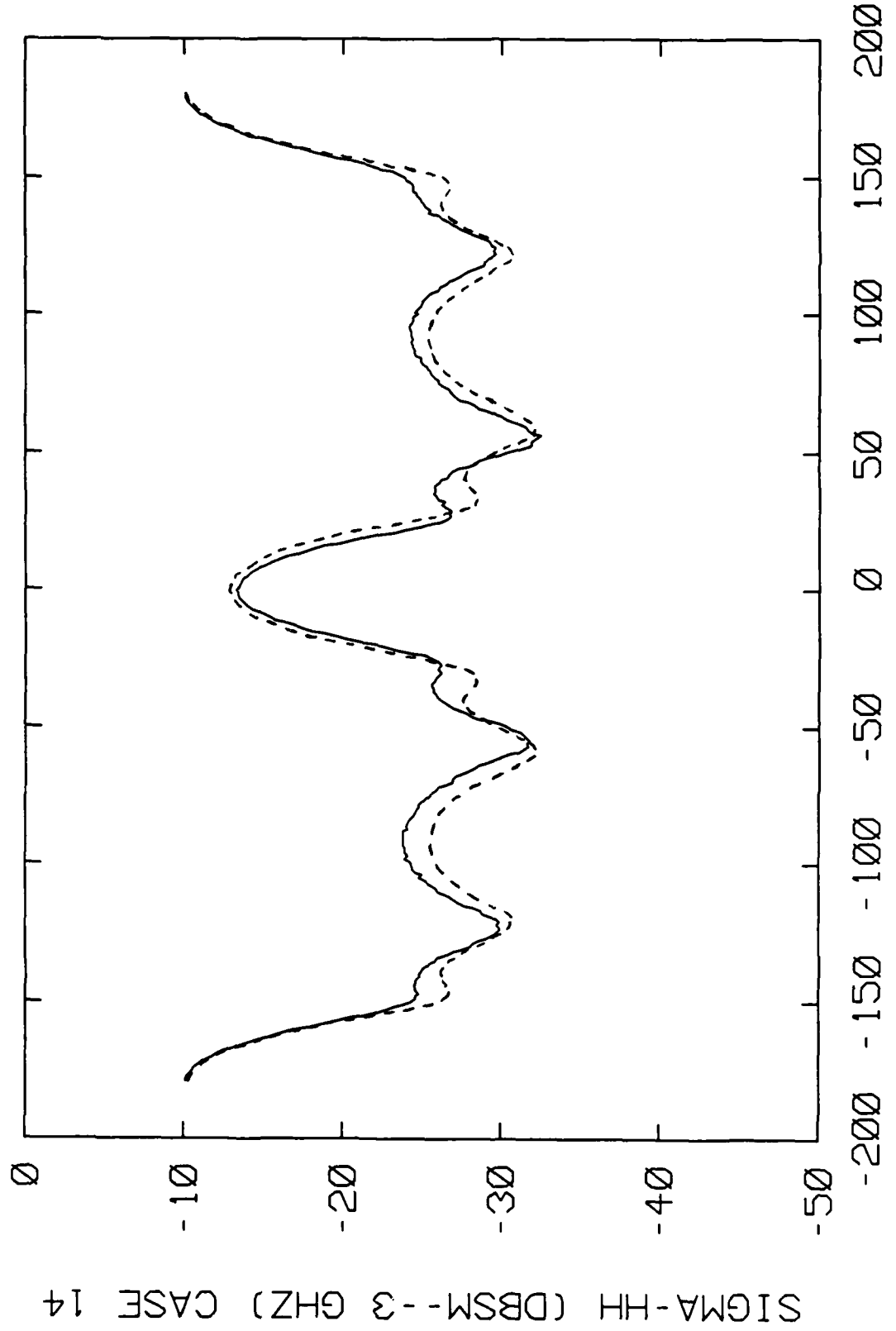

Figure 5.13. Experimental (solid line) and theoretical (dashed line) 3.0 GHz RCS for Eccosorb FGM 40 coated 10cm by 10cm aluminum plate: σ_{hh} versus angle (3 of 5)

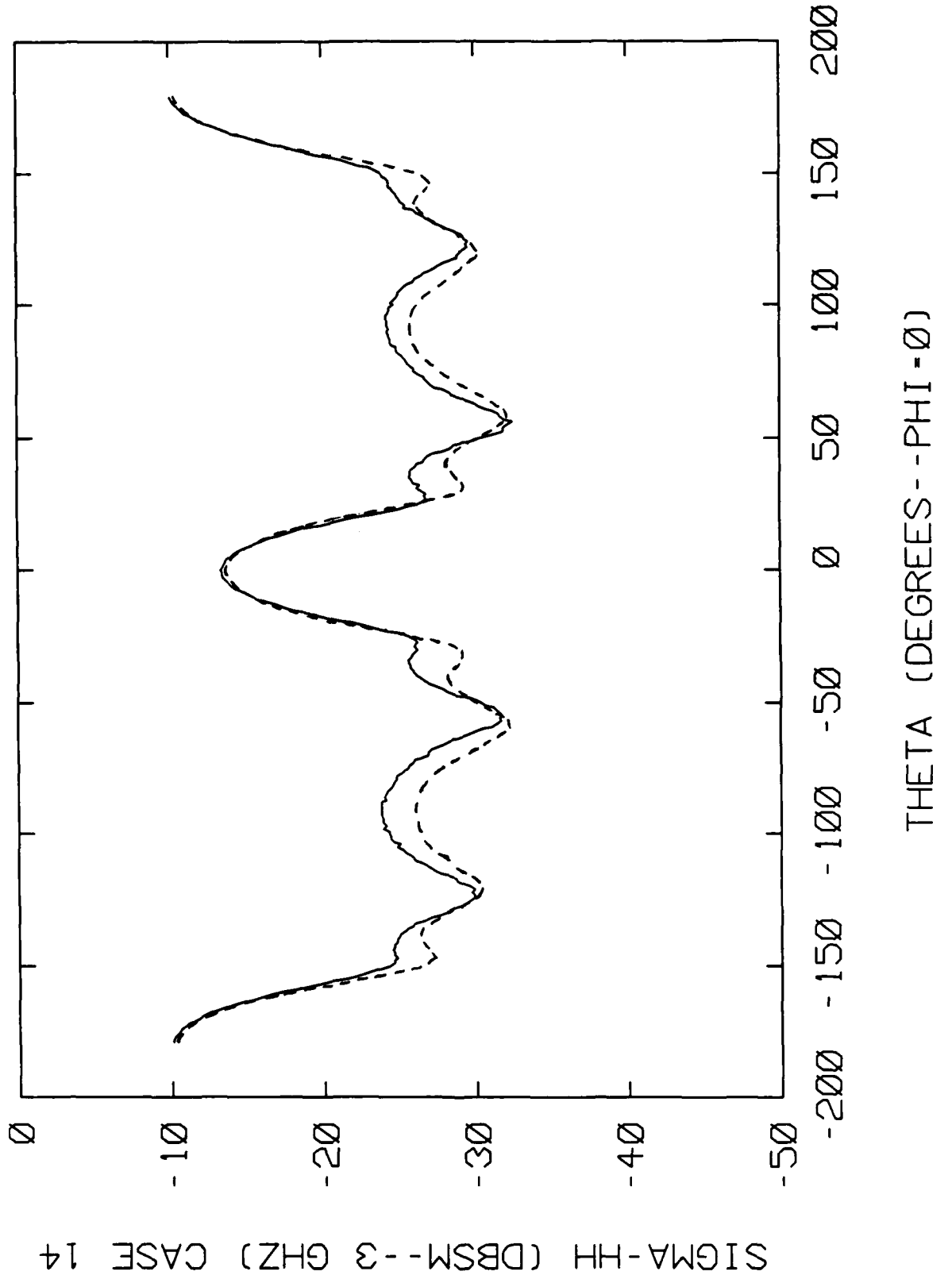

Figure 5.14. Experimental (solid line) and theoretical (dashed line) 3.0 GHz RCS for Eccosorb FGM 40 coated 10cm by 10cm aluminum plate: σ_{hh} versus angle (4 of 5)

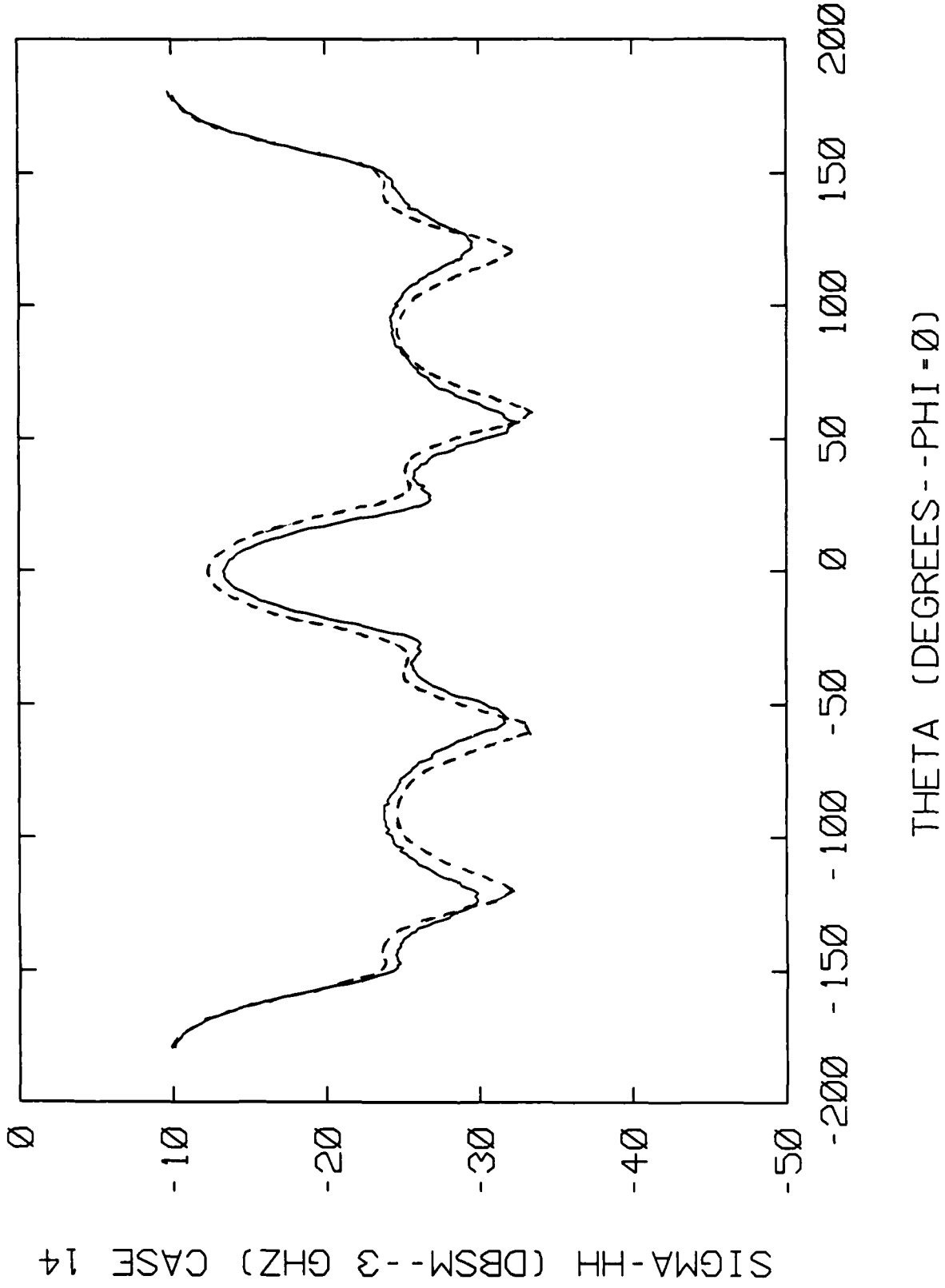

Figure 5.15. Experimental (solid line) and theoretical (dashed line) 3.0 GHz RCS for Eccosorb FGM 40 coated 10cm by 10cm aluminum plate: σ_{hh} versus angle (5 of 5)

Chapter 6

GENERALIZATION TO MULTI-LAYERED COATING

6.1 Introduction

This chapter presents the extension of the procedure discussed in Chapter 3 to a multi-layered coating. Chapter 3 discussed the approach used for a single layer of coating on a perfectly conducting surface. The cases of a completely coated perfect conductor and a partially coated perfect conductor were derived in Chapter 3. This chapter also discusses the cases of a completely coated perfect conductor (section 6.2) and a partially coated perfect conductor (section 6.3) with multi-layered coatings.

6.2 Completely Coated Perfect Conductor

Using Huygens' principle, the equivalence principle, and satisfying the boundary conditions for a completely coated perfect conductor generates a set of integro-differential equations (see Appendix A). Applying the method of moments to this set of integro-differential equations produces a matrix equation. As derived in Appendix A for one layer of coating completely enclosing a perfect conductor (refer to Figure 3.1), the matrix equation is of the form:

$$\begin{pmatrix} \overline{E}_m \\ \overline{H}_{m'} \\ \overline{0}_{m''} \end{pmatrix} = \begin{pmatrix} \overline{\overline{Z}}_{11} & \overline{\overline{Z}}_{12} & \overline{\overline{Z}}_{13} \\ \overline{\overline{Z}}_{21} & \overline{\overline{Z}}_{22} & \overline{\overline{Z}}_{23} \\ \overline{\overline{Z}}_{31} & \overline{\overline{Z}}_{32} & \overline{\overline{Z}}_{33} \end{pmatrix} \begin{pmatrix} \overline{J}_1 \\ \overline{M}_1 \\ \overline{J}_0 \end{pmatrix}. \tag{6.1}$$

The left half of the equation represents the excitation vector, and the right half of the equation represents the interaction matrix, Z-matrix, times the unknown electric and magnetic surface current coefficients. This matrix equation corresponds to three simultaneous equations in three unknowns. Now, the third equation can be used to

back-substitute and reduce the size of the Z-matrix:

$$\overline{J}_0 = -\overline{\overline{Z}}_{33}^{-1}\left[\overline{\overline{Z}}_{31}\cdot\overline{J}_1 + \overline{\overline{Z}}_{32}\cdot\overline{M}_1\right]. \tag{6.2}$$

Back-substituting leaves two simultaneous equations which can be written as the following matrix equation:

$$\begin{pmatrix}\overline{E}_m \\ \overline{H}_{m'}\end{pmatrix} = \begin{pmatrix}\overline{\overline{Z}}'_{11} & \overline{\overline{Z}}'_{12} \\ \overline{\overline{Z}}'_{21} & \overline{\overline{Z}}'_{22}\end{pmatrix}\begin{pmatrix}\overline{J}_1 \\ \overline{M}_1\end{pmatrix} \tag{6.3}$$

where

$$\overline{\overline{Z}}'_{11} = \overline{\overline{Z}}_{11} - \overline{\overline{Z}}_{13}\cdot\overline{\overline{Z}}_{33}^{-1}\cdot\overline{\overline{Z}}_{31} \tag{6.4}$$

$$\overline{\overline{Z}}'_{12} = \overline{\overline{Z}}_{12} - \overline{\overline{Z}}_{13}\cdot\overline{\overline{Z}}_{33}^{-1}\cdot\overline{\overline{Z}}_{32} \tag{6.5}$$

$$\overline{\overline{Z}}'_{21} = \overline{\overline{Z}}_{21} - \overline{\overline{Z}}_{23}\cdot\overline{\overline{Z}}_{33}^{-1}\cdot\overline{\overline{Z}}_{31} \tag{6.6}$$

$$\overline{\overline{Z}}'_{22} = \overline{\overline{Z}}_{22} - \overline{\overline{Z}}_{23}\cdot\overline{\overline{Z}}_{33}^{-1}\cdot\overline{\overline{Z}}_{32}. \tag{6.7}$$

Assume N basis functions are obtained over each boundary surface using the method of moments. Equation 6.1 requires the inversion of a 3N by 3N Z-matrix to compute the unknown surface current coefficients. Back-substitution requires the inversion of an N by N matrix, $\overline{\overline{Z}}_{33}^{-1}$, some matrix multiplications and additions, equations 6.4 through 6.7, and the inversion of a 2N by 2N Z-matrix, equation 6.3. However, all the target structure beneath the coating has been replaced by an equivalent interaction matrix as shown in equation 6.3. This has significance for the extension of the procedure discussed in Chapter 3 to multi-layered coatings.

For two layers of coating on a perfect conductor (refer to Figure 6.1), the matrix equation is of the form:

$$\begin{pmatrix}\overline{E}_m \\ \overline{H}_{m'} \\ \overline{0}_{m''} \\ \overline{0}_{m'''} \\ \overline{0}_{m^{(iv)}}\end{pmatrix} = \begin{pmatrix}\overline{\overline{Z}}_{11} & \overline{\overline{Z}}_{12} & \overline{\overline{Z}}_{13} & \overline{\overline{Z}}_{14} & 0 \\ \overline{\overline{Z}}_{21} & \overline{\overline{Z}}_{22} & \overline{\overline{Z}}_{23} & \overline{\overline{Z}}_{24} & 0 \\ \overline{\overline{Z}}_{31} & \overline{\overline{Z}}_{32} & \overline{\overline{Z}}_{33} & \overline{\overline{Z}}_{34} & \overline{\overline{Z}}_{35} \\ \overline{\overline{Z}}_{41} & \overline{\overline{Z}}_{42} & \overline{\overline{Z}}_{43} & \overline{\overline{Z}}_{44} & \overline{\overline{Z}}_{45} \\ 0 & 0 & \overline{\overline{Z}}_{53} & \overline{\overline{Z}}_{54} & \overline{\overline{Z}}_{55}\end{pmatrix}\begin{pmatrix}\overline{J}_2 \\ \overline{M}_2 \\ \overline{J}_1 \\ \overline{M}_1 \\ \overline{J}_0\end{pmatrix}. \tag{6.8}$$

This matrix equation represents five simultaneous equations in five unknowns. Back-substituting the fifth equation in 6.8 in the manner used for 6.1 yields a matrix equation of the form:

$$\begin{pmatrix} \overline{E}_m \\ \overline{H}_{m'} \\ \overline{0}_{m''} \\ \overline{0}_{m'''} \end{pmatrix} = \begin{pmatrix} \overline{\overline{Z}}_{11} & \overline{\overline{Z}}_{12} & \overline{\overline{Z}}_{13} & \overline{\overline{Z}}_{14} \\ \overline{\overline{Z}}_{21} & \overline{\overline{Z}}_{22} & \overline{\overline{Z}}_{23} & \overline{\overline{Z}}_{24} \\ \overline{\overline{Z}}_{31} & \overline{\overline{Z}}_{32} & \overline{\overline{Z}}_{33} & \overline{\overline{Z}}_{34} \\ \overline{\overline{Z}}_{41} & \overline{\overline{Z}}_{42} & \overline{\overline{Z}}_{43} & \overline{\overline{Z}}_{44} \end{pmatrix} \begin{pmatrix} \overline{J}_2 \\ \overline{M}_2 \\ \overline{J}_1 \\ \overline{M}_1 \end{pmatrix} \tag{6.9}$$

which represents four simultaneous equations in four unknowns. Obviously, the elements of the Z-matrix in equation 6.9 are not the same as the elements of the Z-matrix in equation 6.8 due to the back-substitution. Further, the explicit equation representing the interaction of the perfect conductor surface with the first layer of coating has now been absorbed into the equivalent Z-matrix shown in 6.9. Now, the third and fourth equations in 6.9 can be written as

$$\overline{\overline{Z}}_{33} \cdot \overline{J}_1 + \overline{\overline{Z}}_{34} \cdot \overline{M}_1 = -\left[\overline{\overline{Z}}_{31} \cdot \overline{J}_2 + \overline{\overline{Z}}_{32} \cdot \overline{M}_2\right] \tag{6.10}$$

and

$$\overline{\overline{Z}}_{43} \cdot \overline{J}_1 + \overline{\overline{Z}}_{44} \cdot \overline{M}_1 = -\left[\overline{\overline{Z}}_{41} \cdot \overline{J}_2 + \overline{\overline{Z}}_{42} \cdot \overline{M}_2\right], \tag{6.11}$$

which becomes

$$\begin{pmatrix} \overline{\overline{Z}}_{33} & \overline{\overline{Z}}_{34} \\ \overline{\overline{Z}}_{43} & \overline{\overline{Z}}_{44} \end{pmatrix} \begin{pmatrix} \overline{J}_1 \\ \overline{M}_1 \end{pmatrix} = \begin{pmatrix} -\overline{\overline{Z}}_{31} & -\overline{\overline{Z}}_{32} \\ -\overline{\overline{Z}}_{41} & -\overline{\overline{Z}}_{42} \end{pmatrix} \begin{pmatrix} \overline{J}_2 \\ \overline{M}_2 \end{pmatrix}. \tag{6.12}$$

Therefore,

$$\begin{pmatrix} \overline{J}_1 \\ \overline{M}_1 \end{pmatrix} = -\begin{pmatrix} \overline{\overline{Z}}_{33} & \overline{\overline{Z}}_{34} \\ \overline{\overline{Z}}_{43} & \overline{\overline{Z}}_{44} \end{pmatrix}^{-1} \begin{pmatrix} \overline{\overline{Z}}_{31} & \overline{\overline{Z}}_{32} \\ \overline{\overline{Z}}_{41} & \overline{\overline{Z}}_{42} \end{pmatrix} \begin{pmatrix} \overline{J}_2 \\ \overline{M}_2 \end{pmatrix}. \tag{6.13}$$

Back-substituting equation 6.13 into 6.9 produces a matrix equation of the form:

$$\begin{pmatrix} \overline{E}_m \\ \overline{H}_{m'} \end{pmatrix} = \begin{pmatrix} \overline{\overline{Z}}'_{11} & \overline{\overline{Z}}'_{12} \\ \overline{\overline{Z}}'_{21} & \overline{\overline{Z}}'_{22} \end{pmatrix} \begin{pmatrix} \overline{J}_2 \\ \overline{M}_2 \end{pmatrix} \tag{6.14}$$

Again, assume N basis functions are obtained over each boundary surface using the method of moments. Equation 6.8 requires the inversion of a 5N by 5N Z-matrix

to compute the unknown surface current coefficients. Back-substitution requires the inversion of an N by N matrix, some matrix multiplications and additions, the inversion of a 2N by 2N Z-matrix, equation 6.13, followed by some matrix multiplications and additions, and, finally, the inversion of another 2N by 2N Z-matrix, equation 6.14. All the target structure beneath the second layer of coating has been replaced by an equivalent interaction matrix as shown in equation 6.14. This additional layer of coating only requires the inversion of an additional 2N by 2N Z-matrix over the one layer case.

For three layers of coating on a perfect conductor (refer to Figure 6.2), the matrix equation is of the form:

$$\begin{pmatrix} \overline{E}_m \\ \overline{H}_{m'} \\ \overline{0}_{m''} \\ \overline{0}_{m'''} \\ \overline{0}_{m^{(i*)}} \\ \overline{0}_{m^{(*)}} \\ \overline{0}_{m^{(*i)}} \end{pmatrix} = \begin{pmatrix} \overline{\overline{Z}}_{11} & \overline{\overline{Z}}_{12} & \overline{\overline{Z}}_{13} & \overline{\overline{Z}}_{14} & 0 & 0 & 0 \\ \overline{\overline{Z}}_{21} & \overline{\overline{Z}}_{22} & \overline{\overline{Z}}_{23} & \overline{\overline{Z}}_{24} & 0 & 0 & 0 \\ \overline{\overline{Z}}_{31} & \overline{\overline{Z}}_{32} & \overline{\overline{Z}}_{33} & \overline{\overline{Z}}_{34} & \overline{\overline{Z}}_{35} & \overline{\overline{Z}}_{36} & 0 \\ \overline{\overline{Z}}_{41} & \overline{\overline{Z}}_{42} & \overline{\overline{Z}}_{43} & \overline{\overline{Z}}_{44} & \overline{\overline{Z}}_{45} & \overline{\overline{Z}}_{46} & 0 \\ 0 & 0 & \overline{\overline{Z}}_{53} & \overline{\overline{Z}}_{54} & \overline{\overline{Z}}_{55} & \overline{\overline{Z}}_{56} & \overline{\overline{Z}}_{57} \\ 0 & 0 & \overline{\overline{Z}}_{63} & \overline{\overline{Z}}_{64} & \overline{\overline{Z}}_{65} & \overline{\overline{Z}}_{66} & \overline{\overline{Z}}_{67} \\ 0 & 0 & 0 & 0 & \overline{\overline{Z}}_{75} & \overline{\overline{Z}}_{76} & \overline{\overline{Z}}_{77} \end{pmatrix} \begin{pmatrix} \overline{J}_3 \\ \overline{M}_3 \\ \overline{J}_2 \\ \overline{M}_2 \\ \overline{J}_1 \\ \overline{M}_1 \\ \overline{J}_0 \end{pmatrix} \tag{6.15}$$

By the same logic used for the 2 layer case, back-substitution reduces the size of the Z-matrix for three layers of coating enclosing a perfect conductor:

$$\begin{pmatrix} \overline{E}_m \\ \overline{H}_{m'} \end{pmatrix} = \begin{pmatrix} \overline{\overline{Z}}''_{11} & \overline{\overline{Z}}''_{12} \\ \overline{\overline{Z}}''_{21} & \overline{\overline{Z}}''_{22} \end{pmatrix} \begin{pmatrix} \overline{J}_3 \\ \overline{M}_3 \end{pmatrix} \tag{6.16}$$

since

$$\begin{pmatrix} \overline{J}_2 \\ \overline{M}_2 \end{pmatrix} = -\begin{pmatrix} \overline{\overline{Z}}'_{33} & \overline{\overline{Z}}'_{34} \\ \overline{\overline{Z}}'_{43} & \overline{\overline{Z}}'_{44} \end{pmatrix}^{-1} \begin{pmatrix} \overline{\overline{Z}}'_{31} & \overline{\overline{Z}}'_{32} \\ \overline{\overline{Z}}'_{41} & \overline{\overline{Z}}'_{42} \end{pmatrix} \begin{pmatrix} \overline{J}_3 \\ \overline{M}_3 \end{pmatrix}. \tag{6.17}$$

Again, assume N basis functions are obtained over each boundary surface using the method of moments. Equation 6.15 requires the inversion of a 7N by 7N Z-matrix to compute the unknown surface current coefficients. Back-substitution requires the inversion of one N by N and three 2N by 2N matrices, along with some intermediate matrix multiplications and additions. All the target structure beneath the third layer of coating has been replaced by an equivalent interaction matrix as shown in equation

6.16. This additional layer of coating only requires the inversion of an additional 2N by 2N Z-matrix over the two layer case.

A recursive relationship emerges for multi-layered coatings enclosing a perfect conductor. Instead of the problem involving the inversion of ever larger Z-matrices for each added layer of coating, it becomes one of the intermediate inversion of a 2N by 2N matrix for each added layer of coating. Thus, after each intermediate 2N by 2N inversion and back-substitution, the effects of the inner layer are included, and the inner layer's unknown surface current coefficients are discarded. So, for the three layer example, instead of inverting a 7N by 7N Z-matrix (inversion time increases as N^3), the problem involves the inversion of one N by N and three 2N by 2N matrices. The problem only increases linearly in computation time for each added layer: another 2N by 2N matrix inversion for each added layer of coating.

For n layers of coating on a perfect conductor (refer to Figure 6.3), the matrix equation is of the form:

$$\begin{pmatrix} \overline{E}_m \\ \overline{H}_{m'} \\ \overline{0}_{m''} \\ \overline{0}_{m'''} \\ \vdots \\ \overline{0}_{m^{(2n)}} \end{pmatrix} = \begin{pmatrix} \overline{\overline{Z}}_{11} & \overline{\overline{Z}}_{12} & \overline{\overline{Z}}_{13} & \overline{\overline{Z}}_{14} & \cdots & 0 \\ \overline{\overline{Z}}_{21} & \overline{\overline{Z}}_{22} & \overline{\overline{Z}}_{23} & \overline{\overline{Z}}_{24} & \cdots & 0 \\ \overline{\overline{Z}}_{31} & \overline{\overline{Z}}_{32} & \overline{\overline{Z}}_{33} & \overline{\overline{Z}}_{34} & \cdots & 0 \\ \overline{\overline{Z}}_{41} & \overline{\overline{Z}}_{42} & \overline{\overline{Z}}_{43} & \overline{\overline{Z}}_{44} & \cdots & 0 \\ \vdots & \vdots & \vdots & \vdots & \ddots & \vdots \\ 0 & 0 & 0 & 0 & \cdots & \overline{\overline{Z}}_{(2n+1)(2n+1)} \end{pmatrix} \begin{pmatrix} \overline{J}_n \\ \overline{M}_n \\ \overline{J}_{n-1} \\ \overline{M}_{n-1} \\ \vdots \\ \overline{J}_0 \end{pmatrix} \tag{6.18}$$

The extension to n layers of coating enclosing the perfect conductor is straightforward, given the approach outlined above. Starting with the innermost layer, the Z-matrix elements would be computed as for the single layer case presented in Appendix A. However, instead of the surrounding medium being free-space, it now has the permittivity and permeability of the next layer of coating. Matrix inversion and back-substitution proceeds progressively for each layer of coating added, with the permittivity and permeability of the surrounding medium always being that of the next layer to be added. This process is repeated until the outermost layer of coating is reached. The equivalent electric and magnetic surface current coefficients of the outermost layer are then computed, and the scattered field is calculated as discussed previously.

6.3 Partially Coated Perfect Conductor

The generalization to a multi-layered coating for a partially coated perfect conductor follows the same line of reasoning as presented in section 6.2 for the completely coated perfect conductor. Using Huygens' principle, the equivalence principle, and satisfying the boundary conditions for a partially coated perfect conductor generates a set of integro-differential equations (see Appendix A). Applying the method of moments to this set of integro-differential equations produces a matrix equation. As derived in Appendix A for one layer of coating partially enclosing a perfect conductor (refer to Figure 3.3), the matrix equation is of the form:

$$\begin{pmatrix} \overline{E}_m \\ \overline{H}_{m'} \\ \overline{E}_{m''} \\ \overline{0}_{m'''} \end{pmatrix} = \begin{pmatrix} \overline{\overline{Z}}_{11} & \overline{\overline{Z}}_{12} & \overline{\overline{Z}}_{13} & \overline{\overline{Z}}_{14} \\ \overline{\overline{Z}}_{21} & \overline{\overline{Z}}_{22} & \overline{\overline{Z}}_{23} & \overline{\overline{Z}}_{24} \\ \overline{\overline{Z}}_{31} & \overline{\overline{Z}}_{32} & \overline{\overline{Z}}_{33} & 0 \\ \overline{\overline{Z}}_{41} & \overline{\overline{Z}}_{42} & 0 & \overline{\overline{Z}}_{44} \end{pmatrix} \begin{pmatrix} \overline{J}_1 \\ \overline{M}_1 \\ \overline{J}_2 \\ \overline{J}_3 \end{pmatrix} \tag{6.19}$$

The left half of the equation represents the excitation vector, and the right half of the equation represents the interaction matrix, Z-matrix, times the unknown electric and magnetic surface current coefficients. This matrix equation corresponds to four simultaneous equations in four unknowns. Now, the fourth equation in 6.19 can be used to back-substitute and reduce the size of the Z-matrix:

$$\overline{J}_3 = -\overline{\overline{Z}}_{44}^{-1}\left[\overline{\overline{Z}}_{41} \cdot \overline{J}_1 + \overline{\overline{Z}}_{42} \cdot \overline{M}_1\right]. \tag{6.20}$$

Back-substituting leaves three simultaneous equations which can be written as the following matrix equation:

$$\begin{pmatrix} \overline{E}_m \\ \overline{H}_{m'} \\ \overline{E}_{m''} \end{pmatrix} = \begin{pmatrix} \overline{\overline{Z}}'_{11} & \overline{\overline{Z}}'_{12} & \overline{\overline{Z}}'_{13} \\ \overline{\overline{Z}}'_{21} & \overline{\overline{Z}}'_{22} & \overline{\overline{Z}}'_{23} \\ \overline{\overline{Z}}'_{31} & \overline{\overline{Z}}'_{32} & \overline{\overline{Z}}'_{33} \end{pmatrix} \begin{pmatrix} \overline{J}_1 \\ \overline{M}_1 \\ \overline{J}_2 \end{pmatrix} \tag{6.21}$$

where

$$\overline{\overline{Z}}'_{11} = \overline{\overline{Z}}_{11} - \overline{\overline{Z}}_{14} \cdot \overline{\overline{Z}}_{44}^{-1} \cdot \overline{\overline{Z}}_{41} \tag{6.22}$$

$$\overline{\overline{Z}}'_{12} = \overline{\overline{Z}}_{12} - \overline{\overline{Z}}_{14} \cdot \overline{\overline{Z}}_{44}^{-1} \cdot \overline{\overline{Z}}_{42} \tag{6.23}$$

$$\overline{\overline{Z}}'_{13} = \overline{\overline{Z}}_{13} \tag{6.24}$$

$$\overline{\overline{Z}}'_{21} = \overline{\overline{Z}}_{21} - \overline{\overline{Z}}_{24} \cdot \overline{\overline{Z}}_{44}^{-1} \cdot \overline{\overline{Z}}_{41} \tag{6.25}$$

$$\overline{\overline{Z}}'_{22} = \overline{\overline{Z}}_{22} - \overline{\overline{Z}}_{24} \cdot \overline{\overline{Z}}_{44}^{-1} \cdot \overline{\overline{Z}}_{42}. \tag{6.26}$$

$$\overline{\overline{Z}}'_{23} = \overline{\overline{Z}}_{23} \tag{6.27}$$

$$\overline{\overline{Z}}'_{31} = \overline{\overline{Z}}_{31} \tag{6.28}$$

$$\overline{\overline{Z}}'_{32} = \overline{\overline{Z}}_{32} \tag{6.29}$$

$$\overline{\overline{Z}}'_{33} = \overline{\overline{Z}}_{33} \tag{6.30}$$

Assume N basis functions are obtained over each boundary surface using the method of moments. Equation 6.19 requires the inversion of a 4N by 4N Z-matrix to compute the unknown surface current coefficients for a partially coated perfect conductor. Back-substitution requires the inversion of an N by N matrix, $\overline{\overline{Z}}_{44}^{-1}$, some matrix multiplications and additions, equations 6.22 through 6.30, and the inversion of a 3N by 3N Z-matrix, equation 6.21. However, all the target structure beneath the coating has been replaced by an equivalent interaction matrix as shown in equation 6.21. This has significance for the extension of the procedure discussed in Chapter 3 and section 6.2 to multi-layered coatings over a partially coated perfect conductor.

For two layers of coating on a partially coated perfect conductor (refer to Figure 6.4), the matrix equation is of the form:

$$\begin{pmatrix} \overline{E}_m \\ \overline{H}_{m'} \\ \overline{0}_{m''} \\ \overline{0}_{m'''} \\ \overline{E}_{m^{(iv)}} \\ \overline{0}_{m^{(v)}} \end{pmatrix} = \begin{pmatrix} \overline{\overline{Z}}_{11} & \overline{\overline{Z}}_{12} & \overline{\overline{Z}}_{13} & \overline{\overline{Z}}_{14} & \overline{\overline{Z}}_{15} & 0 \\ \overline{\overline{Z}}_{21} & \overline{\overline{Z}}_{22} & \overline{\overline{Z}}_{23} & \overline{\overline{Z}}_{24} & \overline{\overline{Z}}_{25} & 0 \\ \overline{\overline{Z}}_{31} & \overline{\overline{Z}}_{32} & \overline{\overline{Z}}_{33} & \overline{\overline{Z}}_{34} & 0 & \overline{\overline{Z}}_{36} \\ \overline{\overline{Z}}_{41} & \overline{\overline{Z}}_{42} & \overline{\overline{Z}}_{43} & \overline{\overline{Z}}_{44} & 0 & \overline{\overline{Z}}_{46} \\ \overline{\overline{Z}}_{51} & \overline{\overline{Z}}_{52} & 0 & 0 & \overline{\overline{Z}}_{55} & 0 \\ 0 & 0 & \overline{\overline{Z}}_{63} & \overline{\overline{Z}}_{64} & 0 & \overline{\overline{Z}}_{66} \end{pmatrix} \begin{pmatrix} \overline{J}_2 \\ \overline{M}_2 \\ \overline{J}_1 \\ \overline{M}_1 \\ \overline{J}_3 \\ \overline{J}_4 \end{pmatrix} \tag{6.31}$$

This matrix equation represents six simultaneous equations in six unknowns. Back-substituting the sixth equation in 6.31 in the manner used for 6.19 yields a matrix equation of the form:

$$\begin{pmatrix} \overline{\overline{E}}_m \\ \overline{\overline{H}}_{m'} \\ \overline{\overline{0}}_{m''} \\ \overline{\overline{0}}_{m'''} \\ \overline{\overline{E}}_{m^{(i+)}} \end{pmatrix} = \begin{pmatrix} \overline{\overline{Z}}_{11} & \overline{\overline{Z}}_{12} & \overline{\overline{Z}}_{13} & \overline{\overline{Z}}_{14} & \overline{\overline{Z}}_{15} \\ \overline{\overline{Z}}_{21} & \overline{\overline{Z}}_{22} & \overline{\overline{Z}}_{23} & \overline{\overline{Z}}_{24} & \overline{\overline{Z}}_{25} \\ \overline{\overline{Z}}_{31} & \overline{\overline{Z}}_{32} & \overline{\overline{Z}}_{33} & \overline{\overline{Z}}_{34} & 0 \\ \overline{\overline{Z}}_{41} & \overline{\overline{Z}}_{42} & \overline{\overline{Z}}_{43} & \overline{\overline{Z}}_{44} & 0 \\ \overline{\overline{Z}}_{51} & \overline{\overline{Z}}_{52} & 0 & 0 & \overline{\overline{Z}}_{55} \end{pmatrix} \begin{pmatrix} \overline{J}_2 \\ \overline{M}_2 \\ \overline{J}_1 \\ \overline{M}_1 \\ \overline{J}_3 \end{pmatrix} \tag{6.32}$$

which represents five simultaneous equations in five unknowns. Obviously, the elements of the Z-matrix in equation 6.32 are not the same as the elements of the Z-matrix in equation 6.31 due to the back-substitution. Further, the explicit equation representing the interaction of the coated perfect conductor surface with the first layer of coating has now been absorbed into the equivalent Z-matrix shown in 6.32. Now, the third and fourth equations in 6.32 can be written as

$$\overline{\overline{Z}}_{33} \cdot \overline{J}_1 + \overline{\overline{Z}}_{34} \cdot \overline{M}_1 = -\left[\overline{\overline{Z}}_{31} \cdot \overline{J}_2 + \overline{\overline{Z}}_{32} \cdot \overline{M}_2\right] \tag{6.33}$$

and

$$\overline{\overline{Z}}_{43} \cdot \overline{J}_1 + \overline{\overline{Z}}_{44} \cdot \overline{M}_1 = -\left[\overline{\overline{Z}}_{41} \cdot \overline{J}_2 + \overline{\overline{Z}}_{42} \cdot \overline{M}_2\right], \tag{6.34}$$

which becomes

$$\begin{pmatrix} \overline{\overline{Z}}_{33} & \overline{\overline{Z}}_{34} \\ \overline{\overline{Z}}_{43} & \overline{\overline{Z}}_{44} \end{pmatrix} \begin{pmatrix} \overline{J}_1 \\ \overline{M}_1 \end{pmatrix} = \begin{pmatrix} -\overline{\overline{Z}}_{31} & -\overline{\overline{Z}}_{32} \\ -\overline{\overline{Z}}_{41} & -\overline{\overline{Z}}_{42} \end{pmatrix} \begin{pmatrix} \overline{J}_2 \\ \overline{M}_2 \end{pmatrix}. \tag{6.35}$$

Therefore,

$$\begin{pmatrix} \overline{J}_1 \\ \overline{M}_1 \end{pmatrix} = -\begin{pmatrix} \overline{\overline{Z}}_{33} & \overline{\overline{Z}}_{34} \\ \overline{\overline{Z}}_{43} & \overline{\overline{Z}}_{44} \end{pmatrix}^{-1} \begin{pmatrix} \overline{\overline{Z}}_{31} & \overline{\overline{Z}}_{32} \\ \overline{\overline{Z}}_{41} & \overline{\overline{Z}}_{42} \end{pmatrix} \begin{pmatrix} \overline{J}_2 \\ \overline{M}_2 \end{pmatrix}. \tag{6.36}$$

Back-substituting equation 6.36 into 6.32 produces a matrix equation of the form:

$$\begin{pmatrix} \overline{\overline{E}}_m \\ \overline{\overline{H}}_{m'} \\ \overline{\overline{E}}_{m''} \end{pmatrix} = \begin{pmatrix} \overline{\overline{Z}}'_{11} & \overline{\overline{Z}}'_{12} & \overline{\overline{Z}}'_{13} \\ \overline{\overline{Z}}'_{21} & \overline{\overline{Z}}'_{22} & \overline{\overline{Z}}'_{23} \\ \overline{\overline{Z}}'_{31} & \overline{\overline{Z}}'_{32} & \overline{\overline{Z}}'_{33} \end{pmatrix} \begin{pmatrix} \overline{J}_2 \\ \overline{M}_2 \\ \overline{J}_3 \end{pmatrix} \tag{6.37}$$

Again, assume N basis functions are obtained over each boundary surface using the method of moments. Equation 6.31 requires the inversion of a 6N by 6N Z-matrix to compute the unknown surface current coefficients. Back-substitution requires the

inversion of an N by N matrix, some matrix multiplications and additions, the inversion of a 2N by 2N Z-matrix, equation 6.36, followed by some matrix multiplications and additions, and, finally, the inversion of another 3N by 3N Z-matrix, equation 6.37. All the target structure beneath the second layer of coating has been replaced by an equivalent interaction matrix as shown in equation 6.37. This additional layer of coating only requires the inversion of an additional 2N by 2N Z-matrix over the one layer case.

For three layers of coating on a perfect conductor (refer to Figure 6.5), the matrix equation is of the form:

$$\begin{pmatrix} \overline{E}_m \\ \overline{H}_{m'} \\ \overline{0}_{m''} \\ \overline{0}_{m'''} \\ \overline{0}_{m^{(iv)}} \\ \overline{0}_{m^{(v)}} \\ \overline{E}_{m^{(vi)}} \\ \overline{0}_{m^{(vii)}} \end{pmatrix} = \begin{pmatrix} \overline{\overline{Z}}_{11} & \overline{\overline{Z}}_{12} & \overline{\overline{Z}}_{13} & \overline{\overline{Z}}_{14} & 0 & 0 & \overline{\overline{Z}}_{17} & 0 \\ \overline{\overline{Z}}_{21} & \overline{\overline{Z}}_{22} & \overline{\overline{Z}}_{23} & \overline{\overline{Z}}_{24} & 0 & 0 & \overline{\overline{Z}}_{27} & 0 \\ \overline{\overline{Z}}_{31} & \overline{\overline{Z}}_{32} & \overline{\overline{Z}}_{33} & \overline{\overline{Z}}_{34} & \overline{\overline{Z}}_{35} & \overline{\overline{Z}}_{36} & 0 & 0 \\ \overline{\overline{Z}}_{41} & \overline{\overline{Z}}_{42} & \overline{\overline{Z}}_{43} & \overline{\overline{Z}}_{44} & \overline{\overline{Z}}_{45} & \overline{\overline{Z}}_{46} & 0 & 0 \\ 0 & 0 & \overline{\overline{Z}}_{53} & \overline{\overline{Z}}_{54} & \overline{\overline{Z}}_{55} & \overline{\overline{Z}}_{56} & 0 & \overline{\overline{Z}}_{58} \\ 0 & 0 & \overline{\overline{Z}}_{63} & \overline{\overline{Z}}_{64} & \overline{\overline{Z}}_{65} & \overline{\overline{Z}}_{66} & 0 & \overline{\overline{Z}}_{68} \\ \overline{\overline{Z}}_{71} & \overline{\overline{Z}}_{72} & 0 & 0 & 0 & 0 & \overline{\overline{Z}}_{77} & 0 \\ 0 & 0 & 0 & 0 & \overline{\overline{Z}}_{85} & \overline{\overline{Z}}_{86} & 0 & \overline{\overline{Z}}_{88} \end{pmatrix} \begin{pmatrix} \overline{J}_3 \\ \overline{M}_3 \\ \overline{J}_2 \\ \overline{M}_2 \\ \overline{J}_1 \\ \overline{M}_1 \\ \overline{J}_4 \\ \overline{J}_5 \end{pmatrix} \tag{6.38}$$

By the same logic used for the 2 layer case, back-substitution reduces the size of the Z-matrix for three layers of coating partially enclosing a perfect conductor:

$$\begin{pmatrix} \overline{E}_m \\ \overline{H}_{m'} \\ \overline{E}_{m''} \end{pmatrix} = \begin{pmatrix} \overline{\overline{Z}}''_{11} & \overline{\overline{Z}}''_{12} & \overline{\overline{Z}}''_{13} \\ \overline{\overline{Z}}''_{21} & \overline{\overline{Z}}''_{22} & \overline{\overline{Z}}''_{23} \\ \overline{\overline{Z}}''_{31} & \overline{\overline{Z}}''_{32} & \overline{\overline{Z}}''_{33} \end{pmatrix} \begin{pmatrix} \overline{J}_3 \\ \overline{M}_3 \\ \overline{J}_4 \end{pmatrix} \tag{6.39}$$

since

$$\begin{pmatrix} \overline{J}_2 \\ \overline{M}_2 \end{pmatrix} = - \begin{pmatrix} \overline{\overline{Z}}'_{33} & \overline{\overline{Z}}'_{34} \\ \overline{\overline{Z}}'_{43} & \overline{\overline{Z}}'_{44} \end{pmatrix}^{-1} \begin{pmatrix} \overline{\overline{Z}}'_{31} & \overline{\overline{Z}}'_{32} \\ \overline{\overline{Z}}'_{41} & \overline{\overline{Z}}'_{42} \end{pmatrix} \begin{pmatrix} \overline{J}_3 \\ \overline{M}_3 \end{pmatrix}. \tag{6.40}$$

Again, assume N basis functions are obtained over each boundary surface using the method of moments. Equation 6.38 requires the inversion of an 8N by 8N Z-matrix to compute the unknown surface current coefficients. Back-substitution requires the inversion of one N by N matrix, two 2N by 2N matrices, and one 3N by 3N matrix along with some intermediate matrix multiplications and additions. All the target structure

beneath the third layer of coating has been replaced by an equivalent interaction matrix as shown in equation 6.39. This additional layer of coating only requires the inversion of an additional 2N by 2N Z-matrix over the two layer case.

A recursive relationship emerges for multi-layered coatings partially enclosing a perfect conductor. Instead of the problem involving the inversion of ever larger Z-matrices for each added layer of coating, it becomes one of the intermediate inversion of a 2N by 2N matrix for each added layer of coating. Thus, after each intermediate 2N by 2N inversion and back-substitution, the effects of the inner layer are included, and the inner layer's unknown surface current coefficients are discarded. So, for the three layer example, instead of inverting an 8N by 8N Z-matrix (inversion time increases as N^3), the problem involves the inversion of one N by N matrix, two 2N by 2N matrices, and one 3N by 3N matrix. The problem only increases linearly in computation time for each added layer: another 2N by 2N matrix inversion for each added layer of coating. The extension to n layers of coating partially enclosing the perfect conductor is straightforward, given the approach outlined above. Starting with the innermost layer, the Z-matrix elements would be computed as for the single layer case presented in Appendix A. However, instead of the surrounding medium being free-space, it now has the permittivity and permeability of the next layer of coating. Matrix inversion and back-substitution proceeds progressively for each layer of coating added, with the permittivity and permeability of the surrounding medium always being that of the next layer to be added. This process is repeated until the outermost layer of coating is reached. The equivalent electric and magnetic surface current coefficients of the outermost layer and the exposed perfect conductor are then computed, and the scattered field is calculated as discussed previously.

With the information in this chapter, Chapter 3, and Appendix A, the approach to use for various combinations of coatings and layers of coatings at different locations on the perfect conductor should be obvious. Equivalent interaction matrices which incorporate the cumulative effects of the innermost layers of coatings and perfect conductors would be computed as described above. Then the outermost equivalent electric and magnetic surface current coefficients would be calculated by multiplying the ex-

citation vector by the equivalent interaction matrix. Finally, the far-field radiation pattern would be computed from the equivalent electric and magnetic surface currents for the outermost surfaces. Thus, using Huygens' principle, the equivalence principle, the appropriate boundary conditions, and the method of moments, the radar cross section for coated perfect conductors with arbitrary geometries can be predicted.

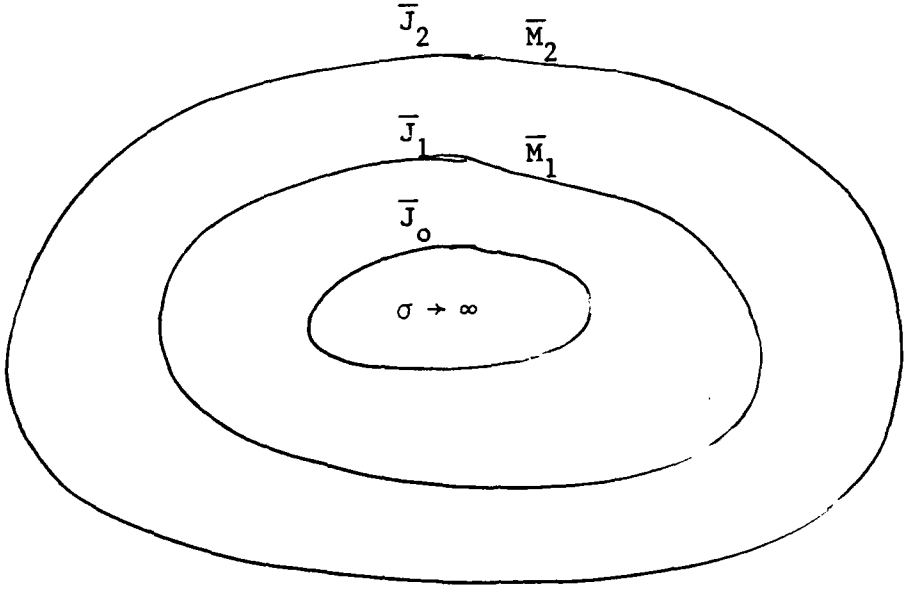

Figure 6.1. Two Layers of Coating Completely Enclosing a Perfect Conductor

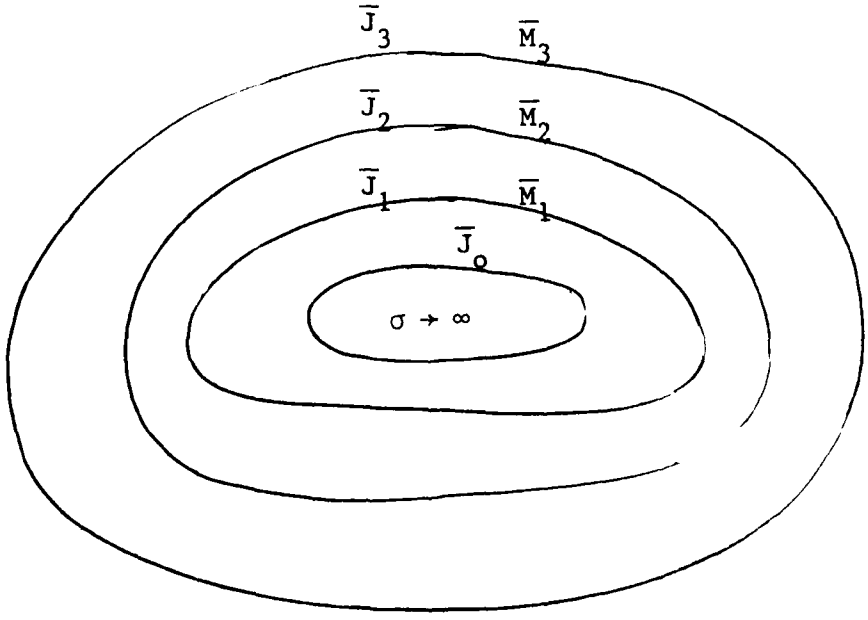

Figure 6.2. Three Layers of Coating Completely Enclosing a Perfect Conductor

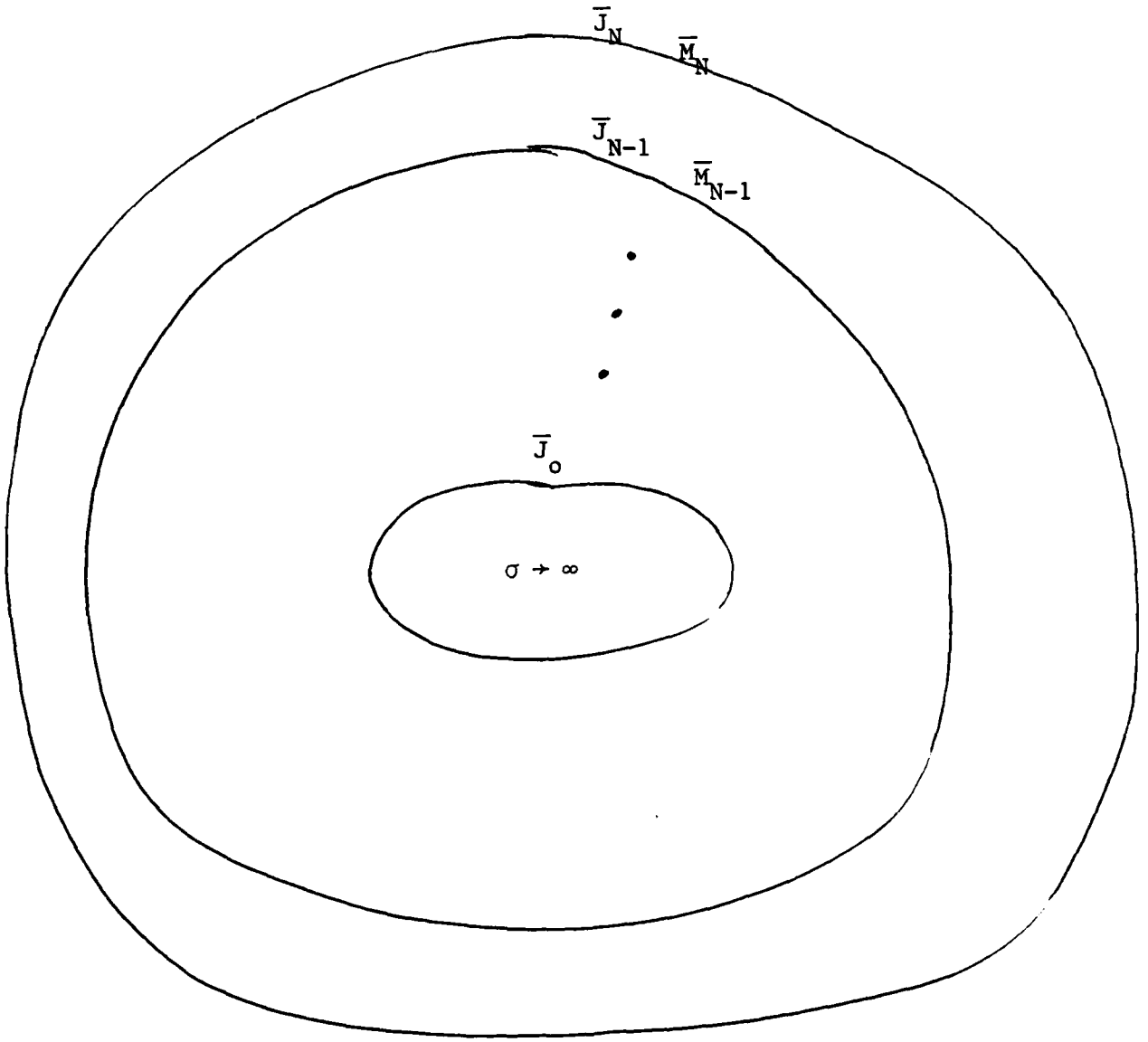

Figure 6.3. N Layers of Coating Completely Enclosing a Perfect Conductor

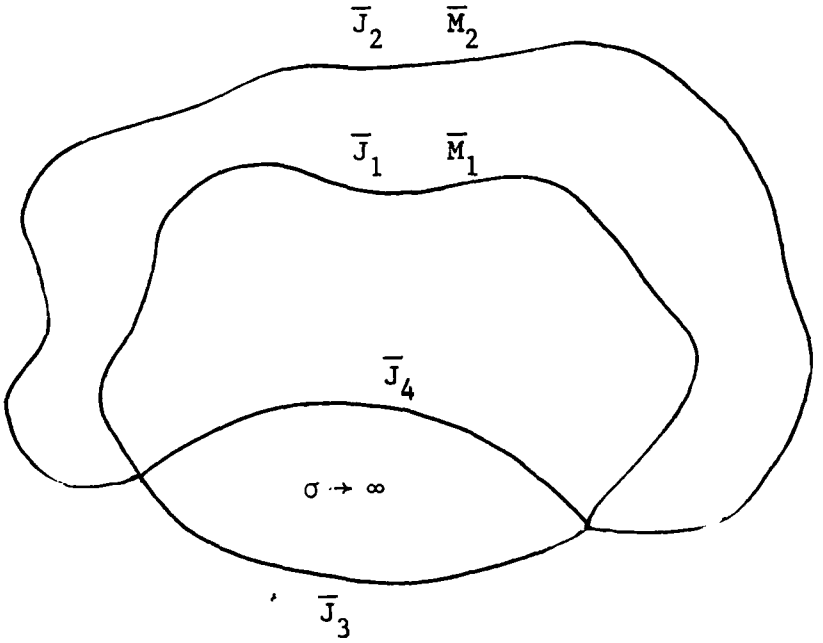

Figure 6.4. Two Layers of Coating Partially Enclosing a Perfect Conductor

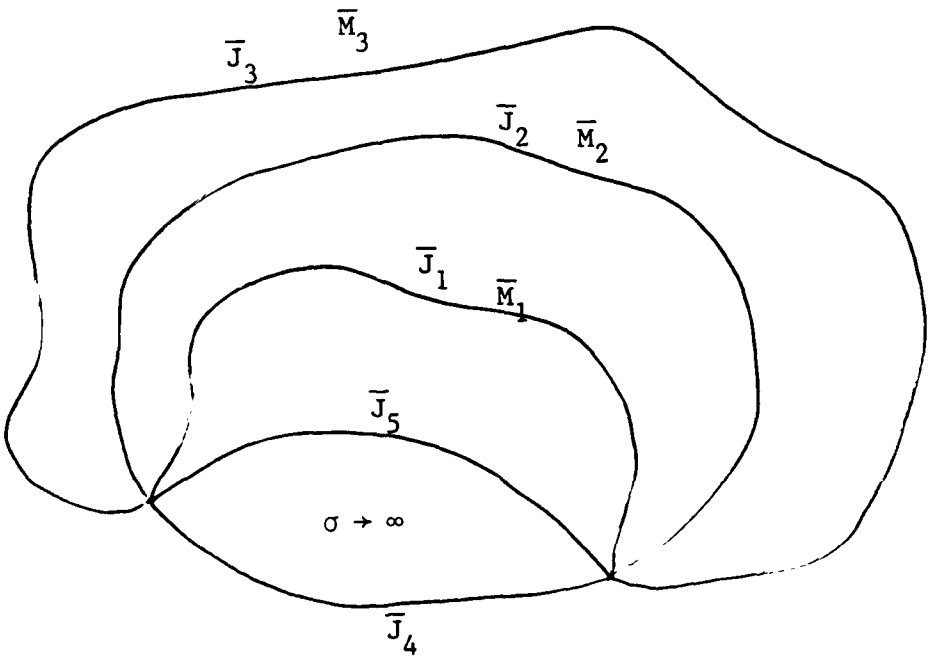

Figure 6.5. Three Layers of Coating Partially Enclosing a Perfect Conductor

Chapter 7

CONCLUSIONS AND SUGGESTED FUTURE EFFORTS

7.1 Conclusions

1. In this thesis, Huygens' principle, the equivalence principle, the appropriate boundary conditions, and the method of moments were used to predict the radar cross section (RCS) for coated perfect conductors with arbitrary geometries. Experimental RCS measurements were performed on square aluminum plates coated on one side with radar absorbing material (Chapter 4). Theoretical RCS predictions were generated using the electric field integral equation (EFIE) series of computer programs (Chapter 3). The EFIE series of computer programs gave a very good match between the experimental RCS measurements and the theoretical RCS predictions for a partially coated plate (Chapter 5), considering the approximations made in the theoretical model. Further, once the equivalent electric and magnetic surface currents have been computed for the coated target, near-field and far-field phenomena can be computed and studied.

2. The matrix equations for multi-layered coatings on a perfect conductor were derived (Chapter 6), and the procedure was discussed to extend the derivations presented in this thesis to multi-layered coatings or various coatings over the same perfectly conducting surface.

3. Some of the approximations and limitations of this approach and method of solution to compute the radar cross section prediction for coated perfect conductors with arbitrary geometries are the following:

   a. An approximation is made of the integration of the weighting function over the

bi-triangular subdomain as its value at the centroid of the triangular patch as is shown in equation (A.69) of Appendix A. This approximation reduces two numerical integrations over every bi-triangular subdomain to just one. This approximation is made when the distance from the observation triangle to the source triangle is more than the length of any edge of the observation triangle. If this criterion is not satisfied, a seven-point numerical quadrature integration is performed over the bi-triangular subdomain.

b. Geometry modelling issues:

1. The sides of the coating which meet the perfect conductor were ignored in the model of the coating surface. Since the coatings were thin, this approximation gave satisfactory results. However, it might not be possible to ignore the sides of the coating if thicker coatings are used.

2. The effects of various triangular patch shapes must be considered when modelling the geometry of the coated perfect conductor [124].

3. The sides of the coating structure were ignored since the triangular patches became too elongated.

4. For the partially coated perfect conductor, there is a discontinuity of electric surface current at the junction between the exposed and the coated perfect conductor surfaces since both are modelled as separate and distinct surfaces.

5. There is a compromise between the size of the target used, the frequency of the RCS calculations, the core memory and magnetic disk storage requirements for the Z-matrix, and the computation time required to calculate the RCS data. These factors must be considered when determining how many triangular patches to use to model the geometry of a coated perfect conductor.

7.2 Suggested Future Efforts

1. Investigate various modellings for the coatings and the perfect conductors. One example would be to incorporate the sides of the coatings which meet the perfect

conductor into the geometry model while keeping the edges of the triangular patches approximately equal. Another example would be to model the square plate as a box. This would then include the effects of the finite thickness of the plate and satisfy the condition of continuity of electric surface current at the boundary between the exposed and coated portion of the perfect conductor.

2. Incorporate continuity of electric surface current at the boundary between the exposed and coated portion of the perfect conductor while still modelling the geometry of each as separate and distinct surfaces.

3. Investigate the results for other numerical quadrature integrations over the bi-triangular subdomains (see Chapter 3).

4. Write the computer programs and generate theoretical RCS predictions for multi-layered coatings over a perfect conductor. Compare to experimental RCS measurements for multi-layered coatings over a metal plate.

5. Incorporate into the EFIE computer programs the ability to add wire antennas to the coated perfect conductor. Compute theoretical RCS predictions with wire antennas added, and compute radiation patterns for the wire antennas near an uncoated and a coated perfect conductor. Compare the results.

6. Incorporate into the EFIE computer programs the ability to compute the RCS for coatings with rough surfaces.

7. Incorporate into the EFIE computer programs the ability to compute the RCS for anisotropic coatings.

REFERENCES

Radar Cross Section

1. Dedrick, K. G., A. R. Hessing, and G. L. Johnson (1978), Bistatic radar scattering by randomly oriented wires, IEEE Trans. Ant. Prop., AP-26, 420-426.

2. Fante, R. L. (1984), Short-wavelength target modeling, IEEE Trans. Ant. Prop., AP-32, 105-111.

3. Glaser, J. I. (1985), Bistatic RCS of complex objects near forward scatter, IEEE Trans. Aero. Electron., AES-21, 70-78.

4. Glisson, A. W. (1984), An integral equation for electromagnetic scattering from homogeneous dielectric bodies, IEEE Trans. Ant. Prop., AP-32, 173-175.

5. Graglia, R. D. and P. L. E. Uslenghi (1984), Electromagnetic scattering from anisotropic materials, Part I: General theory, IEEE Trans. Ant. Prop., AP-32, 867-869.

6. Herman, G. C. and P. M. van den Berg (1982), A least-square iterative technique for solving time-domain scattering problems, J. Acoust. Soc. Am., 72, 1947-1953.

7. Hodge, D. B. (1980), Scattering by circular metallic disks, IEEE Trans. Ant. Prop., AP-28, 707-712.

8. Hwang, Y. M., L. Peters, Jr., and W. D. Burnside (1978), Surface current and charge density induced on aircraft, IEEE Trans. Electromagn. Compat., EMC-20, 77-81.

9. Kao, C. C. (1970), Electromagnetic scattering from a finite tubular cylinder: Numerical solutions, Radio Science, 5, 617-624.

10. Kastner, R. and R. Mittra (1983), A spectral-iteration technique for analyzing scattering from arbitrary bodies, Part I: Cylinder scatterers with E-wave incidence, IEEE Trans. Ant. Prop., AP-31, 499-506.

11. Knott, E. F. (1976), Radar cross section reduction using cylindrical segments, IEEE Trans. Ant. Prop., AP-24, 882-884.

12. Knott, E. F. (1977), RCS reduction of dihedral corners, IEEE Trans. Ant. Prop., AP-25, 406-409.

13. Mautz, J. R. and R. F. Harrington (1969), Radiation and scattering from bodies of revolution, Appl. Sci. Res., 20, 405-435.

14. Mautz, J. R. and R. F. Harrington (1974), Generalized network parameters, radiation and scattering by conducting bodies of revolution, IEEE Trans. Ant. Prop.,

AP-22, 630-631.

15. Miller, E. K. and J. B. Morton (1970), The RCS of a metal plate with a resonant slot, IEEE Trans. Ant. Prop., AP-18, 290-292.

16. Peterson, A. F. and R. Mittra (1985), Method of conjugate gradients for the numerical solution of large-body electromagnetic scattering problems, J. Opt. Soc. Am., 2, 971-977.

17. Mason, J. L. and W. J. Anderson (1985), Finite element solution for electromagnetic scattering from two-dimensional bodies, Int. J. Num. Methods Eng., 21, 909-928.

18. Rahmat-Samii, Y. and R. Mittra (1974), Integral equation solution and RCS computation of a thin rectangular plate, IEEE Trans. Ant. Prop., AP-22, 608-610.

19. Ross, R. A. (1966), Radar cross section of rectangular flat plates as a function of aspect angle, IEEE Trans. Ant. Prop., AP-14, 329-335.

20. Ross, R. A. (1967), Scattering by a finite cylinder, Proc. IEE, 114, 864-868.

21 Ruck, G. T., D. E. Barrick, W. D. Stuart, and C. K. Krichbaum (1970), Radar Cr[illegible] Section Handbook, Vol. 1 and 2, Plenum Press, New York.

22. Saad, Y. and M. H. Schultz (1985), Conjugate gradient-like algorithms for solving nonsymmetric linear systems, Math. Comp., 44, 417-424.

23. Sarkar, T. K. and S. M. Rao (1982), An iterative method for solving electrostatic problems, IEEE Trans. Ant. Prop., AP-30, 611-616.

24. Sarkar, T. K. and S. M. Rao (1984), The application of the conjugate gradient method for the solution of electromagnetic scattering from arbitrarily oriented wire antennas, IEEE Trans. Ant. Prop., AP-32, 398-403.

25. Senior, T. B. A. (1965), A survey of analytical techniques for cross-section estimation, Proc. IEEE, 822-833.

26. Taflove, A., K. R. Umashankar, and T. G. Jurgens (1985), Validation of FD-TD modeling of the radar cross section of three-dimensional sturctures spanning up to nine wavelengths, IEEE Trans. Ant. Prop., AP-33, 662-666.

27. Tsai, L. L., D. G. Dudley, and D. R. Wilton (1974), Electromagnetic scattering by a three-dimensional conducting rectangular box, J. Appl. Phys., 45, 4393-4400.

28. Van Den Berg, P. M. (1984), Iterative computational techniques in scattering based upon the integrated square error criterion, IEEE Trans. Ant. Prop., AP-32, 1063-1071.

29. Walton, E. K. and J. D. Young (1984), The Ohio State University compact range cross-section measurement range, IEEE Trans. Ant. Prop., AP-32, 1218-1223.

30. Wang, D.-S. and L. N. Medgyesi-Mitschang (1985), Electromagnetic scattering from finite circular and elliptic cones, IEEE Trans. Ant. Prop., AP-33, 488-497.

31. Yaghjian, A. D. and R. V. McGahan (1985), Broadside radar cross section of the perfectly conducting cube, IEEE Trans. Ant. Prop., AP-33, 321-329.

Geometrical Optics

32. Deschamps, G. A. (1985), High frequency diffraction by wedges, *IEEE* Trans. Ant. Prop., AP-33, 357-368.

33. Knott, E. F. (1985), A progression of high-frequency RCS prediction techniques, IEEE Proceedings, 73, 252-264.

Physical Optics

34. Asvestas, J. S. (1985), Line integrals and physical optics. Part I. The transformation of the solid-angle surface integral to a line integral, J. Opt. Soc. Am. A, 2, 891-895.

35. Asvestas, J. S. (1985), Line integrals and physical optics. Part II. The conversion of the Kirchhoff surface integral to a line integral, J. Opt. Soc. Am. A, 2, 896-902.

36. Gordon, W. B. (1975), Vector potentials and physical optics, J. Math. Phys., 16, 448-454.

Geometrical Theory of Diffraction

37. Burnside, W. D., R. C. Rudduck, and R. J. Marhefka (1980), Summary of GTD computer codes developed at the Ohio State University, IEEE Trans. Electromagnetic Compatibility, EMC-22, 238-243.

38. James, G. L. (1976), Geometrical Theory of Diffraction for Electromagnetic Waves, Peter Peregrinus Ltd. for IEE, England.

39. Keller, J. B. (1962), Geometrical theory of diffraction, J. Opt. Soc. Am., 52,

AD-A170 973 RADAR CROSS SECTION PREDICTION FOR COATED PERFECT CONDUCTORS WITH ARBITRARY GEOMETRIES(U) AIR FORCE INST OF TECH WRIGHT-PATTERSON AFB OH S W ROGERS 1986 2/3

UNCLASSIFIED AFIT/CI/NR-86-105T F/G 17/9 NL

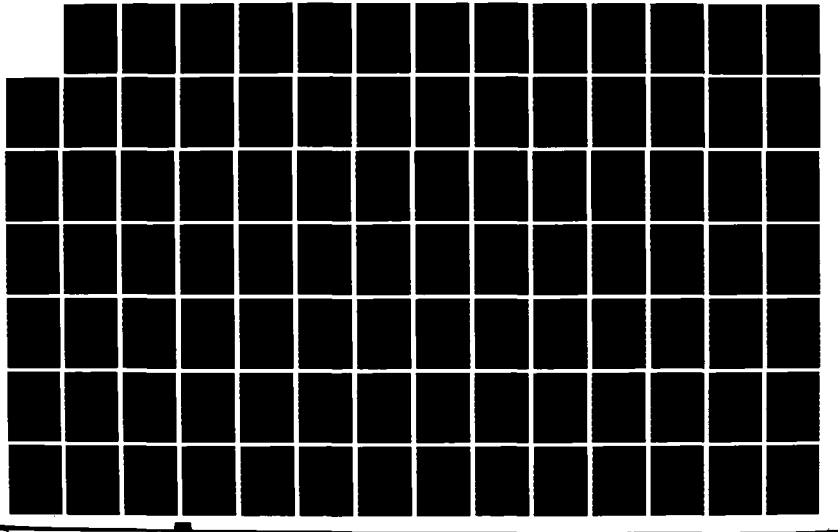

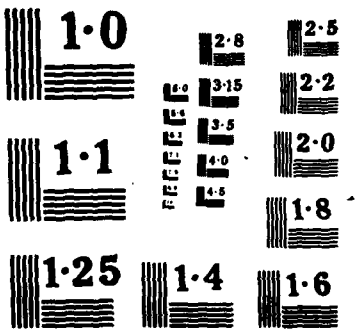
1·0
1·1
1·25
2·8
3·15
3·5
4·0
4·5
1·4
2·5
2·2
2·0
1·8
1·6

116-130.

40. Keller, J. B. (1985), One hundred years of diffraction theory, IEEE Trans. Ant. Prop., AP-33, 123-126.

41. Knott, E. F. and T. B. A. Senior (1974), Comparison of three high-frequency diffraction techniques, Proc. IEEE, 62, 1468-1474.

42. Lee, S. H. (1985), Aperture integration and GTD techniques used in the NEC reflector antenna code, IEEE Trans. Ant. Prop., AP-33, 189-194.

43. Pathak, P. H., N. Wang, W. D. Burnside, and R. G. Kouyoumjian (1981), A uniform GTD solution for the radiation from sources on a convex surface, IEEE Trans. Ant. Prop., AP-29, 609-622.

44. Pathak, P. H., W. D. Burnside, and R. J. Marhefka (1980), A uniform GTD analysis of the diffraction of electromagnetic waves by a smooth convex surface, IEEE Trans. Ant. Prop., AP-28, 631-642.

45. Plonus, M. A., R. Williams, and S. C. H. Wang (1978), Radar cross section of curved plates using geometrical and physical diffraction techniques, IEEE Trans. Ant. Prop., AP-26, 488-493.

46. Tiberio, R. and R. G. Kouyoumjian (1979), A uniform GTD solution for the diffraction by strips illuminated at grazing incidence, Radio Science, 14, 933-941.

Physical Theory of Diffraction

47. Brown, R. T. (1984), Treatment of singularities in the physical theory of diffraction, IEEE Trans. Ant. Prop., AP-32, 640-641.

48. Michaeli, A. (1984), A closed form physical theory of diffraction solution for electromagnetic scattering by strips and 90 deg dihedrals, Radio Science, 19, 609-616.

Uniform Theory of Diffraction

49. Cashman, J. D., R. G. Kouyoumjian, and P. H. Pathak (1977), Comments on "A uniform theory of diffraction for an edge in a perfectly conducting surface", IEEE Trans. Ant. Prop.,AP-25,447-451.

50. Deschamps, G. A., J. Boersma and S. W. Lee (1984), Three-dimensional half-plane

diffraction: exact solution and testing of uniform theories, IEEE Trans. Ant. Prop., AP-32, 264-271.

51. Michaeli, A., M. Kaye, and A. Geva (1984), High-frequency backscatter from a finned cylinder - Comparison of UTD results with experiment, IEEE Trans. Ant. Prop., AP-32, 422-425.

Uniform Asymptotic Theory of Diffraction

52. Borovikov, V. A. and B. Ye. Kinber (1974), Some problems in the asymptotic theory of diffraction, Proc. IEEE, 62, 1416-1437.

53. Lee, S. W. and G. A. Deschamps (1976), A uniform asympotitic theory of electromagnetic diffraction by a curved wedge, IEEE Trans. Ant. Prop., AP-24, 25-34.

54. Lee, S. W. (1977), Comparison of uniform asymptotic theory and Ufimtsev's theory of electromagnetic edge diffraction, IEEE Trans. Ant. Prop., AP-25, 162-170.

55. Lewis, R. M. and J. Boersma (1969), Uniform asymptotic theory of edge diffraction, J. Math. Phys., 10, 2291-2305.

56. Menendez, R. C. and S. W. Lee (1982), Analysis of rectangular horn antennas via uniform asymptotic theory, IEEE Trans. Ant. Prop., AP-30, 241-250.

57. Ott, R. H. (1985), Scattering by a parabolic cylinder - A uniform asymptotic expansion, J. Math. Phys., 26, 854-860.

58. Sanyal, S. and A. K. Bhattacharyya (1984), Electromagnetic scattering by a curved plate - Solution by uniform asymptotic theory of diffraction, IEEE Trans. Ant. Prop., AP-32, 187-189.

59. Stamnes, J. J. (1983), Uniform asymptotic theory of diffraction by apertures, J. Opt. Soc. Am., 73, 96-109.

Method of Moments

60. Ferguson, T. R. (1975), Banded matrix iteration in moments problems, IEEE AP-S International Symposium, Univ. of Illinois, Urbana, IL, 146-149.

61. Ferguson, T. R., T. H. Lehman, and R. J. Balestri (1976), Efficient solution of large moments problems: Theory and small problem results, IEEE Trans. Ant. Prop.,

AP-24, 230-235.

62. Ferguson, T. R. and R. J. Baletri (1976), Solution of large wire grid moments problems, IEEE International Symposium on Elecromagnetic Compatibility, Wash. D.C., 290-294.

63. Glisson, A. W. and D. R. Wilton (1980), Simple and efficient numerical methods for problems of electromagnetic radiation and scattering from surfaces, IEEE Trans. Ant. Prop., AP-28, 593-603.

64. Harrington, R. F. (1968), Field Computation by Moment Methods, The Macmillan Company, New York.

65. Heath, G. E. and D. B. Miron (1984), Comments on 'The singular integral problem in surfaces', IEEE Trans. Ant. Prop., AP-32, 428-430.

66. Klein, C. and R. Mittra (1973), Stability of matrix equations arising in electromagnetics, IEEE Trans. Ant. Prop., AP-21, 902-905.

67. Klein, C. and R. Mittra (1975), An application of the "condition number" concept to the solution of scattering problems in the presence of the interior resonant frequencies, IEEE Trans. Ant. Prop., 431-435.

68. Knepp, D. L. and J. Goldhirsh (1972), Numerical analysis of electromagnetic radiation properties of smooth conducting bodies of arbitrary shape, IEEE Trans. Ant. Prop., AP-20, 383-388.

69. Mautz, J. R. and R. F. Harrington (1979), A combined-source solution for radiation and scattering from a perfectly conducting body, IEEE Trans. Ant. Prop., AP-27, 445-454.

70. Medgyesi-Mitschang and D. Cowdrick (1980), RCS prediction techniques for missile-shaped bodies in the resonance and intermediate frequency regions, Presented at the Radar Camuflage Symposium, Orlando, FL, 18-20 November, 1980.

71. Medgyesi-Mitschang, L. N. and C. Eftimiu (1979), Scattering from axisymmetric obstacles embedded in axisymmetric dielectrics: the method of moments solution, Appl. Phys., 19, 275-285.

72. Medgyesi-Mitschang, L. N. and C. Eftimiu (1982), Scattering from wires and open circular cylinders of finite length using entire domain Galerkin expansions, IEEE Trans. Ant. Prop., AP-30, 628-636.

73. Medgyesi-Mitschang, L. N. and J. M. Putnam (1984), Electromagnetic scattering

from axially inhomogeneous bodies of revolution, IEEE Trans. Ant. Prop., AP-32, 797-806.

74. Miron, D. B. (1983), The singular integral problem in surfaces, IEEE Trans. Ant. Prop., AP-31, 507-509.

75. Mittra, R. ed. (1973), Computer Techniques for Electromagnetics, Pergamon Press, New York.

76. Mittra, R. ed. (1975), Numerical and Asymptotic Techniques in Electromagnetics, Springrer-Verlag, New York.

77. Mittra, R. and C. A. Klien (1975), The use of pivot ratios as a guide to stability of matrix equations arising in the method of moments, IEEE Trans. Ant. Prop., AP-23, 448-450.

78. Moore, J. and R. Pizer (1984), Moment Methods in Electromagnetics: Techniques and Applications, John Wiley & Sons, Inc., Research Studies Press LTD.

79. Pogorzelski, R. J. (1985), The Ludwig integration algorithm for triangular subregions, IEEE Proc., 73, 837-838.

80. Rao, S. M., A. W. Glisson, D. R. Wilton, and B. S. Vidula (1979), A simple numerical solution procedure for statics problems involving arbitrary-shaped surfaces, IEEE Trans. Ant. Prop., AP-27, 604-608.

81. Rao, S. M., D. R. Wilton, and A. W. Glisson (1982), Electromagnetic scattering by surfaces of arbitrary shape, IEEE Trans. Ant. Prop., AP-30, 409-418.

82. Richmond, J. H. (1966), A wire-grid model for scattering by conducting bodies, IEEE Trans. Ant. Prop., AP-14, 782-786.

83. Sarkar, T. K. (1985), A note on the choice weighting functions in the method of moments, IEEE Trans. Ant. Prop., AP-33, 436-441.

84. Sarkar, T. K. (1983), A note on the variational method (Rayleigh-Ritz), Galerkin's method, and the method of least squares, Radio Science, 18, 1207-1224.

85. Sarkar, T. K., K. R. Siarkiewicz, and R. F. Stratton (1981), Survey of numerical methods for solution of large systems of linear equations for electromagnetic field problems, IEEE Trans. Ant. Prop., AP-29, 847-856.

86. Tsai, L. L. and C. E. Smith (1978), Moment methods in electromagnetics for undergraduates, IEEE Trans. Education, E-21, 14-22.

87. Wilton, D. R. and S. Govind (1977), Incorporation of edge conditions in moment method solutions, IEEE Trans. Ant. Prop., AP-25, 845-850.

88. Yaghjian, A. D. (1981), Augmented electric- and magnetic-field integral equations, Radio Science, 16, 987-1001.

Hybrid Methods

89. Burnside, W. D., C. L. Yu, and R. J. Marhefka (1975), A technique to combine the geometrical theory of diffraction and the moment method, IEEE Trans. Ant. Prop., AP-23, 551-558.

90. Davidson, S. A. and G. A. Thiele (1984), A hybrid method of moments - GTD technique for computing electromagnetic coupling between two monopole antennas on a large cylindrical surface, IEEE Trans. Elec. Com., EMC-26, 90-97.

91. Ekelman, E. P. and G. A. Thiele (1980), A hybrid technique for combining the moment method treatment of wire antennas with the GTD for curved surfaces, IEEE Trans. Ant. Prop., AP-28, 831-839.

92. Henderson, L. W. and G. A. Thiele (1982), A hybrid MM-Geometrical Optics technique for the treatment of wire antennas mounted on a curved surface, IEEE Trans. Ant. Prop., AP-30, 1257-1261.

93. Kim, T. J. and G. A. Thiele (1982), A hybrid diffraction technique - general theory and applications, IEEE Trans. Ant. Prop., AP-30, 888-897.

94. Ko, W. L. and R. Mittra (1977), A new approach based on a combination of integral equation and asymptotic techniques for solving electromagnetic scattering problems, IEEE Trans. Ant. Prop., AP-25, 187-197.

95. Li, S. Z. and G. A. Thiele (1984), A hybrid theory of diffraction for the RCS calculation of ogive-like bodies, Radio Science, 19, 1432-1438.

96. Sahalos, J. N. and G. A. Thiele (1981), On the application of the GTD-MM technique and its limitations, IEEE Trans. Ant. Prop., AP-29, 780-786.

97. Thiele, G. A. and T. H. Newhouse (1975), A hybrid technique for combining moment methods with the geometrical theory of diffraction, IEEE Trans. Ant. Prop., AP-23, 62-69.

98. Thiele, G. A. and G. K. Chan (1978), Application of the hybrid technique to time domain problems, IEEE Trans. Elec. Comp., EMC-20, 151-155.

Surface Modeling

99. Kuo, D. C., H. H. Chao, J. R. Mautz, B. J. Strait, and R. F. Harrington (1972), Analysis of radiation and scattering by arbitrary configurations of thin wires, IEEE Trans. Ant. Prop., AP-20, 814-815.

100. Lee, K. S. H., L. Martin, and J. P. Castillo (1976), Limitations of wire-grid modeling of a closed surface, IEEE Trans. Electromagnetic Compatibility, EMC-18, 123-129.

101. Newman, E. H. and D. M. Pozar (1978), Electromagnetic modeling of composite wire and surface geometries, IEEE Trans. Ant. Prop., AP-26, 784-789.

102. Newman, E. H. and D. M. Pozar (1979), Correction to "Electromagnetic modeling of composite wire and surface geometries", IEEE Trans. Ant. Prop., AP-27, 570.

103. Newman, E. H. and D. M. Pozar (1980), Considerations for efficient wire/surface modeling, IEEE Trans. Ant. Prop., AP-28, 121-125.

104. Newman, E. H. and P. Tulyathan (1982), A surface patch model for polygonal plates, IEEE Trans. Ant. Prop., AP-30, 588-593.

105. Newman, E. H., P. Alexandropoulos, and E. K. Walton (1984), Polygonal plate modeling of realistic structures, IEEE Trans. Ant. Prop., AP-32, 742-747.

106. Schaubert, D. H., D. R. Wilton, and A. W. Glisson (1984), A tetrahedral modeling for electromagnetic scattering by arbitrarily shaped inhomogeneous dielectric bodies, IEEE Trans. Ant. Prop., AP-32, 77-85.

107. Singh, J. and A. T Adams (1979), A nonrectangular patch model for scattering from surfaces, IEEE Trans. Ant. Prop., AP-27, 531-535.

108. Wang, J. J. H. (1978), Numerical analysis of three-dimensional arbitrary-shaped conducting scatterers by trilateral surface cell modelling, Radio Science, 13, 947-952.

109. Wang, J. J. H. and C. J. Drane (1982), Numerical analysis of arbitrarily shaped bodies modeled by surface patches, IEEE Trans. Micro. Theo. Tech., MTT-30, 1167-1173.

110. Wilton, D. R., S. M. Rao, A. W. Glisson, D. H. Schaubert, O. M. Al-Bundak and C. M. Butler (1984), Potential integrals for uniform and linear source distributions on polygonal and polyhedral domains, IEEE Trans. Ant. Prop., AP-32, 276-281.

Treated Targets

111. Harrington, R. F. and J. R. Mautz (1975), An impedance sheet approximation for thin dielectric shells, IEEE Trans. Ant. Prop., AP-23, 531-534.

112. Hatakeyama, K. and T. Inui (1984), Electromagnetic wave absorber using ferrite absorbing material dispersed with short metal fibers, IEEE Trans. Magentics, MAG-20, 1261-1263.

113. Hiatt, R. E., K. M. Siegel, and H. Weil (1960), Forward scattering by coated objects illuminated by short wavelength radar, Proc. IRE, 1630-1635.

114. Hiatt, R. E., K. M. Siegel, and H. Weil (1960), The ineffectiveness of absorbing coatings on conducting objects illuminated by long wavelength radar, Proc. IRE, 1636-1642.

115. Iskander, K. A., L. Shafai, A. Frandsen, and J. E. Hensen (1982), Application of impedance boundary conditions to numerical solution of corrugated circular horns, IEEE Trans. Ant. Prop., AP-30, 366-372.

116. Knott, E. F. (1979), The thickness criterion for single-layer radar absorbents, IEEE Trans. Ant. Prop., AP-27, 698-701.

117. Medgyesi-Mitschang, L. N. and J. M. Putnam (1985), Integral equation formulation for imperfectly conducting scatterers, IEEE Trans. Ant. Prop., AP-33, 206-214.

118. Newman, E. H. and M. R. Schrote (1984), An open surface integral formulation for electromagnetic scattering by material plates, IEEE Trans. Ant. Prop., AP-32, 672-678.

119. Newman, E. H. and M. R. Schrote (1983), On the current distribution for open surfaces, IEE Trans. Ant. Prop., AP-31, 515-518.

120. Rogers, J. R. (1985), On combined source solutions for bodies with impedance boundary conditions, IEEE Trans. Ant. Prop., AP-33, 462-465.

121. Senior, T. B. A. (1960), Impedance boundary conditions for imperfectly conducting surfaces, Appl. Sci. Res., Sec. B., 8, 418-436.

122. Senior, T. B. A. (1981), Approximate boundary conditions, IEEE Trans. Ant. Prop., AP-29, 826-829.

123. Senior, T. B. A. (1985), Combined resistive and conductive sheets, IEEE Trans. Ant. Prop., AP-33, 577-579.

Miscellaneous

124. Kiang, J. (1985), Applications of Moment Method to Solve Problems of Scattering by Arbitrarily Shaped Bodies, Masters Thesis, Massachusetts Institute of Technology.

125. Hammer, P. C., O. P. Marloue, and A. H. Stroud (1956), Numerical integration over simplexes and cones, Math. Tables Aids Comp., vol. 10, pp. 130-137.

126. Abramowitz, M. and I. A. Stegun (1972), Handbook of Mathematical Functions, Dover Publications, New York.

127. Van Bladel (1964), Electromagnetic Fields, McGraw-Hill, New York.

128. Kong, J. A. (1984), 6.632 Course Notes for Advanced Electromagnetics course taught at the Massachusetts Institute of Technology.

APPENDICES

APPENDIX A

DERIVATION OF GOVERNING EQUATIONS

A.1 Introduction

This appendix contains a derivation of the governing equations for the method of moments applied to the radar cross section prediction for coated perfect conductors with arbitrary geometries. The equations for the interaction matrices are derived using the equivalence principle, Huygens' principle, the appropriate boundary conditions, and the method of moments. The derivation of the equations for the interaction matrix of a completely coated perfect conductor is presented first, followed by the derivation of the equations for the interaction matrix of a partially coated perfect conductor.

A.2 Completely Coated Perfect Conductor

This section contains the derivation of the equations for the interaction matrix of a completely coated perfect conductor. $e^{-i\omega t}$ is suppressed in the following derivation. This corresponds to a time harmonic solution at a single frequency. Refer to Figures 3.1 and 3.2 as a reference for the following derivation.

Since the boundary surfaces of the coated target will be replaced by an equivalent set of surface currents using the equivalence principle, the dyadic Green's function in an unbounded medium can be used. The dyadic Green's function in an unbounded medium [128] is defined as

$$\overline{\overline{G}}(\bar{r},\bar{r}') = [\overline{\overline{I}} + \frac{1}{k^2}\nabla\nabla]g(\bar{r},\bar{r}') \qquad (A.1)$$

where g is the scalar Green's function defined as

$$g(\bar{r},\bar{r}') = \frac{e^{ik|\bar{r}-\bar{r}'|}}{4\pi|\bar{r}-\bar{r}'|}. \tag{A.2}$$

In region 0, the free space outside the object,

$$\overline{\overline{G}}_0 = [\overline{\overline{I}} + \frac{1}{k_0^2}\nabla\nabla]g_0(\bar{r},\bar{r}') \tag{A.3}$$

where

$$g_0 = \frac{e^{ik_0|\bar{r}-\bar{r}'|}}{4\pi|\bar{r}-\bar{r}'|} \tag{A.4}$$

and

$$k_0 = \omega\sqrt{\mu_0\epsilon_0}.$$

In region 1, the coating on the perfect conductor,

$$\overline{\overline{G}}_1 = [\overline{\overline{I}} + \frac{1}{k_1^2}\nabla\nabla]g_1(\bar{r},\bar{r}') \tag{A.5}$$

where

$$g_1 = \frac{e^{ik_1|\bar{r}-\bar{r}'|}}{4\pi|\bar{r}-\bar{r}'|} \tag{A.6}$$

and

$$k_1 = \omega\sqrt{\mu\epsilon}$$

and μ and ϵ can be complex.

At surface S_1:

$$\hat{n}_0 \times \overline{E}_0 = -\hat{n}_1 \times \overline{E}_1 \tag{A.7}$$

and, therefore, by the equivalence principle

$$\overline{M}_1 = -\overline{M}_1'. \tag{A.8}$$

Also

$$\hat{n}_0 \times \overline{H}_0 = -\hat{n}_1 \times \overline{H}_1 \tag{A.9}$$

and, therefore, by the equivalence principle

$$\overline{J}_1 = -\overline{J}_1^{'}. \tag{A.10}$$

At surface S_2:

$$\hat{n}_2 \times \overline{E}_1 = 0 \tag{A.11}$$

and

$$\hat{n}_2 \times \overline{H}_1 = \overline{J}_2. \tag{A.12}$$

Using Huygens' principle (see equation 3.1) in Region 0:

$$\overline{E}_0 = \overline{E}_{inc} + \overline{E}_s = \overline{E}_{inc} + \int_{S_1} dS_1 \{ i\omega\mu_0 \overline{\overline{G}}_0 \cdot \overline{J}_1 - \nabla \times \overline{\overline{G}}_0 \cdot \overline{M}_1 \} \tag{A.13}$$

and

$$\overline{H}_0 = \overline{H}_{inc} + \overline{H}_s = \overline{H}_{inc} + \int_{S_1} dS_1 \{ i\omega\epsilon_0 \overline{\overline{G}}_0 \cdot \overline{M}_1 + \nabla \times \overline{\overline{G}}_0 \cdot \overline{J}_1 \}. \tag{A.14}$$

Using Huygens' principle in Region 1:

$$\overline{E}_1 = \int_{S_1} dS_1 \{ i\omega\mu \overline{\overline{G}}_1 \cdot \overline{J}_1^{'} - \nabla \times \overline{\overline{G}}_1 \cdot \overline{M}_1^{'} \} + \int_{S_2} dS_2 \{ i\omega\mu \overline{\overline{G}}_1 \cdot \overline{J}_2 \} \tag{A.15}$$

and

$$\overline{H}_1 = \int_{S_1} dS_1 \{ i\omega\epsilon \overline{\overline{G}}_1 \cdot \overline{M}_1^{'} + \nabla \times \overline{\overline{G}}_1 \cdot \overline{J}_1^{'} \} + \int_{S_2} dS_2 \{ \nabla \times \overline{\overline{G}}_1 \cdot \overline{J}_2 \}. \tag{A.16}$$

Applying the boundary conditions at surface S_1:

$$\hat{n}_0 \times \overline{E}_0 = \hat{n}_0 \times \overline{E}_1. \tag{A.17}$$

Therefore, at S_1

$$\hat{n}_0 \times \overline{E}_{inc} + \hat{n}_0 \times \int_{S_1} dS_1 \{ i\omega\mu_0 \overline{\overline{G}}_0 \cdot \overline{J}_1 - \nabla \times \overline{\overline{G}}_0 \cdot \overline{M}_1 \} =$$
$$\hat{n}_0 \times \int_{S_1} dS_1 \{ i\omega\mu \overline{\overline{G}}_1 \cdot \overline{J}_1' - \nabla \times \overline{\overline{G}}_1 \cdot \overline{M}_1' \} + \hat{n}_0 \times \int_{S_2} dS_2 \{ i\omega\mu \overline{\overline{G}}_1 \cdot \overline{J}_2 \} \quad (A.18)$$

Also at S_1

$$\hat{n}_0 \times \overline{H}_0 = \hat{n}_0 \times \overline{H}_1 \quad (A.19)$$

and, therefore, at S_1

$$\hat{n}_0 \times \overline{H}_{inc} + \hat{n}_0 \times \int_{S_1} dS_1 \{ i\omega\epsilon_0 \overline{\overline{G}}_0 \cdot \overline{M}_1 + \nabla \times \overline{\overline{G}}_0 \cdot \overline{J}_1 \} =$$
$$\hat{n}_0 \times \int_{S_1} dS_1 \{ i\omega\epsilon \overline{\overline{G}}_1 \cdot \overline{M}_1' + \nabla \times \overline{\overline{G}}_1 \cdot \overline{J}_1' \} + \hat{n}_0 \times \int_{S_2} dS_2 \{ \nabla \times \overline{\overline{G}}_1 \cdot \overline{J}_2 \} \quad (A.20)$$

Now, at surface S_2

$$\hat{n}_2 \times \overline{E}_1 = 0. \quad (A.21)$$

Therefore, at S_2

$$\hat{n}_2 \times \int_{S_1} dS_1 \{ i\omega\mu \overline{\overline{G}}_1 \cdot \overline{J}_1' - \nabla \times \overline{\overline{G}}_1 \cdot \overline{M}_1' \} + \hat{n}_2 \times \int_{S_2} dS_2 \{ i\omega\mu \overline{\overline{G}}_1 \cdot \overline{J}_2 \} = 0. \quad (A.22)$$

Also at S_2

$$\hat{n}_2 \times \overline{H}_1 = \overline{J}_2 \quad (A.23)$$

and, therefore, at S_2

$$\hat{n}_2 \times \int_{S_1} dS_1 \{ i\omega\epsilon \overline{\overline{G}}_1 \cdot \overline{M}_1' + \nabla \times \overline{\overline{G}}_1 \cdot \overline{J}_1' \} + \hat{n}_2 \times \int_{S_2} dS_2 \{ \nabla \times \overline{\overline{G}}_1 \cdot \overline{J}_2 \} = \overline{J}_2. \quad (A.24)$$

Using equations (A.8) and (A.10) equation (A.18) becomes

$$-\hat{n}_0 \times \int_{S_1} dS_1 \{ i\omega\mu_0 \overline{\overline{G}}_0 \cdot \overline{J}_1 \} - \hat{n}_0 \times \int_{S_1} dS_1 \{ i\omega\mu \overline{\overline{G}}_1 \cdot \overline{J}_1 \} + \hat{n}_0 \times \int_{S_1} dS_1 \{ \nabla \times \overline{\overline{G}}_0 \cdot \overline{M}_1 \}$$

$$+\hat{n}_0 \times \int_{S_1} dS_1\{\nabla \times \overline{\overline{G}}_1 \cdot \overline{M}_1\} + \hat{n}_0 \times \int_{S_2} dS_2\{i\omega\mu\overline{\overline{G}}_1 \cdot \overline{J}_2\} = \hat{n}_0 \times \overline{E}_{inc} \qquad (A.25)$$

and equation (A.20) becomes

$$-\hat{n}_0 \times \int_{S_1} dS_1\{\nabla \times \overline{\overline{G}}_0 \cdot \overline{J}_1\} - \hat{n}_0 \times \int_{S_1} dS_1\{\nabla \times \overline{\overline{G}}_1 \cdot \overline{J}_1\} - \hat{n}_0 \times \int_{S_1} dS_1\{i\omega\epsilon_0\overline{\overline{G}}_0 \cdot \overline{M}_1\}$$

$$-\hat{n}_0 \times \int_{S_1} dS_1\{i\omega\epsilon\overline{\overline{G}}_1 \cdot \overline{M}_1\} + \hat{n}_0 \times \int_{S_2} dS_2\{\nabla \times \overline{\overline{G}}_1 \cdot \overline{J}_2\} = \hat{n}_0 \times \overline{H}_{inc} \qquad (A.26)$$

and equation (A.22) becomes

$$-\hat{n}_2 \times \int_{S_1} dS_1\{i\omega\mu\overline{\overline{G}}_1 \cdot \overline{J}_1\} + \hat{n}_2 \times \int_{S_1} dS_1\{\nabla \times \overline{\overline{G}}_1 \cdot \overline{M}_1\}$$

$$+\hat{n}_2 \times \int_{S_2} dS_2\{i\omega\mu\overline{\overline{G}}_1 \cdot \overline{J}_2\} = 0 \qquad (A.27)$$

and equation (A.24) becomes

$$-\hat{n}_2 \times \int_{S_1} dS_1\{\nabla \times \overline{\overline{G}}_1 \cdot \overline{J}_1\} - \hat{n}_2 \times \int_{S_1} dS_1\{i\omega\epsilon\overline{\overline{G}}_1 \cdot \overline{M}_1\}$$

$$+\hat{n}_2 \times \int_{S_2} dS_2\{\nabla \times \overline{\overline{G}}_1 \cdot \overline{J}_2\} - \overline{J}_2 = 0. \qquad (A.28)$$

Equations (A.25), (A.26), and (A.27) are of the form

$$L_{11} \cdot \overline{J}_1 + L_{12} \cdot \overline{M}_1 + L_{13} \cdot \overline{J}_2 = \hat{n}_0 \times \overline{E}_{inc} \qquad (A.29)$$

$$L_{21} \cdot \overline{J}_1 + L_{22} \cdot \overline{M}_1 + L_{23} \cdot \overline{J}_2 = \hat{n}_0 \times \overline{H}_{inc} \qquad (A.30)$$

$$L_{31} \cdot \overline{J}_1 + L_{32} \cdot \overline{M}_1 + L_{33} \cdot \overline{J}_2 = 0 \qquad (A.31)$$

or the more compact form

$$\begin{pmatrix} L_{11} & L_{12} & L_{13} \\ L_{21} & L_{22} & L_{23} \\ L_{31} & L_{32} & L_{33} \end{pmatrix} \begin{pmatrix} \overline{J}_1 \\ \overline{M}_1 \\ \overline{J}_2 \end{pmatrix} = \begin{pmatrix} \hat{n}_0 \times \overline{E}_{inc} \\ \hat{n}_0 \times \overline{H}_{inc} \\ \overline{0} \end{pmatrix} \qquad (A.32)$$

where

$$L_{11} = -\hat{n}_0 \times \int_{S_1} dS_1 i\omega\{\mu_0\overline{\overline{G}}_0 + \mu\overline{\overline{G}}_1\}\cdot \tag{A.33}$$

$$L_{12} = \hat{n}_0 \times \int_{S_1} dS_1\{\nabla \times \overline{\overline{G}}_0 + \nabla \times \overline{\overline{G}}_1\}\cdot \tag{A.34}$$

$$L_{13} = \hat{n}_0 \times \int_{S_2} dS_2\{i\omega\mu\overline{\overline{G}}_1\}\cdot \tag{A.35}$$

$$L_{21} = -\hat{n}_0 \times \int_{S_1} dS_1\{\nabla \times \overline{\overline{G}}_0 + \nabla \times \overline{\overline{G}}_1\}\cdot \tag{A.36}$$

$$L_{22} = -\hat{n}_0 \times \int_{S_1} dS_1 i\omega\{\epsilon_0\overline{\overline{G}}_0 + \epsilon\overline{\overline{G}}_1\}\cdot \tag{A.37}$$

$$L_{23} = \hat{n}_0 \times \int_{S_2} dS_2\{\nabla \times \overline{\overline{G}}_1\}\cdot \tag{A.38}$$

$$L_{31} = -\hat{n}_2 \times \int_{S_1} dS_1\{i\omega\mu\overline{\overline{G}}_1\}\cdot \tag{A.39}$$

$$L_{32} = \hat{n}_2 \times \int_{S_1} dS_1\{\nabla \times \overline{\overline{G}}_1\}\cdot \tag{A.40}$$

$$L_{33} = \hat{n}_2 \times \int_{S_2} dS_2\{i\omega\mu\overline{\overline{G}}_1\}\cdot\cdot \tag{A.41}$$

Note that L_{12} = -L_{21} and if ϵ and μ are interchanged $L_{11} = L_{22}$. Further, if surfaces S_1 and S_2 are interchanged L_{13} = -L_{31} and $L_{23} = L_{32}$. Equations (A.32) through (A.41) with the G's expanded match Mitschang's derivation [70] in which he used the vector and scalar potential formulation. Finally, using equation (A.27) and not using (A.28) corresponds to the electric field integral equation (EFIE) approach discussed by Rao, Wilton, and Glisson [81]. If (A.28) were used and (A.27) were not used, this would correspond to the magnetic field integral equation (MFIE) approach. If a weighted sum of the EFIE and the MFIE are used, this would correspond to

the combined field integral equation (CFIE) approach discussed by Rogers [120] and Mitschang et al [70].

Now rewriting (A.32) as three distinct equations gives

$$\hat{n}_0 \times \overline{E}_{inc} = -\hat{n}_0 \times \int_{S_1} dS_1 i\omega\{\mu_0 \overline{\overline{G}}_0 + \mu \overline{\overline{G}}_1\} \cdot \overline{J}_1 + \hat{n}_0 \times \int_{S_1} dS_1 \{\nabla \times \overline{\overline{G}}_0 + \nabla \times \overline{\overline{G}}_1\} \cdot \overline{M}_1$$

$$+\hat{n}_0 \times \int_{S_2} dS_2 \{i\omega\mu \overline{\overline{G}}_1\} \cdot \overline{J}_2 \qquad (A.42)$$

$$\hat{n}_0 \times \overline{H}_{inc} = -\hat{n}_0 \times \int_{S_1} dS_1 \{\nabla \times \overline{\overline{G}}_0 + \nabla \times \overline{\overline{G}}_1\} \cdot \overline{J}_1 - \hat{n}_0 \times \int_{S_1} dS_1 i\omega\{\epsilon_0 \overline{\overline{G}}_0 + \epsilon \overline{\overline{G}}_1\} \cdot \overline{M}_1$$

$$+\hat{n}_0 \times \int_{S_2} dS_2 \{\nabla \times \overline{\overline{G}}_1\} \cdot \overline{J}_2 \qquad (A.43)$$

$$\overline{0} = -\hat{n}_2 \times \int_{S_1} dS_1 \{i\omega\mu \overline{\overline{G}}_1\} \cdot \overline{J}_1 + \hat{n}_2 \times \int_{S_1} dS_1 \{\nabla \times \overline{\overline{G}}_1\} \cdot \overline{M}_1$$

$$+\hat{n}_2 \times \int_{S_2} dS_2 \{i\omega\mu \overline{\overline{G}}_1\} \cdot \overline{J}_2 \qquad (A.44)$$

After expanding $\overline{\overline{G}}$, (A.42), (A.43), and (A.44) become (with R= $|\bar{r} - \bar{r}'|$)

$$\begin{aligned}
\hat{n}_0 \times \overline{E}_{inc} = &-\hat{n}_0 \times \int_{S_1} dS_1 i\omega\mu_0 \overline{J}_1 \frac{e^{ik_0 R}}{4\pi R} - \hat{n}_0 \times \nabla \int_{S_1} dS_1 \frac{i\omega\mu_0}{k_0^2} (\nabla \cdot \overline{J}_1) \frac{e^{ik_0 R}}{4\pi R} \\
&- \hat{n}_0 \times \int_{S_1} dS_1 i\omega\mu \overline{J}_1 \frac{e^{ik_1 R}}{4\pi R} - \hat{n}_0 \times \nabla \int_{S_1} dS_1 \frac{i\omega\mu}{k_1^2} (\nabla \cdot \overline{J}_1) \frac{e^{ik_1 R}}{4\pi R} \\
&+ \hat{n}_0 \times \nabla \times \int_{S_1} dS_1 \overline{M}_1 \frac{e^{ik_0 R}}{4\pi R} + \hat{n}_0 \times \nabla \times \nabla \int_{S_1} dS_1 \frac{1}{k_0^2} (\nabla \cdot \overline{M}_1) \frac{e^{ik_0 R}}{4\pi R} \\
&+ \hat{n}_0 \times \nabla \times \int_{S_1} dS_1 \overline{M}_1 \frac{e^{ik_1 R}}{4\pi R} + \hat{n}_0 \times \nabla \times \nabla \int_{S_1} dS_1 \frac{1}{k_1^2} (\nabla \cdot \overline{M}_1) \frac{e^{ik_1 R}}{4\pi R} \\
&\div \hat{n}_0 \times \int_{S_2} dS_2 i\omega\mu \overline{J}_2 \frac{e^{ik_1 R}}{4\pi R} + \hat{n}_0 \times \nabla \int_{S_2} dS_2 \frac{i\omega\mu}{k_1^2} (\nabla \cdot \overline{J}_2) \frac{e^{ik_1 R}}{4\pi R} \qquad (A.45)
\end{aligned}$$

$$\begin{aligned}
\hat{n}_0\times\overline{H}_{inc} = &-\hat{n}_0\times\nabla\times\int_{S_1} dS_1\overline{J}_1\frac{e^{ik_0R}}{4\pi R} - \hat{n}_0\times\nabla\times\nabla\int_{S_1} dS_1\frac{1}{k_0^2}(\nabla\cdot\overline{J}_1)\frac{e^{ik_0R}}{4\pi R}\\
&-\hat{n}_0\times\nabla\times\int_{S_1} dS_1\overline{J}_1\frac{e^{ik_1R}}{4\pi R} - \hat{n}_0\times\nabla\times\nabla\int_{S_1} dS_1\frac{1}{k_1^2}(\nabla\cdot\overline{J}_1)\frac{e^{ik_1R}}{4\pi R}\\
&-\hat{n}_0\times\int_{S_1} dS_1 i\omega\epsilon_0\overline{M}_1\frac{e^{ik_0R}}{4\pi R} - \hat{n}_0\times\nabla\int_{S_1} dS_1\frac{i\omega\epsilon_0}{k_0^2}(\nabla\cdot\overline{M}_1)\frac{e^{ik_0R}}{4\pi R}\\
&-\hat{n}_0\times\int_{S_1} dS_1 i\omega\epsilon\overline{M}_1\frac{e^{ik_1R}}{4\pi R} - \hat{n}_0\times\nabla\int_{S_1} dS_1\frac{i\omega\epsilon}{k_1^2}(\nabla\cdot\overline{M}_1)\frac{e^{ik_1R}}{4\pi R}\\
&+\hat{n}_0\times\nabla\times\int_{S_2} dS_2\overline{J}_2\frac{e^{ik_1R}}{4\pi R} + \hat{n}_0\times\nabla\times\nabla\int_{S_2} dS_2\frac{1}{k_1^2}(\nabla\cdot\overline{J}_2)\frac{e^{ik_1R}}{4\pi R} \qquad (A.46)
\end{aligned}$$

$$\begin{aligned}
\overline{0} = &-\hat{n}_2\times\int_{S_1} dS_1 i\omega\mu\overline{J}_1\frac{e^{ik_1R}}{4\pi R} - \hat{n}_2\times\nabla\int_{S_1} dS_1\frac{i\omega\mu}{k_1^2}(\nabla\cdot\overline{J}_1)\frac{e^{ik_1R}}{4\pi R}\\
&+\hat{n}_2\times\nabla\times\int_{S_1} dS_1\overline{M}_1\frac{e^{ik_1R}}{4\pi R} + \hat{n}_2\times\nabla\times\nabla\int_{S_1} dS_1\frac{1}{k_1^2}(\nabla\cdot\overline{M}_1)\frac{e^{ik_1R}}{4\pi R}\\
&+\hat{n}_2\times\int_{S_2} dS_2 i\omega\mu\overline{J}_2\frac{e^{ik_1R}}{4\pi R} + \hat{n}_2\times\nabla\int_{S_2} dS_2\frac{i\omega\mu}{k_1^2}(\nabla\cdot\overline{J}_2)\frac{e^{ik_1R}}{4\pi R} \qquad (A.47)
\end{aligned}$$

These three equations have functions with the following form:

$$\overline{H}(\bar{r}) = \frac{1}{\mu}\nabla\times\overline{A}(\bar{r}) = \frac{1}{4\pi}\int_V \nabla\times\Big[\overline{J}(\bar{r}')\frac{e^{ik|\bar{r}-\bar{r}'|}}{|\bar{r}-\bar{r}'|}\Big]d\bar{r}' \qquad (A.48)$$

Now from Appendix A-1 equation 14 in Van Bladel [127]

$$\nabla\times(A\bar{a}) = \nabla A\times\bar{a} + A\nabla\times\bar{a} \qquad (A.49)$$

Therefore,

$$\nabla\times\left[\frac{e^{ik|\bar{r}-\bar{r}'|}}{|\bar{r}-\bar{r}'|}\overline{J}(\bar{r}')\right] = \nabla\Big(\frac{e^{ik|\bar{r}-\bar{r}'|}}{|\bar{r}-\bar{r}'|}\Big)\times\overline{J}(\bar{r}') + \Big(\frac{e^{ik|\bar{r}-\bar{r}'|}}{|\bar{r}-\bar{r}'|}\Big)\nabla\times\overline{J}(\bar{r}'). \qquad (A.50)$$

The second term on the right is zero since $\nabla = \nabla(\bar{r})$, and thus

$$\overline{H}(\bar{r}) = \frac{1}{4\pi}\int_V \nabla\Big(\frac{e^{ik|\bar{r}-\bar{r}'|}}{|\bar{r}-\bar{r}'|}\Big)\times\overline{J}(\bar{r}')d\bar{r}' = -\frac{1}{4\pi}\int_V \overline{J}(\bar{r}')\times\nabla\Big(\frac{e^{ik|\bar{r}-\bar{r}'|}}{|\bar{r}-\bar{r}'|}\Big)d\bar{r}' \qquad (A.51)$$

which gives

$$\overline{H}(\bar{r}) = \frac{1}{4\pi}\int_V \overline{J}(\bar{r}') \times \nabla'\left(\frac{e^{ik|\bar{r}-\bar{r}'|}}{|\bar{r}-\bar{r}'|}\right)d\bar{r}' \tag{A.52}$$

and by duality

$$\overline{E}(\bar{r}) = -\nabla \times \frac{1}{4\pi}\int_V \overline{M}(\bar{r}')\frac{e^{ikR}}{R} = -\frac{1}{4\pi}\int_V \overline{M}(\bar{r}') \times \nabla'\left(\frac{e^{ik|\bar{r}-\bar{r}'|}}{|\bar{r}-\bar{r}'|}\right)d\bar{r}'. \tag{A.53}$$

Using these results and the fact that $\nabla \times \nabla A = 0$, (A.45),(A.46), and (A.47) become

$$\begin{aligned}
\hat{n}_0 \times \overline{E}_{inc} = &-\hat{n}_0 \times \int_{S_1} dS_1 i\omega\mu_0 \overline{J}_1 \frac{e^{ik_0R}}{4\pi R} - \hat{n}_0 \times \nabla \int_{S_1} dS_1 \frac{i\omega\mu_0}{k_0^2}(\nabla \cdot \overline{J}_1)\frac{e^{ik_0R}}{4\pi R} \\
&- \hat{n}_0 \times \int_{S_1} dS_1 i\omega\mu \overline{J}_1 \frac{e^{ik_1R}}{4\pi R} - \hat{n}_0 \times \nabla \int_{S_1} dS_1 \frac{i\omega\mu}{k_1^2}(\nabla \cdot \overline{J}_1)\frac{e^{ik_1R}}{4\pi R} \\
&+ \hat{n}_0 \times \int_{S_1} dS_1 \overline{M}_1 \times \nabla'\left(\frac{e^{ik_0R}}{4\pi R}\right) + \hat{n}_0 \times \int_{S_1} dS_1 \overline{M}_1 \times \nabla'\left(\frac{e^{ik_1R}}{4\pi R}\right) \\
&+ \hat{n}_0 \times \int_{S_2} dS_2 i\omega\mu \overline{J}_2 \frac{e^{ik_1R}}{4\pi R} + \hat{n}_0 \times \nabla \int_{S_2} dS_2 \frac{i\omega\mu}{k_1^2}(\nabla \cdot \overline{J}_2)\frac{e^{ik_1R}}{4\pi R}
\end{aligned} \tag{A.54}$$

$$\begin{aligned}
\hat{n}_0 \times \overline{H}_{inc} = &-\hat{n}_0 \times \int_{S_1} dS_1 \overline{J}_1 \times \nabla'\left(\frac{e^{ik_0R}}{4\pi R}\right) - \hat{n}_0 \times \int_{S_1} dS_1 \overline{J}_1 \times \nabla'\left(\frac{e^{ik_1R}}{4\pi R}\right) \\
&- \hat{n}_0 \times \int_{S_1} dS_1 i\omega\epsilon_0 \overline{M}_1 \frac{e^{ik_0R}}{4\pi R} - \hat{n}_0 \times \nabla \int_{S_1} dS_1 \frac{i\omega\epsilon_0}{k_0^2}(\nabla \cdot \overline{M}_1)\frac{e^{ik_0R}}{4\pi R} \\
&- \hat{n}_0 \times \int_{S_1} dS_1 i\omega\epsilon \overline{M}_1 \frac{e^{ik_1R}}{4\pi R} - \hat{n}_0 \times \nabla \int_{S_1} dS_1 \frac{i\omega\epsilon}{k_1^2}(\nabla \cdot \overline{M}_1)\frac{e^{ik_1R}}{4\pi R} \\
&+ \hat{n}_0 \times \int_{S_2} dS_2 \overline{J}_2 \times \nabla'\left(\frac{e^{ik_1R}}{4\pi R}\right)
\end{aligned} \tag{A.55}$$

$$\begin{aligned}
\bar{0} = &-\hat{n}_2 \times \int_{S_1} dS_1 i\omega\mu \overline{J}_1 \frac{e^{ik_1R}}{4\pi R} - \hat{n}_2 \times \nabla \int_{S_1} dS_1 \frac{i\omega\mu}{k_1^2}(\nabla \cdot \overline{J}_1)\frac{e^{ik_1R}}{4\pi R} \\
&+ \hat{n}_2 \times \int_{S_1} dS_1 \overline{M}_1 \times \nabla'\left(\frac{e^{ik_1R}}{4\pi R}\right) + \hat{n}_2 \times \int_{S_2} dS_2 i\omega\mu \overline{J}_2 \frac{e^{ik_1R}}{4\pi R} \\
&+ \hat{n}_2 \times \nabla \int_{S_2} dS_2 \frac{i\omega\mu}{k_1^2}(\nabla \cdot \overline{J}_2)\frac{e^{ik_1R}}{4\pi R}.
\end{aligned} \tag{A.56}$$

The desired approach at this point in the derivation is to change these three integro-differential equations in the three unknown surface current densities into a matrix equation which can be solved using inversion techniques. To this end, the method of moments will be applied using basis functions and a testing procedure developed by Rao, et al [81]. Now the basis functions [81] are

$$\overline{J}_1(\bar{r}') \simeq \sum_{n=1}^{N} I_n \overline{f}_n(\bar{r}') \tag{A.57}$$

$$\overline{M}_1(\bar{r}') \simeq \sum_{n'=1}^{N'} K_{n'} \overline{f}_{n'}(\bar{r}') \tag{A.58}$$

$$\overline{J}_2(\bar{r}') \simeq \sum_{n''=1}^{N''} L_{n''} \overline{f}_{n''}(\bar{r}') \tag{A.59}$$

where n and n' are defined over the surface of the coating, and n'' is defined over the surface of the perfect conductor (see Figure 3.1). Furthermore (see Figure 3.5),

$$\overline{f}_n(\bar{r}') = \begin{cases} \frac{l_n}{2A_n^+}\bar{\rho}_n^+; & \bar{r}' \text{ in } T_n^+ \\ \frac{l_n}{2A_n^-}\bar{\rho}_n^-; & \bar{r}' \text{ in } T_n^- \\ 0; & \text{otherwise} \end{cases} \tag{A.60}$$

and

$$\nabla_s' \cdot \overline{f}_n(\bar{r}') = \begin{cases} \frac{l_n}{A_n^+}; & \bar{r}' \text{ in } T_n^+ \\ -\frac{l_n}{A_n^-}; & \bar{r}' \text{ in } T_n^- \\ 0; & \text{otherwise.} \end{cases} \tag{A.61}$$

Substituting these basis functions into (A.54), (A.55), and (A.56) yields

$$\begin{aligned} \hat{n}_0 \times \overline{E}_{inc} = & -\hat{n}_0 \times \int_{S_1} dS_1 i\omega\mu_0 I_n \overline{f}_n(\bar{r}') \frac{e^{ik_0 R}}{4\pi R} - \hat{n}_0 \times \nabla \int_{S_1} dS_1 \frac{i\omega\mu_0}{k_0^2} (\nabla_s' \cdot I_n \overline{f}_n(\bar{r}')) \frac{e^{ik_0 R}}{4\pi R} \\ & - \hat{n}_0 \times \int_{S_1} dS_1 i\omega\mu I_n \overline{f}_n(\bar{r}') \frac{e^{ik_1 R}}{4\pi R} - \hat{n}_0 \times \nabla \int_{S_1} dS_1 \frac{i\omega\mu}{k_1^2} (\nabla_s' \cdot I_n \overline{f}_n(\bar{r}')) \frac{e^{ik_1 R}}{4\pi R} \\ & + \hat{n}_0 \times \int_{S_1} dS_1 K_{n'} \overline{f}_{n'}(\bar{r}') \times \nabla' \left(\frac{e^{ik_0 R}}{4\pi R}\right) + \hat{n}_0 \times \int_{S_1} dS_1 K_{n'} \overline{f}_{n'}(\bar{r}') \times \nabla' \left(\frac{e^{ik_1 R}}{4\pi R}\right) \\ & + \hat{n}_0 \times \int_{S_2} dS_2 i\omega\mu L_{n''} \overline{f}_{n''}(\bar{r}') \frac{e^{ik_1 R}}{4\pi R} \\ & + \hat{n}_0 \times \nabla \int_{S_2} dS_2 \frac{i\omega\mu}{k_1^2} (\nabla_s' \cdot L_{n''} \overline{f}_{n''}(\bar{r}')) \frac{e^{ik_1 R}}{4\pi R} \end{aligned} \tag{A.62}$$

$$\hat{n}_0\times\overline{H}_{inc} = -\hat{n}_0 \times \int_{S_1} dS_1 I_n \overline{f}_n(\bar{r}') \times \nabla'\left(\frac{e^{ik_0R}}{4\pi R}\right) - \hat{n}_0 \times \int_{S_1} dS_1 I_n \overline{f}_n(\bar{r}') \times \nabla'\left(\frac{e^{ik_1R}}{4\pi R}\right)$$
$$- \hat{n}_0 \times \int_{S_1} dS_1 i\omega\epsilon_0 K_{n'} \overline{f}_{n'}(\bar{r}') \frac{e^{ik_0R}}{4\pi R} - \hat{n}_0 \times \nabla \int_{S_1} dS_1 \frac{i\omega\epsilon_0}{k_0^2} \left(\nabla'_s \cdot K_{n'} \overline{f}_{n'}(\bar{r}')\right) \frac{e^{ik_0R}}{4\pi R}$$
$$- \hat{n}_0 \times \int_{S_1} dS_1 i\omega\epsilon K_{n'} \overline{f}_{n'}(\bar{r}') \frac{e^{ik_1R}}{4\pi R} - \hat{n}_0 \times \nabla \int_{S_1} dS_1 \frac{i\omega\epsilon}{k_1^2} \left(\nabla'_s \cdot K_{n'} \overline{f}_{n'}(\bar{r}')\right) \frac{e^{ik_1R}}{4\pi R}$$
$$+ \hat{n}_0 \times \int_{S_2} dS_2 L_{n''} \overline{f}_{n''}(\bar{r}') \times \nabla'\left(\frac{e^{ik_1R}}{4\pi R}\right) \qquad (A.63)$$

$$\overline{0} = -\hat{n}_2 \times \int_{S_1} dS_1 i\omega\mu I_n \overline{f}_n(\bar{r}') \frac{e^{ik_1R}}{4\pi R} - \hat{n}_2 \times \nabla \int_{S_1} dS_1 \frac{i\omega\mu}{k_1^2} \left(\nabla'_s \cdot I_n \overline{f}_n(\bar{r}')\right) \frac{e^{ik_1R}}{4\pi R}$$
$$+ \hat{n}_2 \times \int_{S_1} dS_1 K_{n'} \overline{f}_{n'}(\bar{r}') \times \nabla'\left(\frac{e^{ik_1R}}{4\pi R}\right) + \hat{n}_2 \times \int_{S_2} dS_2 i\omega\mu L_{n''} \overline{f}_{n''}(\bar{r}') \frac{e^{ik_1R}}{4\pi R}$$
$$+ \hat{n}_2 \times \nabla \int_{S_2} dS_2 \frac{i\omega\mu}{k_1^2} \left(\nabla'_s \cdot L_{n''} \overline{f}_{n''}(\bar{r}')\right) \frac{e^{ik_1R}}{4\pi R}. \qquad (A.64)$$

By using Galerkin's method, where the weighting function equals the basis function, and forming the inner product which is defined as

$$< \overline{f}, \overline{g} > \equiv \int_S dS\, \overline{f} \cdot \overline{g} \qquad (A.65)$$

we get functions of the form

$$< \overline{E}_{inc}, \overline{f}_m > = < \overline{A}, \overline{f}_m > + < \nabla\Phi, \overline{f}_m > \qquad (A.66)$$

By the vector identity $\nabla \cdot (\Phi\overline{A}) = \overline{A} \cdot \nabla\Phi + \Phi\nabla \cdot \overline{A}$, the second term in (A.66) can be rewritten as

$$< \nabla\Phi, \overline{f}_m > = \int_S dS \nabla \cdot (\Phi \overline{f}_m) - \int_S dS \Phi(\nabla \cdot \overline{f}_m). \qquad (A.67)$$

By the two-dimensional divergence theorem, $\int_S dS \nabla \cdot \overline{A} = \oint_C dl\, \overline{A} \cdot \hat{n}$, the first term in (A.67) vanishes due to the fact that the normal component of $\overline{f}_m(\bar{r})$ at the edges of S is zero. Using (A.61), the remaining integral in (A.67) is approximated as follows:

$$\int_S dS\,\Phi(\nabla_s \cdot \overline{f}_m) = l_m\left[\frac{1}{A_m^+}\int_{T_m^+} dS\,\Phi - \frac{1}{A_m^-}\int_{T_m^-} dS\,\Phi\right]$$
$$\simeq l_m[\Phi(\bar{r}_m^{c+}) - \Phi(\bar{r}_m^{c-})] \qquad (A.68)$$

where the average of Φ over each triangle is approximated by the value of Φ at the triangle centroid. Similarly,

$$< \begin{Bmatrix} \overline{E}_{inc} \\ \overline{A} \end{Bmatrix}, \overline{f}_m > = l_m\left[\frac{1}{2A_m^+}\int_{T_m^+} dS \begin{Bmatrix} \overline{E}_{inc} \\ \overline{A} \end{Bmatrix} \cdot \bar{\rho}_m^+ + \frac{1}{2A_m^-}\int_{T_m^-} dS \begin{Bmatrix} \overline{E}_{inc} \\ \overline{A} \end{Bmatrix} \cdot \bar{\rho}_m^-\right]$$
$$\simeq \frac{l_m}{2}\left[\begin{Bmatrix} \overline{E}_{inc}(\bar{r}_m^{c+}) \\ \overline{A}(\bar{r}_m^{c+}) \end{Bmatrix} \cdot \bar{\rho}_m^{c+} + \begin{Bmatrix} \overline{E}_{inc}(\bar{r}_m^{c-}) \\ \overline{A}(\bar{r}_m^{c-}) \end{Bmatrix} \cdot \bar{\rho}_m^{c-}\right] \qquad (A.69)$$

Using the approach outlined above, (A.62) becomes (with $\overline{E}_m^{\pm} = \overline{E}_{inc}(\bar{r}_m^{c\pm})$ and $R_m^{\pm} = |\bar{r}_m^{c\pm} - \bar{r}'|$ and where m is defined over the surface of the coating)

$$l_m\left[\overline{E}_m^+ \cdot \frac{\bar{\rho}_m^{c+}}{2} + \overline{E}_m^- \cdot \frac{\bar{\rho}_m^{c-}}{2}\right] = l_m\left[\overline{A}_{mn}^+ \cdot \frac{\bar{\rho}_m^{c+}}{2} + \overline{A}_{mn}^- \cdot \frac{\bar{\rho}_m^{c-}}{2} + \Phi_{mn}^- - \Phi_{mn}^+\right] \qquad (A.70)$$

where

$$\overline{A}_{mn}^{\pm} = -\int_{S_1} dS_1 i\omega\mu_0 I_n \overline{f}_n(\bar{r}')\frac{e^{ik_0 R_m^{\pm}}}{4\pi R_m^{\pm}} - \int_{S_1} dS_1 i\omega\mu I_n \overline{f}_n(\bar{r}')\frac{e^{ik_1 R_m^{\pm}}}{4\pi R_m^{\pm}}$$
$$+ \int_{S_1} dS_1 K_{n'} \overline{f}_{n'}(\bar{r}') \times \nabla'\left(\frac{e^{ik_0 R_m^{\pm}}}{4\pi R_m^{\pm}}\right) + \int_{S_1} dS_1 K_{n'} \overline{f}_{n'}(\bar{r}') \times \nabla'\left(\frac{e^{ik_1 R_m^{\pm}}}{4\pi R_m^{\pm}}\right)$$
$$+ \int_{S_2} dS_2 i\omega\mu L_{n''} \overline{f}_{n''}(\bar{r}')\frac{e^{ik_1 R_m^{\pm}}}{4\pi R_m^{\pm}} \qquad (A.71)$$

and

$$\Phi_{mn}^{\pm} = -\int_{S_1} dS_1 \frac{i\omega\mu_0}{k_0^2}\left(\nabla'_s \cdot I_n \overline{f}_n(\bar{r}')\right)\frac{e^{ik_0 R_m^{\pm}}}{4\pi R_m^{\pm}}$$
$$- \int_{S_1} dS_1 \frac{i\omega\mu}{k_1^2}\left(\nabla'_s \cdot I_n \overline{f}_n(\bar{r}')\right)\frac{e^{ik_1 R_m^{\pm}}}{4\pi R_m^{\pm}}$$
$$+ \int_{S_2} dS_2 \frac{i\omega\mu}{k_1^2}\left(\nabla'_s \cdot L_{n''} \overline{f}_{n''}(\bar{r}')\right)\frac{e^{ik_1 R_m^{\pm}}}{4\pi R_m^{\pm}}. \qquad (A.72)$$

Similarly, (A.63) becomes (with $\overline{H}^{\pm}_{m'} = \overline{H}_{inc}(\bar{r}^{c\pm}_{m'})$ and $R^{\pm}_{m'} = |\bar{r}^{c\pm}_{m'} - \bar{r}'|$ and where m' is defined over the surface of the coating)

$$l_{m'}\left[\overline{H}^{+}_{m'} \cdot \frac{\bar{\rho}^{c+}_{m'}}{2} + \overline{H}^{-}_{m'} \cdot \frac{\bar{\rho}^{c-}_{m'}}{2}\right] = l_{m'}\left[\overline{B}^{+}_{m'n} \cdot \frac{\bar{\rho}^{c+}_{m'}}{2} + \overline{B}^{-}_{m'n} \cdot \frac{\bar{\rho}^{c-}_{m'}}{2} + \Theta^{-}_{m'n} - \Theta^{+}_{m'n}\right] \quad (A.73)$$

where

$$\begin{aligned}\overline{B}^{\pm}_{m'n} = &- \int_{S_1} dS_1 I_n \overline{f}_n(\bar{r}') \times \nabla'\left(\frac{e^{ik_0 R^{\pm}_{m'}}}{4\pi R^{\pm}_{m'}}\right) - \int_{S_1} dS_1 I_n \overline{f}_n(\bar{r}') \times \nabla'\left(\frac{e^{ik_1 R^{\pm}_{m'}}}{4\pi R^{\pm}_{m'}}\right) \\ &- \int_{S_1} dS_1 i\omega\epsilon_0 K_{n'} \overline{f}_{n'}(\bar{r}') \frac{e^{ik_0 R^{\pm}_{m'}}}{4\pi R^{\pm}_{m'}} - \int_{S_1} dS_1 i\omega\epsilon K_{n'} \overline{f}_{n'}(\bar{r}') \frac{e^{ik_1 R^{\pm}_{m'}}}{4\pi R^{\pm}_{m'}} \\ &+ \int_{S_2} dS_2 L_{n''} \overline{f}_{n''}(\bar{r}') \times \nabla'\left(\frac{e^{ik_1 R^{\pm}_{m'}}}{4\pi R^{\pm}_{m'}}\right) \end{aligned} \quad (A.74)$$

and

$$\begin{aligned}\Theta^{\pm}_{m'n} = &- \int_{S_1} dS_1 \frac{i\omega\epsilon_0}{k_0^2} \left(\nabla'_s \cdot K_{n'} \overline{f}_{n'}(\bar{r}')\right) \frac{e^{ik_0 R^{\pm}_{m'}}}{4\pi R^{\pm}_{m'}} \\ &- \int_{S_1} dS_1 \frac{i\omega\epsilon}{k_1^2} \left(\nabla'_s \cdot K_{n'} \overline{f}_{n'}(\bar{r}')\right) \frac{e^{ik_1 R^{\pm}_{m'}}}{4\pi R^{\pm}_{m'}}. \end{aligned} \quad (A.75)$$

Also, (A.64) becomes (with $R^{\pm}_{m''} = |\bar{r}^{c\pm}_{m''} - \bar{r}'|$ and where m'' is defined over the surface of the perfect conductor)

$$\bar{0}_{m''} = l_{m''}\left[\overline{C}^{+}_{m''n} \cdot \frac{\bar{\rho}^{c+}_{m''}}{2} + \overline{C}^{-}_{m''n} \cdot \frac{\bar{\rho}^{c-}_{m''}}{2} + \Psi^{-}_{m''n} - \Psi^{+}_{m''n}\right] \quad (A.76)$$

where

$$\begin{aligned}\overline{C}^{\pm}_{m''n} = &- \int_{S_1} dS_1 i\omega\mu I_n \overline{f}_n(\bar{r}') \frac{e^{ik_1 R^{\pm}_{m''}}}{4\pi R^{\pm}_{m''}} \\ &+ \int_{S_1} dS_1 K_{n'} \overline{f}_{n'}(\bar{r}') \times \nabla'\left(\frac{e^{ik_1 R^{\pm}_{m''}}}{4\pi R^{\pm}_{m''}}\right) \\ &+ \int_{S_2} dS_2 i\omega\mu L_{n''} \overline{f}_{n''}(\bar{r}') \frac{e^{ik_1 R^{\pm}_{m''}}}{4\pi R^{\pm}_{m''}} \end{aligned} \quad (A.77)$$

and

$$\Psi^{\pm}_{m''n} = -\int_{S_1} dS_1 \frac{i\omega\mu}{k_1^2}\left(\nabla'_s \cdot I_n \overline{f}_n(\bar{r}')\right)\frac{e^{ik_1 R^{\pm}_{m''}}}{4\pi R^{\pm}_{m''}} + \int_{S_2} dS_2 \frac{i\omega\mu}{k_1^2}\left(\nabla'_s \cdot L_{n''} \overline{f}_{n''}(\bar{r}')\right)\frac{e^{ik_1 R^{\pm}_{m''}}}{4\pi R^{\pm}_{m''}}. \quad (A.78)$$

Substituting (A.71) and (A.72), (A.70) becomes

$$\begin{aligned} l_m\left[\overline{E}^{+}_m \cdot \frac{\bar{\rho}^{c+}_m}{2} + \overline{E}^{-}_m \cdot \frac{\bar{\rho}^{c-}_m}{2}\right] = l_m\Bigg[& \frac{\bar{\rho}^{c+}_m}{2} \cdot \Bigg\{ -\int_{T^{\pm}_n} d\bar{r}' i\omega\mu_0 I_n \frac{l_n}{2A^{\pm}_n}\bar{\rho}^{\pm}_n \frac{e^{ik_0 R^{+}_m}}{4\pi R^{+}_m} \\ & - \int_{T^{\pm}_n} d\bar{r}' i\omega\mu I_n \frac{l_n}{2A^{\pm}_n}\bar{\rho}^{\pm}_n \frac{e^{ik_1 R^{+}_m}}{4\pi R^{+}_m} + \int_{T^{\pm}_{n'}} d\bar{r}' K_{n'} \frac{l_{n'}}{2A^{\pm}_{n'}}\bar{\rho}^{\pm}_{n'} \times \nabla'\left(\frac{e^{ik_0 R^{+}_m}}{4\pi R^{+}_m}\right) \\ & + \int_{T^{\pm}_{n'}} d\bar{r}' K_{n'} \frac{l_{n'}}{2A^{\pm}_{n'}}\bar{\rho}^{\pm}_{n'} \times \nabla'\left(\frac{e^{ik_1 R^{+}_m}}{4\pi R^{+}_m}\right) + \int_{T^{\pm}_{n''}} d\bar{r}' i\omega\mu L_{n''} \frac{l_{n''}}{2A^{\pm}_{n''}}\bar{\rho}^{\pm}_{n''} \frac{e^{ik_1 R^{+}_m}}{4\pi R^{+}_m} \Bigg\} \\ & + \frac{\bar{\rho}^{c-}_m}{2} \cdot \Bigg\{ -\int_{T^{\pm}_n} d\bar{r}' i\omega\mu_0 I_n \frac{l_n}{2A^{\pm}_n}\bar{\rho}^{\pm}_n \frac{e^{ik_0 R^{-}_m}}{4\pi R^{-}_m} - \int_{T^{\pm}_n} d\bar{r}' i\omega\mu I_n \frac{l_n}{2A^{\pm}_n}\bar{\rho}^{\pm}_n \frac{e^{ik_1 R^{-}_m}}{4\pi R^{-}_m} \\ & + \int_{T^{\pm}_{n'}} d\bar{r}' K_{n'} \frac{l_{n'}}{2A^{\pm}_{n'}}\bar{\rho}^{\pm}_{n'} \times \nabla'\left(\frac{e^{ik_0 R^{-}_m}}{4\pi R^{-}_m}\right) + \int_{T^{\pm}_{n'}} d\bar{r}' K_{n'} \frac{l_{n'}}{2A^{\pm}_{n'}}\bar{\rho}^{\pm}_{n'} \times \nabla'\left(\frac{e^{ik_1 R^{-}_m}}{4\pi R^{-}_m}\right) \\ & + \int_{T^{\pm}_{n''}} d\bar{r}' i\omega\mu L_{n''} \frac{l_{n''}}{2A^{\pm}_{n''}}\bar{\rho}^{\pm}_{n''} \frac{e^{ik_1 R^{-}_m}}{4\pi R^{-}_m} \Bigg\} \\ & + \Bigg\{ + \int_{T^{\pm}_n} d\bar{r}' \frac{i\omega\mu_0}{k_0^2} I_n\left(\pm\frac{l_n}{A^{\pm}_n}\right)\frac{e^{ik_0 R^{+}_m}}{4\pi R^{+}_m} + \int_{T^{\pm}_n} d\bar{r}' \frac{i\omega\mu}{k_1^2} I_n\left(\pm\frac{l_n}{A^{\pm}_n}\right)\frac{e^{ik_1 R^{+}_m}}{4\pi R^{+}_m} \\ & - \int_{T^{\pm}_{n''}} d\bar{r}' \frac{i\omega\mu}{k_1^2} L_{n''}\left(\pm\frac{l_{n''}}{A^{\pm}_{n''}}\right)\frac{e^{ik_1 R^{+}_m}}{4\pi R^{+}_m} \Bigg\} - \Bigg\{ + \int_{T^{\pm}_n} d\bar{r}' \frac{i\omega\mu_0}{k_0^2} I_n\left(\pm\frac{l_n}{A^{\pm}_n}\right)\frac{e^{ik_0 R^{-}_m}}{4\pi R^{-}_m} \\ & + \int_{T^{\pm}_n} d\bar{r}' \frac{i\omega\mu}{k_1^2} I_n\left(\pm\frac{l_n}{A^{\pm}_n}\right)\frac{e^{ik_1 R^{-}_m}}{4\pi R^{-}_m} - \int_{T^{\pm}_{n''}} d\bar{r}' \frac{i\omega\mu}{k_1^2} L_{n''}\left(\pm\frac{l_{n''}}{A^{\pm}_{n''}}\right)\frac{e^{ik_1 R^{-}_m}}{4\pi R^{-}_m} \Bigg\}\Bigg]. \end{aligned} \quad (A.79)$$

Rearranging (A.79) into a more compact form, it becomes

$$\begin{aligned} & l_m\left[\overline{E}^{+}_m \cdot \frac{\bar{\rho}^{c+}_m}{2} + \overline{E}^{-}_m \cdot \frac{\bar{\rho}^{c-}_m}{2}\right] = \\ & \qquad I_n\left[-\frac{i\omega\mu_0}{4\pi}\frac{l_m l_n}{4A^{\pm}_n}\bar{\rho}^{c\pm}_m \cdot \int_{T^{\pm}_n} d\bar{r}' \bar{\rho}^{\pm}_n \frac{e^{ik_0 R^{\pm}_m}}{R^{\pm}_m} \pm \frac{i}{4\pi\omega\epsilon_0}\frac{l_m l_n}{A^{\pm}_n}\int_{T^{\pm}_n} d\bar{r}' \frac{e^{ik_0 R^{\pm}_m}}{R^{\pm}_m}\right] \end{aligned}$$

$$
\begin{aligned}
&+I_n\left[-\frac{i\omega\mu}{4\pi}\frac{l_m l_n}{4A_n^{\pm}}\bar{\rho}_m^{c\pm}\cdot\int_{T_n^{\pm}}d\bar{r}'\,\bar{\rho}_n^{\pm}\frac{e^{ik_1R_m^{\pm}}}{R_m^{\pm}}\pm\frac{i}{4\pi\omega\epsilon}\frac{l_m l_n}{A_n^{\pm}}\int_{T_n^{\pm}}d\bar{r}'\frac{e^{ik_1R_m^{\pm}}}{R_m^{\pm}}\right]\\
&+K_{n'}\left[\frac{1}{4\pi}\frac{l_m l_{n'}}{4A_{n'}^{\pm}}\bar{\rho}_m^{c\pm}\cdot\int_{T_{n'}^{\pm}}d\bar{r}'\,\bar{\rho}_{n'}^{\pm}\times\nabla'\Big(\frac{e^{ik_0R_m^{\pm}}}{R_m^{\pm}}\Big)\right]\\
&+K_{n'}\left[\frac{1}{4\pi}\frac{l_m l_{n'}}{4A_{n'}^{\pm}}\bar{\rho}_m^{c\pm}\cdot\int_{T_{n'}^{\pm}}d\bar{r}'\,\bar{\rho}_{n'}^{\pm}\times\nabla'\Big(\frac{e^{ik_1R_m^{\pm}}}{R_m^{\pm}}\Big)\right]\\
&+L_{n''}\left[\frac{i\omega\mu}{4\pi}\frac{l_m l_{n''}}{4A_{n''}^{\pm}}\bar{\rho}_m^{c\pm}\cdot\int_{T_{n''}^{\pm}}d\bar{r}'\,\bar{\rho}_{n''}^{\pm}\frac{e^{ik_1R_m^{\pm}}}{R_m^{\pm}}\right.\\
&\qquad\left.\pm\frac{-i}{4\pi\omega\epsilon}\frac{l_m l_{n''}}{A_{n''}^{\pm}}\int_{T_{n''}^{\pm}}d\bar{r}'\frac{e^{ik_1R_m^{\pm}}}{R_m^{\pm}}\right]. \qquad (A.80)
\end{aligned}
$$

Substituting (A.74) and (A.75), (A.73) becomes

$$
\begin{aligned}
l_{m'}\Big[\overline{H}_{m'}^{+}\cdot\frac{\bar{\rho}_{m'}^{c+}}{2}+\overline{H}_{m'}^{-}\cdot\frac{\bar{\rho}_{m'}^{c-}}{2}\Big] &= l_{m'}\left[\frac{\bar{\rho}_{m'}^{c+}}{2}\cdot\left\{-\int_{T_n^{\pm}}d\bar{r}'\,I_n\frac{l_n}{2A_n^{\pm}}\bar{\rho}_n^{\pm}\times\nabla'\Big(\frac{e^{ik_0R_{m'}^{+}}}{4\pi R_{m'}^{+}}\Big)\right.\right.\\
&-\int_{T_n^{\pm}}d\bar{r}'\,I_n\frac{l_n}{2A_n^{\pm}}\bar{\rho}_n^{\pm}\times\nabla'\Big(\frac{e^{ik_1R_{m'}^{+}}}{4\pi R_{m'}^{+}}\Big)-\int_{T_{n'}^{\pm}}d\bar{r}'\,i\omega\epsilon_0K_{n'}\frac{l_{n'}}{2A_{n'}^{\pm}}\bar{\rho}_{n'}^{\pm}\frac{e^{ik_0R_{m'}^{+}}}{4\pi R_{m'}^{+}}\\
&\left.-\int_{T_{n'}^{\pm}}d\bar{r}'\,i\omega\epsilon K_{n'}\frac{l_{n'}}{2A_{n'}^{\pm}}\bar{\rho}_{n'}^{\pm}\frac{e^{ik_1R_{m'}^{+}}}{4\pi R_{m'}^{+}}+\int_{T_{n''}^{\pm}}d\bar{r}'\,L_{n''}\frac{l_{n''}}{2A_{n''}^{\pm}}\bar{\rho}_{n''}^{\pm}\times\nabla'\Big(\frac{e^{ik_1R_{m'}^{+}}}{4\pi R_{m'}^{+}}\Big)\right\}\\
&+\frac{\bar{\rho}_{m'}^{c-}}{2}\cdot\left\{-\int_{T_n^{\pm}}d\bar{r}'\,I_n\frac{l_n}{2A_n^{\pm}}\bar{\rho}_n^{\pm}\times\nabla'\Big(\frac{e^{ik_0R_{m'}^{-}}}{4\pi R_{m'}^{-}}\Big)-\int_{T_n^{\pm}}d\bar{r}'\,I_n\frac{l_n}{2A_n^{\pm}}\bar{\rho}_n^{\pm}\times\nabla'\Big(\frac{e^{ik_1R_{m'}^{-}}}{4\pi R_{m'}^{-}}\Big)\right.\\
&-\int_{T_{n'}^{\pm}}d\bar{r}'\,i\omega\epsilon_0K_{n'}\frac{l_{n'}}{2A_{n'}^{\pm}}\bar{\rho}_{n'}^{\pm}\frac{e^{ik_0R_{m'}^{-}}}{4\pi R_{m'}^{-}}-\int_{T_{n'}^{\pm}}d\bar{r}'\,i\omega\epsilon K_{n'}\frac{l_{n'}}{2A_{n'}^{\pm}}\bar{\rho}_{n'}^{\pm}\frac{e^{ik_1R_{m'}^{-}}}{4\pi R_{m'}^{-}}\\
&\left.+\int_{T_{n''}^{\pm}}d\bar{r}'\,L_{n''}\frac{l_{n''}}{2A_{n''}^{\pm}}\bar{\rho}_{n''}^{\pm}\times\nabla'\Big(\frac{e^{ik_1R_{m'}^{-}}}{4\pi R_{m'}^{-}}\Big)\right\}\\
&+\left\{\int_{T_{n'}^{\pm}}d\bar{r}'\frac{i\omega\epsilon_0}{k_0^2}K_{n'}\Big(\pm\frac{l_{n'}}{A_{n'}^{\pm}}\Big)\frac{e^{ik_0R_{m'}^{+}}}{4\pi R_{m'}^{+}}+\int_{T_{n'}^{\pm}}d\bar{r}'\frac{i\omega\epsilon}{k_1^2}K_{n'}\Big(\pm\frac{l_{n'}}{A_{n'}^{\pm}}\Big)\frac{e^{ik_1R_{m'}^{+}}}{4\pi R_{m'}^{+}}\right\}\\
&-\left\{\int_{T_{n'}^{\pm}}d\bar{r}'\frac{i\omega\epsilon_0}{k_0^2}K_{n'}\Big(\pm\frac{l_{n'}}{A_{n'}^{\pm}}\Big)\frac{e^{ik_0R_{m'}^{-}}}{4\pi R_{m'}^{-}}+\int_{T_{n'}^{\pm}}d\bar{r}'\frac{i\omega\epsilon}{k_1^2}K_{n'}\Big(\pm\frac{l_{n'}}{A_{n'}^{\pm}}\Big)\frac{e^{ik_1R_{m'}^{-}}}{4\pi R_{m'}^{-}}\right\}\Big]. \qquad (A.81)
\end{aligned}
$$

Rearranging (A.81) into a more compact form, it becomes

$$
l_{m'}\Big[\overline{H}_{m'}^{+}\cdot\frac{\bar{\rho}_{m'}^{c+}}{2}+\overline{H}_{m'}^{-}\cdot\frac{\bar{\rho}_{m'}^{c-}}{2}\Big]=
$$

$$
\begin{aligned}
&I_n\left[-\frac{1}{4\pi}\frac{l_{m'}l_n}{4A_n^{\pm}}\bar{\rho}_{m'}^{c\pm}\cdot\int_{T_n^{\pm}}d\bar{r}'\bar{\rho}_n^{\pm}\times\nabla'\Big(\frac{e^{ik_0R_{m'}^{\pm}}}{R_{m'}^{\pm}}\Big)\right]\\
&+I_n\left[-\frac{1}{4\pi}\frac{l_{m'}l_n}{4A_n^{\pm}}\bar{\rho}_{m'}^{c\pm}\cdot\int_{T_n^{\pm}}d\bar{r}'\bar{\rho}_n^{\pm}\times\nabla'\Big(\frac{e^{ik_1R_{m'}^{\pm}}}{R_{m'}^{\pm}}\Big)\right]\\
&+K_{n'}\left[-\frac{i\omega\epsilon_0}{4\pi}\frac{l_{m'}l_{n'}}{4A_{n'}^{\pm}}\bar{\rho}_{m'}^{c\pm}\cdot\int_{T_{n'}^{\pm}}d\bar{r}'\bar{\rho}_{n'}^{\pm}\frac{e^{ik_0R_{m'}^{\pm}}}{R_{m'}^{\pm}}\pm\frac{i}{4\pi\omega\mu_0}\frac{l_{m'}l_{n'}}{A_{n'}^{\pm}}\int_{T_{n'}^{\pm}}d\bar{r}'\frac{e^{ik_0R_{m'}^{\pm}}}{R_{m'}^{\pm}}\right]\\
&+K_{n'}\left[-\frac{i\omega\epsilon}{4\pi}\frac{l_{m'}l_{n'}}{4A_{n'}^{\pm}}\bar{\rho}_{m'}^{c\pm}\cdot\int_{T_{n'}^{\pm}}d\bar{r}'\bar{\rho}_{n'}^{\pm}\frac{e^{ik_1R_{m'}^{\pm}}}{R_{m'}^{\pm}}\pm\frac{i}{4\pi\omega\mu}\frac{l_{m'}l_{n'}}{A_{n'}^{\pm}}\int_{T_{n'}^{\pm}}d\bar{r}'\frac{e^{ik_1R_{m'}^{\pm}}}{R_{m'}^{\pm}}\right]\\
&+L_{n''}\left[\frac{1}{4\pi}\frac{l_{m'}l_{n''}}{4A_{n''}^{\pm}}\bar{\rho}_{m'}^{c\pm}\cdot\int_{T_{n''}^{\pm}}d\bar{r}'\bar{\rho}_{n''}^{\pm}\times\nabla'\Big(\frac{e^{ik_1R_{m'}^{\pm}}}{R_{m'}^{\pm}}\Big)\right]. \qquad (A.82)
\end{aligned}
$$

Substituting (A.77) and (A.78), (A.76) becomes

$$
\begin{aligned}
\bar{0}_{m''} =& l_{m''}\left[\frac{\bar{\rho}_{m''}^{c+}}{2}\cdot\left\{-\int_{T_n^{\pm}}d\bar{r}'i\omega\mu I_n\frac{l_n}{2A_n^{\pm}}\bar{\rho}_n^{\pm}\frac{e^{ik_1R_{m''}^{+}}}{4\pi R_{m''}^{+}}\right.\right.\\
&\left.+\int_{T_{n'}^{\pm}}d\bar{r}'K_{n'}\frac{l_{n'}}{2A_{n'}^{\pm}}\bar{\rho}_{n'}^{\pm}\times\nabla'\Big(\frac{e^{ik_1R_{m''}^{+}}}{4\pi R_{m''}^{+}}\Big)+\int_{T_{n''}^{\pm}}d\bar{r}'i\omega\mu L_{n''}\frac{l_{n''}}{2A_{n''}^{\pm}}\bar{\rho}_{n''}^{\pm}\frac{e^{ik_1R_{m''}^{+}}}{4\pi R_{m''}^{+}}\right\}\\
&+\frac{\bar{\rho}_{m''}^{c-}}{2}\cdot\left\{-\int_{T_n^{\pm}}d\bar{r}'i\omega\mu I_n\frac{l_n}{2A_n^{\pm}}\bar{\rho}_n^{\pm}\frac{e^{ik_1R_{m''}^{-}}}{4\pi R_{m''}^{-}}+\int_{T_{n'}^{\pm}}d\bar{r}'K_{n'}\frac{l_{n'}}{2A_{n'}^{\pm}}\bar{\rho}_{n'}^{\pm}\times\nabla'\Big(\frac{e^{ik_1R_{m''}^{-}}}{4\pi R_{m''}^{-}}\Big)\right.\\
&\left.+\int_{T_{n''}^{\pm}}d\bar{r}'i\omega\mu L_{n''}\frac{l_{n''}}{2A_{n''}^{\pm}}\bar{\rho}_{n''}^{\pm}\frac{e^{ik_1R_{m''}^{-}}}{4\pi R_{m''}^{-}}\right\}\\
&+\left\{\int_{T_n^{\pm}}d\bar{r}'\frac{i\omega\mu}{k_1^2}I_n\Big(\pm\frac{l_n}{A_n^{\pm}}\Big)\frac{e^{ik_1R_{m''}^{+}}}{4\pi R_{m''}^{+}}-\int_{T_{n''}^{\pm}}d\bar{r}'\frac{i\omega\mu}{k_1^2}L_{n''}\Big(\pm\frac{l_{n''}}{A_{n''}^{\pm}}\Big)\frac{e^{ik_1R_{m''}^{+}}}{4\pi R_{m''}^{+}}\right\}\\
&-\left\{\int_{T_n^{\pm}}d\bar{r}'\frac{i\omega\mu}{k_1^2}I_n\Big(\pm\frac{l_n}{A_n^{\pm}}\Big)\frac{e^{ik_1R_{m''}^{-}}}{4\pi R_{m''}^{-}}-\int_{T_{n''}^{\pm}}d\bar{r}'\frac{i\omega\mu}{k_1^2}L_{n''}\Big(\pm\frac{l_{n''}}{A_{n''}^{\pm}}\Big)\frac{e^{ik_1R_{m''}^{-}}}{4\pi R_{m''}^{-}}\right\}\Big]. \qquad (A.83)
\end{aligned}
$$

Rearranging (A.83) into a more compact form, it becomes

$$
\begin{aligned}
\bar{0}_{m''} =& I_n\left[-\frac{i\omega\mu}{4\pi}\frac{l_{m''}l_n}{4A_n^{\pm}}\bar{\rho}_{m''}^{c\pm}\cdot\int_{T_n^{\pm}}d\bar{r}'\bar{\rho}_n^{\pm}\frac{e^{ik_1R_{m''}^{\pm}}}{R_{m''}^{\pm}}\pm\frac{i}{4\pi\omega\epsilon}\frac{l_{m''}l_n}{A_n^{\pm}}\int_{T_n^{\pm}}d\bar{r}'\frac{e^{ik_1R_{m''}^{\pm}}}{R_{m''}^{\pm}}\right]\\
&+K_{n'}\left[\frac{1}{4\pi}\frac{l_{m''}l_{n'}}{4A_{n'}^{\pm}}\bar{\rho}_{m''}^{c\pm}\cdot\int_{T_{n'}^{\pm}}d\bar{r}'\bar{\rho}_{n'}^{\pm}\times\nabla'\Big(\frac{e^{ik_1R_{m''}^{\pm}}}{R_{m''}^{\pm}}\Big)\right]\\
&+L_{n''}\left[\frac{i\omega\mu}{4\pi}\frac{l_{m''}l_{n''}}{4A_{n''}^{\pm}}\bar{\rho}_{m''}^{c\pm}\cdot\int_{T_{n''}^{\pm}}d\bar{r}'\bar{\rho}_{n''}^{\pm}\frac{e^{ik_1R_{m''}^{\pm}}}{R_{m''}^{\pm}}\right.
\end{aligned}
$$

$$\pm \frac{-i}{4\pi\omega\epsilon}\frac{l_{m''}l_{n''}}{A^{\pm}_{n''}}\int_{T^{\pm}_{n''}} d\bar{r}'\frac{e^{ik_1R^{\pm}_{m''}}}{R^{\pm}_{m''}}\Big]. \tag{A.84}$$

By using the fact that

$$\nabla'\Big(\frac{e^{ikR^{\pm}_m}}{R^{\pm}_m}\Big) = (\bar{r}^{c\pm}_m - \bar{r}')(1-ikR^{\pm}_m)\frac{e^{ikR^{\pm}_m}}{(R^{\pm}_m)^3} \tag{A.85}$$

where $R^{\pm}_m = |\bar{r}^{c\pm}_m - \bar{r}'|$, (A.80) becomes

$$\begin{aligned}
l_m\Big[\overline{E}^{+}_m\cdot\frac{\bar{\rho}^{c+}_m}{2}+\overline{E}^{-}_m\cdot\frac{\bar{\rho}^{c-}_m}{2}\Big] = \\
&I_n\Big[-\frac{i\omega\mu_0}{4\pi}\frac{l_ml_n}{4A^{\pm}_n}\bar{\rho}^{c\pm}_m\cdot\int_{T^{\pm}_n}d\bar{r}'\bar{\rho}^{\pm}_n\frac{e^{ik_0R^{\pm}_m}}{R^{\pm}_m}\pm\frac{i}{4\pi\omega\epsilon_0}\frac{l_ml_n}{A^{\pm}_n}\int_{T^{\pm}_n}d\bar{r}'\frac{e^{ik_0R^{\pm}_m}}{R^{\pm}_m}\Big]\\
+&I_n\Big[-\frac{i\omega\mu}{4\pi}\frac{l_ml_n}{4A^{\pm}_n}\bar{\rho}^{c\pm}_m\cdot\int_{T^{\pm}_n}d\bar{r}'\bar{\rho}^{\pm}_n\frac{e^{ik_1R^{\pm}_m}}{R^{\pm}_m}\pm\frac{i}{4\pi\omega\epsilon}\frac{l_ml_n}{A^{\pm}_n}\int_{T^{\pm}_n}d\bar{r}'\frac{e^{ik_1R^{\pm}_m}}{R^{\pm}_m}\Big]\\
+&K_{n'}\Big[\frac{1}{4\pi}\frac{l_ml_{n'}}{4A^{\pm}_{n'}}\bar{\rho}^{c\pm}_m\cdot\int_{T^{\pm}_{n'}}d\bar{r}'\bar{\rho}^{\pm}_{n'}\times(\bar{r}^{c\pm}_m-\bar{r}')(1-ik_0R^{\pm}_m)\frac{e^{ik_0R^{\pm}_m}}{(R^{\pm}_m)^3}\Big]\\
+&K_{n'}\Big[\frac{1}{4\pi}\frac{l_ml_{n'}}{4A^{\pm}_{n'}}\bar{\rho}^{c\pm}_m\cdot\int_{T^{\pm}_{n'}}d\bar{r}'\bar{\rho}^{\pm}_{n'}\times(\bar{r}^{c\pm}_m-\bar{r}')(1-ik_1R^{\pm}_m)\frac{e^{ik_1R^{\pm}_m}}{(R^{\pm}_m)^3}\Big]\\
+&L_{n''}\Big[\frac{i\omega\mu}{4\pi}\frac{l_ml_{n''}}{4A^{\pm}_{n''}}\bar{\rho}^{c\pm}_m\cdot\int_{T^{\pm}_{n''}}d\bar{r}'\bar{\rho}^{\pm}_{n''}\frac{e^{ik_1R^{\pm}_m}}{R^{\pm}_m}\\
&\pm\frac{-i}{4\pi\omega\epsilon}\frac{l_ml_{n''}}{A^{\pm}_{n''}}\int_{T^{\pm}_{n''}}d\bar{r}'\frac{e^{ik_1R^{\pm}_m}}{R^{\pm}_m}\Big].
\end{aligned}\tag{A.86}$$

Similarly, (A.82) becomes

$$\begin{aligned}
l_{m'}\Big[\overline{H}^{+}_{m'}\cdot\frac{\bar{\rho}^{c+}_{m'}}{2}+\overline{H}^{-}_{m'}\cdot\frac{\bar{\rho}^{c-}_{m'}}{2}\Big] = \\
&I_n\Big[-\frac{1}{4\pi}\frac{l_{m'}l_n}{4A^{\pm}_n}\bar{\rho}^{c\pm}_{m'}\cdot\int_{T^{\pm}_n}d\bar{r}'\bar{\rho}^{\pm}_n\times(\bar{r}^{c\pm}_{m'}-\bar{r}')(1-ik_0R^{\pm}_{m'})\frac{e^{ik_0R^{\pm}_{m'}}}{(R^{\pm}_{m'})^3}\Big]\\
+&I_n\Big[-\frac{1}{4\pi}\frac{l_{m'}l_n}{4A^{\pm}_n}\bar{\rho}^{c\pm}_{m'}\int_{T^{\pm}_n}d\bar{r}'\bar{\rho}^{\pm}_n\times(\bar{r}^{c\pm}_{m'}-\bar{r}')(1-ik_1R^{\pm}_{m'})\frac{e^{ik_1R^{\pm}_{m'}}}{(R^{\pm}_{m'})^3}\Big]\\
+&K_{n'}\Big[-\frac{i\omega\epsilon_0}{4\pi}\frac{l_{m'}l_{n'}}{4A^{\pm}_{n'}}\bar{\rho}^{c\pm}_{m'}\cdot\int_{T^{\pm}_{n'}}d\bar{r}'\bar{\rho}^{\pm}_{n'}\frac{e^{ik_0R^{\pm}_{m'}}}{R^{\pm}_{m'}}\pm\frac{i}{4\pi\omega\mu_0}\frac{l_{m'}l_{n'}}{A^{\pm}_{n'}}\int_{T^{\pm}_{n'}}d\bar{r}'\frac{e^{ik_0R^{\pm}_{m'}}}{R^{\pm}_{m'}}\Big]
\end{aligned}$$

$$+K_{n'}\left[-\frac{i\omega\epsilon}{4\pi}\frac{l_{m'}l_{n'}}{4A^{\pm}_{n'}}\bar{\rho}^{c\pm}_{m'}\cdot\int_{T^{\pm}_{n'}}d\bar{r}'\,\bar{\rho}^{\pm}_{n'}\frac{e^{ik_1R^{\pm}_{m'}}}{R^{\pm}_{m'}}\pm\frac{i}{4\pi\omega\mu}\frac{l_{m'}l_{n'}}{A^{\pm}_{n'}}\int_{T^{\pm}_{n'}}d\bar{r}'\frac{e^{ik_1R^{\pm}_{m'}}}{R^{\pm}_{m'}}\right]$$

$$+L_{n''}\left[\frac{1}{4\pi}\frac{l_{m'}l_{n''}}{4A^{\pm}_{n''}}\bar{\rho}^{c\pm}_{m'}\cdot\int_{T^{\pm}_{n''}}d\bar{r}'\,\bar{\rho}^{\pm}_{n''}\times(\bar{r}^{c\pm}_{m'}-\bar{r}')(1-ik_1R^{\pm}_{m'})\frac{e^{ik_1R^{\pm}_{m'}}}{(R^{\pm}_{m'})^3}\right] \qquad (A.87)$$

and (A.84) becomes

$$\bar{0}_{m''}=I_n\left[-\frac{i\omega\mu}{4\pi}\frac{l_{m''}l_n}{4A^{\pm}_n}\bar{\rho}^{c\pm}_{m''}\cdot\int_{T^{\pm}_n}d\bar{r}'\,\bar{\rho}^{\pm}_n\frac{e^{ik_1R^{\pm}_{m''}}}{R^{\pm}_{m''}}\pm\frac{i}{4\pi\omega\epsilon}\frac{l_{m''}l_n}{A^{\pm}_n}\int_{T^{\pm}_n}d\bar{r}'\frac{e^{ik_1R^{\pm}_{m''}}}{R^{\pm}_{m''}}\right]$$

$$+K_{n'}\left[\frac{1}{4\pi}\frac{l_{m''}l_{n'}}{4A^{\pm}_{n'}}\bar{\rho}^{c\pm}_{m''}\cdot\int_{T^{\pm}_{n'}}d\bar{r}'\,\bar{\rho}^{\pm}_{n'}\times(\bar{r}^{c\pm}_{m''}-\bar{r}')(1-ik_1R^{\pm}_{m''})\frac{e^{ik_1R^{\pm}_{m''}}}{(R^{\pm}_{m''})^3}\right]$$

$$+L_{n''}\left[\frac{i\omega\mu}{4\pi}\frac{l_{m''}l_{n''}}{4A^{\pm}_{n''}}\bar{\rho}^{c\pm}_{m''}\cdot\int_{T^{\pm}_{n''}}d\bar{r}'\,\bar{\rho}^{\pm}_{n''}\frac{e^{ik_1R^{\pm}_{m''}}}{R^{\pm}_{m''}}\right.$$

$$\left.\pm\frac{-i}{4\pi\omega\epsilon}\frac{l_{m''}l_{n''}}{A^{\pm}_{n''}}\int_{T^{\pm}_{n''}}d\bar{r}'\frac{e^{ik_1R^{\pm}_{m''}}}{R^{\pm}_{m''}}\right]. \qquad (A.88)$$

Equations (A.86), (A.87), and (A.88) yield a system of equations which can be written in the following form:

$$\begin{pmatrix} l_m\left[\overline{E}^{+}_m\cdot\frac{\bar{\rho}^{c+}_m}{2}+\overline{E}^{-}_m\cdot\frac{\bar{\rho}^{c-}_m}{2}\right] \\ l_{m'}\left[\overline{H}^{+}_{m'}\cdot\frac{\bar{\rho}^{c+}_{m'}}{2}+\overline{H}^{-}_{m'}\cdot\frac{\bar{\rho}^{c-}_{m'}}{2}\right] \\ \bar{0}_{m''} \end{pmatrix}=\begin{pmatrix} Z_{mn} & Z_{mn'} & Z_{mn''} \\ Z_{m'n} & Z_{m'n'} & Z_{m'n''} \\ Z_{m''n} & Z_{m''n'} & Z_{m''n''} \end{pmatrix}\begin{pmatrix} I_n \\ K_{n'} \\ L_{n''} \end{pmatrix}. \qquad (A.89)$$

This equation has the form of $\overline{V}=\overline{\overline{Z}}\cdot\overline{I}$ where $\overline{V}$ represents the incident electric and magnetic field excitation vector at the boundary surfaces. $\overline{I}$ represents the unknown electric and magnetic surface current coefficients, and $\overline{\overline{Z}}$ represents the interaction matrix for all the triangular patches used to model the surfaces. The unknown surface current coefficients can be found by inverting the Z-matrix and multiplying the excitation vector by the inverted Z-matrix. The Z-matrix can now be written as

$$\begin{pmatrix} CZ1 & CZ2 & CZ3 \\ CZ4 & CZ5 & CZ6 \\ CZ7 & CZ8 & CZ9 \end{pmatrix} \qquad (A.90)$$

where the individual elements are

$$CZ1 = \left[-\frac{i\omega\mu_0}{4\pi} \frac{l_m l_n}{4A_n^{\pm}} \bar{\rho}_m^{c\pm} \cdot \int_{T_n^{\pm}} d\bar{r}' \bar{\rho}_n^{\pm} \frac{e^{ik_0 R_m^{\pm}}}{R_m^{\pm}} \pm \frac{i}{4\pi\omega\epsilon_0} \frac{l_m l_n}{A_n^{\pm}} \int_{T_n^{\pm}} d\bar{r}' \frac{e^{ik_0 R_m^{\pm}}}{R_m^{\pm}} \right]$$
$$+ \left[-\frac{i\omega\mu}{4\pi} \frac{l_m l_n}{4A_n^{\pm}} \bar{\rho}_m^{c\pm} \cdot \int_{T_n^{\pm}} d\bar{r}' \bar{\rho}_n^{\pm} \frac{e^{ik_1 R_m^{\pm}}}{R_m^{\pm}} \pm \frac{i}{4\pi\omega\epsilon} \frac{l_m l_n}{A_n^{\pm}} \int_{T_n^{\pm}} d\bar{r}' \frac{e^{ik_1 R_m^{\pm}}}{R_m^{\pm}} \right] \quad (A.91)$$

$$CZ2 = \left[\frac{1}{4\pi} \frac{l_m l_{n'}}{4A_{n'}^{\pm}} \bar{\rho}_m^{c\pm} \cdot \int_{T_{n'}^{\pm}} d\bar{r}' \bar{\rho}_{n'}^{\pm} \times (\bar{r}_m^{c\pm} - \bar{r}')(1 - ik_0 R_m^{\pm}) \frac{e^{ik_0 R_m^{\pm}}}{(R_m^{\pm})^3} \right]$$
$$+ \left[\frac{1}{4\pi} \frac{l_m l_{n'}}{4A_{n'}^{\pm}} \bar{\rho}_m^{c\pm} \cdot \int_{T_{n'}^{\pm}} d\bar{r}' \bar{\rho}_{n'}^{\pm} \times (\bar{r}_m^{c\pm} - \bar{r}')(1 - ik_1 R_m^{\pm}) \frac{e^{ik_1 R_m^{\pm}}}{(R_m^{\pm})^3} \right] \quad (A.92)$$

$$CZ3 = \left[\frac{i\omega\mu}{4\pi} \frac{l_m l_{n''}}{4A_{n''}^{\pm}} \bar{\rho}_m^{c\pm} \cdot \int_{T_{n''}^{\pm}} d\bar{r}' \bar{\rho}_{n''}^{\pm} \frac{e^{ik_1 R_m^{\pm}}}{R_m^{\pm}} \pm \frac{-i}{4\pi\omega\epsilon} \frac{l_m l_{n''}}{A_{n''}^{\pm}} \int_{T_{n''}^{\pm}} d\bar{r}' \frac{e^{ik_1 R_m^{\pm}}}{R_m^{\pm}} \right] \quad (A.93)$$

$$CZ4 = \left[-\frac{1}{4\pi} \frac{l_{m'} l_n}{4A_n^{\pm}} \bar{\rho}_{m'}^{c\pm} \cdot \int_{T_n^{\pm}} d\bar{r}' \bar{\rho}_n^{\pm} \times (\bar{r}_{m'}^{c\pm} - \bar{r}')(1 - ik_0 R_{m'}^{\pm}) \frac{e^{ik_0 R_{m'}^{\pm}}}{(R_{m'}^{\pm})^3} \right]$$
$$+ \left[-\frac{1}{4\pi} \frac{l_{m'} l_n}{4A_n^{\pm}} \bar{\rho}_{m'}^{c\pm} \cdot \int_{T_n^{\pm}} d\bar{r}' \bar{\rho}_n^{\pm} \times (\bar{r}_{m'}^{c\pm} - \bar{r}')(1 - ik_1 R_{m'}^{\pm}) \frac{e^{ik_1 R_{m'}^{\pm}}}{(R_{m'}^{\pm})^3} \right] \quad (A.94)$$

$$CZ5 = \left[-\frac{i\omega\epsilon_0}{4\pi} \frac{l_{m'} l_{n'}}{4A_{n'}^{\pm}} \bar{\rho}_{m'}^{c\pm} \cdot \int_{T_{n'}^{\pm}} d\bar{r}' \bar{\rho}_{n'}^{\pm} \frac{e^{ik_0 R_{m'}^{\pm}}}{R_{m'}^{\pm}} \pm \frac{i}{4\pi\omega\mu_0} \frac{l_{m'} l_{n'}}{A_{n'}^{\pm}} \int_{T_{n'}^{\pm}} d\bar{r}' \frac{e^{ik_0 R_{m'}^{\pm}}}{R_{m'}^{\pm}} \right]$$
$$+ \left[-\frac{i\omega\epsilon}{4\pi} \frac{l_{m'} l_{n'}}{4A_{n'}^{\pm}} \bar{\rho}_{m'}^{c\pm} \cdot \int_{T_{n'}^{\pm}} d\bar{r}' \bar{\rho}_{n'}^{\pm} \frac{e^{ik_1 R_{m'}^{\pm}}}{R_{m'}^{\pm}} \pm \frac{i}{4\pi\omega\mu} \frac{l_{m'} l_{n'}}{A_{n'}^{\pm}} \int_{T_{n'}^{\pm}} d\bar{r}' \frac{e^{ik_1 R_{m'}^{\pm}}}{R_{m'}^{\pm}} \right] \quad (A.95)$$

$$CZ6 = \left[\frac{1}{4\pi} \frac{l_{m'} l_{n''}}{4A_{n''}^{\pm}} \bar{\rho}_{m'}^{c\pm} \cdot \int_{T_{n''}^{\pm}} d\bar{r}' \bar{\rho}_{n''}^{\pm} \times (\bar{r}_{m'}^{c\pm} - \bar{r}')(1 - ik_1 R_{m'}^{\pm}) \frac{e^{ik_1 R_{m'}^{\pm}}}{(R_{m'}^{\pm})^3} \right] \quad (A.96)$$

$$CZ7 = \left[-\frac{i\omega\mu}{4\pi} \frac{l_{m''} l_n}{4A_n^{\pm}} \bar{\rho}_{m''}^{c\pm} \cdot \int_{T_n^{\pm}} d\bar{r}' \bar{\rho}_n^{\pm} \frac{e^{ik_1 R_{m''}^{\pm}}}{R_{m''}^{\pm}} \pm \frac{i}{4\pi\omega\epsilon} \frac{l_{m''} l_n}{A_n^{\pm}} \int_{T_n^{\pm}} d\bar{r}' \frac{e^{ik_1 R_{m''}^{\pm}}}{R_{m''}^{\pm}} \right] \quad (A.97)$$

$$CZ8 = \left[\frac{1}{4\pi} \frac{l_{m''} l_{n'}}{4A_{n'}^{\pm}} \bar{\rho}_{m''}^{c\pm} \cdot \int_{T_{n'}^{\pm}} d\bar{r}' \bar{\rho}_{n'}^{\pm} \times (\bar{r}_{m''}^{c\pm} - \bar{r}')(1 - ik_1 R_{m''}^{\pm}) \frac{e^{ik_1 R_{m''}^{\pm}}}{(R_{m''}^{\pm})^3} \right] \quad (A.98)$$

$$CZ9 = \left[\frac{i\omega\mu}{4\pi} \frac{l_{m''} l_{n''}}{4A_{n''}^{\pm}} \bar{\rho}_{m''}^{c\pm} \cdot \int_{T_{n''}^{\pm}} d\bar{r}' \bar{\rho}_{n''}^{\pm} \frac{e^{ik_1 R_{m''}^{\pm}}}{R_{m''}^{\pm}} \right.$$

$$\pm \frac{-i}{4\pi\omega\epsilon}\frac{l_{m''}l_{n''}}{A^{\pm}_{n''}}\int_{T^{\pm}_{n''}} d\bar{r}'\frac{e^{ik_1R^{\pm}_{m''}}}{R^{\pm}_{m''}}\Bigg]. \tag{A.99}$$

Now to satisfy duality, CZ2 = -CZ4. Further, to satisfy reciprocity, CZ2 = -$CZ4^T$, CZ3 = $CZ7^T$, and CZ6 = -$CZ8^T$. Multiplying (A.88) by -1 gives

$$\begin{aligned}\bar{0}_{m''} = I_n&\left[\frac{i\omega\mu}{4\pi}\frac{l_{m''}l_n}{4A^{\pm}_n}\bar{\rho}^{c\pm}_{m''}\cdot\int_{T^{\pm}_n} d\bar{r}'\bar{\rho}^{\pm}_n\frac{e^{ik_1R^{\pm}_{m''}}}{R^{\pm}_{m''}} \pm \frac{-i}{4\pi\omega\epsilon}\frac{l_{m''}l_n}{A^{\pm}_n}\int_{T^{\pm}_n} d\bar{r}'\frac{e^{ik_1R^{\pm}_{m''}}}{R^{\pm}_{m''}}\right]\\
&+ K_{n'}\left[-\frac{1}{4\pi}\frac{l_{m''}l_{n'}}{4A^{\pm}_{n'}}\bar{\rho}^{c\pm}_{m''}\cdot\int_{T^{\pm}_{n'}} d\bar{r}'\bar{\rho}^{\pm}_{n'}\times(\bar{r}^{c\pm}_{m''}-\bar{r}')(1-ik_1R^{\pm}_{m''})\frac{e^{ik_1R^{\pm}_{m''}}}{(R^{\pm}_{m''})^3}\right]\\
&+ L_{n''}\left[-\frac{i\omega\mu}{4\pi}\frac{l_{m''}l_{n''}}{4A^{\pm}_{n''}}\bar{\rho}^{c\pm}_{m''}\cdot\int_{T^{\pm}_{n''}} d\bar{r}'\bar{\rho}^{\pm}_{n''}\frac{e^{ik_1R^{\pm}_{m''}}}{R^{\pm}_{m''}}\right.\\
&\left.\pm\frac{i}{4\pi\omega\epsilon}\frac{l_{m''}l_{n''}}{A^{\pm}_{n''}}\int_{T^{\pm}_{n''}} d\bar{r}'\frac{e^{ik_1R^{\pm}_{m''}}}{R^{\pm}_{m''}}\right].\end{aligned} \tag{A.100}$$

and therefore,

$$CZ7 = \left[\frac{i\omega\mu}{4\pi}\frac{l_{m''}l_n}{4A^{\pm}_n}\bar{\rho}^{c\pm}_{m''}\cdot\int_{T^{\pm}_n} d\bar{r}'\bar{\rho}^{\pm}_n\frac{e^{ik_1R^{\pm}_{m''}}}{R^{\pm}_{m''}} \pm \frac{-i}{4\pi\omega\epsilon}\frac{l_{m''}l_n}{A^{\pm}_n}\int_{T^{\pm}_n} d\bar{r}'\frac{e^{ik_1R^{\pm}_{m''}}}{R^{\pm}_{m''}}\right] \tag{A.101}$$

$$CZ8 = \left[-\frac{1}{4\pi}\frac{l_{m''}l_{n'}}{4A^{\pm}_{n'}}\bar{\rho}^{c\pm}_{m''}\cdot\int_{T^{\pm}_{n'}} d\bar{r}'\bar{\rho}^{\pm}_{n'}\times(\bar{r}^{c\pm}_{m''}-\bar{r}')(1-ik_1R^{\pm}_{m''})\frac{e^{ik_1R^{\pm}_{m''}}}{(R^{\pm}_{m''})^3}\right] \tag{A.102}$$

$$\begin{aligned}CZ9 = \Bigg[&-\frac{i\omega\mu}{4\pi}\frac{l_{m''}l_{n''}}{4A^{\pm}_{n''}}\bar{\rho}^{c\pm}_{m''}\cdot\int_{T^{\pm}_{n''}} d\bar{r}'\bar{\rho}^{\pm}_{n''}\frac{e^{ik_1R^{\pm}_{m''}}}{R^{\pm}_{m''}}\\
&\pm\frac{i}{4\pi\omega\epsilon}\frac{l_{m''}l_{n''}}{A^{\pm}_{n''}}\int_{T^{\pm}_{n''}} d\bar{r}'\frac{e^{ik_1R^{\pm}_{m''}}}{R^{\pm}_{m''}}\Bigg].\end{aligned} \tag{A.103}$$

Thus, the system of equations becomes

$$\begin{pmatrix} l_m\left[\overline{E}^{+}_m\cdot\frac{\bar{\rho}^{c+}_m}{2}+\overline{E}^{-}_m\cdot\frac{\bar{\rho}^{c-}_m}{2}\right]\\ l_{m'}\left[\overline{H}^{+}_{m'}\cdot\frac{\bar{\rho}^{c+}_{m'}}{2}+\overline{H}^{-}_{m'}\cdot\frac{\bar{\rho}^{c-}_{m'}}{2}\right]\\ \bar{0}_{m''}\end{pmatrix} = \begin{pmatrix} Z_{mn} & Z_{mn'} & Z_{mn''}\\ Z_{m'n} & Z_{m'n'} & Z_{m'n''}\\ Z_{m''n} & Z_{m''n'} & Z_{m''n''}\end{pmatrix}\begin{pmatrix} I_n\\ K_{n'}\\ L_{n''}\end{pmatrix}. \tag{A.104}$$

where now CZ1 $\simeq$ CZ1^T, CZ2 $\simeq$ -CZ4^T, CZ3 $\simeq$ CZ7^T, CZ5 $\simeq$ CZ5^T, CZ6 $\simeq$ -CZ8^T, and CZ9 $\simeq$ CZ9^T. Finally, multiplying the middle set of equations by -1 yields a symmetric Z-matrix:

$$\begin{pmatrix} l_m\left[\overline{E}_m^+ \cdot \frac{\bar{\rho}_m^{c+}}{2} + \overline{E}_m^- \cdot \frac{\bar{\rho}_m^{c-}}{2}\right] \\ -l_{m'}\left[\overline{H}_{m'}^+ \cdot \frac{\bar{\rho}_{m'}^{c+}}{2} + \overline{H}_{m'}^- \cdot \frac{\bar{\rho}_{m'}^{c-}}{2}\right] \\ \vec{0}_{m''} \end{pmatrix} = \begin{pmatrix} CZ1 & CZ2 & CZ3 \\ CZ4 & CZ5 & CZ6 \\ CZ7 & CZ8 & CZ9 \end{pmatrix} \begin{pmatrix} I_n \\ K_{n'} \\ L_{n''} \end{pmatrix}. \quad (A.105)$$

where the individual elements are

$$CZ1 = \left[-\frac{i\omega\mu_0}{4\pi}\frac{l_m l_n}{4A_n^\pm}\bar{\rho}_m^{c\pm} \cdot \int_{T_n^\pm} d\bar{r}'\,\bar{\rho}_n^\pm \frac{e^{ik_0 R_m^\pm}}{R_m^\pm} \pm \frac{i}{4\pi\omega\epsilon_0}\frac{l_m l_n}{A_n^\pm}\int_{T_n^\pm} d\bar{r}'\frac{e^{ik_0 R_m^\pm}}{R_m^\pm}\right]$$
$$+\left[-\frac{i\omega\mu}{4\pi}\frac{l_m l_n}{4A_n^\pm}\bar{\rho}_m^{c\pm} \cdot \int_{T_n^\pm} d\bar{r}'\,\bar{\rho}_n^\pm \frac{e^{ik_1 R_m^\pm}}{R_m^\pm} \pm \frac{i}{4\pi\omega\epsilon}\frac{l_m l_n}{A_n^\pm}\int_{T_n^\pm} d\bar{r}'\frac{e^{ik_1 R_m^\pm}}{R_m^\pm}\right] \quad (A.106)$$

$$CZ2 = \left[\frac{1}{4\pi}\frac{l_m l_{n'}}{4A_{n'}^\pm}\bar{\rho}_m^{c\pm} \cdot \int_{T_{n'}^\pm} d\bar{r}'\,\bar{\rho}_{n'}^\pm \times (\bar{r}_m^{c\pm} - \bar{r}')(1 - ik_0 R_m^\pm)\frac{e^{ik_0 R_m^\pm}}{(R_m^\pm)^3}\right]$$
$$+\left[\frac{1}{4\pi}\frac{l_m l_{n'}}{4A_{n'}^\pm}\bar{\rho}_m^{c\pm} \cdot \int_{T_{n'}^\pm} d\bar{r}'\,\bar{\rho}_{n'}^\pm \times (\bar{r}_m^{c\pm} - \bar{r}')(1 - ik_1 R_m^\pm)\frac{e^{ik_1 R_m^\pm}}{(R_m^\pm)^3}\right] \quad (A.107)$$

$$CZ3 = \left[\frac{i\omega\mu}{4\pi}\frac{l_m l_{n''}}{4A_{n''}^\pm}\bar{\rho}_m^{c\pm} \cdot \int_{T_{n''}^\pm} d\bar{r}'\,\bar{\rho}_{n''}^\pm \frac{e^{ik_1 R_m^\pm}}{R_m^\pm} \pm \frac{-i}{4\pi\omega\epsilon}\frac{l_m l_{n''}}{A_{n''}^\pm}\int_{T_{n''}^\pm} d\bar{r}'\frac{e^{ik_1 R_m^\pm}}{R_m^\pm}\right] \quad (A.108)$$

$$CZ4 = \left[\frac{1}{4\pi}\frac{l_{m'} l_n}{4A_n^\pm}\bar{\rho}_{m'}^{c\pm} \cdot \int_{T_n^\pm} d\bar{r}'\,\bar{\rho}_n^\pm \times (\bar{r}_{m'}^{c\pm} - \bar{r}')(1 - ik_0 R_{m'}^\pm)\frac{e^{ik_0 R_{m'}^\pm}}{(R_{m'}^\pm)^3}\right]$$
$$+\left[\frac{1}{4\pi}\frac{l_{m'} l_n}{4A_n^\pm}\bar{\rho}_{m'}^{c\pm} \cdot \int_{T_n^\pm} d\bar{r}'\,\bar{\rho}_n^\pm \times (\bar{r}_{m'}^{c\pm} - \bar{r}')(1 - ik_1 R_{m'}^\pm)\frac{e^{ik_1 R_{m'}^\pm}}{(R_{m'}^\pm)^3}\right] \quad (A.109)$$

$$CZ5 = \left[\frac{i\omega\epsilon_0}{4\pi}\frac{l_{m'} l_{n'}}{4A_{n'}^\pm}\bar{\rho}_{m'}^{c\pm} \cdot \int_{T_{n'}^\pm} d\bar{r}'\,\bar{\rho}_{n'}^\pm \frac{e^{ik_0 R_{m'}^\pm}}{R_{m'}^\pm} \pm \frac{-i}{4\pi\omega\mu_0}\frac{l_{m'} l_{n'}}{A_{n'}^\pm}\int_{T_{n'}^\pm} d\bar{r}'\frac{e^{ik_0 R_{m'}^\pm}}{R_{m'}^\pm}\right]$$
$$+\left[\frac{i\omega\epsilon}{4\pi}\frac{l_{m'} l_{n'}}{4A_{n'}^\pm}\bar{\rho}_{m'}^{c\pm} \cdot \int_{T_{n'}^\pm} d\bar{r}'\,\bar{\rho}_{n'}^\pm \frac{e^{ik_1 R_{m'}^\pm}}{R_{m'}^\pm} \pm \frac{-i}{4\pi\omega\mu}\frac{l_{m'} l_{n'}}{A_{n'}^\pm}\int_{T_{n'}^\pm} d\bar{r}'\frac{e^{ik_1 R_{m'}^\pm}}{R_{m'}^\pm}\right] \quad (A.110)$$

$$CZ6 = \left[-\frac{1}{4\pi}\frac{l_{m'} l_{n''}}{4A_{n''}^\pm}\bar{\rho}_{m'}^{c\pm} \cdot \int_{T_{n''}^\pm} d\bar{r}'\,\bar{\rho}_{n''}^\pm \times (\bar{r}_{m'}^{c\pm} - \bar{r}')(1 - ik_1 R_{m'}^\pm)\frac{e^{ik_1 R_{m'}^\pm}}{(R_{m'}^\pm)^3}\right] \quad (A.111)$$

$$CZ7 = \left[\frac{i\omega\mu}{4\pi}\frac{l_{m''}l_n}{4A_n^{\pm}}\bar{\rho}_{m''}^{c\pm}\cdot\int_{T_n^{\pm}}d\bar{r}'\bar{\rho}_n^{\pm}\frac{e^{ik_1R_{m''}^{\pm}}}{R_{m''}^{\pm}} \pm \frac{-i}{4\pi\omega\epsilon}\frac{l_{m''}l_n}{A_n^{\pm}}\int_{T_n^{\pm}}d\bar{r}'\frac{e^{ik_1R_{m''}^{\pm}}}{R_{m''}^{\pm}}\right] \quad (A.112)$$

$$CZ8 = \left[-\frac{1}{4\pi}\frac{l_{m''}l_{n'}}{4A_{n'}^{\pm}}\bar{\rho}_{m''}^{c\pm}\cdot\int_{T_{n'}^{\pm}}d\bar{r}'\bar{\rho}_{n'}^{\pm}\times(\bar{r}_{m''}^{c\pm}-\bar{r}')(1-ik_1R_{m''}^{\pm})\frac{e^{ik_1R_{m''}^{\pm}}}{(R_{m''}^{\pm})^3}\right] \quad (A.113)$$

$$CZ9 = \left[-\frac{i\omega\mu}{4\pi}\frac{l_{m''}l_{n''}}{4A_{n''}^{\pm}}\bar{\rho}_{m''}^{c\pm}\cdot\int_{T_{n''}^{\pm}}d\bar{r}'\bar{\rho}_{n''}^{\pm}\frac{e^{ik_1R_{m''}^{\pm}}}{R_{m''}^{\pm}} \pm \frac{i}{4\pi\omega\epsilon}\frac{l_{m''}l_{n''}}{A_{n''}^{\pm}}\int_{T_{n''}^{\pm}}d\bar{r}'\frac{e^{ik_1R_{m''}^{\pm}}}{R_{m''}^{\pm}}\right]. \quad (A.114)$$

A symmetric matrix can be inverted by techniques such as border inversion or LU decomposition. For border inversion the entire matrix does not have to reside in core memory at the same time. This can be important for coated targets of any appreciable dimension with respect to wavelength since the size of the Z-matrix will be very large. Equations (A.106) through (A.114) represent the symmetric Z-matrix as computed by program EFIE2C.FOR (see Appendix B).

A.3 Partially Coated Perfect Conductor

This section contains the derivation of the equations for the interaction matrix of a partially coated perfect conductor. The derivation of the governing equations for this interaction matrix follows the same approach as that presented above for the completely coated perfect conductor. Refer to Figure 3.3 as a reference for the following derivation.

Using Huygens' principle (see equation 3.1) in Region 0:

$$\begin{aligned}\overline{E}_0 &= \overline{E}_{inc} + \overline{E}_s \\ &= \overline{E}_{inc} + \int_{S_1} dS_1\{i\omega\mu_0\overline{\overline{G}}_0\cdot\overline{J}_1 - \nabla\times\overline{\overline{G}}_0\cdot\overline{M}_1\} \\ &\quad + \int_{S_2} dS_2\{i\omega\mu_0\overline{\overline{G}}_0\cdot\overline{J}_2\} \end{aligned} \quad (A.115)$$

and

$$\begin{aligned}\overline{H}_0 &= \overline{H}_{inc} + \overline{H}_s \\ &= \overline{H}_{inc} + \int_{S_1} dS_1\{i\omega\epsilon_0\overline{\overline{G}}_0 \cdot \overline{M}_1 + \nabla \times \overline{\overline{G}}_0 \cdot \overline{J}_1\} \\ &\quad + \int_{S_2} dS_2\{\nabla \times \overline{\overline{G}}_0 \cdot \overline{J}_2\}. \end{aligned} \tag{A.116}$$

Using Huygens' principle in Region 1:

$$\overline{E}_1 = \int_{S_1} dS_1\{i\omega\mu\overline{\overline{G}}_1 \cdot \overline{J}_1' - \nabla \times \overline{\overline{G}}_1 \cdot \overline{M}_1'\} + \int_{S_3} dS_3\{i\omega\mu\overline{\overline{G}}_1 \cdot \overline{J}_3\} \tag{A.117}$$

and

$$\overline{H}_1 = \int_{S_1} dS_1\{i\omega\epsilon\overline{\overline{G}}_1 \cdot \overline{M}_1' + \nabla \times \overline{\overline{G}}_1 \cdot \overline{J}_1'\} + \int_{S_3} dS_3\{\nabla \times \overline{\overline{G}}_1 \cdot \overline{J}_3\}. \tag{A.118}$$

Applying the boundary conditions at surface S_1:

$$\hat{n}_0 \times \overline{E}_0 = \hat{n}_0 \times \overline{E}_1. \tag{A.119}$$

Therefore, at S_1

$$\begin{aligned}&\hat{n}_0 \times \overline{E}_{inc} + \hat{n}_0 \times \int_{S_1} dS_1\{i\omega\mu_0\overline{\overline{G}}_0 \cdot \overline{J}_1 - \nabla \times \overline{\overline{G}}_0 \cdot \overline{M}_1\} + \hat{n}_0 \times \int_{S_2} dS_2\{i\omega\mu_0\overline{\overline{G}}_0 \cdot \overline{J}_2\} \\ &\quad = \hat{n}_0 \times \int_{S_1} dS_1\{i\omega\mu\overline{\overline{G}}_1 \cdot \overline{J}_1' - \nabla \times \overline{\overline{G}}_1 \cdot \overline{M}_1'\} \\ &\quad\quad + \hat{n}_0 \times \int_{S_3} dS_3\{i\omega\mu\overline{\overline{G}}_1 \cdot \overline{J}_3\}. \end{aligned} \tag{A.120}$$

Also at S_1

$$\hat{n}_0 \times \overline{H}_0 = \hat{n}_0 \times \overline{H}_1 \tag{A.121}$$

and, therefore, at S_1

$$\hat{n}_0 \times \overline{H}_{inc} + \hat{n}_0 \times \int_{S_1} dS_1 \{ i\omega\epsilon_0 \overline{\overline{G}}_0 \cdot \overline{M}_1 + \nabla \times \overline{\overline{G}}_0 \cdot \overline{J}_1 \} + \hat{n}_0 \times \int_{S_2} dS_2 \{ \nabla \times \overline{\overline{G}}_0 \cdot \overline{J}_2 \}$$
$$= \hat{n}_0 \times \int_{S_1} dS_1 \{ i\omega\epsilon \overline{\overline{G}}_1 \cdot \overline{M}_1' + \nabla \times \overline{\overline{G}}_1 \cdot \overline{J}_1' \}$$
$$+ \hat{n}_0 \times \int_{S_3} dS_3 \{ \nabla \times \overline{\overline{G}}_1 \cdot \overline{J}_3 \}. \qquad (A.122)$$

Now, at surface S_2

$$\hat{n}_2 \times \overline{E}_0 = 0. \qquad (A.123)$$

Therefore, at S_2

$$\hat{n}_2 \times \overline{E}_{inc} + \hat{n}_2 \times \int_{S_1} dS_1 \{ i\omega\mu_0 \overline{\overline{G}}_0 \cdot \overline{J}_1 - \nabla \times \overline{\overline{G}}_0 \cdot \overline{M}_1 \} + \hat{n}_2 \times \int_{S_2} dS_2 \{ i\omega\mu_0 \overline{\overline{G}}_0 \cdot \overline{J}_2 \} = 0. \qquad (A.124)$$

Now, at surface S_3

$$\hat{n}_3 \times \overline{E}_1 = 0. \qquad (A.125)$$

Therefore, at S_3

$$\hat{n}_3 \times \int_{S_1} dS_1 \{ i\omega\mu \overline{\overline{G}}_1 \cdot \overline{J}_1' - \nabla \times \overline{\overline{G}}_1 \cdot \overline{M}_1' \} + \hat{n}_3 \times \int_{S_3} dS_3 \{ i\omega\mu \overline{\overline{G}}_1 \cdot \overline{J}_3 \} = 0. \qquad (A.126)$$

This yields four equations in four unknowns: $\overline{J}_1, \overline{M}_1, \overline{J}_2, \overline{J}_3$.

Using equations (A.8) and (A.10), equation (A.120) becomes

$$\hat{n}_0 \times \overline{E}_{inc} = -\hat{n}_0 \times \int_{S_1} dS_1 \{ i\omega\mu_0 \overline{\overline{G}}_0 \cdot \overline{J}_1 - \nabla \times \overline{\overline{G}}_0 \cdot \overline{M}_1 \}$$
$$- \hat{n}_0 \times \int_{S_2} dS_2 \{ i\omega\mu_0 \overline{\overline{G}}_0 \cdot \overline{J}_2 \}$$
$$- \hat{n}_0 \times \int_{S_1} dS_1 \{ i\omega\mu \overline{\overline{G}}_1 \cdot \overline{J}_1 - \nabla \times \overline{\overline{G}}_1 \cdot \overline{M}_1 \}$$
$$+ \hat{n}_0 \times \int_{S_3} dS_3 \{ i\omega\mu \overline{\overline{G}}_1 \cdot \overline{J}_3 \} \qquad (A.127)$$

and equation (A.122) becomes

$$\hat{n}_0 \times \overline{H}_{inc} = -\hat{n}_0 \times \int_{S_1} dS_1 \{ i\omega\epsilon_0 \overline{\overline{G}}_0 \cdot \overline{M}_1 + \{ \nabla \times \overline{\overline{G}}_0 \cdot \overline{J}_1 \}$$
$$- \hat{n}_0 \times \int_{S_2} dS_2 \nabla \times \overline{\overline{G}}_0 \cdot \overline{J}_2 \}$$
$$- \hat{n}_0 \times \int_{S_1} dS_1 \{ i\omega\epsilon \overline{\overline{G}}_1 \cdot \overline{M}_1 + \nabla \times \overline{\overline{G}}_1 \cdot \overline{J}_1 \}$$
$$+ \hat{n}_0 \times \int_{S_3} dS_3 \{ \nabla \times \overline{\overline{G}}_1 \cdot \overline{J}_3 \} \qquad (A.128)$$

and equation (A.124) becomes

$$\hat{n}_2 \times \overline{E}_{inc} = -\hat{n}_2 \times \int_{S_1} dS_1 \{ i\omega\mu_0 \overline{\overline{G}}_0 \cdot \overline{J}_1 - \nabla \times \overline{\overline{G}}_0 \cdot \overline{M}_1 \} - \hat{n}_2 \times \int_{S_2} dS_2 \{ i\omega\mu_0 \overline{\overline{G}}_0 \cdot \overline{J}_2 \} \qquad (A.129)$$

and equation (A.126) becomes

$$\overline{0} = -\hat{n}_3 \times \int_{S_1} dS_1 \{ i\omega\mu \overline{\overline{G}}_1 \cdot \overline{J}_1 - \nabla \times \overline{\overline{G}}_1 \cdot \overline{M}_1 \} + \hat{n}_3 \times \int_{S_3} dS_3 \{ i\omega\mu \overline{\overline{G}}_1 \cdot \overline{J}_3 \}. \qquad (A.130)$$

Equations (A.127) through (A.130) are of the form

$$L_{11} \cdot \overline{J}_1 + L_{12} \cdot \overline{M}_1 + L_{13} \cdot \overline{J}_2 + L_{14} \cdot \overline{J}_3 = \hat{n}_0 \times \overline{E}_{inc} \qquad (A.131)$$

$$L_{21} \cdot \overline{J}_1 + L_{22} \cdot \overline{M}_1 + L_{23} \cdot \overline{J}_2 + L_{24} \cdot \overline{J}_3 = \hat{n}_0 \times \overline{H}_{inc} \qquad (A.132)$$

$$L_{31} \cdot \overline{J}_1 + L_{32} \cdot \overline{M}_1 + L_{33} \cdot \overline{J}_2 + L_{34} \cdot \overline{J}_3 = \hat{n}_2 \times \overline{E}_{inc} \qquad (A.133)$$

$$L_{41} \cdot \overline{J}_1 + L_{42} \cdot \overline{M}_1 + L_{43} \cdot \overline{J}_2 + L_{44} \cdot \overline{J}_3 = \overline{0} \qquad (A.134)$$

or the more compact form

$$\begin{pmatrix} L_{11} & L_{12} & L_{13} & L_{14} \\ L_{21} & L_{22} & L_{23} & L_{24} \\ L_{31} & L_{32} & L_{33} & L_{34} \\ L_{41} & L_{42} & L_{43} & L_{44} \end{pmatrix} \begin{pmatrix} \overline{J}_1 \\ \overline{M}_1 \\ \overline{J}_2 \\ \overline{J}_3 \end{pmatrix} = \begin{pmatrix} \hat{n}_0 \times \overline{E}_{inc} \\ \hat{n}_0 \times \overline{H}_{inc} \\ \hat{n}_2 \times \overline{E}_{inc} \\ \overline{0} \end{pmatrix} \qquad (A.135)$$

where

$$L_{11} = -\hat{n}_0 \times \int_{S_1} dS_1 i\omega\{\mu_0 \overline{\overline{G}}_0 + \mu \overline{\overline{G}}_1\} \cdot \tag{A.136}$$

$$L_{12} = \hat{n}_0 \times \int_{S_1} dS_1 \{\nabla \times \overline{\overline{G}}_0 + \nabla \times \overline{\overline{G}}_1\} \cdot \tag{A.137}$$

$$L_{13} = -\hat{n}_0 \times \int_{S_2} dS_2 \{i\omega\mu_0 \overline{\overline{G}}_0\} \cdot \tag{A.138}$$

$$L_{14} = \hat{n}_0 \times \int_{S_3} dS_3 \{i\omega\mu \overline{\overline{G}}_1\} \cdot \tag{A.139}$$

$$L_{21} = -\hat{n}_0 \times \int_{S_1} dS_1 \{\nabla \times \overline{\overline{G}}_0 + \nabla \times \overline{\overline{G}}_1\} \cdot \tag{A.140}$$

$$L_{22} = -\hat{n}_0 \times \int_{S_1} dS_1 i\omega\{\epsilon_0 \overline{\overline{G}}_0 + \epsilon \overline{\overline{G}}_1\} \cdot \tag{A.141}$$

$$L_{23} = -\hat{n}_0 \times \int_{S_2} dS_2 \{\nabla \times \overline{\overline{G}}_0\} \cdot \tag{A.142}$$

$$L_{24} = \hat{n}_0 \times \int_{S_3} dS_3 \{\nabla \times \overline{\overline{G}}_1\} \cdot \tag{A.143}$$

$$L_{31} = -\hat{n}_2 \times \int_{S_1} dS_1 \{i\omega\mu_0 \overline{\overline{G}}_0\} \cdot \tag{A.144}$$

$$L_{32} = \hat{n}_2 \times \int_{S_1} dS_1 \{\nabla \times \overline{\overline{G}}_0\} \cdot \tag{A.145}$$

$$L_{33} = -\hat{n}_2 \times \int_{S_2} dS_2 \{i\omega\mu_0 \overline{\overline{G}}_0\} \cdot \tag{A.146}$$

$$L_{34} = \overline{0} \tag{A.147}$$

$$L_{41} = -\hat{n}_3 \times \int_{S_1} dS_1 \{i\omega\mu \overline{\overline{G}}_1\} \cdot \tag{A.148}$$

$$L_{42} = \hat{n}_3 \times \int_{S_1} dS_1 \{\nabla \times \overline{\overline{G}}_1\} \cdot \tag{A.149}$$

$$L_{43} = \overline{0} \tag{A.150}$$

$$L_{44} = \hat{n}_3 \times \int_{S_3} dS_3 \{i\omega\mu\overline{\overline{G}}_1\} \cdot . \tag{A.151}$$

Note that L_{12} = -L_{21} and if ϵ and μ are interchanged $L_{11} = L_{22}$. Further, if surfaces S_1 and S_2 are interchanged $L_{13} = L_{31}$ and L_{23} = -L_{32}. Also, if surfaces S_1 and S_3 are interchanged $L_{24} = L_{42}$ and L_{14} = -L_{41}. Finally, this approach corresponds to the electric field integral equation (EFIE) approach discussed by Rao, Wilton, and Glisson [81]. If the boundary conditions on the tangential magnetic field at the surface of the perfect conductors had been used, this would correspond to the magnetic field integral equation (MFIE) approach, and if a weighted sum of the EFIE and MFIE had been used, this would correspond to the combined field integral equation (CFIE) approach [70,120].

Now rewriting (A.135) as four distinct equations, as done previously for the completely coated perfect conductor, gives

$$\begin{aligned}
\hat{n}_0 \times \overline{E}_{inc} = &-\hat{n}_0 \times \int_{S_1} dS_1 i\omega\mu_0 \overline{J}_1 \frac{e^{ik_0 R}}{4\pi R} - \hat{n}_0 \times \nabla \int_{S_1} dS_1 \frac{i\omega\mu_0}{k_0^2} (\nabla \cdot \overline{J}_1) \frac{e^{ik_0 R}}{4\pi R} \\
&- \hat{n}_0 \times \int_{S_1} dS_1 i\omega\mu \overline{J}_1 \frac{e^{ik_1 R}}{4\pi R} - \hat{n}_0 \times \nabla \int_{S_1} dS_1 \frac{i\omega\mu}{k_1^2} (\nabla \cdot \overline{J}_1) \frac{e^{ik_1 R}}{4\pi R} \\
&+ \hat{n}_0 \times \int_{S_1} dS_1 \overline{M}_1 \times \nabla' \left(\frac{e^{ik_0 R}}{4\pi R}\right) + \hat{n}_0 \times \int_{S_1} dS_1 \overline{M}_1 \times \nabla' \left(\frac{e^{ik_1 R}}{4\pi R}\right) \\
&- \hat{n}_0 \times \int_{S_2} dS_2 i\omega\mu_0 \overline{J}_2 \frac{e^{ik_0 R}}{4\pi R} - \hat{n}_0 \times \nabla \int_{S_2} dS_2 \frac{i\omega\mu_0}{k_0^2} (\nabla \cdot \overline{J}_2) \frac{e^{ik_0 R}}{4\pi R} \\
&+ \hat{n}_0 \times \int_{S_3} dS_3 i\omega\mu \overline{J}_3 \frac{e^{ik_1 R}}{4\pi R} + \hat{n}_0 \times \nabla \int_{S_3} dS_3 \frac{i\omega\mu}{k_1^2} (\nabla \cdot \overline{J}_3) \frac{e^{ik_1 R}}{4\pi R}
\end{aligned} \tag{A.152}$$

$$\begin{aligned}
\hat{n}_0 \times \overline{H}_{inc} = &-\hat{n}_0 \times \int_{S_1} dS_1 \overline{J}_1 \times \nabla' \left(\frac{e^{ik_0 R}}{4\pi R}\right) - \hat{n}_0 \times \int_{S_1} dS_1 \overline{J}_1 \times \nabla' \left(\frac{e^{ik_1 R}}{4\pi R}\right) \\
&- \hat{n}_0 \times \int_{S_1} dS_1 i\omega\epsilon_0 \overline{M}_1 \frac{e^{ik_0 R}}{4\pi R} - \hat{n}_0 \times \nabla \int_{S_1} dS_1 \frac{i\omega\epsilon_0}{k_0^2} (\nabla \cdot \overline{M}_1) \frac{e^{ik_0 R}}{4\pi R}
\end{aligned}$$

$$- \hat{n}_0 \times \int_{S_1} dS_1 i\omega\epsilon \overline{M}_1 \frac{e^{ik_1 R}}{4\pi R} - \hat{n}_0 \times \nabla \int_{S_1} dS_1 \frac{i\omega\epsilon}{k_1^2} (\nabla \cdot \overline{M}_1) \frac{e^{ik_1 R}}{4\pi R}$$
$$- \hat{n}_0 \times \int_{S_2} dS_2 \overline{J}_2 \times \nabla' (\frac{e^{ik_0 R}}{4\pi R}) + \hat{n}_0 \times \int_{S_3} dS_3 \overline{J}_3 \times \nabla' (\frac{e^{ik_1 R}}{4\pi R}) \quad (A.153)$$

$$\hat{n}_2 \times \overline{E}_{inc} = -\hat{n}_2 \times \int_{S_1} dS_1 i\omega\mu_0 \overline{J}_1 \frac{e^{ik_0 R}}{4\pi R} - \hat{n}_2 \times \nabla \int_{S_1} dS_1 \frac{i\omega\mu_0}{k_0^2} (\nabla \cdot \overline{J}_1) \frac{e^{ik_0 R}}{4\pi R}$$
$$+ \hat{n}_2 \times \int_{S_1} dS_1 \overline{M}_1 \times \nabla' (\frac{e^{ik_0 R}}{4\pi R}) - \hat{n}_2 \times \int_{S_2} dS_2 i\omega\mu_0 \overline{J}_2 \frac{e^{ik_0 R}}{4\pi R}$$
$$- \hat{n}_2 \times \nabla \int_{S_2} dS_2 \frac{i\omega\mu_0}{k_0^2} (\nabla \cdot \overline{J}_2) \frac{e^{ik_0 R}}{4\pi R} \quad (A.154)$$

$$\overline{0} = -\hat{n}_3 \times \int_{S_1} dS_1 i\omega\mu \overline{J}_1 \frac{e^{ik_1 R}}{4\pi R} - \hat{n}_3 \times \nabla \int_{S_1} dS_1 \frac{i\omega\mu}{k_1^2} (\nabla \cdot \overline{J}_1) \frac{e^{ik_1 R}}{4\pi R}$$
$$+ \hat{n}_3 \times \int_{S_1} dS_1 \overline{M}_1 \times \nabla' (\frac{e^{ik_1 R}}{4\pi R})$$
$$+ \hat{n}_3 \times \int_{S_3} dS_3 i\omega\mu \overline{J}_3 \frac{e^{ik_1 R}}{4\pi R} + \hat{n}_3 \times \nabla \int_{S_3} dS_3 \frac{i\omega\mu}{k_1^2} (\nabla \cdot \overline{J}_3) \frac{e^{ik_1 R}}{4\pi R} \quad (A.155)$$

where $R = |\bar{r} - \bar{r}'|$.

The desired approach at this point in the derivation is to change these four integro-differential equations in the four unknown surface current densities into a matrix equation which can be solved using inversion techniques. To this end the method of moments will be applied using the basis functions as defined previously in equations (A.60) and (A.61). Now the basis functions [81] are

$$\overline{J}_1(\bar{r}') \simeq \sum_{n=1}^{N} I_n \overline{f}_n(\bar{r}') \quad (A.156)$$

$$\overline{M}_1(\bar{r}') \simeq \sum_{n'=1}^{N'} K_{n'} \overline{f}_{n'}(\bar{r}') \quad (A.157)$$

$$\overline{J}_2(\bar{r}') \simeq \sum_{n''=1}^{N''} L_{n''} \overline{f}_{n''}(\bar{r}') \quad (A.158)$$

$$\overline{J}_3(\vec{r}') \simeq \sum_{n'''=1}^{N'''} P_{n'''}\overline{f}_{n'''}(\vec{r}') \qquad (A.159)$$

where n and n' are defined over the surface of the coating, n'' is defined over the surface of the exposed perfect conductor, and n''' is defined over the surface of the coated perfect conductor (see Figure 3.3).

Substituting these basis functions into (A.152) through (A.155) yields

$$\begin{aligned}
\hat{n}_0 \times \overline{E}_{inc} = &-\hat{n}_0 \times \int_{S_1} dS_1 i\omega\mu_0 I_n \overline{f}_n(\vec{r}')\frac{e^{ik_0R}}{4\pi R} - \hat{n}_0 \times \nabla \int_{S_1} dS_1 \frac{i\omega\mu_0}{k_0^2}\left(\nabla_s' \cdot I_n \overline{f}_n(\vec{r}')\right)\frac{e^{ik_0R}}{4\pi R} \\
&- \hat{n}_0 \times \int_{S_1} dS_1 i\omega\mu I_n \overline{f}_n(\vec{r}')\frac{e^{ik_1R}}{4\pi R} - \hat{n}_0 \times \nabla \int_{S_1} dS_1 \frac{i\omega\mu}{k_1^2}\left(\nabla_s' \cdot I_n \overline{f}_n(\vec{r}')\right)\frac{e^{ik_1R}}{4\pi R} \\
&+ \hat{n}_0 \times \int_{S_1} dS_1 K_{n'} \overline{f}_{n'}(\vec{r}') \times \nabla'\left(\frac{e^{ik_0R}}{4\pi R}\right) + \hat{n}_0 \times \int_{S_1} dS_1 K_{n'} \overline{f}_{n'}(\vec{r}') \times \nabla'\left(\frac{e^{ik_1R}}{4\pi R}\right) \\
&- \hat{n}_0 \times \int_{S_2} dS_2 i\omega\mu_0 L_{n''} \overline{f}_{n''}(\vec{r}')\frac{e^{ik_0R}}{4\pi R} - \hat{n}_0 \times \nabla \int_{S_2} dS_2 \frac{i\omega\mu_0}{k_0^2}\left(\nabla_s' \cdot L_{n''} \overline{f}_{n''}(\vec{r}')\right)\frac{e^{ik_0R}}{4\pi R} \\
&+ \hat{n}_0 \times \int_{S_3} dS_3 i\omega\mu P_{n'''} \overline{f}_{n'''}(\vec{r}')\frac{e^{ik_1R}}{4\pi R} \\
&+ \hat{n}_0 \times \nabla \int_{S_3} dS_3 \frac{i\omega\mu}{k_1^2}\left(\nabla_s' \cdot P_{n'''} \overline{f}_{n'''}(\vec{r}')\right)\frac{e^{ik_1R}}{4\pi R} \qquad (A.160)
\end{aligned}$$

$$\begin{aligned}
\hat{n}_0 \times \overline{H}_{inc} = &-\hat{n}_0 \times \int_{S_1} dS_1 I_n \overline{f}_n(\vec{r}') \times \nabla'\left(\frac{e^{ik_0R}}{4\pi R}\right) - \hat{n}_0 \times \int_{S_1} dS_1 I_n \overline{f}_n(\vec{r}') \times \nabla'\left(\frac{e^{ik_1R}}{4\pi R}\right) \\
&- \hat{n}_0 \times \int_{S_1} dS_1 i\omega\epsilon_0 K_{n'} \overline{f}_{n'}(\vec{r}')\frac{e^{ik_0R}}{4\pi R} - \hat{n}_0 \times \nabla \int_{S_1} dS_1 \frac{i\omega\epsilon_0}{k_0^2}\left(\nabla_s' \cdot K_{n'} \overline{f}_{n'}(\vec{r}')\right)\frac{e^{ik_0R}}{4\pi R} \\
&- \hat{n}_0 \times \int_{S_1} dS_1 i\omega\epsilon K_{n'} \overline{f}_{n'}(\vec{r}')\frac{e^{ik_1R}}{4\pi R} - \hat{n}_0 \times \nabla \int_{S_1} dS_1 \frac{i\omega\epsilon}{k_1^2}\left(\nabla_s' \cdot K_{n'} \overline{f}_{n'}(\vec{r}')\right)\frac{e^{ik_1R}}{4\pi R} \\
&- \hat{n}_0 \times \int_{S_2} dS_2 L_{n''} \overline{f}_{n''}(\vec{r}') \times \nabla'\left(\frac{e^{ik_0R}}{4\pi R}\right) \\
&+ \hat{n}_0 \times \int_{S_3} dS_3 P_{n'''} \overline{f}_{n'''}(\vec{r}') \times \nabla'\left(\frac{e^{ik_1R}}{4\pi R}\right) \qquad (A.161)
\end{aligned}$$

$$\hat{n}_2 \times \overline{E}_{inc} = -\hat{n}_2 \times \int_{S_1} dS_1 i\omega\mu_0 I_n \overline{f}_n(\vec{r}')\frac{e^{ik_0R}}{4\pi R} - \hat{n}_2 \times \nabla \int_{S_1} dS_1 \frac{i\omega\mu_0}{k_0^2}\left(\nabla_s' \cdot I_n \overline{f}_n(\vec{r}')\right)\frac{e^{ik_0R}}{4\pi R}$$

$$+\hat{n}_2\times\int_{S_1}dS_1K_{n'}\overline{f}_{n'}(\bar{r}')\times\nabla'\left(\frac{e^{ik_0R}}{4\pi R}\right)-\hat{n}_2\times\int_{S_2}dS_2i\omega\mu_0L_{n''}\overline{f}_{n''}(\bar{r}')\frac{e^{ik_0R}}{4\pi R}$$
$$-\hat{n}_2\times\nabla\int_{S_2}dS_2\frac{i\omega\mu_0}{k_0^2}\left(\nabla'_s\cdot L_{n''}\overline{f}_{n''}(\bar{r}')\right)\frac{e^{ik_0R}}{4\pi R} \qquad (A.162)$$

$$\overline{0}=-\hat{n}_3\times\int_{S_1}dS_1i\omega\mu I_n\overline{f}_n(\bar{r}')\frac{e^{ik_1R}}{4\pi R}-\hat{n}_3\times\nabla\int_{S_1}dS_1\frac{i\omega\mu}{k_1^2}\left(\nabla'_s\cdot I_n\overline{f}_n(\bar{r}')\right)\frac{e^{ik_1R}}{4\pi R}$$
$$+\hat{n}_3\times\int_{S_1}dS_1K_{n'}\overline{f}_{n'}(\bar{r}')\times\nabla'\left(\frac{e^{ik_1R}}{4\pi R}\right)+\hat{n}_3\times\int_{S_3}dS_3i\omega\mu P_{n'''}\overline{f}_{n'''}(\bar{r}')\frac{e^{ik_1R}}{4\pi R}$$
$$+\hat{n}_3\times\nabla\int_{S_3}dS_3\frac{i\omega\mu}{k_1^2}\left(\nabla'_s\cdot P_{n'''}\overline{f}_{n'''}(\bar{r}')\right)\frac{e^{ik_1R}}{4\pi R}. \qquad (A.163)$$

By using Galerkin's method, where the weighting function equals the basis function, and forming the inner product, which is defined as

$$<\overline{f},\overline{g}>\equiv\int_S dS\overline{f}\cdot\overline{g} \qquad (A.164)$$

we again get functions of the form

$$<\overline{E}_{inc},\overline{f}_m>=<\overline{A},\overline{f}_m>+<\nabla\Phi,\overline{f}_m> \qquad (A.165)$$

Following the same approach as previously discussed for the completely coated perfect conductor, (A.160) becomes (with $\overline{E}_m^{\pm}=\overline{E}_{inc}(\bar{r}_m^{c\pm})$ and $R_m^{\pm}=|\bar{r}_m^{c\pm}-\bar{r}'|$ and where m is defined over the surface of the coating)

$$l_m\left[\overline{E}_m^{+}\cdot\frac{\bar{\rho}_m^{c+}}{2}+\overline{E}_m^{-}\cdot\frac{\bar{\rho}_m^{c-}}{2}\right]=l_m\left[\overline{A}_{mn}^{+}\cdot\frac{\bar{\rho}_m^{c+}}{2}+\overline{A}_{mn}^{-}\cdot\frac{\bar{\rho}_m^{c-}}{2}+\Phi_{mn}^{-}-\Phi_{mn}^{+}\right] \qquad (A.166)$$

where

$$\overline{A}_{mn}^{\pm}=-\int_{S_1}dS_1i\omega\mu_0I_n\overline{f}_n(\bar{r}')\frac{e^{ik_0R_m^{\pm}}}{4\pi R_m^{\pm}}-\int_{S_1}dS_1i\omega\mu I_n\overline{f}_n(\bar{r}')\frac{e^{ik_1R_m^{\pm}}}{4\pi R_m^{\pm}}$$
$$+\int_{S_1}dS_1K_{n'}\overline{f}_{n'}(\bar{r}')\times\nabla'\left(\frac{e^{ik_0R_m^{\pm}}}{4\pi R_m^{\pm}}\right)+\int_{S_1}dS_1K_{n'}\overline{f}_{n'}(\bar{r}')\times\nabla'\left(\frac{e^{ik_1R_m^{\pm}}}{4\pi R_m^{\pm}}\right)$$
$$-\int_{S_2}dS_2i\omega\mu_0L_{n''}\overline{f}_{n''}(\bar{r}')\frac{e^{ik_0R_m^{\pm}}}{4\pi R_m^{\pm}}+\int_{S_3}dS_3i\omega\mu P_{n'''}\overline{f}_{n'''}(\bar{r}')\frac{e^{ik_1R_m^{\pm}}}{4\pi R_m^{\pm}} \qquad (A.167)$$

and

$$\Phi^{\pm}_{mn} = -\int_{S_1} dS_1 \frac{i\omega\mu_0}{k_0^2}\left(\nabla'_s \cdot I_n \overline{f}_n(\bar{r}')\right)\frac{e^{ik_0 R^{\pm}_m}}{4\pi R^{\pm}_m}$$
$$-\int_{S_1} dS_1 \frac{i\omega\mu}{k_1^2}\left(\nabla'_s \cdot I_n \overline{f}_n(\bar{r}')\right)\frac{e^{ik_1 R^{\pm}_m}}{4\pi R^{\pm}_m}$$
$$-\int_{S_2} dS_2 \frac{i\omega\mu_0}{k_0^2}\left(\nabla'_s \cdot L_{n''} \overline{f}_{n''}(\bar{r}')\right)\frac{e^{ik_0 R^{\pm}_m}}{4\pi R^{\pm}_m}$$
$$+\int_{S_3} dS_3 \frac{i\omega\mu}{k_1^2}\left(\nabla'_s \cdot P_{n'''} \overline{f}_{n'''}(\bar{r}')\right)\frac{e^{ik_1 R^{\pm}_m}}{4\pi R^{\pm}_m}. \qquad (A.168)$$

Similarly, (A.161) becomes (with $\overline{H}^{\pm}_{m'} = \overline{H}_{inc}(\bar{r}^{c\pm}_{m'})$ and $R^{\pm}_{m'} = |\bar{r}^{c\pm}_{m'} - \bar{r}'|$ and where m' is defined over the surface of the coating)

$$l_{m'}\left[\overline{H}^{+}_{m'} \cdot \frac{\bar{\rho}^{c+}_{m'}}{2} + \overline{H}^{-}_{m'} \cdot \frac{\bar{\rho}^{c-}_{m'}}{2}\right] = l_{m'}\left[\overline{B}^{+}_{m'n} \cdot \frac{\bar{\rho}^{c+}_{m'}}{2} + \overline{B}^{-}_{m'n} \cdot \frac{\bar{\rho}^{c-}_{m'}}{2} + \Theta^{-}_{m'n} - \Theta^{+}_{m'n}\right] \quad (A.169)$$

where

$$\overline{B}^{\pm}_{m'n} = -\int_{S_1} dS_1 I_n \overline{f}_n(\bar{r}') \times \nabla'\left(\frac{e^{ik_0 R^{\pm}_{m'}}}{4\pi R^{\pm}_{m'}}\right) - \int_{S_1} dS_1 I_n \overline{f}_n(\bar{r}') \times \nabla'\left(\frac{e^{ik_1 R^{\pm}_{m'}}}{4\pi R^{\pm}_{m'}}\right)$$
$$-\int_{S_1} dS_1 i\omega\epsilon_0 K_{n'} \overline{f}_{n'}(\bar{r}')\frac{e^{ik_0 R^{\pm}_{m'}}}{4\pi R^{\pm}_{m'}} - \int_{S_1} dS_1 i\omega\epsilon K_{n'} \overline{f}_{n'}(\bar{r}')\frac{e^{ik_1 R^{\pm}_{m'}}}{4\pi R^{\pm}_{m'}}$$
$$-\int_{S_2} dS_2 L_{n''} \overline{f}_{n''}(\bar{r}') \times \nabla'\left(\frac{e^{ik_0 R^{\pm}_{m'}}}{4\pi R^{\pm}_{m'}}\right)$$
$$+\int_{S_3} dS_3 P_{n'''} \overline{f}_{n'''}(\bar{r}') \times \nabla'\left(\frac{e^{ik_1 R^{\pm}_{m'}}}{4\pi R^{\pm}_{m'}}\right) \qquad (A.170)$$

and

$$\Theta^{\pm}_{m'n} = -\int_{S_1} dS_1 \frac{i\omega\epsilon_0}{k_0^2}\left(\nabla'_s \cdot K_{n'} \overline{f}_{n'}(\bar{r}')\right)\frac{e^{ik_0 R^{\pm}_{m'}}}{4\pi R^{\pm}_{m'}}$$
$$-\int_{S_1} dS_1 \frac{i\omega\epsilon}{k_1^2}\left(\nabla'_s \cdot K_{n'} \overline{f}_{n'}(\bar{r}')\right)\frac{e^{ik_1 R^{\pm}_{m'}}}{4\pi R^{\pm}_{m'}}. \qquad (A.171)$$

Also, (A.162) becomes (with $R^{\pm}_{m''} = |\bar{r}^{c\pm}_{m''} - \bar{r}'|$ and where m'' is defined over the surface of the exposed perfect conductor)

$$l_{m''}\left[\overline{E}^{+}_{m''}\cdot\frac{\bar{\rho}^{c+}_{m''}}{2}+\overline{E}^{-}_{m''}\cdot\frac{\bar{\rho}^{c-}_{m''}}{2}\right] = l_{m''}\left[\overline{C}^{+}_{m''n}\cdot\frac{\bar{\rho}^{c+}_{m''}}{2}+\overline{C}^{-}_{m''n}\cdot\frac{\bar{\rho}^{c-}_{m''}}{2}+\Psi^{-}_{m''n}-\Psi^{+}_{m''n}\right] \quad (A.172)$$

where

$$\overline{C}^{\pm}_{m''n} = -\int_{S_1} dS_1 i\omega\mu_0 I_n \overline{f}_n(\bar{r}')\frac{e^{ik_0R^{\pm}_{m''}}}{4\pi R^{\pm}_{m''}} + \int_{S_1} dS_1 K_{n'}\overline{f}_{n'}(\bar{r}')\times\nabla'\left(\frac{e^{ik_0R^{\pm}_{m''}}}{4\pi R^{\pm}_{m''}}\right)$$
$$-\int_{S_2} dS_2 i\omega\mu_0 L_{n''}\overline{f}_{n''}(\bar{r}')\frac{e^{ik_0R^{\pm}_{m''}}}{4\pi R^{\pm}_{m''}} \quad (A.173)$$

and

$$\Psi^{\pm}_{m''n} = -\int_{S_1} dS_1\frac{i\omega\mu_0}{k_0^2}\left(\nabla'_s\cdot I_n\overline{f}_n(\bar{r}')\right)\frac{e^{ik_0R^{\pm}_{m''}}}{4\pi R^{\pm}_{m''}}$$
$$-\int_{S_2} dS_2\frac{i\omega\mu_0}{k_0^2}\left(\nabla'_s\cdot L_{n''}\overline{f}_{n''}(\bar{r}')\right)\frac{e^{ik_0R^{\pm}_{m''}}}{4\pi R^{\pm}_{m''}}. \quad (A.174)$$

Finally, (A.163) becomes (with $R^{\pm}_{m'''} = |\bar{r}^{c\pm}_{m'''} - \bar{r}'|$ and where m''' is defined over the surface of the coated perfect conductor)

$$\bar{0}_{m'''} = l_{m'''}\left[\overline{D}^{+}_{m'''n}\cdot\frac{\bar{\rho}^{c+}_{m'''}}{2}+\overline{D}^{-}_{m'''n}\cdot\frac{\bar{\rho}^{c-}_{m'''}}{2}+\Lambda^{-}_{m'''n}-\Lambda^{+}_{m'''n}\right] \quad (A.175)$$

where

$$\overline{D}^{\pm}_{m'''n} = -\int_{S_1} dS_1 i\omega\mu I_n\overline{f}_n(\bar{r}')\frac{e^{ik_1R^{\pm}_{m'''}}}{4\pi R^{\pm}_{m'''}} + \int_{S_1} dS_1 K_{n'}\overline{f}_{n'}(\bar{r}')\times\nabla'\left(\frac{e^{ik_1R^{\pm}_{m'''}}}{4\pi R^{\pm}_{m'''}}\right)$$
$$+\int_{S_3} dS_3 i\omega\mu P_{n'''}\overline{f}_{n'''}(\bar{r}')\frac{e^{ik_1R^{\pm}_{m'''}}}{4\pi R^{\pm}_{m'''}} \quad (A.176)$$

and

$$\Lambda^{\pm}_{m'''n} = -\int_{S_1} dS_1 \frac{i\omega\mu}{k_1^2}\left(\nabla'_s \cdot I_n \overline{f}_n(\bar{r}')\right)\frac{e^{ik_1 R^{\pm}_{m'''}}}{4\pi R^{\pm}_{m'''}} + \int_{S_3} dS_3 \frac{i\omega\mu}{k_1^2}\left(\nabla'_s \cdot P_{n'''}\overline{f}_{n'''}(\bar{r}')\right)\frac{e^{ik_1 R^{\pm}_{m'''}}}{4\pi R^{\pm}_{m'''}}. \quad (A.177)$$

Substituting (A.167) and (A.168), (A.166) becomes

$$\begin{aligned} l_m\left[\overline{E}^{+}_m \cdot \frac{\bar{\rho}^{c+}_m}{2} + \overline{E}^{-}_m \cdot \frac{\bar{\rho}^{c-}_m}{2}\right] = \\ I_n\left[-\frac{i\omega\mu_0}{4\pi}\frac{l_m l_n}{4A^{\pm}_n}\bar{\rho}^{c\pm}_m \cdot \int_{T^{\pm}_n} d\bar{r}'\bar{\rho}^{\pm}_n \frac{e^{ik_0 R^{\pm}_m}}{R^{\pm}_m} \pm \frac{i}{4\pi\omega\epsilon_0}\frac{l_m l_n}{A^{\pm}_n}\int_{T^{\pm}_n} d\bar{r}'\frac{e^{ik_0 R^{\pm}_m}}{R^{\pm}_m}\right] \\ +I_n\left[-\frac{i\omega\mu}{4\pi}\frac{l_m l_n}{4A^{\pm}_n}\bar{\rho}^{c\pm}_m \cdot \int_{T^{\pm}_n} d\bar{r}'\bar{\rho}^{\pm}_n \frac{e^{ik_1 R^{\pm}_m}}{R^{\pm}_m} \pm \frac{i}{4\pi\omega\epsilon}\frac{l_m l_n}{A^{\pm}_n}\int_{T^{\pm}_n} d\bar{r}'\frac{e^{ik_1 R^{\pm}_m}}{R^{\pm}_m}\right] \\ +K_{n'}\left[\frac{1}{4\pi}\frac{l_m l_{n'}}{4A^{\pm}_{n'}}\bar{\rho}^{c\pm}_m \cdot \int_{T^{\pm}_{n'}} d\bar{r}'\bar{\rho}^{\pm}_{n'} \times \nabla'\left(\frac{e^{ik_0 R^{\pm}_m}}{R^{\pm}_m}\right)\right] \\ +K_{n'}\left[\frac{1}{4\pi}\frac{l_m l_{n'}}{4A^{\pm}_{n'}}\bar{\rho}^{c\pm}_m \cdot \int_{T^{\pm}_{n'}} d\bar{r}'\bar{\rho}^{\pm}_{n'} \times \nabla'\left(\frac{e^{ik_1 R^{\pm}_m}}{R^{\pm}_m}\right)\right] \\ +L_{n''}\left[-\frac{i\omega\mu_0}{4\pi}\frac{l_m l_{n''}}{4A^{\pm}_{n''}}\bar{\rho}^{c\pm}_m \cdot \int_{T^{\pm}_{n''}} d\bar{r}'\bar{\rho}^{\pm}_{n''} \frac{e^{ik_0 R^{\pm}_m}}{R^{\pm}_m} \pm \frac{i}{4\pi\omega\epsilon_0}\frac{l_m l_{n''}}{A^{\pm}_{n''}}\int_{T^{\pm}_{n''}} d\bar{r}'\frac{e^{ik_0 R^{\pm}_m}}{R^{\pm}_m}\right] \\ +P_{n'''}\left[\frac{i\omega\mu}{4\pi}\frac{l_m l_{n'''}}{4A^{\pm}_{n'''}}\bar{\rho}^{c\pm}_m \cdot \int_{T^{\pm}_{n'''}} d\bar{r}'\bar{\rho}^{\pm}_{n'''} \frac{e^{ik_1 R^{\pm}_m}}{R^{\pm}_m} \pm \frac{-i}{4\pi\omega\epsilon}\frac{l_m l_{n'''}}{A^{\pm}_{n'''}}\int_{T^{\pm}_{n'''}} d\bar{r}'\frac{e^{ik_1 R^{\pm}_m}}{R^{\pm}_m}\right]. \end{aligned} \quad (A.178)$$

Substituting (A.170) and (A.171), (A.169) becomes

$$\begin{aligned} l_{m'}\left[\overline{H}^{+}_{m'} \cdot \frac{\bar{\rho}^{c+}_{m'}}{2} + \overline{H}^{-}_{m'} \cdot \frac{\bar{\rho}^{c-}_{m'}}{2}\right] = \\ I_n\left[-\frac{1}{4\pi}\frac{l_{m'} l_n}{4A^{\pm}_n}\bar{\rho}^{c\pm}_{m'} \cdot \int_{T^{\pm}_n} d\bar{r}'\bar{\rho}^{\pm}_n \times \nabla'\left(\frac{e^{ik_0 R^{\pm}_{m'}}}{R^{\pm}_{m'}}\right)\right] \\ +I_n\left[-\frac{1}{4\pi}\frac{l_{m'} l_n}{4A^{\pm}_n}\bar{\rho}^{c\pm}_{m'} \cdot \int_{T^{\pm}_n} d\bar{r}'\bar{\rho}^{\pm}_n \times \nabla'\left(\frac{e^{ik_1 R^{\pm}_{m'}}}{R^{\pm}_{m'}}\right)\right] \\ +K_{n'}\left[-\frac{i\omega\epsilon_0}{4\pi}\frac{l_{m'} l_{n'}}{4A^{\pm}_{n'}}\bar{\rho}^{c\pm}_{m'} \cdot \int_{T^{\pm}_{n'}} d\bar{r}'\bar{\rho}^{\pm}_{n'} \frac{e^{ik_0 R^{\pm}_{m'}}}{R^{\pm}_{m'}} \pm \frac{i}{4\pi\omega\mu_0}\frac{l_{m'} l_{n'}}{A^{\pm}_{n'}}\int_{T^{\pm}_{n'}} d\bar{r}'\frac{e^{ik_0 R^{\pm}_{m'}}}{R^{\pm}_{m'}}\right] \end{aligned}$$

$$+K_{n'}\left[-\frac{i\omega\epsilon}{4\pi}\frac{l_{m'}l_{n'}}{4A^{\pm}_{n'}}\bar{\rho}^{c\pm}_{m'}\cdot\int_{T^{\pm}_{n'}}d\bar{r}'\bar{\rho}^{\pm}_{n'}\frac{e^{ik_1R^{\pm}_{m'}}}{R^{\pm}_{m'}}\pm\frac{i}{4\pi\omega\mu}\frac{l_{m'}l_{n'}}{A^{\pm}_{n'}}\int_{T^{\pm}_{n'}}d\bar{r}'\frac{e^{ik_1R^{\pm}_{m'}}}{R^{\pm}_{m'}}\right]$$

$$+L_{n''}\left[-\frac{1}{4\pi}\frac{l_{m'}l_{n''}}{4A^{\pm}_{n''}}\bar{\rho}^{c\pm}_{m'}\cdot\int_{T^{\pm}_{n''}}d\bar{r}'\bar{\rho}^{\pm}_{n''}\times\nabla'\left(\frac{e^{ik_0R^{\pm}_{m'}}}{R^{\pm}_{m'}}\right)\right]$$

$$+P_{n'''}\left[\frac{1}{4\pi}\frac{l_{m'}l_{n'''}}{4A^{\pm}_{n'''}}\bar{\rho}^{c\pm}_{m'}\cdot\int_{T^{\pm}_{n'''}}d\bar{r}'\bar{\rho}^{\pm}_{n'''}\times\nabla'\left(\frac{e^{ik_1R^{\pm}_{m'}}}{R^{\pm}_{m'}}\right)\right]. \qquad (A.179)$$

Substituting (A.173) and (A.174), (A.172) becomes

$$l_{m''}\left[\overline{E^{+}_{m''}}\cdot\frac{\bar{\rho}^{c+}_{m''}}{2}+\overline{E^{-}_{m''}}\cdot\frac{\bar{\rho}^{c-}_{m''}}{2}\right]=$$

$$I_n\left[-\frac{i\omega\mu_0}{4\pi}\frac{l_{m''}l_n}{4A^{\pm}_n}\bar{\rho}^{c\pm}_{m''}\cdot\int_{T^{\pm}_n}d\bar{r}'\bar{\rho}^{\pm}_n\frac{e^{ik_0R^{\pm}_{m''}}}{R^{\pm}_{m''}}\pm\frac{i}{4\pi\omega\epsilon_0}\frac{l_{m''}l_n}{A^{\pm}_n}\int_{T^{\pm}_n}d\bar{r}'\frac{e^{ik_0R^{\pm}_{m''}}}{R^{\pm}_{m''}}\right]$$

$$+K_{n'}\left[\frac{1}{4\pi}\frac{l_{m''}l_{n'}}{4A^{\pm}_{n'}}\bar{\rho}^{c\pm}_{m''}\cdot\int_{T^{\pm}_{n'}}d\bar{r}'\bar{\rho}^{\pm}_{n'}\times\nabla'\left(\frac{e^{ik_0R^{\pm}_{m''}}}{R^{\pm}_{m''}}\right)\right]$$

$$+L_{n''}\left[-\frac{i\omega\mu_0}{4\pi}\frac{l_{m''}l_{n''}}{4A^{\pm}_{n''}}\bar{\rho}^{c\pm}_{m''}\cdot\int_{T^{\pm}_{n''}}d\bar{r}'\bar{\rho}^{\pm}_{n''}\frac{e^{ik_0R^{\pm}_{m''}}}{R^{\pm}_{m''}}\right.$$

$$\left.\pm\frac{i}{4\pi\omega\epsilon_0}\frac{l_{m''}l_{n''}}{A^{\pm}_{n''}}\int_{T^{\pm}_{n''}}d\bar{r}'\frac{e^{ik_0R^{\pm}_{m''}}}{R^{\pm}_{m''}}\right]. \qquad (A.180)$$

Substituting (A.176) and (A.177), (A.175) becomes

$$\bar{0}_{m'''}=I_n\left[-\frac{i\omega\mu}{4\pi}\frac{l_{m'''}l_n}{4A^{\pm}_n}\bar{\rho}^{c\pm}_{m'''}\cdot\int_{T^{\pm}_n}d\bar{r}'\bar{\rho}^{\pm}_n\frac{e^{ik_1R^{\pm}_{m'''}}}{R^{\pm}_{m'''}}\pm\frac{i}{4\pi\omega\epsilon}\frac{l_{m'''}l_n}{A^{\pm}_n}\int_{T^{\pm}_n}d\bar{r}'\frac{e^{ik_1R^{\pm}_{m'''}}}{R^{\pm}_{m'''}}\right]$$

$$+K_{n'}\left[\frac{1}{4\pi}\frac{l_{m'''}l_{n'}}{4A^{\pm}_{n'}}\bar{\rho}^{c\pm}_{m'''}\cdot\int_{T^{\pm}_{n'}}d\bar{r}'\bar{\rho}^{\pm}_{n'}\times\nabla'\left(\frac{e^{ik_1R^{\pm}_{m'''}}}{R^{\pm}_{m'''}}\right)\right]$$

$$+P_{n'''}\left[\frac{i\omega\mu}{4\pi}\frac{l_{m'''}l_{n'''}}{4A^{\pm}_{n'''}}\bar{\rho}^{c\pm}_{m'''}\cdot\int_{T^{\pm}_{n'''}}d\bar{r}'\bar{\rho}^{\pm}_{n'''}\frac{e^{ik_1R^{\pm}_{m'''}}}{R^{\pm}_{m'''}}\right.$$

$$\left.\pm\frac{-i}{4\pi\omega\epsilon}\frac{l_{m'''}l_{n'''}}{A^{\pm}_{n'''}}\int_{T^{\pm}_{n'''}}d\bar{r}'\frac{e^{ik_1R^{\pm}_{m'''}}}{R^{\pm}_{m'''}}\right]. \qquad (A.181)$$

By using (A.85), equations (A.178) through (A.181) yield a system of equations which can be written in the following form:

$$\begin{pmatrix} l_m\left[\overline{E}_m^+ \cdot \frac{\bar{\rho}_m^{c+}}{2} + \overline{E}_m^- \cdot \frac{\bar{\rho}_m^{c-}}{2}\right] \\ l_{m'}\left[\overline{H}_{m'}^+ \cdot \frac{\bar{\rho}_{m'}^{c+}}{2} + \overline{H}_{m'}^- \cdot \frac{\bar{\rho}_{m'}^{c-}}{2}\right] \\ l_{m''}\left[\overline{E}_{m''}^+ \cdot \frac{\bar{\rho}_{m''}^{c+}}{2} + \overline{E}_{m''}^- \cdot \frac{\bar{\rho}_{m''}^{c-}}{2}\right] \\ 0_{m'''} \end{pmatrix} = \begin{pmatrix} Z_{mn} & Z_{mn'} & Z_{mn''} & Z_{mn'''} \\ Z_{m'n} & Z_{m'n'} & Z_{m'n''} & Z_{m'n'''} \\ Z_{m''n} & Z_{m''n'} & Z_{m''n''} & Z_{m''n'''} \\ Z_{m'''n} & Z_{m'''n'} & Z_{m'''n''} & Z_{m'''n'''} \end{pmatrix} \begin{pmatrix} I_n \\ K_{n'} \\ L_{n''} \\ P_{n'''} \end{pmatrix} \tag{A.182}$$

This equation has the form of $\overline{V} = \overline{\overline{Z}} \cdot \overline{I}$ where $\overline{V}$ represents the incident electric and magnetic field excitation vector at the boundary surfaces. $\overline{I}$ represents the unknown electric and magnetic surface current coefficients, and $\overline{\overline{Z}}$ represents the interaction matrix for all the triangular patches used to model the surfaces. The unknown surface current coefficients can be found by inverting the Z-matrix and multiplying the excitation vector by the inverted Z-matrix. The Z-matrix can now be written as

$$\begin{pmatrix} CZ1 & CZ2 & CZ3 & CZ4 \\ CZ5 & CZ6 & CZ7 & CZ8 \\ CZ9 & CZ10 & CZ11 & CZ12 \\ CZ13 & CZ14 & CZ15 & CZ16 \end{pmatrix} \tag{A.183}$$

where the individual elements are

$$\begin{aligned} CZ1 = &\left[-\frac{i\omega\mu_0}{4\pi}\frac{l_m l_n}{4A_n^{\pm}}\bar{\rho}_m^{c\pm} \cdot \int_{T_n^{\pm}} d\bar{r}'\,\bar{\rho}_n^{\pm}\frac{e^{ik_0 R_m^{\pm}}}{R_m^{\pm}} \pm \frac{i}{4\pi\omega\epsilon_0}\frac{l_m l_n}{A_n^{\pm}}\int_{T_n^{\pm}} d\bar{r}'\frac{e^{ik_0 R_m^{\pm}}}{R_m^{\pm}}\right] \\ &+ \left[-\frac{i\omega\mu}{4\pi}\frac{l_m l_n}{4A_n^{\pm}}\bar{\rho}_m^{c\pm} \cdot \int_{T_n^{\pm}} d\bar{r}'\,\bar{\rho}_n^{\pm}\frac{e^{ik_1 R_m^{\pm}}}{R_m^{\pm}} \pm \frac{i}{4\pi\omega\epsilon}\frac{l_m l_n}{A_n^{\pm}}\int_{T_n^{\pm}} d\bar{r}'\frac{e^{ik_1 R_m^{\pm}}}{R_m^{\pm}}\right] \end{aligned} \tag{A.184}$$

$$\begin{aligned} CZ2 = &\left[\frac{1}{4\pi}\frac{l_m l_{n'}}{4A_{n'}^{\pm}}\bar{\rho}_m^{c\pm} \cdot \int_{T_{n'}^{\pm}} d\bar{r}'\,\bar{\rho}_{n'}^{\pm} \times (\bar{r}_m^{c\pm} - \bar{r}')(1 - ik_0 R_m^{\pm})\frac{e^{ik_0 R_m^{\pm}}}{(R_m^{\pm})^3}\right] \\ &+ \left[\frac{1}{4\pi}\frac{l_m l_{n'}}{4A_{n'}^{\pm}}\bar{\rho}_m^{c\pm} \cdot \int_{T_{n'}^{\pm}} d\bar{r}'\,\bar{\rho}_{n'}^{\pm} \times (\bar{r}_m^{c\pm} - \bar{r}')(1 - ik_1 R_m^{\pm})\frac{e^{ik_1 R_m^{\pm}}}{(R_m^{\pm})^3}\right] \end{aligned} \tag{A.185}$$

$$\begin{aligned} CZ3 = &\left[-\frac{i\omega\mu_0}{4\pi}\frac{l_m l_{n''}}{4A_{n''}^{\pm}}\bar{\rho}_m^{c\pm} \cdot \int_{T_{n''}^{\pm}} d\bar{r}'\,\bar{\rho}_{n''}^{\pm}\frac{e^{ik_0 R_m^{\pm}}}{R_m^{\pm}}\right. \\ &\left. \pm \frac{i}{4\pi\omega\epsilon_0}\frac{l_m l_{n''}}{A_{n''}^{\pm}}\int_{T_{n''}^{\pm}} d\bar{r}'\frac{e^{ik_0 R_m^{\pm}}}{R_m^{\pm}}\right] \end{aligned} \tag{A.186}$$

$$CZ4 = \left[\frac{i\omega\mu}{4\pi}\frac{l_m l_{n'''}}{4A^{\pm}_{n'''}}\bar{\rho}^{c\pm}_{m} \cdot \int_{T^{\pm}_{n'''}} d\bar{r}'\,\bar{\rho}^{\pm}_{n'''}\frac{e^{ik_1 R^{\pm}_m}}{R^{\pm}_m} \pm \frac{-i}{4\pi\omega\epsilon}\frac{l_m l_{n'''}}{A^{\pm}_{n'''}}\int_{T^{\pm}_{n'''}} d\bar{r}'\frac{e^{ik_1 R^{\pm}_m}}{R^{\pm}_m}\right] \tag{A.187}$$

$$CZ5 = \left[-\frac{1}{4\pi}\frac{l_{m'}l_n}{4A^{\pm}_n}\bar{\rho}^{c\pm}_{m'} \cdot \int_{T^{\pm}_n} d\bar{r}'\,\bar{\rho}^{\pm}_n \times (\bar{r}^{c\pm}_{m'} - \bar{r}')(1 - ik_0 R^{\pm}_{m'})\frac{e^{ik_0 R^{\pm}_{m'}}}{(R^{\pm}_{m'})^3}\right] + \left[-\frac{1}{4\pi}\frac{l_{m'}l_n}{4A^{\pm}_n}\bar{\rho}^{c\pm}_{m'} \cdot \int_{T^{\pm}_n} d\bar{r}'\,\bar{\rho}^{\pm}_n \times (\bar{r}^{c\pm}_{m'} - \bar{r}')(1 - ik_1 R^{\pm}_{m'})\frac{e^{ik_1 R^{\pm}_{m'}}}{(R^{\pm}_{m'})^3}\right] \tag{A.188}$$

$$CZ6 = \left[-\frac{i\omega\epsilon_0}{4\pi}\frac{l_{m'}l_{n'}}{4A^{\pm}_{n'}}\bar{\rho}^{c\pm}_{m'} \cdot \int_{T^{\pm}_{n'}} d\bar{r}'\,\bar{\rho}^{\pm}_{n'}\frac{e^{ik_0 R^{\pm}_{m'}}}{R^{\pm}_{m'}} \pm \frac{i}{4\pi\omega\mu_0}\frac{l_{m'}l_{n'}}{A^{\pm}_{n'}}\int_{T^{\pm}_{n'}} d\bar{r}'\frac{e^{ik_0 R^{\pm}_{m'}}}{R^{\pm}_{m'}}\right] + \left[-\frac{i\omega\epsilon}{4\pi}\frac{l_{m'}l_{n'}}{4A^{\pm}_{n'}}\bar{\rho}^{c\pm}_{m'} \cdot \int_{T^{\pm}_{n'}} d\bar{r}'\,\bar{\rho}^{\pm}_{n'}\frac{e^{ik_1 R^{\pm}_{m'}}}{R^{\pm}_{m'}} \pm \frac{i}{4\pi\omega\mu}\frac{l_{m'}l_{n'}}{A^{\pm}_{n'}}\int_{T^{\pm}_{n'}} d\bar{r}'\frac{e^{ik_1 R^{\pm}_{m'}}}{R^{\pm}_{m'}}\right] \tag{A.189}$$

$$CZ7 = \left[-\frac{1}{4\pi}\frac{l_{m'}l_{n''}}{4A^{\pm}_{n''}}\bar{\rho}^{c\pm}_{m'} \cdot \int_{T^{\pm}_{n''}} d\bar{r}'\,\bar{\rho}^{\pm}_{n''} \times (\bar{r}^{c\pm}_{m'} - \bar{r}')(1 - ik_0 R^{\pm}_{m'})\frac{e^{ik_0 R^{\pm}_{m'}}}{(R^{\pm}_{m'})^3}\right] \tag{A.190}$$

$$CZ8 = \left[\frac{1}{4\pi}\frac{l_{m'}l_{n'''}}{4A^{\pm}_{n'''}}\bar{\rho}^{c\pm}_{m'} \cdot \int_{T^{\pm}_{n'''}} d\bar{r}'\,\bar{\rho}^{\pm}_{n'''} \times (\bar{r}^{c\pm}_{m'} - \bar{r}')(1 - ik_1 R^{\pm}_{m'})\frac{e^{ik_1 R^{\pm}_{m'}}}{(R^{\pm}_{m'})^3}\right] \tag{A.191}$$

$$CZ9 = \left[-\frac{i\omega\mu_0}{4\pi}\frac{l_{m''}l_n}{4A^{\pm}_n}\bar{\rho}^{c\pm}_{m''} \cdot \int_{T^{\pm}_n} d\bar{r}'\,\bar{\rho}^{\pm}_n\frac{e^{ik_0 R^{\pm}_{m''}}}{R^{\pm}_{m''}} \pm \frac{i}{4\pi\omega\epsilon_0}\frac{l_{m''}l_n}{A^{\pm}_n}\int_{T^{\pm}_n} d\bar{r}'\frac{e^{ik_0 R^{\pm}_{m''}}}{R^{\pm}_{m''}}\right] \tag{A.192}$$

$$CZ10 = \left[\frac{1}{4\pi}\frac{l_{m''}l_{n'}}{4A^{\pm}_{n'}}\bar{\rho}^{c\pm}_{m''} \cdot \int_{T^{\pm}_{n'}} d\bar{r}'\,\bar{\rho}^{\pm}_{n'} \times (\bar{r}^{c\pm}_{m''} - \bar{r}')(1 - ik_0 R^{\pm}_{m''})\frac{e^{ik_0 R^{\pm}_{m''}}}{(R^{\pm}_{m''})^3}\right] \tag{A.193}$$

$$CZ11 = \left[-\frac{i\omega\mu_0}{4\pi}\frac{l_{m''}l_{n''}}{4A^{\pm}_{n''}}\bar{\rho}^{c\pm}_{m''} \cdot \int_{T^{\pm}_{n''}} d\bar{r}'\,\bar{\rho}^{\pm}_{n''}\frac{e^{ik_0 R^{\pm}_{m''}}}{R^{\pm}_{m''}}\right.$$

$$\pm \frac{i}{4\pi\omega\epsilon_0}\frac{l_{m''}l_{n''}}{A^{\pm}_{n''}}\int_{T^{\pm}_{n''}} d\bar{r}'\frac{e^{ik_0R^{\pm}_{m''}}}{R^{\pm}_{m''}}\Bigg] \tag{A.194}$$

$$CZ12 = \bar{0}_{m''n'''} \tag{A.195}$$

$$CZ13 = \Bigg[-\frac{i\omega\mu}{4\pi}\frac{l_{m'''}l_n}{4A^{\pm}_n}\bar{\rho}^{c\pm}_{m'''}\cdot\int_{T^{\pm}_n} d\bar{r}'\bar{\rho}^{\pm}_n\frac{e^{ik_1R^{\pm}_{m'''}}}{R^{\pm}_{m'''}}$$
$$\pm \frac{i}{4\pi\omega\epsilon}\frac{l_{m'''}l_n}{A^{\pm}_n}\int_{T^{\pm}_n} d\bar{r}'\frac{e^{ik_1R^{\pm}_{m'''}}}{R^{\pm}_{m'''}}\Bigg] \tag{A.196}$$

$$CZ14 = \left[\frac{1}{4\pi}\frac{l_{m'''}l_{n'}}{4A^{\pm}_{n'}}\bar{\rho}^{c\pm}_{m'''}\cdot\int_{T^{\pm}_{n'}} d\bar{r}'\bar{\rho}^{\pm}_{n'}\times(\bar{r}^{c\pm}_{m'''}-\bar{r}')(1-ik_1R^{\pm}_{m'''})\frac{e^{ik_1R^{\pm}_{m'''}}}{(R^{\pm}_{m'''})^3}\right] \tag{A.197}$$

$$CZ15 = \bar{0}_{m'''n''} \tag{A.198}$$

$$CZ16 = \Bigg[\frac{i\omega\mu}{4\pi}\frac{l_{m'''}l_{n'''}}{4A^{\pm}_{n'''}}\bar{\rho}^{c\pm}_{m'''}\cdot\int_{T^{\pm}_{n'''}} d\bar{r}'\bar{\rho}^{\pm}_{n'''}\frac{e^{ik_1R^{\pm}_{m'''}}}{R^{\pm}_{m'''}}$$
$$\pm \frac{-i}{4\pi\omega\epsilon}\frac{l_{m'''}l_{n'''}}{A^{\pm}_{n'''}}\int_{T^{\pm}_{n'''}} d\bar{r}'\frac{e^{ik_1R^{\pm}_{m'''}}}{R^{\pm}_{m'''}}\Bigg]. \tag{A.199}$$

Now to satisfy duality, CZ2 = -CZ5. Further, to satisfy reciprocity, CZ2 = -$CZ5^T$, CZ3 = $CZ9^T$, CZ4 = $CZ13^T$, CZ7 = -$CZ10^T$, CZ8 = -$CZ14^T$, and CZ12 = $CZ15^T$. Multiplying the second and fourth sets of equations by -1 yields a symmetric Z-matrix:

$$\begin{pmatrix} l_m\left[\overline{E}^{+}_m\cdot\frac{\bar{\rho}^{c+}_m}{2}+\overline{E}^{-}_m\cdot\frac{\bar{\rho}^{c-}_m}{2}\right] \\ -l_{m'}\left[\overline{H}^{+}_{m'}\cdot\frac{\bar{\rho}^{c+}_{m'}}{2}+\overline{H}^{-}_{m'}\cdot\frac{\bar{\rho}^{c-}_{m'}}{2}\right] \\ l_{m''}\left[\overline{E}^{+}_{m''}\cdot\frac{\bar{\rho}^{c+}_{m''}}{2}+\overline{E}^{-}_{m''}\cdot\frac{\bar{\rho}^{c-}_{m''}}{2}\right] \\ \bar{0}_{m'''} \end{pmatrix} = \begin{pmatrix} CZ1 & CZ2 & CZ3 & CZ4 \\ CZ5 & CZ6 & CZ7 & CZ8 \\ CZ9 & CZ10 & CZ11 & CZ12 \\ CZ13 & CZ14 & CZ15 & CZ16 \end{pmatrix}\begin{pmatrix} I_n \\ K_{n'} \\ L_{n''} \\ P_{n'''} \end{pmatrix} \tag{A.200}$$

where the individual elements are

$$CZ1 = \left[-\frac{i\omega\mu_0}{4\pi}\frac{l_ml_n}{4A^{\pm}_n}\bar{\rho}^{c\pm}_m\cdot\int_{T^{\pm}_n} d\bar{r}'\bar{\rho}^{\pm}_n\frac{e^{ik_0R^{\pm}_m}}{R^{\pm}_m}\pm\frac{i}{4\pi\omega\epsilon_0}\frac{l_ml_n}{A^{\pm}_n}\int_{T^{\pm}_n} d\bar{r}'\frac{e^{ik_0R^{\pm}_m}}{R^{\pm}_m}\right]$$

$$+\left[-\frac{i\omega\mu}{4\pi}\frac{l_m l_n}{4A_n^{\pm}}\bar{\rho}_m^{c\pm}\cdot\int_{T_n^{\pm}}d\bar{r}'\bar{\rho}_n^{\pm}\frac{e^{ik_1R_m^{\pm}}}{R_m^{\pm}}\pm\frac{i}{4\pi\omega\epsilon}\frac{l_m l_n}{A_n^{\pm}}\int_{T_n^{\pm}}d\bar{r}'\frac{e^{ik_1R_m^{\pm}}}{R_m^{\pm}}\right] \quad (A.201)$$

$$CZ2=\left[\frac{1}{4\pi}\frac{l_m l_{n'}}{4A_{n'}^{\pm}}\bar{\rho}_m^{c\pm}\cdot\int_{T_{n'}^{\pm}}d\bar{r}'\bar{\rho}_{n'}^{\pm}\times(\bar{r}_m^{c\pm}-\bar{r}')(1-ik_0R_m^{\pm})\frac{e^{ik_0R_m^{\pm}}}{(R_m^{\pm})^3}\right]$$
$$+\left[\frac{1}{4\pi}\frac{l_m l_{n'}}{4A_{n'}^{\pm}}\bar{\rho}_m^{c\pm}\cdot\int_{T_{n'}^{\pm}}d\bar{r}'\bar{\rho}_{n'}^{\pm}\times(\bar{r}_m^{c\pm}-\bar{r}')(1-ik_1R_m^{\pm})\frac{e^{ik_1R_m^{\pm}}}{(R_m^{\pm})^3}\right] \quad (A.202)$$

$$CZ3=\left[-\frac{i\omega\mu_0}{4\pi}\frac{l_m l_{n''}}{4A_{n''}^{\pm}}\bar{\rho}_m^{c\pm}\cdot\int_{T_{n''}^{\pm}}d\bar{r}'\bar{\rho}_{n''}^{\pm}\frac{e^{ik_0R_m^{\pm}}}{R_m^{\pm}}\right.$$
$$\left.\pm\frac{i}{4\pi\omega\epsilon_0}\frac{l_m l_{n''}}{A_{n''}^{\pm}}\int_{T_{n''}^{\pm}}d\bar{r}'\frac{e^{ik_0R_m^{\pm}}}{R_m^{\pm}}\right] \quad (A.203)$$

$$CZ4=\left[\frac{i\omega\mu}{4\pi}\frac{l_m l_{n'''}}{4A_{n'''}^{\pm}}\bar{\rho}_m^{c\pm}\cdot\int_{T_{n'''}^{\pm}}d\bar{r}'\bar{\rho}_{n'''}^{\pm}\frac{e^{ik_1R_m^{\pm}}}{R_m^{\pm}}\right.$$
$$\left.\pm\frac{-i}{4\pi\omega\epsilon}\frac{l_m l_{n'''}}{A_{n'''}^{\pm}}\int_{T_{n'''}^{\pm}}d\bar{r}'\frac{e^{ik_1R_m^{\pm}}}{R_m^{\pm}}\right] \quad (A.204)$$

$$CZ5=\left[\frac{1}{4\pi}\frac{l_{m'}l_n}{4A_n^{\pm}}\bar{\rho}_{m'}^{c\pm}\cdot\int_{T_n^{\pm}}d\bar{r}'\bar{\rho}_n^{\pm}\times(\bar{r}_{m'}^{c\pm}-\bar{r}')(1-ik_0R_{m'}^{\pm})\frac{e^{ik_0R_{m'}^{\pm}}}{(R_{m'}^{\pm})^3}\right]$$
$$+\left[\frac{1}{4\pi}\frac{l_{m'}l_n}{4A_n^{\pm}}\bar{\rho}_{m'}^{c\pm}\cdot\int_{T_n^{\pm}}d\bar{r}'\bar{\rho}_n^{\pm}\times(\bar{r}_{m'}^{c\pm}-\bar{r}')(1-ik_1R_{m'}^{\pm})\frac{e^{ik_1R_{m'}^{\pm}}}{(R_{m'}^{\pm})^3}\right] \quad (A.205)$$

$$CZ6=\left[\frac{i\omega\epsilon_0}{4\pi}\frac{l_{m'}l_{n'}}{4A_{n'}^{\pm}}\bar{\rho}_{m'}^{c\pm}\cdot\int_{T_{n'}^{\pm}}d\bar{r}'\bar{\rho}_{n'}^{\pm}\frac{e^{ik_0R_{m'}^{\pm}}}{R_{m'}^{\pm}}\pm\frac{-i}{4\pi\omega\mu_0}\frac{l_{m'}l_{n'}}{A_{n'}^{\pm}}\int_{T_{n'}^{\pm}}d\bar{r}'\frac{e^{ik_0R_{m'}^{\pm}}}{R_{m'}^{\pm}}\right]$$
$$+\left[\frac{i\omega\epsilon}{4\pi}\frac{l_{m'}l_{n'}}{4A_{n'}^{\pm}}\bar{\rho}_{m'}^{c\pm}\cdot\int_{T_{n'}^{\pm}}d\bar{r}'\bar{\rho}_{n'}^{\pm}\frac{e^{ik_1R_{m'}^{\pm}}}{R_{m'}^{\pm}}\pm\frac{-i}{4\pi\omega\mu}\frac{l_{m'}l_{n'}}{A_{n'}^{\pm}}\int_{T_{n'}^{\pm}}d\bar{r}'\frac{e^{ik_1R_{m'}^{\pm}}}{R_{m'}^{\pm}}\right] \quad (A.206)$$

$$CZ7=\left[\frac{1}{4\pi}\frac{l_{m'}l_{n''}}{4A_{n''}^{\pm}}\bar{\rho}_{m'}^{c\pm}\cdot\int_{T_{n''}^{\pm}}d\bar{r}'\bar{\rho}_{n''}^{\pm}\times(\bar{r}_{m'}^{c\pm}-\bar{r}')(1-ik_0R_{m'}^{\pm})\frac{e^{ik_0R_{m'}^{\pm}}}{(R_{m'}^{\pm})^3}\right] \quad (A.207)$$

$$CZ8=\left[-\frac{1}{4\pi}\frac{l_{m'}l_{n'''}}{4A_{n'''}^{\pm}}\bar{\rho}_{m'}^{c\pm}\cdot\int_{T_{n'''}^{\pm}}d\bar{r}'\bar{\rho}_{n'''}^{\pm}\times(\bar{r}_{m'}^{c\pm}-\bar{r}')(1-ik_1R_{m'}^{\pm})\frac{e^{ik_1R_{m'}^{\pm}}}{(R_{m'}^{\pm})^3}\right] \quad (A.208)$$

$$CZ9 = \left[-\frac{i\omega\mu_0}{4\pi} \frac{l_{m''} l_n}{4A_n^{\pm}} \bar{\rho}_{m''}^{c\pm} \cdot \int_{T_n^{\pm}} d\bar{r}' \bar{\rho}_n^{\pm} \frac{e^{ik_0 R_{m''}^{\pm}}}{R_{m''}^{\pm}} \right.$$
$$\left. \pm \frac{i}{4\pi\omega\epsilon_0} \frac{l_{m''} l_n}{A_n^{\pm}} \int_{T_n^{\pm}} d\bar{r}' \frac{e^{ik_0 R_{m''}^{\pm}}}{R_{m''}^{\pm}} \right] \tag{A.209}$$

$$CZ10 = \left[\frac{1}{4\pi} \frac{l_{m''} l_{n'}}{4A_{n'}^{\pm}} \bar{\rho}_{m''}^{c\pm} \cdot \int_{T_{n'}^{\pm}} d\bar{r}' \bar{\rho}_{n'}^{\pm} \times (\bar{r}_{m''}^{c\pm} - \bar{r}')(1 - ik_0 R_{m''}^{\pm}) \frac{e^{ik_0 R_{m''}^{\pm}}}{(R_{m''}^{\pm})^3} \right] \tag{A.210}$$

$$CZ11 = \left[-\frac{i\omega\mu_0}{4\pi} \frac{l_{m''} l_{n''}}{4A_{n''}^{\pm}} \bar{\rho}_{m''}^{c\pm} \cdot \int_{T_{n''}^{\pm}} d\bar{r}' \bar{\rho}_{n''}^{\pm} \frac{e^{ik_0 R_{m''}^{\pm}}}{R_{m''}^{\pm}} \right.$$
$$\left. \pm \frac{i}{4\pi\omega\epsilon_0} \frac{l_{m''} l_{n''}}{A_{n''}^{\pm}} \int_{T_{n''}^{\pm}} d\bar{r}' \frac{e^{ik_0 R_{m''}^{\pm}}}{R_{m''}^{\pm}} \right] \tag{A.211}$$

$$CZ12 = \bar{0}_{m''n'''} \tag{A.212}$$

$$CZ13 = \left[\frac{i\omega\mu}{4\pi} \frac{l_{m'''} l_n}{4A_n^{\pm}} \bar{\rho}_{m'''}^{c\pm} \cdot \int_{T_n^{\pm}} d\bar{r}' \bar{\rho}_n^{\pm} \frac{e^{ik_1 R_{m'''}^{\pm}}}{R_{m'''}^{\pm}} \right.$$
$$\left. \pm \frac{-i}{4\pi\omega\epsilon} \frac{l_{m'''} l_n}{A_n^{\pm}} \int_{T_n^{\pm}} d\bar{r}' \frac{e^{ik_1 R_{m'''}^{\pm}}}{R_{m'''}^{\pm}} \right] \tag{A.213}$$

$$CZ14 = \left[-\frac{1}{4\pi} \frac{l_{m'''} l_{n'}}{4A_{n'}^{\pm}} \bar{\rho}_{m'''}^{c\pm} \cdot \int_{T_{n'}^{\pm}} d\bar{r}' \bar{\rho}_{n'}^{\pm} \times (\bar{r}_{m'''}^{c\pm} - \bar{r}')(1 - ik_1 R_{m'''}^{\pm}) \frac{e^{ik_1 R_{m'''}^{\pm}}}{(R_{m'''}^{\pm})^3} \right] \tag{A.214}$$

$$CZ15 = \bar{0}_{m'''n''} \tag{A.215}$$

$$CZ16 = \left[-\frac{i\omega\mu}{4\pi} \frac{l_{m'''} l_{n'''}}{4A_{n'''}^{\pm}} \bar{\rho}_{m'''}^{c\pm} \cdot \int_{T_{n'''}^{\pm}} d\bar{r}' \bar{\rho}_{n'''}^{\pm} \frac{e^{ik_1 R_{m'''}^{\pm}}}{R_{m'''}^{\pm}} \right.$$
$$\left. \pm \frac{i}{4\pi\omega\epsilon} \frac{l_{m'''} l_{n'''}}{A_{n'''}^{\pm}} \int_{T_{n'''}^{\pm}} d\bar{r}' \frac{e^{ik_1 R_{m'''}^{\pm}}}{R_{m'''}^{\pm}} \right]. \tag{A.216}$$

Equations (A.201) through (A.216) represent the symmetric Z-matrix as computed by program EFIE2PC.FOR (see Appendices B and D).

Appendix B

DESCRIPTION OF COMPUTER PROGRAMS

B.1 Introduction

The electric field integral equation (EFIE) programs are discussed in this appendix. This set of programs uses the method of moments to calculate the equivalent electric and magnetic surface currents and the far-field radiation pattern of a user specified geometrical construction. This geometrical construction is a triangular patch model of the coated perfect conductor. The user specifies a geometry by creating the file GMETRY.DAT using the commands outlined in INPUT.DOC. GMETRY.DAT is the input for the EFIE series of programs. Various output files are generated by these programs. EFIE5R and EFIE5V will generate plots on a graphics terminal. These plots can be viewed and manipulated in an interactive mode. The source code uses PENPLOT graphics software.

B.2 Program Description

A brief description of the EFIE files and programs follows:

GMETRY.DAT– a user created file which uses condensed commands to create the desired geometry. The condensed commands can be found in the INPUT.DOC file. This file is the input to EFIE1. To view the geometry created by the GMETRY.DAT commands, run EFIE1 and rename or copy the output file STORAGE.DAT to RESULT.DAT. Then run EFIE5V.

EFIE1– translates condensed geometry specifications into EFIE usable data. Surface modelling by triangular patches.

INPUT: GMETRY.DAT–condensed geometry specs

OUTPUT: STORAGE.DAT–geometry modelled using triangular patches

EFIE2C– calculates the "generalized" symmetric Z-matrix of an arbitrary configuration of completely coated, perfectly conducting surfaces. Surface modelling is by triangular patches.

INPUT: complex relative permittivity, ϵ_R, and permeability, μ_R.

INPUT: STORAGE.DAT–perfect conductor geometry

INPUT: CSTORAGE.DAT–coating geometry (generated by EFIE1 and renamed from STORAGE.DAT)

OUTPUT: RESMAT.DAT–Z-matrix

EFIE2PC– calculates the "generalized" symmetric Z-matrix of an arbitrary configuration of partially coated, perfectly conducting surfaces. Surface modelling is by triangular patches.

INPUT: complex relative permittivity, ϵ_R, and permeability, μ_R.

INPUT: STORAGE.DAT–coated perfect conductor geometry

INPUT: KSTORAGE.DAT–exposed perfect conductor geometry (generated by EFIE1 and renamed from STORAGE.DAT)

INPUT: CSTORAGE.DAT–coating geometry (generated by EFIE1 and renamed from STORAGE.DAT)

OUTPUT: RESMAT.DAT–Z-matrix

EFIE3– inverts the symmetric Z-matrix by border inversion

INPUT: RESMAT.DAT–Z-matrix

OUTPUT: RESMAT.DAT–inverse Z-matrix, $\overline{\overline{Z}}^{-1}$

EFIE5BC– calculates scattered electromagnetic field, E_s, far-field radiation pattern from the equivalent electric and magnetic surface current distribution of an arbitrary configuration of completely coated perfect conductors (triangular patches used to model surfaces). Current density calculated across edges of triangles. This is an interactive program.

INPUT: RESMAT.DAT–inverse Z-matrix, $\overline{\overline{Z}}^{-1}$

INPUT: CSTORAGE.DAT–coating geometry

OUTPUT: SPATTERN.DAT–stored far-field radiation pattern

EFIE5PC– calculates scattered electromagnetic field, E_s, far-field radiation pattern from the equivalent electric and magnetic surface current distribution of an arbitrary configuration of partially coated perfect conductors (triangular patches used to model surfaces). Current density calculated across edges of triangles. This is an interactive program.

INPUT: RESMAT.DAT–inverse Z-matrix, $\overline{\overline{Z}}^{-1}$

INPUT: CSTORAGE.DAT–coating geometry

INPUT: KSTORAGE.DAT–exposed perfect conductor geometry

OUTPUT: SPATTERN.DAT–stored far-field radiation pattern

EFIE5R– calculates far-field radar cross section (RCS), σ, patterns from the previously stored far-field radiation pattern of an arbitrary configuration of coated surfaces (triangular patches). This is an interactive program. Output is plotted on a graphics terminal. The plotting subroutines called by this program can be found in PLOTR2.FOR which uses PENPLOT graphics software.

INPUT: RPATTERN.DAT–this file is necessary if user asks program to read a previously stored pattern such as SPATTERN.DAT generated by EFIE5B. RPATTERN.DAT is simply SPATTERN.DAT renamed or copied.

OUTPUT: far-field RCS plots on a graphics terminal.

OUTPUT: DPATTERN.DAT–user readable file containing the far-field RCS, σ, versus angle data

OUTPUT: HDCOPY.PLT–far-field RCS patterns (user requested) ready for printing.

EFIE5V– outputs GMETRY.DAT data in user viewable form. The geometry created by the user can be viewed on graphics terminal. The plot

produced is a 3-D graphics view of the geometry, and the viewing angle can be changed. This is an interactive program.

INPUT: RESULT.DAT–renamed or copied STORAGE.DAT or CSTORAGE.DAT file.

OUTPUT: plots on a graphics terminal.

OUTPUT: HDCOPY.PLT–3-D geometry (user requested) ready for printing.

HDCOPY.PLT– file containing plots requested by user. They can be viewed on a graphics terminal or sent to a printer.

B.3 Flowchart of Computer Programs

Figure B.1 is a flowchart of the computer programs described in Section B.2. It is not a flowchart of the individual computer programs, but a flowchart to show the progression through the EFIE series of computer programs used to calculate the desired far-field radar cross section patterns.

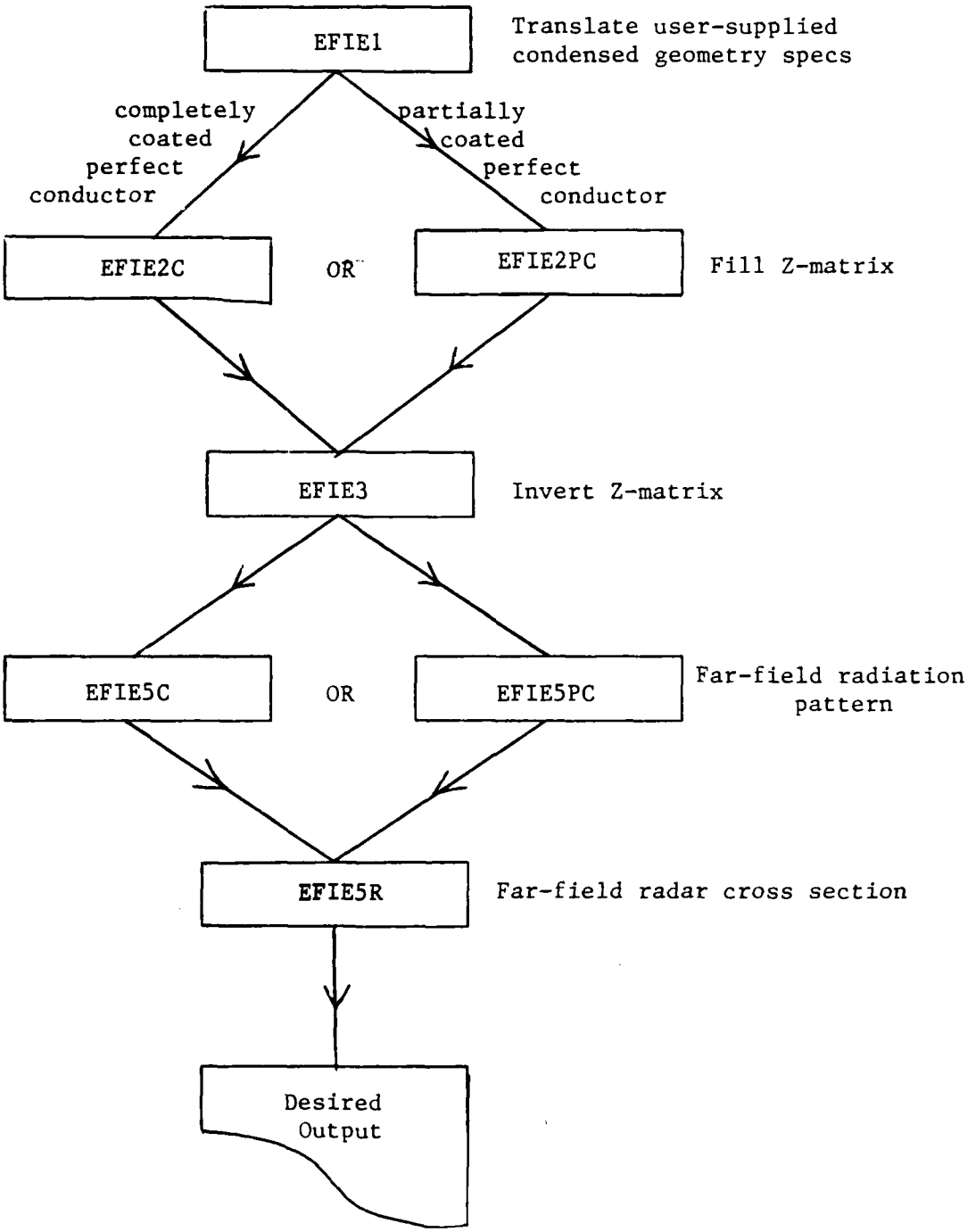

Figure B.1. Flowchart of EFIE Computer Programs

Appendix C

SEVEN-POINT NUMERICAL INTEGRATION OVER TRIANGULAR SUBDOMAINS

C.1 Introduction

To calculate the elements of the interaction matrix, Z-matrix, an integration of several types of functions over each triangular patch is required as shown in Appendix A, equations *A*.106 through *A*.114 and *A*.201 through *A*.216. The integration of these functions over the triangular patches is accomplished numerically using a quadrature technique for surface integration over a triangular surface. The following sections of this appendix discuss the numerical integration of these functions over the triangular patches.

C.2 Integration of $\int_{T_n^\pm} d\bar{r}' \bar{\rho}_n^\pm \frac{e^{ik_0 R_m^\pm}}{R_m^\pm}$ and $\int_{T_n^\pm} d\bar{r}' \frac{e^{ik_0 R_m^\pm}}{R_m^\pm}$

The integrations of $\int_{T_n^\pm} d\bar{r}' \bar{\rho}_n^\pm \frac{e^{ik_0 R_m^\pm}}{R_m^\pm}$ and $\int_{T_n^\pm} d\bar{r}' \frac{e^{ik_0 R_m^\pm}}{R_m^\pm}$ are accomplished using a seven-point numerical integration scheme over each triangular patch. When the source triangle and the observation triangle are the same triangular patch, $m = n$, and the singularity in these integrals presents a difficulty. The seven-point numerical integration scheme used is discussed in Chapter 3 of Kiang's thesis [124], and will not be repeated here. Further, Kiang's thesis discusses the effects of various triangular patch shapes on the computation of the scattering from perfect conductors. The seven-point numerical integration over the triangular patches is an adaptation of the numerical quadrature technique discussed in reference [125]. The quadrature values used in the integration can also be found in Abramowitz and Stegun [126] on page 893. The integration of $\int_{T_n^\pm} d\bar{r}' \bar{\rho}_n^\pm \frac{e^{ik_0 R_m^\pm}}{R_m^\pm}$ and $\int_{T_n^\pm} d\bar{r}' \frac{e^{ik_0 R_m^\pm}}{R_m^\pm}$ are accomplished in subroutine NINT7

of fortran program EFIE2PC (Appendix D), and the integration of $\int_{T_n^\pm} d\bar{r}' \bar{\rho}_n^\pm \frac{e^{ik_1 R_m^\pm}}{R_m^\pm}$ and $\int_{T_n^\pm} d\bar{r}' \frac{e^{ik_1 R_m^\pm}}{R_m^\pm}$ are accomplished in subroutine NINT7A of EFIE2PC.

C.3 Integration of $\int_{T_n^\pm} d\bar{r}' \bar{\rho}_n^\pm \times (\bar{r}_m^{c\pm} - \bar{r}')(1 - ik_0 R_m^\pm) \frac{e^{ik_0 R_m^\pm}}{(R_m^\pm)^3}$

The integration of $\int_{T_n^\pm} d\bar{r}' \bar{\rho}_n^\pm \times (\bar{r}_m^{c\pm} - \bar{r}')(1 - ik_0 R_m^\pm) \frac{e^{ik_0 R_m^\pm}}{(R_m^\pm)^3}$ uses a modified version of the seven-point numerical integration scheme discussed in Section C.2. Refer to Figure C.1. Let

$$I_{mn} = \int_{T_n^\pm} d\bar{r}' \bar{\rho}_n^\pm \times (\bar{r}_m^{c\pm} - \bar{r}')(1 - ik_0 R_m^\pm) \frac{e^{ik_0 R_m^\pm}}{(R_m^\pm)^3}. \tag{C.1}$$

Now, referring to Figure C.1, let

$$\bar{\rho}_n = (\bar{r}' - \bar{r}_i) \tag{C.2}$$

where $\bar{r}_i = \bar{r}_1, \bar{r}_2, \bar{r}_3$ in turn. Now

$$\bar{r}' = \bar{r}_1 + (\bar{r}_2 - \bar{r}_1)\xi + (\bar{r}_3 - \bar{r}_1)\eta \tag{C.3}$$

where

$$\xi = \frac{A_2}{A_n}, \tag{C.4}$$

and

$$\eta = \frac{A_3}{A_n}, \tag{C.5}$$

and A_n is the area of the nth triangular patch. $\bar{r}_1$ is the vector from the global origin to vertex 1 of the nth triangular patch. Similarly, $\bar{r}_2$ and $\bar{r}_3$ are the vectors from the global origin to vertices 2 and 3, respectively, of the nth triangular patch.

Substituting $C.2$ into $C.1$, I_{mn} becomes

$$I_{mn} = \int_{T_n^\pm} d\bar{r}' (\bar{r}' - \bar{r}_i) \times (\bar{r}_m^{c\pm} - \bar{r}')(1 - ik_0 R_m^\pm) \frac{e^{ik_0 R_m^\pm}}{(R_m^\pm)^3}. \tag{C.6}$$

Now

$$
\begin{aligned}
(\bar{r}' - \bar{r}_i) \times (\bar{r}_m^{c\pm} - \bar{r}') &= \bar{r}' \times \bar{r}_m^{c\pm} - \bar{r}_i \times \bar{r}_m^{c\pm} + \bar{r}_i \times \bar{r}' \\
&= (\bar{r}_m^{c\pm} \times \bar{r}_i) + \bar{r}_i \times \bar{r}' - \bar{r}_m^{c\pm} \times \bar{r}' \\
&= (\bar{r}_m^{c\pm} \times \bar{r}_i) + (\bar{r}_i - \bar{r}_m^{c\pm}) \times \bar{r}'. \qquad (C.7)
\end{aligned}
$$

Therefore, using $C.3$ in $C.7$ and $C.7$ in $C.6$ yields

$$
\begin{aligned}
I_{mn} &= \int_{T_n^\pm} d\bar{r}' \left[(\bar{r}_m^{c\pm} \times \bar{r}_i) + (\bar{r}_i - \bar{r}_m^{c\pm}) \times \bar{r}' \right] (1 - ik_0 R_m^\pm) \frac{e^{ik_0 R_m^\pm}}{(R_m^\pm)^3} \\
&= 2A_n \int_0^1 \int_0^{1-\eta} d\xi d\eta \Big[(\bar{r}_m^{c\pm} \times \bar{r}_i) \\
&\quad + (\bar{r}_i - \bar{r}_m^{c\pm}) \times \{ \bar{r}_1 + (\bar{r}_2 - \bar{r}_1)\xi + (\bar{r}_3 - \bar{r}_1)\eta \} \Big] (1 - ik_0 R_m^\pm) \frac{e^{ik_0 R_m^\pm}}{(R_m^\pm)^3} \\
&= 2A_n (\bar{r}_m^{c\pm} \times \bar{r}_i) \int_0^1 \int_0^{1-\eta} d\xi d\eta (1 - ik_0 R_m^\pm) \frac{e^{ik_0 R_m^\pm}}{(R_m^\pm)^3} \\
&\quad + 2A_n (\bar{r}_i - \bar{r}_m^{c\pm}) \times \int_0^1 \int_0^{1-\eta} d\xi d\eta \Big[\{ \bar{r}_1 + (\bar{r}_2 - \bar{r}_1)\xi \\
&\qquad + (\bar{r}_3 - \bar{r}_1)\eta \} \Big] (1 - ik_0 R_m^\pm) \frac{e^{ik_0 R_m^\pm}}{(R_m^\pm)^3} \\
&= 2A_n (\bar{r}_m^{c\pm} \times \bar{r}_i) \int_0^1 \int_0^{1-\eta} d\xi d\eta (1 - ik_0 R_m^\pm) \frac{e^{ik_0 R_m^\pm}}{(R_m^\pm)^3} \\
&\quad + 2A_n (\bar{r}_i - \bar{r}_m^{c\pm}) \times \bar{r}_1 \int_0^1 \int_0^{1-\eta} d\xi d\eta (1 - ik_0 R_m^\pm) \frac{e^{ik_0 R_m^\pm}}{(R_m^\pm)^3} \\
&\quad + 2A_n (\bar{r}_i - \bar{r}_m^{c\pm}) \times (\bar{r}_2 - \bar{r}_1) \int_0^1 \int_0^{1-\eta} d\xi d\eta \, \xi (1 - ik_0 R_m^\pm) \frac{e^{ik_0 R_m^\pm}}{(R_m^\pm)^3} \\
&\quad + 2A_n (\bar{r}_i - \bar{r}_m^{c\pm}) \times (\bar{r}_3 - \bar{r}_1) \int_0^1 \int_0^{1-\eta} d\xi d\eta \, \eta (1 - ik_0 R_m^\pm) \frac{e^{ik_0 R_m^\pm}}{(R_m^\pm)^3} \\
&= 2A_n (\bar{r}_m^{c\pm} \times \bar{r}_i) J_m + 2A_n (\bar{r}_i - \bar{r}_m^{c\pm}) \times \bar{r}_1 J_m \\
&\quad + 2A_n (\bar{r}_i - \bar{r}_m^{c\pm}) \times (\bar{r}_2 - \bar{r}_1) J_m^\xi + 2A_n (\bar{r}_i - \bar{r}_m^{c\pm}) \times (\bar{r}_3 - \bar{r}_1) J_m^\eta. \qquad (C.8)
\end{aligned}
$$

Finally,

$$
I_{mn} = 2A_n \left[(\bar{r}_m^{c\pm} \times \bar{r}_i) J_m + (\bar{r}_i - \bar{r}_m^{c\pm}) \times \{ \bar{r}_1 J_m + (\bar{r}_2 - \bar{r}_1) J_m^\xi + (\bar{r}_3 - \bar{r}_1) J_m^\eta \} \right]; m \neq n \quad (C.9)
$$

where

$$J_m = \int_0^1 \int_0^{1-\eta} d\xi d\eta (1 - ik_0 R_m^{\pm}) \frac{e^{ik_0 R_m^{\pm}}}{(R_m^{\pm})^3} \tag{C.10}$$

$$J_m^{\xi} = \int_0^1 \int_0^{1-\eta} d\xi d\eta \; \xi (1 - ik_0 R_m^{\pm}) \frac{e^{ik_0 R_m^{\pm}}}{(R_m^{\pm})^3} \tag{C.11}$$

$$J_m^{\eta} = \int_0^1 \int_0^{1-\eta} d\xi d\eta \; \eta (1 - ik_0 R_m^{\pm}) \frac{e^{ik_0 R_m^{\pm}}}{(R_m^{\pm})^3}. \tag{C.12}$$

A singularity occurs in these integrals when $m = n$. For $m = n$, which corresponds to the source triangle and the observation triangle being the same triangular patch, I_{mn} is set equal to zero since

$$\bar{\rho}_m^{c\pm} \cdot \int_{T_n^{\pm}} d\bar{r}' \bar{\rho}_n^{\pm} \times (\bar{r}_m^{c\pm} - \bar{r}')(1 - ik_0 R_m^{\pm}) \frac{e^{ik_0 R_m^{\pm}}}{(R_m^{\pm})^3} \tag{C.13}$$

yields a vector in the plane of the triangular patch, $\bar{\rho}_m^{c\pm}$, dotted with a vector perpendicular to the plane of the triangular patch, $\bar{\rho}_n^{\pm} \times (\bar{r}_m^{c\pm} - \bar{r}')$.

The seven-point numerical integration over the triangular patches is an adaptation of the numerical quadrature technique discussed in reference [125]. The values used in the quadrature integration can also be found in Abramowitz and Stegun [126] on page 893. The integration of $\int_{T_n^{\pm}} d\bar{r}' \bar{\rho}_n^{\pm} \times (\bar{r}_m^{c\pm} - \bar{r}')(1 - ik_0 R_m^{\pm}) \frac{e^{ik_0 R_m^{\pm}}}{(R_m^{\pm})^3}$ is accomplished in subroutine NINT7B of fortran program EFIE2PC (Appendix D), and the integration of $\int_{T_n^{\pm}} d\bar{r}' \bar{\rho}_n^{\pm} \times (\bar{r}_m^{c\pm} - \bar{r}')(1 - ik_1 R_m^{\pm}) \frac{e^{ik_1 R_m^{\pm}}}{(R_m^{\pm})^3}$ is accomplished in subroutine NINT7C of EFIE2PC.

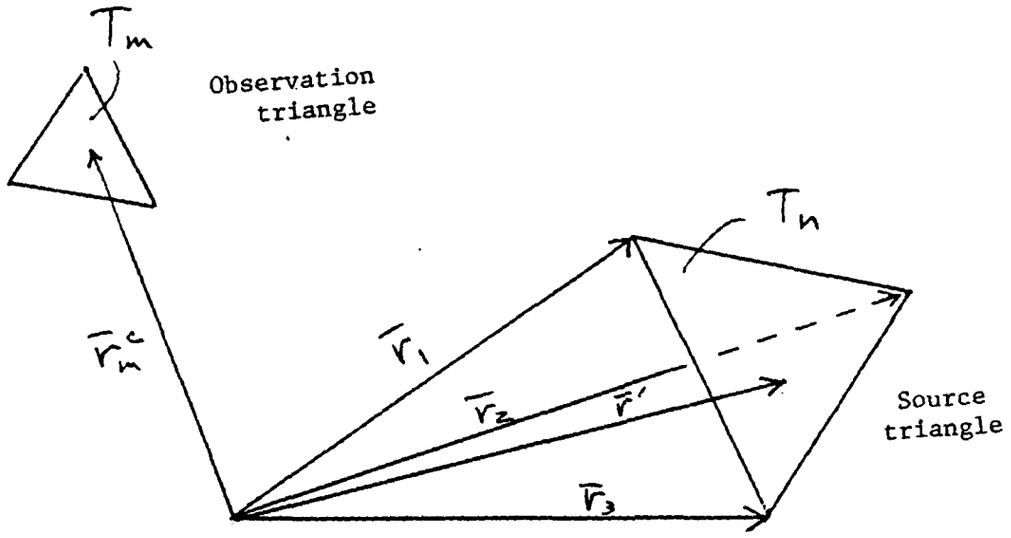

Source triangle

$$A_1 + A_2 + A_3 = A_n$$

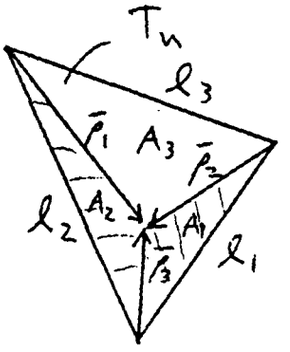

Figure C.1. Source and Observation Triangular Patches

Appendix D

EFIE2PC COMPUTER PROGRAM

This appendix contains the EFIE2PC computer program. The EFIE2C program discussed in Chapter 3 and Appendix B uses similar logic. The EFIE2PC computer program is written in the FORTRAN computer language. This program calculates the elements of the interaction matrix, Z-matrix, for a partially coated perfect conductor (see Chapter 3). The individual elements of the Z-matrix are computed according to equations *A*.201 through *A*.216 in Appendix A. The Z-matrix elements computed from each of these equations are calculated in subroutines ZPLPL1 through ZPLPL16 respectively. The PLPL designation is an abbreviation for plate-plate interaction since triangular patches are used to model the surfaces.

```
C
C EFIE2PC
C
C modified version of EFIE2 to handle PARTIALLY coated perfect conductors
C
C version 1.0  September 1985     MIT
C
C this program calculates the "generalized" impedance matrix of
C of an arbitrary configuration of PARTIALLY COATED conducting surfaces
C
C inverting and multiplying this matrix by an excitation will obtain
C the current distribution and the far field radiation pattern
C
C excitation may be by either plane waves or voltage sources
C
C modelling of the surface is done by triangular patches
C
C surfaces may be multiply connected
C
C input file:  STORAGE – geometry for COATED perfect conductor
C input file:  CSTORAGE – geometry for coating
C input file:  KSTORAGE – geometry for EXPOSED perfect conductor
C output file: RESMAT  – Z-matrix
C
C at present 1000 unknowns are permitted
C
      PROGRAM CMPUTE
C
      INTEGER MNODES,MEDGES,MFACES,MWCRDS,MUNKNS
      INTEGER NNODES,NEDGES,NFACES,NWCRDS,NUNKNS,NWSEGS
      INTEGER JNODES,JEDGES,JFACES,JWCRDS,JUNKNS,JWSEGS
      INTEGER KNODES,KEDGES,KFACES,KWCRDS,KUNKNS,KWSEGS
      PARAMETER (MNODES=300)
      PARAMETER (MEDGES=900)
      PARAMETER (MFACES=600)
      PARAMETER (MWCRDS=2)
      PARAMETER (MUNKNS=600)
C
      INTEGER WIRE,PLATE,STATE
      PARAMETER (WIRE=2)
      PARAMETER (PLATE=3)
C
      COMPLEX JI,KN1,JWU14P,X14PWE,JWE14P,X14PWU
      COMPLEX CZ(MUNKNS,MUNKNS),CV(MUNKNS),CI(MUNKNS)
      COMPLEX CCV(MUNKNS),CCI(MUNKNS)
      COMPLEX KCV(MUNKNS),KCI(MUNKNS)
      REAL PI,KN,JWU04P,X14PJE,JWE04P,X14PJU,X14PI
      REAL DATNOD(4,MNODES),WR(4,MWCRDS)
      REAL CDATNOD(4,MNODES),CWR(4,MWCRDS)
      REAL KDATNOD(4,MNODES),KWR(4,MWCRDS)
      INTEGER NCONN(2,MEDGES),NBOUND(6,MFACES)
      INTEGER JCONN(2,MEDGES),JBOUND(6,MFACES)
```

```
      INTEGER KCONN(2,MEDGES),KBOUND(6,MFACES)
      INTEGER SEG(4,MWCRDS-1),MAPUNK(MEDGES+MWCRDS)
      INTEGER SEGJ(4,MWCRDS-1),MAPUNKJ(MEDGES+MWCRDS)
      INTEGER SEGK(4,MWCRDS-1),MAPUNKK(MEDGES+MWCRDS)
C
      COMMON/DIMEN/NNODES,NEDGES,NFACES
      COMMON/DIMWR/NWCRDS,NWSEGS
      COMMON/NMBRS/NUNKNS
      COMMON/RWIRE/WR
      COMMON/SWIRE/SEG
      COMMON/PLAT1/DATNOD
      COMMON/PLAT2/NCONN
      COMMON/PLAT3/NBOUND
      COMMON/CONST/PI,KN,JI,JWU04P,X14PJE,JWE04P,X14PJU
      COMMON/MAPUS/MAPUNK
      COMMON/MATRX3/CI
      COMMON/MATRX2/CV
      COMMON/MATRX1/CZ
C
      COMMON/CDIMEN/JNODES,JEDGES,JFACES
      COMMON/CDIMWR/JWCRDS,JWSEGS
      COMMON/CNMBRS/JUNKNS
      COMMON/CRWIRE/CWR
      COMMON/CSWIRE/SEGJ
      COMMON/CPLAT1/CDATNOD
      COMMON/CPLAT2/JCONN
      COMMON/CPLAT3/JBOUND
      COMMON/CONST1/KN1,JWU14P,X14PWE,X14PI,JWE14P,X14PWU
      COMMON/CMAPUS/MAPUNKJ
      COMMON/CMATRX3/CCI
      COMMON/CMATRX2/CCV
C
      COMMON/KDIMEN/KNODES,KEDGES,KFACES
      COMMON/KDIMWR/KWCRDS,KWSEGS
      COMMON/KNMBRS/KUNKNS
      COMMON/KRWIRE/KWR
      COMMON/KSWIRE/SEGK
      COMMON/KPLAT1/KDATNOD
      COMMON/KPLAT2/KCONN
      COMMON/KPLAT3/KBOUND
      COMMON/KMAPUS/MAPUNKK
      COMMON/KMATRX3/KCI
      COMMON/KMATRX2/KCV
C
C read the geometry for the COATED perfect conductor
C
      OPEN(FILE='STORAGE',STATUS='OLD',UNIT=55,FORM='UNFORMATTED')
      CALL HFILE(MNODES,MEDGES,MFACES,MWCRDS,MUNKNS,STATE)
      CLOSE(55)
      IF (STATE.NE.0) THEN
        WRITE(6,101)
        STOP
```

```
        ENDIF
C
C read the geometry for the EXPOSED perfect conductor
C
      OPEN(FILE='KSTORAGE',STATUS='OLD',UNIT=54,FORM='UNFORMATTED')
      CALL HFILEK(MNODES,MEDGES,MFACES,MWCRDS,MUNKNS,STATE)
      CLOSE(54)
      IF (STATE.NE.0) THEN
       WRITE(6,101)
       STOP
       ENDIF
C
C read the geometry for the coating
C
      OPEN(FILE='CSTORAGE',STATUS='OLD',UNIT=56,FORM='UNFORMATTED')
      CALL HFILEC(MNODES,MEDGES,MFACES,MWCRDS,MUNKNS,STATE)
      CLOSE(56)
      IF (STATE.NE.0) THEN
       WRITE(6,101)
       STOP
       ENDIF
101   FORMAT(3X,'*** currents have already been computed ***')
C
C establish Z-matrix
C
      OPEN(FILE='RESMAT',STATUS='NEW',UNIT=57,FORM='UNFORMATTED')
      CALL ZINIT(CZ,JUNKNS,JUNKNS)
      CALL ZPLPL1(CZ,JUNKNS,NUNKNS,KUNKNS)
      CALL ZINIT(CZ,JUNKNS,JUNKNS)
      CALL ZPLPL2(CZ,JUNKNS)
      CALL ZPLPL5(CZ,JUNKNS)
      CALL ZINIT(CZ,JUNKNS,JUNKNS)
      CALL ZPLPL6(CZ,JUNKNS)
      CALL SAFE(CZ,JUNKNS,KUNKNS,NUNKNS,1)
      CALL ZINIT(CZ,JUNKNS,KUNKNS)
      CALL ZPLPL3(CZ,JUNKNS,KUNKNS)
      CALL ZPLPL9(CZ,JUNKNS,KUNKNS)
      CALL ZINIT(CZ,JUNKNS,KUNKNS)
      CALL ZPLPL7(CZ,JUNKNS,KUNKNS)
      CALL ZPLPL10(CZ,JUNKNS,KUNKNS)
      CALL ZINIT(CZ,KUNKNS,KUNKNS)
      CALL ZPLPL11(CZ,KUNKNS)
      CALL SAFE(CZ,JUNKNS,KUNKNS,NUNKNS,2)
      CALL ZINIT(CZ,JUNKNS,NUNKNS)
      CALL ZPLPL4(CZ,JUNKNS,NUNKNS)
      CALL ZPLPL13(CZ,JUNKNS,NUNKNS)
      CALL ZINIT(CZ,JUNKNS,NUNKNS)
      CALL ZPLPL8(CZ,JUNKNS,NUNKNS)
      CALL ZPLPL14(CZ,JUNKNS,NUNKNS)
      CALL ZINIT(CZ,NUNKNS,NUNKNS)
      CALL ZPLPL16(CZ,NUNKNS)
      CALL SAFE(CZ,JUNKNS,KUNKNS,NUNKNS,3)
```

```
      CLOSE(57)
C
      STOP
      END
C
C read necessary geometry information for COATED perfect conductor
C
      SUBROUTINE HFILE(MNODES,MEDGES,MFACES,MWCRDS,MUNKNS,STATE)
C
      INTEGER I,J,STATE
      INTEGER MNODES,MEDGES,MFACES,MWCRDS,MUNKNS
      INTEGER NNODES,NEDGES,NFACES,NWCRDS,NUNKNS,NWSEGS
      COMPLEX JI,CI(1),CV(1)
      REAL PI,KN,JWU04P,X14PJE
      REAL DATNOD(4,1),WR(4,1)
      INTEGER NCONN(2,1),NBOUND(6,1),SEG(4,1),MAPUNK(1)
C
      COMMON/DIMEN/NNODES,NEDGES,NFACES
      COMMON/DIMWR/NWCRDS,NWSEGS
      COMMON/NMBRS/NUNKNS
      COMMON/RWIRE/WR
      COMMON/SWIRE/SEG
      COMMON/PLAT1/DATNOD
      COMMON/PLAT2/NCONN
      COMMON/PLAT3/NBOUND
      COMMON/CONST/PI,KN,JI,JWU04P,X14PJE,JWE04P,X14PJU
      COMMON/MAPUS/MAPUNK
      COMMON/MATRX3/CI
      COMMON/MATRX2/CV
C
      READ(55,ERR=990) STATE
      READ(55,ERR=990) NNODES,NEDGES,NFACES,NWCRDS,NWSEGS,NUNKNS
C
      IF (NNODES.GT.MNODES) WRITE(6,91) MNODES
      IF (NEDGES.GT.MEDGES) WRITE(6,92) MEDGES
      IF (NFACES.GT.MFACES) WRITE(6,93) MFACES
      IF (NWCRDS.GT.MWCRDS) WRITE(6,94) MWCRDS
      IF (NUNKNS.GT.MUNKNS) WRITE(6,95) MUNKNS
      IF (NNODES.GT.MNODES.OR.NEDGES.GT.MEDGES.OR.NFACES.GT.MFACES.OR.
     + NWCRDS.GT.MWCRDS.OR.NUNKNS.GT.MUNKNS) STOP
C
      READ(55,ERR=990) ((WR(I,J),I=1,4),J=1,NWCRDS)
      READ(55,ERR=990) ((SEG(I,J),I=1,4),J=1,NWSEGS)
      READ(55,ERR=990) ((DATNOD(I,J),I=1,4),J=1,NNODES)
      READ(55,ERR=990) ((NCONN(I,J),I=1,2),J=1,NEDGES)
      READ(55,ERR=990) ((NBOUND(I,J),I=1,6),J=1,NFACES)
      READ(55,ERR=990) PI,KN,JI,JWU04P,X14PJE
      READ(55,ERR=990) (MAPUNK(I),I=1,NEDGES)
      READ(55,ERR=990) (MAPUNK(I+NEDGES),I=1,NWCRDS)
C
      READ(55,ERR=990) (CV(I),I=1,NUNKNS)
      READ(55,ERR=990) (CI(I),I=1,NUNKNS)
```

```
C
      REWIND 55
      RETURN
C
91    FORMAT(/2X,'nodes exceeds dimension of',I5)
92    FORMAT(/2X,'edges exceeds dimension of',I5)
93    FORMAT(/2X,'faces exceeds dimension of',I5)
94    FORMAT(/2X,'wire nodes exceeds dimension of',I5)
95    FORMAT(/2X,'unknowns exceeds dimension of',I5)
99    FORMAT(/2X,'*** unexpected error in read ***')
990   WRITE(6,99)
      STOP
C
      END
C
C read necessary geometry information for EXPOSED perfect conductor
C
      SUBROUTINE HFILEK(MNODES,MEDGES,MFACES,MWCRDS,MUNKNS,STATE)
C
      INTEGER I,J,STATE
      INTEGER MNODES,MEDGES,MFACES,MWCRDS,MUNKNS
      INTEGER KNODES,KEDGES,KFACES,KWCRDS,KUNKNS,KWSEGS
      COMPLEX JI,KCI(1),KCV(1)
      REAL PI,KN,JWU04P,X14PJE
      REAL KDATNOD(4,1),KWR(4,1)
      INTEGER KCONN(2,1),KBOUND(6,1),SEGK(4,1),MAPUNKK(1)
C
      COMMON/KDIMEN/KNODES,KEDGES,KFACES
      COMMON/KDIMWR/KWCRDS,KWSEGS
      COMMON/KNMBRS/KUNKNS
      COMMON/KRWIRE/KWR
      COMMON/KSWIRE/SEGK
      COMMON/KPLAT1/KDATNOD
      COMMON/KPLAT2/KCONN
      COMMON/KPLAT3/KBOUND
      COMMON/CONST/PI,KN,JI,JWU04P,X14PJE,JWE04P,X14PJU
      COMMON/KMAPUS/MAPUNKK
      COMMON/KMATRX3/KCI
      COMMON/KMATRX2/KCV
C
      READ(54,ERR=990) STATE
      READ(54,ERR=990) KNODES,KEDGES,KFACES,KWCRDS,KWSEGS,KUNKNS
C
      IF (KNODES.GT.MNODES) WRITE(6,91) MNODES
      IF (KEDGES.GT.MEDGES) WRITE(6,92) MEDGES
      IF (KFACES.GT.MFACES) WRITE(6,93) MFACES
      IF (KWCRDS.GT.MWCRDS) WRITE(6,94) MWCRDS
      IF (KUNKNS.GT.MUNKNS) WRITE(6,95) MUNKNS
      IF (KNODES.GT.MNODES.OR.KEDGES.GT.MEDGES.OR.KFACES.GT.MFACES.OR.
     + KWCRDS.GT.MWCRDS.OR.KUNKNS.GT.MUNKNS) STOP
C
      READ(54,ERR=990) ((KWR(I,J),I=1,4),J=1,KWCRDS)
```

```
      READ(54,ERR=990) ((SEGK(I,J),I=1,4),J=1,KWSEGS)
      READ(54,ERR=990) ((KDATNOD(I,J),I=1,4),J=1,KNODES)
      READ(54,ERR=990) ((KCONN(I,J),I=1,2),J=1,KEDGES)
      READ(54,ERR=990) ((KBOUND(I,J),I=1,6),J=1,KFACES)
      READ(54,ERR=990) PI,KN,JI,JWU04P,X14PJE
      READ(54,ERR=990) (MAPUNKK(I),I=1,KEDGES)
      READ(54,ERR=990) (MAPUNKK(I+KEDGES),I=1,KWCRDS)
C
      READ(54,ERR=990) (KCV(I),I=1,KUNKNS)
      READ(54,ERR=990) (KCI(I),I=1,KUNKNS)
C
      REWIND 54
      RETURN
C
91    FORMAT(/2X,'nodes exceeds dimension of',I5)
92    FORMAT(/2X,'edges exceeds dimension of',I5)
93    FORMAT(/2X,'faces exceeds dimension of',I5)
94    FORMAT(/2X,'wire nodes exceeds dimension of',I5)
95    FORMAT(/2X,'unknowns exceeds dimension of',I5)
99    FORMAT(/2X,'*** unexpected error in read ***')
990   WRITE(6,99)
      STOP
C
      END
C
C read necessary geometry information for coating
C
      SUBROUTINE HFILEC(MNODES,MEDGES,MFACES,MWCRDS,MUNKNS,STATE)
C
      INTEGER I,J,STATE
      INTEGER MNODES,MEDGES,MFACES,MWCRDS,MUNKNS
      INTEGER JNODES,JEDGES,JFACES,JWCRDS,JUNKNS,JWSEGS
      COMPLEX JI,CCI(1),CCV(1)
      COMPLEX EPSILON,MU,KN1,JWU14P,X14PWE,JWE14P,X14PWU
      REAL PI,KN,JWU04P,X14PJE
      REAL C,LAMBDA,MU0,OMEGA,EPSLON0,JWE04P,X14PJU,X14PI
      REAL CDATNOD(4,1),CWR(4,1)
      INTEGER JCONN(2,1),JBOUND(6,1),SEGJ(4,1),MAPUNKJ(1)
C
      COMMON/CDIMEN/JNODES,JEDGES,JFACES
      COMMON/CDIMWR/JWCRDS,JWSEGS
      COMMON/CNMBRS/JUNKNS
      COMMON/CRWIRE/CWR
      COMMON/CSWIRE/SEGJ
      COMMON/CPLAT1/CDATNOD
      COMMON/CPLAT2/JCONN
      COMMON/CPLAT3/JBOUND
      COMMON/CONST/PI,KN,JI,JWU04P,X14PJE,JWE04P,X14PJU
      COMMON/CONST1/KN1,JWU14P,X14PWE,X14PI,JWE14P,X14PWU
      COMMON/CMAPUS/MAPUNKJ
      COMMON/CMATRX3/CCI
      COMMON/CMATRX2/CCV
```

```
C
      READ(56,ERR=990) STATE
      READ(56,ERR=990) JNODES,JEDGES,JFACES,JWCRDS,JWSEGS,JUNKNS
C
      IF (JNODES.GT.MNODES) WRITE(6,91) MNODES
      IF (JEDGES.GT.MEDGES) WRITE(6,92) MEDGES
      IF (JFACES.GT.MFACES) WRITE(6,93) MFACES
      IF (JWCRDS.GT.MWCRDS) WRITE(6,94) MWCRDS
      IF (JUNKNS.GT.MUNKNS) WRITE(6,95) MUNKNS
      IF (JNODES.GT.MNODES.OR.JEDGES.GT.MEDGES.OR.JFACES.GT.MFACES.OR.
     + JWCRDS.GT.MWCRDS.OR.JUNKNS.GT.MUNKNS) STOP
C
      READ(56,ERR=990) ((CWR(I,J),I=1,4),J=1,JWCRDS)
      READ(56,ERR=990) ((SEGJ(I,J),I=1,4),J=1,JWSEGS)
      READ(56,ERR=990) ((CDATNOD(I,J),I=1,4),J=1,JNODES)
      READ(56,ERR=990) ((JCONN(I,J),I=1,2),J=1,JEDGES)
      READ(56,ERR=990) ((JBOUND(I,J),I=1,6),J=1,JFACES)
      READ(56,ERR=990) PI,KN,JI,JWU04P,X14PJE
      READ(56,ERR=990) (MAPUNKJ(I),I=1,JEDGES)
      READ(56,ERR=990) (MAPUNKJ(I+JEDGES),I=1,JWCRDS)
C
      READ(56,ERR=990) (CCV(I),I=1,JUNKNS)
      READ(56,ERR=990) (CCI(I),I=1,JUNKNS)
C
      REWIND 56
C
C calculate constants
C
      TYPE *,'ENTER RELATIVE EPS & MU OF COATING: EPS(RE,IM),MU(RE,IM)'
      READ(*,*) EPSILON,MU
        TYPE *,'EPSILON RELATIVE=',EPSILON
        TYPE *,'MU RELATIVE=',MU
      PI= 3.1415926535897932
      C= 299792456
      LAMBDA= 1.0
      MU0= 4*PI*1D-7
        TYPE *,'MU0=',MU0
      KN= 2*PI/LAMBDA
        TYPE *,'KN=',KN
      OMEGA= KN*C
        TYPE *,'OMEGA=',OMEGA
      EPSLON0= 1/(MU0*C**2)
        TYPE *,'EPSLON0=',EPSLON0
      MU= MU*MU0
        TYPE *,'MU=',MU
      EPSILON= EPSILON*EPSLON0
        TYPE *,'EPSILON=',EPSILON
      JWU04P= OMEGA*MU0/(4*PI)
        TYPE *,'JWU04P=',JWU04P
      X14PJE= -1/(4*PI*OMEGA*EPSLON0)
        TYPE *,'X14PJE=',X14PJE
      JI= CMPLX(0,-1)
```

```
        TYPE *,'JI=',JI
      JWE04P= OMEGA*EPSLON0/(4*PI)
        TYPE *,'JWE04P=',JWE04P
      X14PJU= -1/(4*PI*OMEGA*MU0)
        TYPE *,'X14PJU=',X14PJU
      KN1= OMEGA*SQRT(MU*EPSILON)
        TYPE *,'KN1=',KN1
      JWU14P= OMEGA*MU/(4*PI)
        TYPE *,'JWU14P=',JWU14P
      X14PWE= -1/(4*PI*OMEGA*EPSILON)
        TYPE *,'X14PWE=',X14PWE
      X14PI= 1/(4*PI)
        TYPE *,'X14PI=',X14PI
      JWE14P= OMEGA*EPSILON/(4*PI)
        TYPE *,'JWE14P=',JWE14P
      X14PWU= -1/(4*PI*OMEGA*MU)
        TYPE *,'X14PWU=',X14PWU
C
      RETURN
C
91    FORMAT(/2X,'nodes exceeds dimension of',I5)
92    FORMAT(/2X,'edges exceeds dimension of',I5)
93    FORMAT(/2X,'faces exceeds dimension of',I5)
94    FORMAT(/2X,'wire nodes exceeds dimension of',I5)
95    FORMAT(/2X,'unknowns exceeds dimension of',I5)
99    FORMAT(/2X,'*** unexpected error in read ***')
990   WRITE(6,99)
      STOP
C
      END
C
C Z-MATRIX contributions
C
C
C init cz matrix
C
      SUBROUTINE ZINIT(CZ,JUNKNS,NUNKNS)
      INTEGER JUNKNS,NUNKNS
      COMPLEX CZ(JUNKNS,NUNKNS)
       DO 2001 I=1,JUNKNS
         DO 2001 J=1,NUNKNS
           CZ(I,J)=0
2001     CONTINUE
      RETURN
      END
C
C plate - plate coupling
C
      SUBROUTINE ZPLPL1(CZ,JUNKNS,NUNKNS,KUNKNS)
C
      INTEGER JUNKNS,NUNKNS,KUNKNS
      COMPLEX JL,A,P,SGNPOT
```

```
      COMPLEX CVEC,CXSI,CETA,CPHI,A1(3),CDOT
      COMPLEX CVEC1,CXSI1,CETA1,CPHI1,A2(3)
      COMPLEX CZ(JUNKNS,JUNKNS),CX1,CF,CFX
      COMPLEX KN1,JWU14P,X14PWE,JWE14P,X14PWU
      REAL PI,KN,JWU04P,X14PJE,JWE04P,X14PJU,X14PI
      REAL MAGNI,GTAREA,AREA1N,VDOT,AREA1M,TRASH
      REAL DR,POT,RLN1(3),R01(3),L1M(3),L1N(3)
      REAL R11M(3,3),R1M(3),RC1M(3),RHO1M(3),R11N(3,3)
      REAL XSI(7),ETA(7),WGHT(7)
      INTEGER JNODES,JEDGES,JFACES,JWCRDS,JWSEGS
      INTEGER I,J,K,M(2),M0,M1,N(2),N0,N1,MAP1,E1M(3),E1N(3),ISGN
C
      INTEGER WIRE,PLATE
      PARAMETER (WIRE=2)
      PARAMETER (PLATE=3)
C
      COMMON/CDIMEN/JNODES,JEDGES,JFACES
      COMMON/CDIMWR/JWCRDS,JWSEGS
      COMMON/CONST/PI,KN,JI,JWU04P,X14PJE,JWE04P,X14PJU
      COMMON/CONST1/KN1,JWU14P,X14PWE,X14PI,JWE14P,X14PWU
      COMMON/NUMINT/XSI,ETA,WGHT
C
      EXTERNAL MAGNI,GTAREA,VDOT,MAP1
      EXTERNAL SGNPOT,ISGN,CDOT
C
C source triangles
C
      DO 2005 N0=1,JFACES
       CALL VTXCRD1(N0,R11N)
       AREA1N = GTAREA(R11N,PLATE)
       CALL LENGTH(R11N,L1N)
       CALL FACEDG1(N0,E1N(1),E1N(2),E1N(3))
C
C observation triangles
C
      DO 2004 M0=1,JFACES
       CALL VTXCRD1(M0,R11M)
       AREA1M = GTAREA(R11M,PLATE)
       CALL CENTER(R11M,RC1M,PLATE)
       CALL LENGTH(R11M,L1M)
       CALL FACEDG1(M0,E1M(1),E1M(2),E1M(3))
C
C compute integrals
C
      CALL NINT7(R11N,RC1M,CVEC,CXSI,CETA,POT,CPHI,RLN1,R01,AREA1N,DR)
      CALL NINT7A(R11N,RC1M,CVEC1,CXSI1,CETA1,POT,CPHI1,
     +                    RLN1,R01,AREA1N,DR)
C
      DO 2003 N1=1,PLATE
       N(1) = MAP1(N0,N1,PLATE)
       N(2) = MAP1(N0,N1+PLATE,PLATE)
       IF (N(1).NE.0.OR.N(2).NE.0) THEN
```

```
      P = ISGN(E1N(N1)) * L1N(N1)/AREA1N * JI * X14PJE * CPHI +
     +        ISGN(E1N(N1)) * L1N(N1)/AREA1N * JI * X14PWE * CPHI1
      DO 2001 I=1,3
       A1(I) = ( R11N(I,1) - R11N(I,N1) ) * CVEC +
     +   ( R11N(I,2) - R11N(I,1) ) * CXSI +
     +   ( R11N(I,3) - R11N(I,1) ) * CETA +
     +   ( R01(I) - R11N(I,N1) ) * POT + RLN1(I)
       A2(I) = ( R11N(I,1) - R11N(I,N1) ) * CVEC1 +
     +   ( R11N(I,2) - R11N(I,1) ) * CXSI1 +
     +   ( R11N(I,3) - R11N(I,1) ) * CETA1 +
     +   ( R01(I) - R11N(I,N1) ) * POT + RLN1(I)
       A1(I) = ISGN(E1N(N1)) * L1N(N1)/(2*AREA1N) * A1(I)
       A2(I) = ISGN(E1N(N1)) * L1N(N1)/(2*AREA1N) * A2(I)
2001   CONTINUE
C
       DO 2002 M1=1,PLATE
        M(1) = MAP1(M0,M1,PLATE)
        M(2) = MAP1(M0,M1+PLATE,PLATE)
        IF (M(1).NE.0.OR.M(2).NE.0) THEN
         CALL P1RHO(R11M,M1,RHO1M)
         A = JI * JWU04P * CDOT(RHO1M,A1) +
     +          JI * JWU14P * CDOT(RHO1M,A2)
         CX1 = ISGN(E1M(M1))*L1M(M1)*(A+P)
C
      IF (DR.LT.L1M(1).OR.DR.LT.L1M(2).OR.DR.LT.L1M(3)) THEN
C
C do the 7-pt integration over the observation triangle
C
       CF = 0
       CFX = 0
       DO 2051 II=1,7
         DO 2050 JJ=1,3
           R1M(JJ) = R11M(JJ,1) + (R11M(JJ,2)-R11M(JJ,1))*XSI(II) +
     +        (R11M(JJ,3)-R11M(JJ,1))*ETA(II)
           RHO1M(JJ) = R1M(JJ)-R11M(JJ,M1)
2050     CONTINUE
       CALL NINT7(R11N,R1M,CVEC,CXSI,CETA,POT,CPHI,RLN1,R01,AREA1N,TRASH)
       CALL NINT7A(R11N,R1M,CVEC1,CXSI1,CETA1,POT,CPHI1,
     +                  RLN1,R01,AREA1N,TRASH)
       P = ISGN(E1N(N1)) * L1N(N1)/AREA1N * JI * X14PJE * CPHI +
     +        ISGN(E1N(N1)) * L1N(N1)/AREA1N * JI * X14PWE * CPHI1
       DO 2049 I=1,3
        A1(I) = ( R11N(I,1) - R11N(I,N1) ) * CVEC +
     +   ( R11N(I,2) - R11N(I,1) ) * CXSI +
     +   ( R11N(I,3) - R11N(I,1) ) * CETA +
     +   ( R01(I) - R11N(I,N1) ) * POT + RLN1(I)
        A2(I) = ( R11N(I,1) - R11N(I,N1) ) * CVEC1 +
     +   ( R11N(I,2) - R11N(I,1) ) * CXSI1 +
     +   ( R11N(I,3) - R11N(I,1) ) * CETA1 +
     +   ( R01(I) - R11N(I,N1) ) * POT + RLN1(I)
        A1(I) = ISGN(E1N(N1)) * L1N(N1)/(4*AREA1N) * A1(I)
        A2(I) = ISGN(E1N(N1)) * L1N(N1)/(4*AREA1N) * A2(I)
```

```
2049      CONTINUE
            A = JI * JWU04P * CDOT(RHO1M,A1) +
     +              JI * JWU14P * CDOT(RHO1M,A2)
            CFX = ISGN(E1M(M1))*L1M(M1)/AREA1M*(A+P)
            CF = CF + CFX*WGHT(II)
2051   CONTINUE
            CX1 = CF * AREA1M
C
       ENDIF
C
            DO 3001 J=1,2
            DO 3001 K=1,2
             IF (M(K).NE.0.AND.N(J).NE.0) THEN
               IF(M(K).NE.N(J)) THEN
                CZ(M(K),N(J)) = CZ(M(K),N(J)) + SGNPOT(CX1,J,K)/2
                CZ(N(J),M(K)) = CZ(N(J),M(K)) + SGNPOT(CX1,J,K)/2
               ELSE
                CZ(M(K),N(J)) = CZ(M(K),N(J)) + SGNPOT(CX1,J,K)
               ENDIF
              ENDIF
3001         CONTINUE
            ENDIF
2002       CONTINUE
          ENDIF
2003     CONTINUE
2004    CONTINUE
2005    CONTINUE
C
C ***************
       WRITE(57) 2*JUNKNS+NUNKNS+KUNKNS,0
       DO 147 J=1,JUNKNS
147     WRITE(57)(CZ(I,J),I=1,J)
C ***************
C
       TYPE *,' CZ1 COMPLETED'
C
       RETURN
       END
C
       SUBROUTINE ZPLPL2(CZ,JUNKNS)
C
       INTEGER JUNKNS
       COMPLEX JI,A,P,SGNPOT
       COMPLEX CVECK0,CXSIK0,CETAK0,A1(3),A3(3),CDOT
       COMPLEX CVECK1,CXSIK1,CETAK1,A2(3),A4(3)
       COMPLEX CZ(JUNKNS,JUNKNS),CX2,CF,CFX
       COMPLEX KN1,JWU14P,X14PWE,JWE14P,X14PWU
       REAL PI,KN,JWU04P,X14PJE,JWE04P,X14PJU,X14PI
       REAL MAGNI,GTAREA,AREA1N,VDOT,AREA1M,TRASH
       REAL DR,POT,RLN1(3),R01(3),L1M(3),L1N(3)
       REAL R11M(3,3),R1M(3),RC1M(3),RHO1M(3),R11N(3,3)
       REAL RI(3),RIMRCM(3),RCMXRI(3)
```

```
      REAL XSI(7),ETA(7),WGHT(7)
      INTEGER JNODES,JEDGES,JFACES,JWCRDS,JWSEGS
      INTEGER I,J,K,M(2),M0,M1,N(2),N0,N1,MAP1,E1M(3),E1N(3),ISGN
C
      INTEGER WIRE,PLATE
      PARAMETER (WIRE=2)
      PARAMETER (PLATE=3)
C
      COMMON/CDIMEN/JNODES,JEDGES,JFACES
      COMMON/CDIMWR/JWCRDS,JWSEGS
      COMMON/CONST/PI,KN,JI,JWU04P,X14PJE,JWE04P,X14PJU
      COMMON/CONST1/KN1,JWU14P,X14PWE,X14PI,JWE14P,X14PWU
      COMMON/NUMINT/XSI,ETA,WGHT
C
      EXTERNAL MAGNI,GTAREA,VDOT,MAP1
      EXTERNAL SGNPOT,ISGN,CDOT
C
C source triangles
C
      DO 2005 N0=1,JFACES
       CALL VTXCRD1(N0,R11N)
       AREA1N = GTAREA(R11N,PLATE)
       CALL LENGTH(R11N,L1N)
       CALL FACEDG1(N0,E1N(1),E1N(2),E1N(3))
C
C observation triangles
C
      DO 2004 M0=1,JFACES
       CALL VTXCRD1(M0,R11M)
       AREA1M = GTAREA(R11M,PLATE)
       CALL CENTER(R11M,RC1M,PLATE)
       CALL LENGTH(R11M,L1M)
       CALL FACEDG1(M0,E1M(1),E1M(2),E1M(3))
C
C compute integrals
C
      IF(M0.EQ.N0) THEN
         CVECK0 = 0
         CXSIK0 = 0
         CETAK0 = 0
         CVECK1 = 0
         CXSIK1 = 0
         CETAK1 = 0
      ELSE
        CALL NINT7B(R11N,RC1M,CVECK0,CXSIK0,CETAK0,AREA1N,DR)
        CALL NINT7C(R11N,RC1M,CVECK1,CXSIK1,CETAK1,AREA1N,DR)
      ENDIF
C
      DO 2003 N1=1,PLATE
       N(1) = MAP1(N0,N1,PLATE)
       N(2) = MAP1(N0,N1+PLATE,PLATE)
       IF (N(1).NE.0.OR.N(2).NE.0) THEN
```

```
          DO 2001 I=1,3
           A1(I) = R11N(I,1) * CVECK0 +
     +      ( R11N(I,2) - R11N(I,1) ) * CXSIK0 +
     +      ( R11N(I,3) - R11N(I,1) ) * CETAK0
           A2(I) = R11N(I,1) * CVECK1 +
     +      ( R11N(I,2) - R11N(I,1) ) * CXSIK1 +
     +      ( R11N(I,3) - R11N(I,1) ) * CETAK1
           RI(I) = R11N(I,N1)
           RIMRCM(I) = RI(I) - RC1M(I)
2001       CONTINUE
          CALL CROSS2(RC1M,RI,RCMXRI)
          CALL CROSS3(RIMRCM,A1,A3)
          CALL CROSS3(RIMRCM,A2,A4)
          DO 2025 I=1,3
           A1(I) = A3(I) + RCMXRI(I) * CVECK0
           A2(I) = A4(I) + RCMXRI(I) * CVECK1
           A1(I) = ISGN(E1N(N1)) * L1N(N1)/(2*AREA1N) * A1(I)
           A2(I) = ISGN(E1N(N1)) * L1N(N1)/(2*AREA1N) * A2(I)
2025       CONTINUE
C
          DO 2002 M1=1,PLATE
           M(1) = MAP1(M0,M1,PLATE)
           M(2) = MAP1(M0,M1+PLATE,PLATE)
           IF (M(1).NE.0.OR.M(2).NE.0) THEN
            CALL P1RHO(R11M,M1,RHO1M)
            A = X14PI * ( CDOT(RHO1M,A1) + CDOT(RHO1M,A2) )
            CX2 = ISGN(E1M(M1)) * L1M(M1) * A
C
        IF (DR.LT.L1M(1).OR.DR.LT.L1M(2).OR.DR.LT.L1M(3)) THEN
C
C do the 7-pt integration over the observation triangle
C
        CF = 0
        CFX = 0
        DO 2051 II=1,7
          DO 2050 JJ=1,3
            R1M(JJ) = R11M(JJ,1) + (R11M(JJ,2)-R11M(JJ,1))*XSI(II) +
     +          (R11M(JJ,3)-R11M(JJ,1))*ETA(II)
           RHO1M(JJ) = R1M(JJ)-R11M(JJ,M1)
2050      CONTINUE
        IF(M0.EQ.N0) THEN
           CVECK0 = 0
           CXSIK0 = 0
           CETAK0 = 0
           CVECK1 = 0
           CXSIK1 = 0
           CETAK1 = 0
        ELSE
          CALL NINT7B(R11N,R1M,CVECK0,CXSIK0,CETAK0,AREA1N,TRASH)
          CALL NINT7C(R11N,R1M,CVECK1,CXSIK1,CETAK1,AREA1N,TRASH)
        ENDIF
          DO 2049 I=1,3
```

```
          A1(I) = R11N(I,1) * CVECK0 +
     +     ( R11N(I,2) - R11N(I,1) ) * CXSIK0 +
     +     ( R11N(I,3) - R11N(I,1) ) * CETAK0
          A2(I) = R11N(I,1) * CVECK1 +
     +     ( R11N(I,2) - R11N(I,1) ) * CXSIK1 +
     +     ( R11N(I,3) - R11N(I,1) ) * CETAK1
          RI(I) = R11N(I,N1)
          RIMRCM(I) = RI(I) - R1M(I)
2049      CONTINUE
         CALL CROSS2(R1M,RI,RCMXRI)
         CALL CROSS3(RIMRCM,A1,A3)
         CALL CROSS3(RIMRCM,A2,A4)
         DO 2048 I=1,3
          A1(I) = A3(I) + RCMXRI(I) * CVECK0
          A2(I) = A4(I) + RCMXRI(I) * CVECK1
          A1(I) = ISGN(E1N(N1)) * L1N(N1)/(4*AREA1N) * A1(I)
          A2(I) = ISGN(E1N(N1)) * L1N(N1)/(4*AREA1N) * A2(I)
2048      CONTINUE
           A = X14PI * ( CDOT(RHO1M,A1) + CDOT(RHO1M,A2) )
           CFX = ISGN(E1M(M1)) * L1M(M1)/AREA1M * A
           CF = CF + CFX*WGHT(II)
2051   CONTINUE
           CX2 = CF * AREA1M
C
       ENDIF
C
           DO 3001 J=1,2
           DO 3001 K=1,2
            IF (M(K).NE.0.AND.N(J).NE.0) THEN
              CZ(M(K),N(J)) = CZ(M(K),N(J)) + SGNPOT(CX2,J,K)/2
             ENDIF
3001         CONTINUE
           ENDIF
2002      CONTINUE
         ENDIF
2003    CONTINUE
2004   CONTINUE
2005   CONTINUE
C
       TYPE *,' CZ2 COMPLETED'
C
       RETURN
       END
C
       SUBROUTINE ZPLPL3(CZ,JUNKNS,KUNKNS)
C
       INTEGER JUNKNS,KUNKNS
       COMPLEX JI,A,P,SGNPOT
       COMPLEX CVEC,CXSI,CETA,CPHI,A1(3),CDOT
       COMPLEX CZ(JUNKNS,KUNKNS),CX3,CF,CFX
       COMPLEX KN1,JWU14P,X14PWE,JWE14P,X14PWU
       REAL PI,KN,JWU04P,X14PJE,JWE04P,X14PJU,X14PI
```

```
      REAL MAGNI,GTAREA,AREA1N,VDOT,AREA1M,TRASH
      REAL DR,POT,RLN1(3),R01(3),L1M(3),L1N(3)
      REAL R11M(3,3),R1M(3),RC1M(3),RHO1M(3),R11N(3,3)
      REAL XSI(7),ETA(7),WGHT(7)
      INTEGER KNODES,KEDGES,KFACES,KWCRDS,KWSEGS
      INTEGER JNODES,JEDGES,JFACES,JWCRDS,JWSEGS
      INTEGER I,J,K,M(2),M0,M1,N(2),N0,N1,MAP1,MAP2
      INTEGER E1M(3),E1N(3),ISGN
C
      INTEGER WIRE,PLATE
      PARAMETER (WIRE=2)
      PARAMETER (PLATE=3)
C
      COMMON/KDIMEN/KNODES,KEDGES,KFACES
      COMMON/KDIMWR/KWCRDS,KWSEGS
      COMMON/CDIMEN/JNODES,JEDGES,JFACES
      COMMON/CDIMWR/JWCRDS,JWSEGS
      COMMON/CONST/PI,KN,JI,JWU04P,X14PJE,JWE04P,X14PJU
      COMMON/CONST1/KN1,JWU14P,X14PWE,X14PI,JWE14P,X14PWU
      COMMON/NUMINT/XSI,ETA,WGHT
C
      EXTERNAL MAGNI,GTAREA,VDOT,MAP1,MAP2
      EXTERNAL SGNPOT,ISGN,CDOT
C
C source triangles
C
      DO 2005 N0=1,KFACES
       CALL VTXCRD2(N0,R11N)
       AREA1N = GTAREA(R11N,PLATE)
       CALL LENGTH(R11N,L1N)
       CALL FACEDG2(N0,E1N(1),E1N(2),E1N(3))
C
C observation triangles
C
      DO 2004 M0=1,JFACES
       CALL VTXCRD1(M0,R11M)
       AREA1M = GTAREA(R11M,PLATE)
       CALL CENTER(R11M,RC1M,PLATE)
       CALL LENGTH(R11M,L1M)
       CALL FACEDG1(M0,E1M(1),E1M(2),E1M(3))
C
C compute integrals
C
      CALL NINT7(R11N,RC1M,CVEC,CXSI,CETA,POT,CPHI,
     +                    RLN1,R01,AREA1N,DR)
C
      DO 2003 N1=1,PLATE
       N(1) = MAP2(N0,N1,PLATE)
       N(2) = MAP2(N0,N1+PLATE,PLATE)
       IF (N(1).NE.0.OR.N(2).NE.0) THEN
        P = ISGN(E1N(N1)) * L1N(N1)/AREA1N * JI * X14PJE * CPHI
        DO 2001 I=1,3
```

```
          A1(I) = ( R11N(I,1) - R11N(I,N1) ) * CVEC +
     +     ( R11N(I,2) - R11N(I,1) ) * CXSI +
     +     ( R11N(I,3) - R11N(I,1) ) * CETA +
     +     ( R01(I) - R11N(I,N1) ) * POT + RLN1(I)
          A1(I) = ISGN(E1N(N1)) * L1N(N1)/(2*AREA1N) * A1(I)
2001      CONTINUE
C
          DO 2002 M1=1,PLATE
           M(1) = MAP1(M0,M1,PLATE)
           M(2) = MAP1(M0,M1+PLATE,PLATE)
           IF (M(1).NE.0.OR.M(2).NE.0) THEN
            CALL P1RHO(R11M,M1,RHO1M)
            A = JI * JWU04P * CDOT(RHO1M,A1)
            CX3 = ISGN(E1M(M1))*L1M(M1)*(A+P)
C
       IF (DR.LT.L1M(1).OR.DR.LT.L1M(2).OR.DR.LT.L1M(3)) THEN
C
C do the 7-pt integration over the observation triangle
C
       CF = 0
       CFX = 0
       DO 2051 II=1,7
         DO 2050 JJ=1,3
           R1M(JJ) = R11M(JJ,1) + (R11M(JJ,2)-R11M(JJ,1))*XSI(II) +
     +         (R11M(JJ,3)-R11M(JJ,1))*ETA(II)
           RHO1M(JJ) = R1M(JJ)-R11M(JJ,M1)
2050     CONTINUE
       CALL NINT7(R11N,R1M,CVEC,CXSI,CETA,POT,CPHI,
     +                    RLN1,R01,AREA1N,TRASH)
         P = ISGN(E1N(N1)) * L1N(N1)/AREA1N * JI * X14PJE * CPHI
         DO 2049 I=1,3
          A1(I) = ( R11N(I,1) - R11N(I,N1) ) * CVEC +
     +     ( R11N(I,2) - R11N(I,1) ) * CXSI +
     +     ( R11N(I,3) - R11N(I,1) ) * CETA +
     +     ( R01(I) - R11N(I,N1) ) * POT + RLN1(I)
          A1(I) = ISGN(E1N(N1)) * L1N(N1)/(4*AREA1N) * A1(I)
2049      CONTINUE
           A = JI * JWU04P * CDOT(RHO1M,A1)
           CFX = ISGN(E1M(M1))*L1M(M1)/AREA1M*(A+P)
           CF = CF + CFX*WGHT(II)
2051   CONTINUE
          CX3 = CF * AREA1M
C
       ENDIF
C
          DO 3001 J=1,2
          DO 3001 K=1,2
           IF (M(K).NE.0.AND.N(J).NE.0) THEN
             CZ(M(K),N(J)) = CZ(M(K),N(J)) + SGNPOT(CX3,J,K)/2
            ENDIF
3001       CONTINUE
          ENDIF
```

```
2002       CONTINUE
          ENDIF
2003     CONTINUE
2004    CONTINUE
2005    CONTINUE
C
        TYPE *,' CZ3 COMPLETED'
C
        RETURN
        END
C
        SUBROUTINE ZPLPL4(CZ,JUNKNS,NUNKNS)
C
        INTEGER JUNKNS,NUNKNS
        COMPLEX JI,A,P,SGNPOT
        COMPLEX CVEC1,CXSI1,CETA1,CPHI1,A2(3),CDOT
        COMPLEX CZ(JUNKNS,NUNKNS),CX4,CF,CFX
        COMPLEX KN1,JWU14P,X14PWE,JWE14P,X14PWU
        REAL PI,KN,JWU04P,X14PJE,JWE04P,X14PJU,X14PI
        REAL MAGNI,GTAREA,AREA1N,VDOT,AREA1M,TRASH
        REAL DR,POT,RLN1(3),R01(3),L1M(3),L1N(3)
        REAL R11M(3,3),R1M(3),RC1M(3),RHO1M(3),R11N(3,3)
        REAL XSI(7),ETA(7),WGHT(7)
        INTEGER NNODES,NEDGES,NFACES,NWCRDS,NWSEGS
        INTEGER JNODES,JEDGES,JFACES,JWCRDS,JWSEGS
        INTEGER I,J,K,M(2),M0,M1,N(2),N0,N1,MAP,MAP1
        INTEGER E1M(3),E1N(3),ISGN
C
        INTEGER WIRE,PLATE
        PARAMETER (WIRE=2)
        PARAMETER (PLATE=3)
C
        COMMON/DIMEN/NNODES,NEDGES,NFACES
        COMMON/DIMWR/NWCRDS,NWSEGS
        COMMON/CDIMEN/JNODES,JEDGES,JFACES
        COMMON/CDIMWR/JWCRDS,JWSEGS
        COMMON/CONST/PI,KN,JI,JWU04P,X14PJE,JWE04P,X14PJU
        COMMON/CONST1/KN1,JWU14P,X14PWE,X14PI,JWE14P,X14PWU
        COMMON/NUMINT/XSI,ETA,WGHT
C
        EXTERNAL MAGNI,GTAREA,VDOT,MAP,MAP1
        EXTERNAL SGNPOT,ISGN,CDOT
C
C source triangles
C
        DO 2005 N0=1,NFACES
         CALL VTXCRD(N0,R11N)
         AREA1N = GTAREA(R11N,PLATE)
         CALL LENGTH(R11N,L1N)
         CALL FACEDG(N0,E1N(1),E1N(2),E1N(3))
C
C observation triangles
```

```
C
      DO 2004 M0=1,JFACES
       CALL VTXCRD1(M0,R11M)
       AREA1M = GTAREA(R11M,PLATE)
       CALL CENTER(R11M,RC1M,PLATE)
       CALL LENGTH(R11M,L1M)
       CALL FACEDG1(M0,E1M(1),E1M(2),E1M(3))
C
C compute integrals
C
      CALL NINT7A(R11N,RC1M,CVEC1,CXSI1,CETA1,POT,CPHI1,
     +                    RLN1,R01,AREA1N,DR)
C
      DO 2003 N1=1,PLATE
       N(1) = MAP(N0,N1,PLATE)
       N(2) = MAP(N0,N1+PLATE,PLATE)
       IF (N(1).NE.0.OR.N(2).NE.0) THEN
        P = ISGN(E1N(N1)) * L1N(N1)/AREA1N * (-JI) * X14PWE * CPHI1
        DO 2001 I=1,3
         A2(I) = ( R11N(I,1) - R11N(I,N1) ) * CVEC1 +
     +    ( R11N(I,2) - R11N(I,1) ) * CXSI1 +
     +    ( R11N(I,3) - R11N(I,1) ) * CETA1 +
     +    ( R01(I) - R11N(I,N1) ) * POT + RLN1(I)
         A2(I) = ISGN(E1N(N1)) * L1N(N1)/(2*AREA1N) * A2(I)
2001     CONTINUE
C
        DO 2002 M1=1,PLATE
         M(1) = MAP1(M0,M1,PLATE)
         M(2) = MAP1(M0,M1+PLATE,PLATE)
         IF (M(1).NE.0.OR.M(2).NE.0) THEN
          CALL P1RHO(R11M,M1,RHO1M)
          A = -JI * JWU14P * CDOT(RHO1M,A2)
          CX4 = ISGN(E1M(M1))*L1M(M1)*(A+P)
C
      IF (DR.LT.L1M(1).OR.DR.LT.L1M(2).OR.DR.LT.L1M(3)) THEN
C
C do the 7-pt integration over the observation triangle
C
      CF = 0
      CFX = 0
      DO 2051 II=1,7
        DO 2050 JJ=1,3
          R1M(JJ) = R11M(JJ,1) + (R11M(JJ,2)-R11M(JJ,1))*XSI(II) +
     +        (R11M(JJ,3)-R11M(JJ,1))*ETA(II)
          RHO1M(JJ) = R1M(JJ)-R11M(JJ,M1)
2050    CONTINUE
       CALL NINT7A(R11N,R1M,CVEC1,CXSI1,CETA1,POT,CPHI1,
     +                    RLN1,R01,AREA1N,TRASH)
        P = ISGN(E1N(N1)) * L1N(N1)/AREA1N * (-JI) * X14PWE * CPHI1
        DO 2049 I=1,3
         A2(I) = ( R11N(I,1) - R11N(I,N1) ) * CVEC1 +
     +    ( R11N(I,2) - R11N(I,1) ) * CXSI1 +
```

```
     +     ( R11N(I,3) - R11N(I,1) ) * CETA1 +
     +     ( R01(I) - R11N(I,N1) ) * POT + RLN1(I)
           A2(I) = ISGN(E1N(N1)) * L1N(N1)/(4*AREA1N) * A2(I)
2049       CONTINUE
           A = -JI * JWU14P * CDOT(RHO1M,A2)
           CFX = ISGN(E1M(M1))*L1M(M1)/AREA1M*(A+P)
           CF = CF + CFX*WGHT(II)
2051   CONTINUE
           CX4 = CF * AREA1M
C
       ENDIF
C
           DO 3001 J=1,2
           DO 3001 K=1,2
            IF (M(K).NE.0.AND.N(J).NE.0) THEN
              CZ(M(K),N(J)) = CZ(M(K),N(J)) + SGNPOT(CX4,J,K)/2
             ENDIF
3001        CONTINUE
           ENDIF
2002      CONTINUE
         ENDIF
2003    CONTINUE
2004   CONTINUE
2005   CONTINUE
C
       TYPE *,' CZ4 COMPLETED'
C
       RETURN
       END
C
       SUBROUTINE ZPLPL5(CZ,JUNKNS)
C
       INTEGER JUNKNS
       COMPLEX JI,A,P,SGNPOT
       COMPLEX CVECK0,CXSIK0,CETAK0,A1(3),A3(3),CDOT
       COMPLEX CVECK1,CXSIK1,CETAK1,A2(3),A4(3)
       COMPLEX CZ(JUNKNS,JUNKNS),CX5,CF,CFX
       COMPLEX KN1,JWU14P,X14PWE,JWE14P,X14PWU
       REAL PI,KN,JWU04P,X14PJE,JWE04P,X14PJU,X14PI
       REAL MAGNI,GTAREA,AREA1N,VDOT,AREA1M,TRASH
       REAL DR,POT,RLN1(3),R01(3),L1M(3),L1N(3)
       REAL R11M(3,3),R1M(3),RC1M(3),RHO1M(3),R11N(3,3)
       REAL RI(3),RIMRCM(3),RCMXRI(3)
       REAL XSI(7),ETA(7),WGHT(7)
       INTEGER JNODES,JEDGES,JFACES,JWCRDS,JWSEGS
       INTEGER LJ,K,M(2),M0,M1,N(2),N0,N1,MAP1,E1M(3),E1N(3),ISGN
C
       INTEGER WIRE,PLATE
       PARAMETER (WIRE=2)
       PARAMETER (PLATE=3)
C
       COMMON/CDIMEN/JNODES,JEDGES,JFACES
```

```
      COMMON/CDIMWR/JWCRDS,JWSEGS
      COMMON/CONST/PI,KN,JI,JWU04P,X14PJE,JWE04P,X14PJU
      COMMON/CONST1/KN1,JWU14P,X14PWE,X14PI,JWE14P,X14PWU
      COMMON/NUMINT/XSI,ETA,WGHT
C
      EXTERNAL MAGNI,GTAREA,VDOT,MAP1
      EXTERNAL SGNPOT,ISGN,CDOT
C
C source triangles
C
      DO 2005 N0=1,JFACES
       CALL VTXCRD1(N0,R11N)
       AREA1N = GTAREA(R11N,PLATE)
       CALL LENGTH(R11N,L1N)
       CALL FACEDG1(N0,E1N(1),E1N(2),E1N(3))
C
C observation triangles
C
      DO 2004 M0=1,JFACES
       CALL VTXCRD1(M0,R11M)
       AREA1M = GTAREA(R11M,PLATE)
       CALL CENTER(R11M,RC1M,PLATE)
       CALL LENGTH(R11M,L1M)
       CALL FACEDG1(M0,E1M(1),E1M(2),E1M(3))
C
C compute integrals
C
      IF(M0.EQ.N0) THEN
         CVECK0 = 0
         CXSIK0 = 0
         CETAK0 = 0
         CVECK1 = 0
         CXSIK1 = 0
         CETAK1 = 0
      ELSE
        CALL NINT7B(R11N,RC1M,CVECK0,CXSIK0,CETAK0,AREA1N,DR)
        CALL NINT7C(R11N,RC1M,CVECK1,CXSIK1,CETAK1,AREA1N,DR)
      ENDIF
C
      DO 2003 N1=1,PLATE
       N(1) = MAP1(N0,N1,PLATE)
       N(2) = MAP1(N0,N1+PLATE,PLATE)
       IF (N(1).NE.0.OR.N(2).NE.0) THEN
        DO 2001 I=1,3
         A1(I) = R11N(I,1) * CVECK0 +
     +     ( R11N(I,2) - R11N(I,1) ) * CXSIK0 +
     +     ( R11N(I,3) - R11N(I,1) ) * CETAK0
         A2(I) = R11N(I,1) * CVECK1 +
     +     ( R11N(I,2) - R11N(I,1) ) * CXSIK1 +
     +     ( R11N(I,3) - R11N(I,1) ) * CETAK1
         RI(I) = R11N(I,N1)
         RIMRCM(I) = RI(I) - RC1M(I)
```

```
2001      CONTINUE
          CALL CROSS2(RC1M,RI,RCMXRI)
          CALL CROSS3(RIMRCM,A1,A3)
          CALL CROSS3(RIMRCM,A2,A4)
          DO 2025 I=1,3
           A1(I) = A3(I) + RCMXRI(I) * CVECK0
           A2(I) = A4(I) + RCMXRI(I) * CVECK1
           A1(I) = ISGN(E1N(N1)) * L1N(N1)/(2*AREA1N) * A1(I)
           A2(I) = ISGN(E1N(N1)) * L1N(N1)/(2*AREA1N) * A2(I)
2025      CONTINUE
C
          DO 2002 M1=1,PLATE
           M(1) = MAP1(M0,M1,PLATE)
           M(2) = MAP1(M0,M1+PLATE,PLATE)
           IF (M(1).NE.0.OR.M(2).NE.0) THEN
            CALL P1RHO(R11M,M1,RHO1M)
            A = X14PI * ( CDOT(RHO1M,A1) + CDOT(RHO1M,A2) )
            CX5 = ISGN(E1M(M1)) * L1M(M1) * A
C
       IF (DR.LT.L1M(1).OR.DR.LT.L1M(2).OR.DR.LT.L1M(3)) THEN
C
C do the 7-pt integration over the observation triangle
C
       CF = 0
       CFX = 0
       DO 2051 II=1,7
         DO 2050 JJ=1,3
           R1M(JJ) = R11M(JJ,1) + (R11M(JJ,2)-R11M(JJ,1))*XSI(II) +
     +         (R11M(JJ,3)-R11M(JJ,1))*ETA(II)
           RHO1M(JJ) = R1M(JJ)-R11M(JJ,M1)
2050     CONTINUE
       IF(M0.EQ.N0) THEN
          CVECK0 = 0
          CXSIK0 = 0
          CETAK0 = 0
          CVECK1 = 0
          CXSIK1 = 0
          CETAK1 = 0
       ELSE
         CALL NINT7B(R11N,R1M,CVECK0,CXSIK0,CETAK0,AREA1N,TRASH)
         CALL NINT7C(R11N,R1M,CVECK1,CXSIK1,CETAK1,AREA1N,TRASH)
       ENDIF
         DO 2049 I=1,3
          A1(I) = R11N(I,1) * CVECK0 +
     +     ( R11N(I,2) - R11N(I,1) ) * CXSIK0 +
     +     ( R11N(I,3) - R11N(I,1) ) * CETAK0
          A2(I) = R11N(I,1) * CVECK1 +
     +     ( R11N(I,2) - R11N(I,1) ) * CXSIK1 +
     +     ( R11N(I,3) - R11N(I,1) ) * CETAK1
          RI(I) = R11N(I,N1)
          RIMRCM(I) = RI(I) - R1M(I)
2049      CONTINUE
```

```
          CALL CROSS2(R1M,RI,RCMXRI)
          CALL CROSS3(RIMRCM,A1,A3)
          CALL CROSS3(RIMRCM,A2,A4)
          DO 2048 I=1,3
           A1(I) = A3(I) + RCMXRI(I) * CVECK0
           A2(I) = A4(I) + RCMXRI(I) * CVECK1
           A1(I) = ISGN(E1N(N1)) * L1N(N1)/(4*AREA1N) * A1(I)
           A2(I) = ISGN(E1N(N1)) * L1N(N1)/(4*AREA1N) * A2(I)
2048       CONTINUE
            A = X14PI * ( CDOT(RHO1M,A1) + CDOT(RHO1M,A2) )
            CFX = ISGN(E1M(M1)) * L1M(M1)/AREA1M * A
            CF = CF + CFX*WGHT(II)
2051    CONTINUE
            CX5 = CF * AREA1M
C
        ENDIF
C
            DO 3001 J=1,2
            DO 3001 K=1,2
             IF (M(K).NE.0.AND.N(J).NE.0) THEN
               CZ(N(J),M(K)) = CZ(N(J),M(K)) + SGNPOT(CX5,J,K)/2
              ENDIF
3001         CONTINUE
            ENDIF
2002       CONTINUE
          ENDIF
2003     CONTINUE
2004    CONTINUE
2005    CONTINUE
C
C ***************
        OPEN(FILE='CZ2',STATUS='NEW',DISPOSE='DELETE',
       +                  UNIT=22,FORM='UNFORMATTED')
        DO 147 J=1,JUNKNS
147      WRITE(22)(CZ(I,J),I=1,JUNKNS)
C ***************
C
        TYPE *,' CZ5 COMPLETED'
C
        RETURN
        END
C
        SUBROUTINE ZPLPL6(CZ,JUNKNS)
C
        INTEGER JUNKNS
        COMPLEX JI,A,P,SGNPOT
        COMPLEX CVEC,CXSI,CETA,CPHI,A1(3),CDOT
        COMPLEX CVEC1,CXSI1,CETA1,CPHI1,A2(3)
        COMPLEX CZ(JUNKNS,JUNKNS),CX6,CF,CFX
        COMPLEX KN1,JWU14P,X14PWE,JWE14P,X14PWU
        REAL PI,KN,JWU04P,X14PJE,JWE04P,X14PJU,X14PI
        REAL MAGNI,GTAREA,AREA1N,VDOT,AREA1M,TRASH
```

```
      REAL DR,POT,RLN1(3),R01(3),L1M(3),L1N(3)
      REAL R11M(3,3),R1M(3),RC1M(3),RHO1M(3),R11N(3,3)
      REAL XSI(7),ETA(7),WGHT(7)
      INTEGER JNODES,JEDGES,JFACES,JWCRDS,JWSEGS
      INTEGER I,J,K,M(2),M0,M1,N(2),N0,N1,MAP1,E1M(3),E1N(3),ISGN
C
      INTEGER WIRE,PLATE
      PARAMETER (WIRE=2)
      PARAMETER (PLATE=3)
C
      COMMON/CDIMEN/JNODES,JEDGES,JFACES
      COMMON/CDIMWR/JWCRDS,JWSEGS
      COMMON/CONST/PI,KN,JI,JWU04P,X14PJE,JWE04P,X14PJU
      COMMON/CONST1/KN1,JWU14P,X14PWE,X14PI,JWE14P,X14PWU
      COMMON/NUMINT/XSI,ETA,WGHT
C
      EXTERNAL MAGNI,GTAREA,VDOT,MAP1
      EXTERNAL SGNPOT,ISGN,CDOT
C
C source triangles
C
      DO 2005 N0=1,JFACES
       CALL VTXCRD1(N0,R11N)
       AREA1N = GTAREA(R11N,PLATE)
       CALL LENGTH(R11N,L1N)
       CALL FACEDG1(N0,E1N(1),E1N(2),E1N(3))
C
C observation triangles
C
      DO 2004 M0=1,JFACES
       CALL VTXCRD1(M0,R11M)
       AREA1M = GTAREA(R11M,PLATE)
       CALL CENTER(R11M,RC1M,PLATE)
       CALL LENGTH(R11M,L1M)
       CALL FACEDG1(M0,E1M(1),E1M(2),E1M(3))
C
C compute integrals
C
      CALL NINT7(R11N,RC1M,CVEC,CXSI,CETA,POT,CPHI,RLN1,R01,AREA1N,DR)
      CALL NINT7A(R11N,RC1M,CVEC1,CXSI1,CETA1,POT,CPHI1,
     +                    RLN1,R01,AREA1N,DR)
C
      DO 2003 N1=1,PLATE
       N(1) = MAP1(N0,N1,PLATE)
       N(2) = MAP1(N0,N1+PLATE,PLATE)
       IF (N(1).NE.0.OR.N(2).NE.0) THEN
        P = ISGN(E1N(N1)) * L1N(N1)/AREA1N * (-JI) * X14PJU * CPHI +
     +          ISGN(E1N(N1)) * L1N(N1)/AREA1N * (-JI) * X14PWU * CPHI1
        DO 2001 I=1,3
         A1(I) = ( R11N(I,1) - R11N(I,N1) ) * CVEC +
     +    ( R11N(I,2) - R11N(I,1) ) * CXSI +
     +    ( R11N(I,3) - R11N(I,1) ) * CETA +
```

```
     +     ( R01(I) - R11N(I,N1) ) * POT + RLN1(I)
           A2(I) = ( R11N(I,1) - R11N(I,N1) ) * CVEC1 +
     +     ( R11N(I,2) - R11N(I,1) ) * CXSI1 +
     +     ( R11N(I,3) - R11N(I,1) ) * CETA1 +
     +     ( R01(I) - R11N(I,N1) ) * POT + RLN1(I)
           A1(I) = ISGN(E1N(N1)) * L1N(N1)/(2*AREA1N) * A1(I)
           A2(I) = ISGN(E1N(N1)) * L1N(N1)/(2*AREA1N) * A2(I)
2001       CONTINUE
C
           DO 2002 M1=1,PLATE
            M(1) = MAP1(M0,M1,PLATE)
            M(2) = MAP1(M0,M1+PLATE,PLATE)
            IF (M(1).NE.0.OR.M(2).NE.0) THEN
             CALL P1RHO(R11M,M1,RHO1M)
             A = -JI * JWE04P * CDOT(RHO1M,A1) +
     +           (-JI) * JWE14P * CDOT(RHO1M,A2)
            CX6 = ISGN(E1M(M1))*L1M(M1)*(A+P)
C
       IF (DR.LT.L1M(1).OR.DR.LT.L1M(2).OR.DR.LT.L1M(3)) THEN
C
C do the 7-pt integration over the observation triangle
C
        CF = 0
        CFX = 0
        DO 2051 II=1,7
          DO 2050 JJ=1,3
            R1M(JJ) = R11M(JJ,1) + (R11M(JJ,2)-R11M(JJ,1))*XSI(II) +
     +         (R11M(JJ,3)-R11M(JJ,1))*ETA(II)
            RHO1M(JJ) = R1M(JJ)-R11M(JJ,M1)
2050      CONTINUE
        CALL NINT7(R11N,R1M,CVEC,CXSI,CETA,POT,CPHI,RLN1,R01,AREA1N,TRASH)
        CALL NINT7A(R11N,R1M,CVEC1,CXSI1,CETA1,POT,CPHI1,
     +                    RLN1,R01,AREA1N,TRASH)
          P = ISGN(E1N(N1)) * L1N(N1)/AREA1N * (-JI) * X14PJU * CPHI +
     +          ISGN(E1N(N1)) * L1N(N1)/AREA1N * (-JI) * X14PWU * CPHI1
          DO 2049 I=1,3
           A1(I) = ( R11N(I,1) - R11N(I,N1) ) * CVEC +
     +     ( R11N(I,2) - R11N(I,1) ) * CXSI +
     +     ( R11N(I,3) - R11N(I,1) ) * CETA +
     +     ( R01(I) - R11N(I,N1) ) * POT + RLN1(I)
           A2(I) = ( R11N(I,1) - R11N(I,N1) ) * CVEC1 +
     +     ( R11N(I,2) - R11N(I,1) ) * CXSI1 +
     +     ( R11N(I,3) - R11N(I,1) ) * CETA1 +
     +     ( R01(I) - R11N(I,N1) ) * POT + RLN1(I)
           A1(I) = ISGN(E1N(N1)) * L1N(N1)/(4*AREA1N) * A1(I)
           A2(I) = ISGN(E1N(N1)) * L1N(N1)/(4*AREA1N) * A2(I)
2049       CONTINUE
            A = -JI * JWE04P * CDOT(RHO1M,A1) +
     +          (-JI) * JWE14P * CDOT(RHO1M,A2)
           CFX = ISGN(E1M(M1))*L1M(M1)/AREA1M*(A+P)
           CF = CF + CFX*WGHT(II)
2051   CONTINUE
```

```
            CX6 = CF * AREA1M
C
          ENDIF
C
               DO 3001 J=1,2
               DO 3001 K=1,2
                IF (M(K).NE.0.AND.N(J).NE.0) THEN
                  IF(M(K).NE.N(J)) THEN
                   CZ(M(K),N(J)) = CZ(M(K),N(J)) + SGNPOT(CX6,J,K)/2
                   CZ(N(J),M(K)) = CZ(N(J),M(K)) + SGNPOT(CX6,J,K)/2
                  ELSE
                   CZ(M(K),N(J)) = CZ(M(K),N(J)) + SGNPOT(CX6,J,K)
                  ENDIF
                 ENDIF
3001             CONTINUE
                ENDIF
2002           CONTINUE
              ENDIF
2003         CONTINUE
2004       CONTINUE
2005       CONTINUE
C
C ***************
          OPEN(FILE='CZ6',STATUS='NEW',DISPOSE='DELETE',
         +                        UNIT=26,FORM='UNFORMATTED')
          DO 147 J=1,JUNKNS
147        WRITE(26)(CZ(I,J),I=1,J)
C ***************
C
          TYPE *,' CZ6 COMPLETED'
C
          RETURN
          END
C
          SUBROUTINE ZPLPL7(CZ,JUNKNS,KUNKNS)
C
          INTEGER JUNKNS,KUNKNS
          COMPLEX JL,A,P,SGNPOT
          COMPLEX CVECK0,CXSIK0,CETAK0,A1(3),A3(3),CDOT
          COMPLEX CZ(JUNKNS,KUNKNS),CX7,CF,CFX
          COMPLEX KN1,JWU14P,X14PWE,JWE14P,X14PWU
          REAL PI,KN,JWU04P,X14PJE,JWE04P,X14PJU,X14PI
          REAL MAGNI,GTAREA,AREA1N,VDOT,AREA1M,TRASH
          REAL DR,POT,RLN1(3),R01(3),L1M(3),L1N(3)
          REAL R11M(3,3),R1M(3),RC1M(3),RHO1M(3),R11N(3,3)
          REAL RI(3),RIMRCM(3),RCMXRI(3)
          REAL XSI(7),ETA(7),WGHT(7)
          INTEGER KNODES,KEDGES,KFACES,KWCRDS,KWSEGS
          INTEGER JNODES,JEDGES,JFACES,JWCRDS,JWSEGS
          INTEGER I,J,K,M(2),M0,M1,N(2),N0,N1,MAP1,MAP2
          INTEGER E1M(3),E1N(3),ISGN
C
```

```
      INTEGER WIRE,PLATE
      PARAMETER (WIRE=2)
      PARAMETER (PLATE=3)
C
      COMMON/KDIMEN/KNODES,KEDGES,KFACES
      COMMON/KDIMWR/KWCRDS,KWSEGS
      COMMON/CDIMEN/JNODES,JEDGES,JFACES
      COMMON/CDIMWR/JWCRDS,JWSEGS
      COMMON/CONST/PI,KN,JI,JWU04P,X14PJE,JWE04P,X14PJU
      COMMON/CONST1/KN1,JWU14P,X14PWE,X14PI,JWE14P,X14PWU
      COMMON/NUMINT/XSI,ETA,WGHT
C
      EXTERNAL MAGNI,GTAREA,VDOT,MAP1,MAP2
      EXTERNAL SGNPOT,ISGN,CDOT
C
C source triangles
C
      DO 2005 N0=1,KFACES
       CALL VTXCRD2(N0,R11N)
       AREA1N = GTAREA(R11N,PLATE)
       CALL LENGTH(R11N,L1N)
       CALL FACEDG2(N0,E1N(1),E1N(2),E1N(3))
C
C observation triangles
C
      DO 2004 M0=1,JFACES
       CALL VTXCRD1(M0,R11M)
       AREA1M = GTAREA(R11M,PLATE)
       CALL CENTER(R11M,RC1M,PLATE)
       CALL LENGTH(R11M,L1M)
       CALL FACEDG1(M0,E1M(1),E1M(2),E1M(3))
C
C compute integrals
C
      CALL NINT7B(R11N,RC1M,CVECK0,CXSIK0,CETAK0,AREA1N,DR)
C
      DO 2003 N1=1,PLATE
       N(1) = MAP2(N0,N1,PLATE)
       N(2) = MAP2(N0,N1+PLATE,PLATE)
       IF (N(1).NE.0.OR.N(2).NE.0) THEN
        DO 2001 I=1,3
         A1(I) = R11N(I,1) * CVECK0 +
     +    ( R11N(I,2) - R11N(I,1) ) * CXSIK0 +
     +    ( R11N(I,3) - R11N(I,1) ) * CETAK0
         RI(I) = R11N(I,N1)
         RIMRCM(I) = RI(I) - RC1M(I)
2001     CONTINUE
        CALL CROSS2(RC1M,RI,RCMXRI)
        CALL CROSS3(RIMRCM,A1,A3)
        DO 2025 I=1,3
         A1(I) = A3(I) + RCMXRI(I) * CVECK0
         A1(I) = ISGN(E1N(N1)) * L1N(N1)/(2*AREA1N) * A1(I)
```

```
2025      CONTINUE
C
         DO 2002 M1=1,PLATE
          M(1) = MAP1(M0,M1,PLATE)
          M(2) = MAP1(M0,M1+PLATE,PLATE)
          IF (M(1).NE.0.OR.M(2).NE.0) THEN
           CALL P1RHO(R11M,M1,RHO1M)
           A = X14PI * CDOT(RHO1M,A1)
           CX7 = ISGN(E1M(M1)) * L1M(M1) * A
C
      IF (DR.LT.L1M(1).OR.DR.LT.L1M(2).OR.DR.LT.L1M(3)) THEN
C
C do the 7-pt integration over the observation triangle
C
       CF = 0
       CFX = 0
       DO 2051 II=1,7
          DO 2050 JJ=1,3
            R1M(JJ) = R11M(JJ,1) + (R11M(JJ,2)-R11M(JJ,1))*XSI(II) +
     +          (R11M(JJ,3)-R11M(JJ,1))*ETA(II)
            RHO1M(JJ) = R1M(JJ)-R11M(JJ,M1)
2050      CONTINUE
       CALL NINT7B(R11N,R1M,CVECK0,CXSIK0,CETAK0,AREA1N,TRASH)
          DO 2049 I=1,3
           A1(I) = R11N(I,1) * CVECK0 +
     +      ( R11N(I,2) - R11N(I,1) ) * CXSIK0 +
     +      ( R11N(I,3) - R11N(I,1) ) * CETAK0
           RI(I) = R11N(I,N1)
           RIMRCM(I) = RI(I) - R1M(I)
2049       CONTINUE
          CALL CROSS2(R1M,RI,RCMXRI)
          CALL CROSS3(RIMRCM,A1,A3)
          DO 2048 I=1,3
           A1(I) = A3(I) + RCMXRI(I) * CVECK0
           A1(I) = ISGN(E1N(N1)) * L1N(N1)/(4*AREA1N) * A1(I)
2048       CONTINUE
            A = X14PI * CDOT(RHO1M,A1)
            CFX = ISGN(E1M(M1)) * L1M(M1)/AREA1M * A
            CF = CF + CFX*WGHT(II)
2051   CONTINUE
            CX7 = CF * AREA1M
C
       ENDIF
C
            DO 3001 J=1,2
            DO 3001 K=1,2
             IF (M(K).NE.0.AND.N(J).NE.0) THEN
               CZ(M(K),N(J)) = CZ(M(K),N(J)) + SGNPOT(CX7,J,K)/2
              ENDIF
3001         CONTINUE
            ENDIF
2002       CONTINUE
```

```
        ENDIF
2003    CONTINUE
2004   CONTINUE
2005   CONTINUE
C
       TYPE *,' CZ7 COMPLETED'
C
       RETURN
       END
C
       SUBROUTINE ZPLPL8(CZ,JUNKNS,NUNKNS)
C
       INTEGER JUNKNS,NUNKNS
       COMPLEX JI,A,P,SGNPOT
       COMPLEX CVECK1,CXSIK1,CETAK1,A2(3),A4(3),CDOT
       COMPLEX CZ(JUNKNS,NUNKNS),CX8,CF,CFX
       COMPLEX KN1,JWU14P,X14PWE,JWE14P,X14PWU
       REAL PI,KN,JWU04P,X14PJE,JWE04P,X14PJU,X14PI
       REAL MAGNI,GTAREA,AREA1N,VDOT,AREA1M,TRASH
       REAL DR,POT,RLN1(3),R01(3),L1M(3),L1N(3)
       REAL R11M(3,3),R1M(3),RC1M(3),RHO1M(3),R11N(3,3)
       REAL RI(3),RIMRCM(3),RCMXRI(3)
       REAL XSI(7),ETA(7),WGHT(7)
       INTEGER NNODES,NEDGES,NFACES,NWCRDS,NWSEGS
       INTEGER JNODES,JEDGES,JFACES,JWCRDS,JWSEGS
       INTEGER I,J,K,M(2),M0,M1,N(2),N0,N1,MAP,MAP1
       INTEGER E1M(3),E1N(3),ISGN
C
       INTEGER WIRE,PLATE
       PARAMETER (WIRE=2)
       PARAMETER (PLATE=3)
C
       COMMON/DIMEN/NNODES,NEDGES,NFACES
       COMMON/DIMWR/NWCRDS,NWSEGS
       COMMON/CDIMEN/JNODES,JEDGES,JFACES
       COMMON/CDIMWR/JWCRDS,JWSEGS
       COMMON/CONST/PI,KN,JI,JWU04P,X14PJE,JWE04P,X14PJU
       COMMON/CONST1/KN1,JWU14P,X14PWE,X14PI,JWE14P,X14PWU
       COMMON/NUMINT/XSI,ETA,WGHT
C
       EXTERNAL MAGNI,GTAREA,VDOT,MAP,MAP1
       EXTERNAL SGNPOT,ISGN,CDOT
C
C source triangles
C
       DO 2005 N0=1,NFACES
        CALL VTXCRD(N0,R11N)
        AREA1N = GTAREA(R11N,PLATE)
        CALL LENGTH(R11N,L1N)
        CALL FACEDG(N0,E1N(1),E1N(2),E1N(3))
C
C observation triangles
```

```
C
      DO 2004 M0=1,JFACES
       CALL VTXCRD1(M0,R11M)
       AREA1M = GTAREA(R11M,PLATE)
       CALL CENTER(R11M,RC1M,PLATE)
       CALL LENGTH(R11M,L1M)
       CALL FACEDG1(M0,E1M(1),E1M(2),E1M(3))
C
C compute integrals
C
      CALL NINT7C(R11N,RC1M,CVECK1,CXSIK1,CETAK1,AREA1N,DR)
C
      DO 2003 N1=1,PLATE
       N(1) = MAP(N0,N1,PLATE)
       N(2) = MAP(N0,N1+PLATE,PLATE)
       IF (N(1).NE.0.OR.N(2).NE.0) THEN
        DO 2001 I=1,3
         A2(I) = R11N(I,1) * CVECK1 +
     +     ( R11N(I,2) - R11N(I,1) ) * CXSIK1 +
     +     ( R11N(I,3) - R11N(I,1) ) * CETAK1
         RI(I) = R11N(I,N1)
         RIMRCM(I) = RI(I) - RC1M(I)
2001     CONTINUE
        CALL CROSS2(RC1M,RI,RCMXRI)
        CALL CROSS3(RIMRCM,A2,A4)
        DO 2025 I=1,3
         A2(I) = A4(I) + RCMXRI(I) * CVECK1
         A2(I) = ISGN(E1N(N1)) * L1N(N1)/(2*AREA1N) * A2(I)
2025     CONTINUE
C
        DO 2002 M1=1,PLATE
         M(1) = MAP1(M0,M1,PLATE)
         M(2) = MAP1(M0,M1+PLATE,PLATE)
         IF (M(1).NE.0.OR.M(2).NE.0) THEN
          CALL P1RHO(R11M,M1,RHO1M)
          A = -X14PI * CDOT(RHO1M,A2)
          CX8 = ISGN(E1M(M1)) * L1M(M1) * A
C
      IF (DR.LT.L1M(1).OR.DR.LT.L1M(2).OR.DR.LT.L1M(3)) THEN
C
C do the 7-pt integration over the observation triangle
C
      CF = 0
      CFX = 0
      DO 2051 II=1,7
        DO 2050 JJ=1,3
          R1M(JJ) = R11M(JJ,1) + (R11M(JJ,2)-R11M(JJ,1))*XSI(II) +
     +        (R11M(JJ,3)-R11M(JJ,1))*ETA(II)
          RHO1M(JJ) = R1M(JJ)-R11M(JJ,M1)
2050    CONTINUE
      CALL NINT7C(R11N,R1M,CVECK1,CXSIK1,CETAK1,AREA1N,TRASH)
        DO 2049 I=1,3
```

```
          A2(I) = R11N(I,1) * CVECK1 +
     +     ( R11N(I,2) - R11N(I,1) ) * CXSIK1 +
     +     ( R11N(I,3) - R11N(I,1) ) * CETAK1
          RI(I) = R11N(I,N1)
          RIMRCM(I) = RI(I) - R1M(I)
2049      CONTINUE
         CALL CROSS2(R1M,RI,RCMXRI)
         CALL CROSS3(RIMRCM,A2,A4)
         DO 2048 I=1,3
          A2(I) = A4(I) + RCMXRI(I) * CVECK1
          A2(I) = ISGN(E1N(N1)) * L1N(N1)/(4*AREA1N) * A2(I)
2048      CONTINUE
           A = -X14PI * CDOT(RHO1M,A2)
           CFX = ISGN(E1M(M1)) * L1M(M1)/AREA1M * A
           CF = CF + CFX*WGHT(II)
2051   CONTINUE
          CX8 = CF * AREA1M
C
       ENDIF
C
          DO 3001 J=1,2
          DO 3001 K=1,2
           IF (M(K).NE.0.AND.N(J).NE.0) THEN
             CZ(M(K),N(J)) = CZ(M(K),N(J)) + SGNPOT(CX8,J,K)/2
            ENDIF
3001       CONTINUE
          ENDIF
2002      CONTINUE
         ENDIF
2003    CONTINUE
2004   CONTINUE
2005   CONTINUE
C
       TYPE *,' CZ8 COMPLETED'
C
       RETURN
       END
C
       SUBROUTINE ZPLPL9(CZ,JUNKNS,KUNKNS)
C
       INTEGER JUNKNS,KUNKNS
       COMPLEX JL,A,P,SGNPOT
       COMPLEX CVEC,CXSI,CETA,CPHI,A1(3),CDOT
       COMPLEX CZ(JUNKNS,KUNKNS),CX9,CF,CFX
       COMPLEX KN1,JWU14P,X14PWE,JWE14P,X14PWU
       REAL PI,KN,JWU04P,X14PJE,JWE04P,X14PJU,X14PI
       REAL MAGNI,GTAREA,AREA1N,VDOT,AREA1M,TRASH
       REAL DR,POT,RLN1(3),R01(3),L1M(3),L1N(3)
       REAL R11M(3,3),R1M(3),RC1M(3),RHO1M(3),R11N(3,3)
       REAL XSI(7),ETA(7),WGHT(7)
       INTEGER KNODES,KEDGES,KFACES,KWCRDS,KWSEGS
       INTEGER JNODES,JEDGES,JFACES,JWCRDS,JWSEGS
```

```
      INTEGER I,J,K,M(2),M0,M1,N(2),N0,N1,MAP1,MAP2
      INTEGER E1M(3),E1N(3),ISGN
C
      INTEGER WIRE,PLATE
      PARAMETER (WIRE=2)
      PARAMETER (PLATE=3)
C
      COMMON/KDIMEN/KNODES,KEDGES,KFACES
      COMMON/KDIMWR/KWCRDS,KWSEGS
      COMMON/CDIMEN/JNODES,JEDGES,JFACES
      COMMON/CDIMWR/JWCRDS,JWSEGS
      COMMON/CONST/PI,KN,JI,JWU04P,X14PJE,JWE04P,X14PJU
      COMMON/CONST1/KN1,JWU14P,X14PWE,X14PI,JWE14P,X14PWU
      COMMON/NUMINT/XSI,ETA,WGHT
C
      EXTERNAL MAGNI,GTAREA,VDOT,MAP1,MAP2
      EXTERNAL SGNPOT,ISGN,CDOT
C
C source triangles
C
      DO 2005 N0=1,JFACES
       CALL VTXCRD1(N0,R11N)
       AREA1N = GTAREA(R11N,PLATE)
       CALL LENGTH(R11N,L1N)
       CALL FACEDG1(N0,E1N(1),E1N(2),E1N(3))
C
C observation triangles
C
      DO 2004 M0=1,KFACES
       CALL VTXCRD2(M0,R11M)
       AREA1M = GTAREA(R11M,PLATE)
       CALL CENTER(R11M,RC1M,PLATE)
       CALL LENGTH(R11M,L1M)
       CALL FACEDG2(M0,E1M(1),E1M(2),E1M(3))
C
C compute integrals
C
      CALL NINT7(R11N,RC1M,CVEC,CXSI,CETA,POT,CPHI,
     +                    RLN1,R01,AREA1N,DR)
C
      DO 2003 N1=1,PLATE
       N(1) = MAP1(N0,N1,PLATE)
       N(2) = MAP1(N0,N1+PLATE,PLATE)
       IF (N(1).NE.0.OR.N(2).NE.0) THEN
        P = ISGN(E1N(N1)) * L1N(N1)/AREA1N * JI * X14PJE * CPHI
        DO 2001 I=1,3
         A1(I) = ( R11N(I,1) - R11N(I,N1) ) * CVEC +
     +    ( R11N(I,2) - R11N(I,1) ) * CXSI +
     +    ( R11N(I,3) - R11N(I,1) ) * CETA +
     +    ( R01(I) - R11N(I,N1) ) * POT + RLN1(I)
         A1(I) = ISGN(E1N(N1)) * L1N(N1)/(2*AREA1N) * A1(I)
2001     CONTINUE
```

```
C
        DO 2002 M1=1,PLATE
         M(1) = MAP2(M0,M1,PLATE)
         M(2) = MAP2(M0,M1+PLATE,PLATE)
         IF (M(1).NE.0.OR.M(2).NE.0) THEN
          CALL P1RHO(R11M,M1,RHO1M)
          A = JI * JWU04P * CDOT(RHO1M,A1)
          CX9 = ISGN(E1M(M1))*L1M(M1)*(A+P)
C
      IF (DR.LT.L1M(1).OR.DR.LT.L1M(2).OR.DR.LT.L1M(3)) THEN
C
C do the 7-pt integration over the observation triangle
C
      CF = 0
      CFX = 0
      DO 2051 II=1,7
        DO 2050 JJ=1,3
          R1M(JJ) = R11M(JJ,1) + (R11M(JJ,2)-R11M(JJ,1))*XSI(II) +
     +        (R11M(JJ,3)-R11M(JJ,1))*ETA(II)
          RHO1M(JJ) = R1M(JJ)-R11M(JJ,M1)
2050    CONTINUE
      CALL NINT7(R11N,R1M,CVEC,CXSI,CETA,POT,CPHI,
     +                    RLN1,R01,AREA1N,TRASH)
        P = ISGN(E1N(N1)) * L1N(N1)/AREA1N * JI * X14PJE * CPHI
        DO 2049 I=1,3
         A1(I) = ( R11N(I,1) - R11N(I,N1) ) * CVEC +
     +    ( R11N(I,2) - R11N(I,1) ) * CXSI +
     +    ( R11N(I,3) - R11N(I,1) ) * CETA +
     +    ( R01(I) - R11N(I,N1) ) * POT + RLN1(I)
         A1(I) = ISGN(E1N(N1)) * L1N(N1)/(4*AREA1N) * A1(I)
2049    CONTINUE
          A = JI * JWU04P * CDOT(RHO1M,A1)
          CFX = ISGN(E1M(M1))*L1M(M1)/AREA1M*(A+P)
          CF = CF + CFX*WGHT(II)
2051  CONTINUE
          CX9 = CF * AREA1M
C
      ENDIF
C
          DO 3001 J=1,2
          DO 3001 K=1,2
           IF (M(K).NE.0.AND.N(J).NE.0) THEN
             CZ(N(J),M(K)) = CZ(N(J),M(K)) + SGNPOT(CX9,J,K)/2
            ENDIF
3001       CONTINUE
          ENDIF
2002     CONTINUE
        ENDIF
2003   CONTINUE
2004  CONTINUE
2005  CONTINUE
C
```

```
C ************
      OPEN(FILE='CZ3',STATUS='NEW',DISPOSE='DELETE',
     +           UNIT=23,FORM='UNFORMATTED')
      DO 147 J=1,KUNKNS
147    WRITE(23)(CZ(I,J),I=1,JUNKNS)
C ************
C
      TYPE *,' CZ9 COMPLETED'
C
      RETURN
      END
C
      SUBROUTINE ZPLPL10(CZ,JUNKNS,KUNKNS)
C
      INTEGER JUNKNS,KUNKNS
      COMPLEX JI,A,P,SGNPOT
      COMPLEX CVECK0,CXSIK0,CETAK0,A1(3),A3(3),CDOT
      COMPLEX CZ(JUNKNS,KUNKNS),CX10,CF,CFX
      COMPLEX KN1,JWU14P,X14PWE,JWE14P,X14PWU
      REAL PI,KN,JWU04P,X14PJE,JWE04P,X14PJU,X14PI
      REAL MAGNI,GTAREA,AREA1N,VDOT,AREA1M,TRASH
      REAL DR,POT,RLN1(3),R01(3),L1M(3),L1N(3)
      REAL R11M(3,3),R1M(3),RC1M(3),RHO1M(3),R11N(3,3)
      REAL RI(3),RIMRCM(3),RCMXRI(3)
      REAL XSI(7),ETA(7),WGHT(7)
      INTEGER KNODES,KEDGES,KFACES,KWCRDS,KWSEGS
      INTEGER JNODES,JEDGES,JFACES,JWCRDS,JWSEGS
      INTEGER I,J,K,M(2),M0,M1,N(2),N0,N1,MAP1,MAP2
      INTEGER E1M(3),E1N(3),ISGN
C
      INTEGER WIRE,PLATE
      PARAMETER (WIRE=2)
      PARAMETER (PLATE=3)
C
      COMMON/KDIMEN/KNODES,KEDGES,KFACES
      COMMON/KDIMWR/KWCRDS,KWSEGS
      COMMON/CDIMEN/JNODES,JEDGES,JFACES
      COMMON/CDIMWR/JWCRDS,JWSEGS
      COMMON/CONST/PI,KN,JI,JWU04P,X14PJE,JWE04P,X14PJU
      COMMON/CONST1/KN1,JWU14P,X14PWE,X14PI,JWE14P,X14PWU
      COMMON/NUMINT/XSI,ETA,WGHT
C
      EXTERNAL MAGNI,GTAREA,VDOT,MAP1,MAP2
      EXTERNAL SGNPOT,ISGN,CDOT
C
C source triangles
C
      DO 2005 N0=1,JFACES
       CALL VTXCRD1(N0,R11N)
       AREA1N = GTAREA(R11N,PLATE)
       CALL LENGTH(R11N,L1N)
       CALL FACEDG1(N0,E1N(1),E1N(2),E1N(3))
```

```
C
C observation triangles
C
      DO 2004 M0=1,KFACES
       CALL VTXCRD2(M0,R11M)
       AREA1M = GTAREA(R11M,PLATE)
       CALL CENTER(R11M,RC1M,PLATE)
       CALL LENGTH(R11M,L1M)
       CALL FACEDG2(M0,E1M(1),E1M(2),E1M(3))
C
C compute integrals
C
      CALL NINT7B(R11N,RC1M,CVECK0,CXSIK0,CETAK0,AREA1N,DR)
C
      DO 2003 N1=1,PLATE
       N(1) = MAP1(N0,N1,PLATE)
       N(2) = MAP1(N0,N1+PLATE,PLATE)
       IF (N(1).NE.0.OR.N(2).NE.0) THEN
        DO 2001 I=1,3
         A1(I) = R11N(I,1) * CVECK0 +
     +    ( R11N(I,2) - R11N(I,1) ) * CXSIK0 +
     +    ( R11N(I,3) - R11N(I,1) ) * CETAK0
         RI(I) = R11N(I,N1)
         RIMRCM(I) = RI(I) - RC1M(I)
2001     CONTINUE
        CALL CROSS2(RC1M,RI,RCMXRI)
        CALL CROSS3(RIMRCM,A1,A3)
        DO 2025 I=1,3
         A1(I) = A3(I) + RCMXRI(I) * CVECK0
         A1(I) = ISGN(E1N(N1)) * L1N(N1)/(2*AREA1N) * A1(I)
2025     CONTINUE
        DO 2002 M1=1,PLATE
         M(1) = MAP2(M0,M1,PLATE)
         M(2) = MAP2(M0,M1+PLATE,PLATE)
         IF (M(1).NE.0.OR.M(2).NE.0) THEN
          CALL P1RHO(R11M,M1,RHO1M)
          A = X14PI * CDOT(RHO1M,A1)
          CX10 = ISGN(E1M(M1)) * L1M(M1) * A
C
      IF (DR.LT.L1M(1).OR.DR.LT.L1M(2).OR.DR.LT.L1M(3)) THEN
C
C do the 7-pt integration over the observation triangle
C
      CF = 0
      CFX = 0
      DO 2051 II=1,7
        DO 2050 JJ=1,3
          R1M(JJ) = R11M(JJ,1) + (R11M(JJ,2)-R11M(JJ,1))*XSI(II) +
     +        (R11M(JJ,3)-R11M(JJ,1))*ETA(II)
          RHO1M(JJ) = R1M(JJ)-R11M(JJ,M1)
2050    CONTINUE
      CALL NINT7B(R11N,R1M,CVECK0,CXSIK0,CETAK0,AREA1N,TRASH)
```

```
          DO 2049 I=1,3
           A1(I) = R11N(I,1) * CVECK0 +
     +      ( R11N(I,2) - R11N(I,1) ) * CXSIK0 +
     +      ( R11N(I,3) - R11N(I,1) ) * CETAK0
           RI(I) = R11N(I,N1)
           RIMRCM(I) = RI(I) - R1M(I)
2049       CONTINUE
          CALL CROSS2(R1M,RI,RCMXRI)
          CALL CROSS3(RIMRCM,A1,A3)
          DO 2048 I=1,3
           A1(I) = A3(I) + RCMXRI(I) * CVECK0
           A1(I) = ISGN(E1N(N1)) * L1N(N1)/(4*AREA1N) * A1(I)
2048       CONTINUE
            A = X14PI * CDOT(RHO1M,A1)
            CFX = ISGN(E1M(M1)) * L1M(M1)/AREA1M * A
            CF = CF + CFX*WGHT(II)
2051    CONTINUE
            CX10 = CF * AREA1M
C
        ENDIF
C
            DO 3001 J=1,2
            DO 3001 K=1,2
             IF (M(K).NE.0.AND.N(J).NE.0) THEN
               CZ(N(J),M(K)) = CZ(N(J),M(K)) + SGNPOT(CX10,J,K)/2
              ENDIF
3001         CONTINUE
            ENDIF
2002       CONTINUE
          ENDIF
2003     CONTINUE
2004    CONTINUE
2005    CONTINUE
C
C ***************
        OPEN(FILE='CZ7',STATUS='NEW',DISPOSE='DELETE',
     +                  UNIT=27,FORM='UNFORMATTED')
        DO 147 J=1,KUNKNS
147      WRITE(27)(CZ(I,J),I=1,JUNKNS)
C ***************
C
        TYPE *,' CZ10 COMPLETED'
C
        RETURN
        END
C
        SUBROUTINE ZPLPL11(CZ,KUNKNS)
C
        INTEGER KUNKNS
        COMPLEX JI,A,P,SGNPOT
        COMPLEX CVEC,CXSI,CETA,CPHI,A1(3),CDOT
        COMPLEX CZ(KUNKNS,KUNKNS),CX11,CF,CFX
```

```
      COMPLEX KN1,JWU14P,X14PWE,JWE14P,X14PWU
      REAL PI,KN,JWU04P,X14PJE,JWE04P,X14PJU,X14PI
      REAL MAGNI,GTAREA,AREA1N,VDOT,AREA1M,TRASH
      REAL DR,POT,RLN1(3),R01(3),L1M(3),L1N(3)
      REAL R11M(3,3),R1M(3),RC1M(3),RHO1M(3),R11N(3,3)
      REAL XSI(7),ETA(7),WGHT(7)
      INTEGER KNODES,KEDGES,KFACES,KWCRDS,KWSEGS
      INTEGER I,J,K,M(2),M0,M1,N(2),N0,N1,MAP2,E1M(3),E1N(3),ISGN
C
      INTEGER WIRE,PLATE
      PARAMETER (WIRE=2)
      PARAMETER (PLATE=3)
C
      COMMON/KDIMEN/KNODES,KEDGES,KFACES
      COMMON/KDIMWP/KWCRDS,KWSEGS
      COMMON/CONST/PI,KN,JI,JWU04P,X14PJE,JWE04P,X14PJU
      COMMON/CONST1/KN1,JWU14P,X14PWE,X14PI,JWE14P,X14PWU
      COMMON/NUMINT/XSI,ETA,WGHT
C
      EXTERNAL MAGNI,GTAREA,VDOT,MAP2
      EXTERNAL SGNPOT,ISGN,CDOT
C
C source triangles
C
      DO 2005 N0=1,KFACES
       CALL VTXCRD2(N0,R11N)
       AREA1N = GTAREA(R11N,PLATE)
       CALL LENGTH(R11N,L1N)
       CALL FACEDG2(N0,E1N(1),E1N(2),E1N(3))
C
C observation triangles
C
      DO 2004 M0=1,KFACES
       CALL VTXCRD2(M0,R11M)
       AREA1M = GTAREA(R11M,PLATE)
       CALL CENTER(R11M,RC1M,PLATE)
       CALL LENGTH(R11M,L1M)
       CALL FACEDG2(M0,E1M(1),E1M(2),E1M(3))
C
C compute integrals
C
      CALL NINT7(R11N,RC1M,CVEC,CXSI,CETA,POT,CPHI,
     +                    RLN1,R01,AREA1N,DR)
C
      DO 2003 N1=1,PLATE
       N(1) = MAP2(N0,N1,PLATE)
       N(2) = MAP2(N0,N1+PLATE,PLATE)
       IF (N(1).NE.0.OR.N(2).NE.0) THEN
        P = ISGN(E1N(N1)) * L1N(N1)/AREA1N * JI * X14PJE * CPHI
        DO 2001 I=1,3
         A1(I) = ( R11N(I,1) - R11N(I,N1) ) * CVEC +
     +    ( R11N(I,2) - R11N(I,1) ) * CXSI +
```

```
     +     ( R11N(I,3) - R11N(I,1) ) * CETA +
     +     ( R01(I) - R11N(I,N1) ) * POT + RLN1(I)
           A1(I) = ISGN(E1N(N1)) * L1N(N1)/(2*AREA1N) * A1(I)
2001       CONTINUE
C
          DO 2002 M1=1,PLATE
           M(1) = MAP2(M0,M1,PLATE)
           M(2) = MAP2(M0,M1+PLATE,PLATE)
           IF (M(1).NE.0.OR.M(2).NE.0) THEN
            CALL P1RHO(R11M,M1,RHO1M)
            A = JI * JWU04P * CDOT(RHO1M,A1)
            CX11 = ISGN(E1M(M1))*L1M(M1)*(A+P)
C
       IF (DR.LT.L1M(1).OR.DR.LT.L1M(2).OR.DR.LT.L1M(3)) THEN
C
C do the 7-pt integration over the observation triangle
C
        CF = 0
        CFX = 0
        DO 2051 II=1,7
          DO 2050 JJ=1,3
            R1M(JJ) = R11M(JJ,1) + (R11M(JJ,2)-R11M(JJ,1))*XSI(II) +
     +          (R11M(JJ,3)-R11M(JJ,1))*ETA(II)
           RHO1M(JJ) = R1M(JJ)-R11M(JJ,M1)
2050      CONTINUE
        CALL NINT7(R11N,R1M,CVEC,CXSI,CETA,POT,CPHI,
     +                    RLN1,R01,AREA1N,TRASH)
          P = ISGN(E1N(N1)) * L1N(N1)/AREA1N * JI * X14PJE * CPHI
          DO 2049 I=1,3
           A1(I) = ( R11N(I,1) - R11N(I,N1) ) * CVEC +
     +     ( R11N(I,2) - R11N(I,1) ) * CXSI +
     +     ( R11N(I,3) - R11N(I,1) ) * CETA +
     +     ( R01(I) - R11N(I,N1) ) * POT + RLN1(I)
           A1(I) = ISGN(E1N(N1)) * L1N(N1)/(4*AREA1N) * A1(I)
2049       CONTINUE
           A = JI * JWU04P * CDOT(RHO1M,A1)
           CFX = ISGN(E1M(M1))*L1M(M1)/AREA1M*(A+P)
           CF = CF + CFX*WGHT(II)
2051   CONTINUE
           CX11 = CF * AREA1M
C
        ENDIF
C
           DO 3001 J=1,2
           DO 3001 K=1,2
            IF (M(K).NE.0.AND.N(J).NE.0) THEN
              IF(M(K).NE.N(J)) THEN
               CZ(M(K),N(J)) = CZ(M(K),N(J)) + SGNPOT(CX11,J,K)/2
               CZ(N(J),M(K)) = CZ(N(J),M(K)) + SGNPOT(CX11,J,K)/2
              ELSE
               CZ(M(K),N(J)) = CZ(M(K),N(J)) + SGNPOT(CX11,J,K)
              ENDIF
```

AD-A170 973 RADAR CROSS SECTION PREDICTION FOR COATED PERFECT CONDUCTORS WITH ARBITRARY GEOMETRIES(U) AIR FORCE INST OF TECH WRIGHT-PATTERSON AFB OH S W ROGERS 1986 3/3

UNCLASSIFIED AFIT/CI/NR-86-105T F/G 17/9 NL

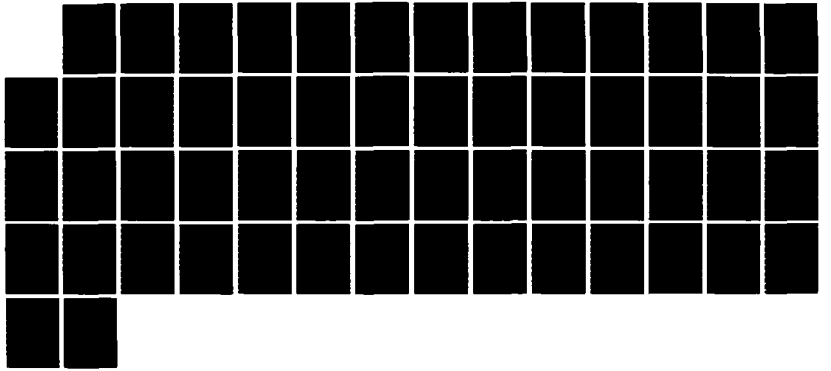

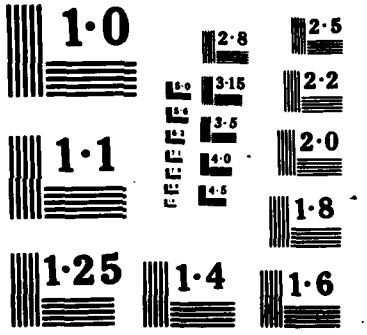
1·0
1·1
1·25
2·8
3·15
3·5
4·0
4·5
1·4
2·5
2·2
2·0
1·8
1·6

```
            ENDIF
3001        CONTINUE
           ENDIF
2002      CONTINUE
         ENDIF
2003    CONTINUE
2004   CONTINUE
2005   CONTINUE
C
C ***************
      OPEN(FILE='CZ11',STATUS='NEW',DISPOSE='DELETE',
     +                    UNIT=31,FORM='UNFORMATTED')
      DO 147 J=1,KUNKNS
147    WRITE(31)(CZ(I,J),I=1,J)
C ***************
C
      TYPE *,' CZ11 COMPLETED'
C
      RETURN
      END
C
      SUBROUTINE ZPLPL13(CZ,JUNKNS,NUNKNS)
C
      INTEGER JUNKNS,NUNKNS
      COMPLEX JI,A,P,SGNPOT
      COMPLEX CVEC1,CXSI1,CETA1,CPHI1,A2(3),CDOT
      COMPLEX CZ(JUNKNS,NUNKNS),CX13,CF,CFX
      COMPLEX KN1,JWU14P,X14PWE,JWE14P,X14PWU
      REAL PI,KN,JWU04P,X14PJE,JWE04P,X14PJU,X14PI
      REAL MAGNI,GTAREA,AREA1N,VDOT,AREA1M,TRASH
      REAL DR,POT,RLN1(3),R01(3),L1M(3),L1N(3)
      REAL R11M(3,3),R1M(3),RC1M(3),RHO1M(3),R11N(3,3)
      REAL XSI(7),ETA(7),WGHT(7)
      INTEGER NNODES,NEDGES,NFACES,NWCRDS,NWSEGS
      INTEGER JNODES,JEDGES,JFACES,JWCRDS,JWSEGS
      INTEGER I,J,K,M(2),M0,M1,N(2),N0,N1,MAP,MAP1
      INTEGER E1M(3),E1N(3),ISGN
C
      INTEGER WIRE,PLATE
      PARAMETER (WIRE=2)
      PARAMETER (PLATE=3)
C
      COMMON/DIMEN/NNODES,NEDGES,NFACES
      COMMON/DIMWR/NWCRDS,NWSEGS
      COMMON/CDIMEN/JNODES,JEDGES,JFACES
      COMMON/CDIMWR/JWCRDS,JWSEGS
      COMMON/CONST/PI,KN,JI,JWU04P,X14PJE,JWE04P,X14PJU
      COMMON/CONST1/KN1,JWU14P,X14PWE,X14PI,JWE14P,X14PWU
      COMMON/NUMINT/XSI,ETA,WGHT
C
      EXTERNAL MAGNI,GTAREA,VDOT,MAP,MAP1
      EXTERNAL SGNPOT,ISGN,CDOT
```

```
C
C source triangles
C
      DO 2005 N0=1,JFACES
       CALL VTXCRD1(N0,R11N)
       AREA1N = GTAREA(R11N,PLATE)
       CALL LENGTH(R11N,L1N)
       CALL FACEDG1(N0,E1N(1),E1N(2),E1N(3))
C
C observation triangles
C
      DO 2004 M0=1,NFACES
       CALL VTXCRD(M0,R11M)
       AREA1M = GTAREA(R11M,PLATE)
       CALL CENTER(R11M,RC1M,PLATE)
       CALL LENGTH(R11M,L1M)
       CALL FACEDG(M0,E1M(1),E1M(2),E1M(3))
C
C compute integrals
C
      CALL NINT7A(R11N,RC1M,CVEC1,CXSI1,CETA1,POT,CPHI1,
     +                    RLN1,R01,AREA1N,DR)
C
      DO 2003 N1=1,PLATE
       N(1) = MAP1(N0,N1,PLATE)
       N(2) = MAP1(N0,N1+PLATE,PLATE)
       IF (N(1).NE.0.OR.N(2).NE.0) THEN
        P = ISGN(E1N(N1)) * L1N(N1)/AREA1N * (-JI) * X14PWE * CPHI1
        DO 2001 I=1,3
         A2(I) = ( R11N(I,1) - R11N(I,N1) ) * CVEC1 +
     +     ( R11N(I,2) - R11N(I,1) ) * CXSI1 +
     +     ( R11N(I,3) - R11N(I,1) ) * CETA1 +
     +     ( R01(I) - R11N(I,N1) ) * POT + RLN1(I)
         A2(I) = ISGN(E1N(N1)) * L1N(N1)/(2*AREA1N) * A2(I)
2001     CONTINUE
C
        DO 2002 M1=1,PLATE
         M(1) = MAP(M0,M1,PLATE)
         M(2) = MAP(M0,M1+PLATE,PLATE)
         IF (M(1).NE.0.OR.M(2).NE.0) THEN
          CALL P1RHO(R11M,M1,RHO1M)
          A = -JI * JWU14P * CDOT(RHO1M,A2)
          CX13 = ISGN(E1M(M1))*L1M(M1)*(A+P)
C
      IF (DR.LT.L1M(1).OR.DR.LT.L1M(2).OR.DR.LT.L1M(3)) THEN
C
C do the 7-pt integration over the observation triangle
C
      CF = 0
      CFX = 0
      DO 2051 II=1,7
        DO 2050 JJ=1,3
```

```
          R1M(JJ) = R11M(JJ,1) + (R11M(JJ,2)-R11M(JJ,1))*XSI(II) +
     +         (R11M(JJ,3)-R11M(JJ,1))*ETA(II)
          RHO1M(JJ) = R1M(JJ)-R11M(JJ,M1)
2050     CONTINUE
       CALL NINT7A(R11N,R1M,CVEC1,CXSI1,CETA1,POT,CPHI1,
     +                    RLN1,R01,AREA1N,TRASH)
         P = ISGN(E1N(N1)) * L1N(N1)/AREA1N * (-JI) * X14PWE * CPHI1
         DO 2049 I=1,3
          A2(I) = ( R11N(I,1) - R11N(I,N1) ) * CVEC1 +
     +     ( R11N(I,2) - R11N(I,1) ) * CXSI1 +
     +     ( R11N(I,3) - R11N(I,1) ) * CETA1 +
     +     ( R01(I) - R11N(I,N1) ) * POT + RLN1(I)
          A2(I) = ISGN(E1N(N1)) * L1N(N1)/(4*AREA1N) * A2(I)
2049      CONTINUE
           A = -JI * JWU14P * CDOT(RHO1M,A2)
           CFX = ISGN(E1M(M1))*L1M(M1)/AREA1M*(A+P)
           CF = CF + CFX*WGHT(II)
2051   CONTINUE
          CX13 = CF * AREA1M
C
       ENDIF
C
          DO 3001 J=1,2
          DO 3001 K=1,2
           IF (M(K).NE.0.AND.N(J).NE.0) THEN
             CZ(N(J),M(K)) = CZ(N(J),M(K)) + SGNPOT(CX13,J,K)/2
            ENDIF
3001        CONTINUE
          ENDIF
2002      CONTINUE
         ENDIF
2003    CONTINUE
2004   CONTINUE
2005   CONTINUE
C
C ***************
       OPEN(FILE='CZ4',STATUS='NEW',DISPOSE='DELETE',
     +           UNIT=24,FORM='UNFORMATTED')
       DO 147 J=1,NUNKNS
147     WRITE(24)(CZ(I,J),I=1,JUNKNS)
C ***************
C
       TYPE *,' CZ13 COMPLETED'
C
       RETURN
       END
C
       SUBROUTINE ZPLPL14(CZ,JUNKNS,NUNKNS)
C
       INTEGER JUNKNS,NUNKNS
       COMPLEX JI,A,P,SGNPOT
       COMPLEX CVECK1,CXSIK1,CETAK1,A2(3),A4(3),CDOT
```

```
      COMPLEX CZ(JUNKNS,NUNKNS),CX14,CF,CFX
      COMPLEX KN1,JWU14P,X14PWE,JWE14P,X14PWU
      REAL PI,KN,JWU04P,X14PJE,JWE04P,X14PJU,X14PI
      REAL MAGNI,GTAREA,AREA1N,VDOT,ARE/ :M,TRASH
      REAL DR,POT,RLN1(3),R01(3),L1M(3),L1N(3)
      REAL R11M(3,3),R1M(3),RC1M(3),RHO1M(3),R11N(3,3)
      REAL RI(3),RIMRCM(3),RCMXRI(3)
      REAL XSI(7),ETA(7),WGHT(7)
      INTEGER NNODES,NEDGES,NFACES,NWCRDS,NWSEGS
      INTEGER JNODES,JEDGES,JFACES,JWCRDS,JWSEGS
      INTEGER I,J,K,M(2),M0,M1,N(2),N0,N1,MAP,MAP1
      INTEGER E1M(3),E1N(3),ISGN
C
      INTEGER WIRE,PLATE
      PARAMETER (WIRE=2)
      PARAMETER (PLATE=3)
C
      COMMON/DIMEN/NNODES,NEDGES,NFACES
      COMMON/DIMWR/NWCRDS,NWSEGS
      COMMON/CDIMEN/JNODES,JEDGES,JFACES
      COMMON/CDIMWR/JWCRDS,JWSEGS
      COMMON/CONST/PI,KN,JI,JWU04P,X14PJE,JWE04P,X14PJU
      COMMON/CONST1/KN1,JWU14P,X14PWE,X14PI,JWE14P,X14PWU
      COMMON/NUMINT/XSI,ETA,WGHT
C
      EXTERNAL MAGNI,GTAREA,VDOT,MAP,MAP1
      EXTERNAL SGNPOT,ISGN,CDOT
C
C source triangles
C
      DO 2005 N0=1,JFACES
       CALL VTXCRD1(N0,R11N)
       AREA1N = GTAREA(R11N,PLATE)
       CALL LENGTH(R11N,L1N)
       CALL FACEDG1(N0,E1N(1),E1N(2),E1N(3))
C
C observation triangles
C
      DO 2004 M0=1,NFACES
       CALL VTXCRD(M0,R11M)
       AREA1M = GTAREA(R11M,PLATE)
       CALL CENTER(R11M,RC1M,PLATE)
       CALL LENGTH(R11M,L1M)
       CALL FACEDG(M0,E1M(1),E1M(2),E1M(3))
C
C compute integrals
C
      CALL NINT7C(R11N,RC1M,CVECK1,CXSIK1,CETAK1,AREA1N,DR)
C
      DO 2003 N1=1,PLATE
       N(1) = MAP1(N0,N1,PLATE)
       N(2) = MAP1(N0,N1+PLATE,PLATE)
```

```
      IF (N(1).NE.0.OR.N(2).NE.0) THEN
       DO 2001 I=1,3
        A2(I) = R11N(I,1) * CVECK1 +
     +    ( R11N(I,2) - R11N(I,1) ) * CXSIK1 +
     +    ( R11N(I,3) - R11N(I,1) ) * CETAK1
        RI(I) = R11N(I,N1)
        RIMRCM(I) = RI(I) - RC1M(I)
2001    CONTINUE
       CALL CROSS2(RC1M,RI,RCMXRI)
       CALL CROSS3(RIMRCM,A2,A4)
       DO 2025 I=1,3
        A2(I) = A4(I) + RCMXRI(I) * CVECK1
        A2(I) = ISGN(E1N(N1)) * L1N(N1)/(2*AREA1N) * A2(I)
2025    CONTINUE
       DO 2002 M1=1,PLATE
        M(1) = MAP(M0,M1,PLATE)
        M(2) = MAP(M0,M1+PLATE,PLATE)
        IF (M(1).NE.0.OR.M(2).NE.0) THEN
         CALL P1RHO(R11M,M1,RHO1M)
         A = -X14PI * CDOT(RHO1M,A2)
         CX14 = ISGN(E1M(M1)) * L1M(M1) * A
C
      IF (DR.LT.L1M(1).OR.DR.LT.L1M(2).OR.DR.LT.L1M(3)) THEN
C
C do the 7-pt integration over the observation triangle
C
       CF = 0
       CFX = 0
       DO 2051 II=1,7
         DO 2050 JJ=1,3
           R1M(JJ) = R11M(JJ,1) + (R11M(JJ,2)-R11M(JJ,1))*XSI(II) +
     +         (R11M(JJ,3)-R11M(JJ,1))*ETA(II)
          RHO1M(JJ) = R1M(JJ)-R11M(JJ,M1)
2050     CONTINUE
       CALL NINT7C(R11N,R1M,CVECK1,CXSIK1,CETAK1,AREA1N,TRASH)
         DO 2049 I=1,3
          A2(I) = R11N(I,1) * CVECK1 +
     +    ( R11N(I,2) - R11N(I,1) ) * CXSIK1 +
     +    ( R11N(I,3) - R11N(I,1) ) * CETAK1
          RI(I) = R11N(I,N1)
          RIMRCM(I) = RI(I) - R1M(I)
2049      CONTINUE
         CALL CROSS2(R1M,RI,RCMXRI)
         CALL CROSS3(RIMRCM,A2,A4)
         DO 2048 I=1,3
          A2(I) = A4(I) + RCMXRI(I) * CVECK1
          A2(I) = ISGN(E1N(N1)) * L1N(N1)/(4*AREA1N) * A2(I)
2048      CONTINUE
           A = -X14PI * CDOT(RHO1M,A2)
           CFX = ISGN(E1M(M1)) * L1M(M1)/AREA1M * A
           CF = CF + CFX*WGHT(II)
2051   CONTINUE
```

```
            CX14 = CF * AREA1M
C
          ENDIF
C
            DO 3001 J=1,2
            DO 3001 K=1,2
             IF (M(K).NE.0.AND.N(J).NE.0) THEN
               CZ(N(J),M(K)) = CZ(N(J),M(K)) + SGNPOT(CX14,J,K)/2
             ENDIF
3001         CONTINUE
            ENDIF
2002       CONTINUE
          ENDIF
2003     CONTINUE
2004    CONTINUE
2005    CONTINUE
C
C ***************
        OPEN(FILE='CZ8',STATUS='NEW',DISPOSE='DELETE',
       +                        UNIT=28,FORM='UNFORMATTED')
        DO 147 J=1,NUNKNS
147      WRITE(28)(CZ(I,J),I=1,JUNKNS)
C ***************
C
        TYPE *,' CZ14 COMPLETED'
C
        RETURN
        END
C
        SUBROUTINE ZPLPL16(CZ,NUNKNS)
C
        INTEGER NUNKNS
        COMPLEX JI,A,P,SGNPOT
        COMPLEX CVEC1,CXSI1,CETA1,CPHI1,A2(3),CDOT
        COMPLEX CZ(NUNKNS,NUNKNS),CX16,CF,CFX
        COMPLEX KN1,JWU14P,X14PWE,JWE14P,X14PWU
        REAL PI,KN,JWU04P,X14PJE,JWE04P,X14PJU,X14PI
        REAL MAGNI,GTAREA,AREA1N,VDOT,AREA1M,TRASH
        REAL DR,POT,RLN1(3),R01(3),L1M(3),L1N(3)
        REAL R11M(3,3),R1M(3),RC1M(3),RHO1M(3),R11N(3,3)
        REAL XSI(7),ETA(7),WGHT(7)
        INTEGER NNODES,NEDGES,NFACES,NWCRDS,NWSEGS
        INTEGER I,J,K,M(2),M0,M1,N(2),N0,N1,MAP,E1M(3),E1N(3),ISGN
C
        INTEGER WIRE,PLATE
        PARAMETER (WIRE=2)
        PARAMETER (PLATE=3)
C
        COMMON/DIMEN/NNODES,NEDGES,NFACES
        COMMON/DIMWR/NWCRDS,NWSEGS
        COMMON/CONST/PI,KN,JI,JWU04P,X14PJE,JWE04P,X14PJU
        COMMON/CONST1/KN1,JWU14P,X14PWE,X14PI,JWE14P,X14PWU
```

```
      COMMON/NUMINT/XSI,ETA,WGHT
C
      EXTERNAL MAGNI,GTAREA,VDOT,MAP
      EXTERNAL SGNPOT,ISGN,CDOT
C
C source triangles
C
      DO 2005 N0=1,NFACES
       CALL VTXCRD(N0,R11N)
       AREA1N = GTAREA(R11N,PLATE)
       CALL LENGTH(R11N,L1N)
       CALL FACEDG(N0,E1N(1),E1N(2),E1N(3))
C
C observation triangles
C
      DO 2004 M0=1,NFACES
       CALL VTXCRD(M0,R11M)
       AREA1M = GTAREA(R11M,PLATE)
       CALL CENTER(R11M,RC1M,PLATE)
       CALL LENGTH(R11M,L1M)
       CALL FACEDG(M0,E1M(1),E1M(2),E1M(3))
C
C compute integrals
C
      CALL NINT7A(R11N,RC1M,CVEC1,CXSI1,CETA1,POT,CPHI1,
     +                    RLN1,R01,AREA1N,DR)
C
      DO 2003 N1=1,PLATE
       N(1) = MAP(N0,N1,PLATE)
       N(2) = MAP(N0,N1+PLATE,PLATE)
       IF (N(1).NE.0.OR.N(2).NE.0) THEN
        P = ISGN(E1N(N1)) * L1N(N1)/AREA1N * JI * X14PWE * CPHI1
        DO 2001 I=1,3
         A2(I) = ( R11N(I,1) - R11N(I,N1) ) * CVEC1 +
     +     ( R11N(I,2) - R11N(I,1) ) * CXSI1 +
     +     ( R11N(I,3) - R11N(I,1) ) * CETA1 +
     +     ( R01(I) - R11N(I,N1) ) * POT + RLN1(I)
         A2(I) = ISGN(E1N(N1)) * L1N(N1)/(2*AREA1N) * A2(I)
2001     CONTINUE
C
        DO 2002 M1=1,PLATE
         M(1) = MAP(M0,M1,PLATE)
         M(2) = MAP(M0,M1+PLATE,PLATE)
         IF (M(1).NE.0.OR.M(2).NE.0) THEN
          CALL P1RHO(R11M,M1,RHO1M)
          A = JI * JWU14P * CDOT(RHO1M,A2)
          CX16 = ISGN(E1M(M1))*L1M(M1)*(A+P)
C
      IF (DR.LT.L1M(1).OR.DR.LT.L1M(2).OR.DR.LT.L1M(3)) THEN
C
C do the 7-pt integration over the observation triangle
C
```

```
      CF = 0
      CFX = 0
      DO 2051 II=1,7
        DO 2050 JJ=1,3
          R1M(JJ) = R11M(JJ,1) + (R11M(JJ,2)-R11M(JJ,1))*XSI(II) +
     +         (R11M(JJ,3)-R11M(JJ,1))*ETA(II)
          RHO1M(JJ) = R1M(JJ)-R11M(JJ,M1)
2050    CONTINUE
      CALL NINT7A(R11N,R1M,CVEC1,CXSI1,CETA1,POT,CPHI1,
     +                    RLN1,R01,AREA1N,TRASH)
        P = ISGN(E1N(N1)) * L1N(N1)/AREA1N * JI * X14PWE * CPHI1
        DO 2049 I=1,3
         A2(I) = ( R11N(I,1) - R11N(I,N1) ) * CVEC1 +
     +     ( R11N(I,2) - R11N(I,1) ) * CXSI1 +
     +     ( R11N(I,3) - R11N(I,1) ) * CETA1 +
     +     ( R01(I) - R11N(I,N1) ) * POT + RLN1(I)
         A2(I) = ISGN(E1N(N1)) * L1N(N1)/(4*AREA1N) * A2(I)
2049     CONTINUE
          A = JI * JWU14P * CDOT(RHO1M,A2)
          CFX = ISGN(E1M(M1))*L1M(M1)/AREA1M*(A+P)
          CF = CF + CFX*WGHT(II)
2051  CONTINUE
          CX16 = CF * AREA1M
C
      ENDIF
C
          DO 3001 J=1,2
          DO 3001 K=1,2
           IF (M(K).NE.0.AND.N(J).NE.0) THEN
             IF(M(K).NE.N(J)) THEN
              CZ(M(K),N(J)) = CZ(M(K),N(J)) + SGNPOT(CX16,J,K)/2
              CZ(N(J),M(K)) = CZ(N(J),M(K)) + SGNPOT(CX16,J,K)/2
             ELSE
              CZ(M(K),N(J)) = CZ(M(K),N(J)) + SGNPOT(CX16,J,K)
             ENDIF
            ENDIF
3001       CONTINUE
          ENDIF
2002     CONTINUE
        ENDIF
2003   CONTINUE
2004  CONTINUE
2005  CONTINUE
C
C ***************
      OPEN(FILE='CZ16',STATUS='NEW',DISPOSE='DELETE',
     +                 UNIT=36,FORM='UNFORMATTED')
      DO 147 J=1,NUNKNS
147    WRITE(36)(CZ(I,J),I=1,J)
C ***************
C
      TYPE *,' CZ16 COMPLETED'
```

```
C
      RETURN
      END
C
C
      COMPLEX FUNCTION SGNPOT(P,M1,N1)
C USED FOR MULTIPLE EDGE CONNECTIONS
      INTEGER M1,N1
      COMPLEX P
      SGNPOT = P
      IF (M1.NE.1) SGNPOT = -SGNPOT
      IF (N1.NE.1) SGNPOT = -SGNPOT
      RETURN
      END
C
C vector functions
C
C  for use with z-matrix
C
      SUBROUTINE COPY(V1,V2)
      REAL V1(3),V2(3)
      INTEGER I
       DO 2001 I=1,3
        V2(I)=V1(I)
2001    CONTINUE
      RETURN
      END
C
      REAL FUNCTION VDOT(V1,V2)
      INTEGER I
      REAL V1(3),V2(3)
       VDOT = 0
       DO 2001 I=1,3
        VDOT = VDOT + V1(I)*V2(I)
2001    CONTINUE
      RETURN
      END
C
      COMPLEX FUNCTION CDOT(V1,V2)
      INTEGER I
      REAL V1(3)
      COMPLEX V2(3)
       CDOT = 0
       DO 2001 I=1,3
        CDOT = CDOT + V1(I)*V2(I)
2001    CONTINUE
      RETURN
      END
C
      REAL FUNCTION MAGNI(V)
      REAL VDOT
      REAL V(3)
```

```
      EXTERNAL VDOT
       MAGNI=SQRT(VDOT(V,V))
      RETURN
      END
C
      SUBROUTINE UNIT(V1,V2)
      INTEGER I
      REAL V1(3),V2(3)
      REAL MAGNI,R
      EXTERNAL MAGNI
       R=MAGNI(V1)
       DO 2001 I=1,3
        V2(I)=V1(I)/R
2001    CONTINUE
      RETURN
      END
C
      SUBROUTINE CENTER(VTX,V,CASE)
      REAL VTX(3,3),V(3)
      INTEGER I,J,CASE
       DO 2002 I=1,3
        V(I)=0
        DO 2001 J=1,CASE
         V(I)=V(I)+VTX(I,J)
2001     CONTINUE
        V(I)=V(I)/CASE
2002    CONTINUE
      RETURN
      END
C
      SUBROUTINE MIDPTS(VTX,V)
      REAL VTX(3,3),V(3,3)
      INTEGER I,J,K
      EXTERNAL MAGNI
       DO 2002 I=1,3
        J=MOD(I,3)+1
        K=MOD(J,3)+1
        DO 2001 L=1,3
         V(L,I) = ( VTX(L,J) + VTX(L,K) ) / 2
2001     CONTINUE
2002    CONTINUE
      RETURN
      END
C
      SUBROUTINE LENGTH(VTX,S)
      REAL VTX(3,3),V(3)
      REAL S(3),MAGNI
      INTEGER I,J,K
      EXTERNAL MAGNI
       DO 2002 I=1,3
        J=MOD(I,3)+1
        K=MOD(J,3)+1
```

```
          DO 2001 L=1,3
           V(L)=VTX(L,J)-VTX(L,K)
2001       CONTINUE
          S(I)=MAGNI(V)
2002      CONTINUE
        RETURN
        END
C
        REAL FUNCTION GTAREA(VTX,CASE)
        REAL MAGNI
        REAL V(3),VTX(3,3)
        INTEGER I,CASE
        EXTERNAL MAGNI
C
C "area" of wire segment = length
C "area" of triangle is 1/2 cross product of two sides
C
         IF (CASE.EQ.2) THEN
          DO 2001 I=1,3
           V(I) = VTX(I,2) - VTX(I,1)
2001       CONTINUE
          GTAREA=MAGNI(V)
         ELSE IF (CASE.EQ.3) THEN
          CALL CROSS1(VTX,V)
          GTAREA=MAGNI(V)/2
         ENDIF
        RETURN
        END
C
        SUBROUTINE CROSS1(VTX,V)
        REAL VTX(3,3),V(3)
        INTEGER I,J,K
         DO 2001 I=1,3
          J=MOD(I,3)+1
          K=MOD(J,3)+1
         V(I) = (VTX(J,2)-VTX(J,1)) * (VTX(K,3)-VTX(K,1)) -
     +   (VTX(J,3)-VTX(J,1)) * (VTX(K,2)-VTX(K,1))
2001      CONTINUE
        RETURN
        END
C
        SUBROUTINE CROSS2(V1,V2,V3)
        REAL V1(3),V2(3),V3(3)
        INTEGER I,J,K
         DO 2001 I=1,3
          J=MOD(I,3)+1
          K=MOD(J,3)+1
          V3(I) = V1(J)*V2(K) - V1(K)*V2(J)
2001      CONTINUE
        RETURN
        END
C
```

```
      SUBROUTINE CROSS3(V1,V2,V3)
      REAL V1(3)
      COMPLEX V2(3),V3(3)
      INTEGER I,J,K
       DO 2001 I=1,3
        J=MOD(I,3)+1
        K=MOD(J,3)+1
        V3(I) = V1(J)*V2(K) - V1(K)*V2(J)
2001    CONTINUE
      RETURN
      END
C
      INTEGER FUNCTION MAP(I,J,CASE)
      INTEGER I,J,CASE
      INTEGER NNODES,NEDGES,MAPUNK(1),SEG(4,1),NBOUND(6,1)
      COMMON/DIMEN/NNODES,NEDGES
      COMMON/MAPUS/MAPUNK
      COMMON/SWIRE/SEG
      COMMON/PLAT3/NBOUND
       IF (CASE.EQ.2) THEN
        MAP = ABS(SEG(J,I))
        IF (MAP.NE.0) MAP=MAPUNK(NEDGES+MAP)
       ELSE IF (CASE.EQ.3) THEN
        MAP=ABS(NBOUND(J,I))
        IF (MAP.NE.0) MAP=MAPUNK(MAP)
        ENDIF
      RETURN
      END
C
      INTEGER FUNCTION MAP1(I,J,CASE)
      INTEGER I,J,CASE
      INTEGER JNODES,JEDGES,MAPUNKJ(1),SEGJ(4,1),JBOUND(6,1)
      COMMON/CDIMEN/JNODES,JEDGES
      COMMON/CMAPUS/MAPUNKJ
      COMMON/CSWIRE/SEGJ
      COMMON/CPLAT3/JBOUND
       IF (CASE.EQ.2) THEN
        MAP1 = ABS(SEGJ(J,I))
        IF (MAP1.NE.0) MAP1=MAPUNKJ(JEDGES+MAP1)
       ELSE IF (CASE.EQ.3) THEN
        MAP1=ABS(JBOUND(J,I))
        IF (MAP1.NE.0) MAP1=MAPUNKJ(MAP1)
        ENDIF
      RETURN
      END
C
      INTEGER FUNCTION MAP2(I,J,CASE)
      INTEGER I,J,CASE
      INTEGER KNODES,KEDGES,MAPUNKK(1),SEGK(4,1),KBOUND(6,1)
      COMMON/KDIMEN/KNODES,KEDGES
      COMMON/KMAPUS/MAPUNKK
      COMMON/KSWIRE/SEGK
```

```
      COMMON/KPLAT3/KBOUND
       IF (CASE.EQ.2) THEN
        MAP2 = ABS(SEGK(J,I))
        IF (MAP2.NE.0) MAP2=MAPUNKK(KEDGES+MAP2)
       ELSE IF (CASE.EQ.3) THEN
        MAP2=ABS(KBOUND(J,I))
        IF (MAP2.NE.0) MAP2=MAPUNKK(MAP2)
        ENDIF
      RETURN
      END
C
      SUBROUTINE GETRHO(VTX,V)
      INTEGER I
      REAL VTX(3,3),V(3)
       DO 2001 I=1,3
        V(I) = ( VTX(I,2) - VTX(I,1) ) / 2
2001    CONTINUE
      RETURN
      END
C
      SUBROUTINE P1RHO(VTX,I,V)
      REAL VTX(3,3),V(3)
      INTEGER I,J,K,L
       J=MOD(I,3)+1
       K=MOD(J,3)+1
       DO 2001 L=1,3
        V(L) = ( VTX(L,J) + VTX(L,K) ) / 2
        V(L) = ( V(L) - VTX(L,I) ) / 3
2001    CONTINUE
      RETURN
      END
C
C this routine returns the edges of face F on the perfect conductor
C
      SUBROUTINE FACEDG(F,E1,E2,E3)
C
      INTEGER E1,E2,E3,F
      INTEGER NBOUND(6,1)
      COMMON/PLAT3/NBOUND
C
      E1=NBOUND(1,F)
      E2=NBOUND(2,F)
      E3=NBOUND(3,F)
      RETURN
      END
C
C this routine returns the edges of face F on the coating
C
      SUBROUTINE FACEDG1(F,E1,E2,E3)
C
      INTEGER E1,E2,E3,F
      INTEGER JBOUND(6,1)
```

```
      COMMON/CPLAT3/JBOUND
C
      E1=JBOUND(1,F)
      E2=JBOUND(2,F)
      E3=JBOUND(3,F)
      RETURN
      END
C
C this routine returns the edges of face F on the coating
C
      SUBROUTINE FACEDG2(F,E1,E2,E3)
C
      INTEGER E1,E2,E3,F
      INTEGER KBOUND(6,1)
      COMMON/KPLAT3/KBOUND
C
      E1=KBOUND(1,F)
      E2=KBOUND(2,F)
      E3=KBOUND(3,F)
      RETURN
      END
C
C this routine returns the vertices of face F on the perfect conductor
C v(i,j) = vertex opposite jth edge; i=1=x, i=2=y, i=3=z
C
      SUBROUTINE VTXCRD(F,V)
C
      INTEGER I,J,F,E1,E2,E3,P(3),NCONN(2,1)
      REAL V(3,3),DATNOD(4,1)
      COMMON/PLAT1/DATNOD
      COMMON/PLAT2/NCONN
C
      CALL FACEDG(F,E1,E2,E3)
C
      IF (E1.GT.0) THEN
       P(2)=NCONN(1,E1)
       P(3)=NCONN(2,E1)
        ELSE
       P(2)=NCONN(2,-E1)
       P(3)=NCONN(1,-E1)
       ENDIF
C
      IF (E2.GT.0) THEN
       P(1)=NCONN(2,E2)
        ELSE
       P(1)=NCONN(1,-E2)
       ENDIF
C
      DO 2002 I=1,3
      DO 2001 J=1,3
       V(J,I)=DATNOD(J,P(I))
2001   CONTINUE
```

```
2002    CONTINUE
C
        RETURN
        END
C
C this routine returns the vertices of face F on the coating
C v(i,j) = vertex opposite jth edge; i=1=x, i=2=y, i=3=z
C
        SUBROUTINE VTXCRD1(F,V)
C
        INTEGER I,J,F,E1,E2,E3,P(3),JCONN(2,1)
        REAL V(3,3),CDATNOD(4,1)
        COMMON/CPLAT1/CDATNOD
        COMMON/CPLAT2/JCONN
C
        CALL FACEDG1(F,E1,E2,E3)
C
        IF (E1.GT.0) THEN
         P(2)=JCONN(1,E1)
         P(3)=JCONN(2,E1)
          ELSE
         P(2)=JCONN(2,-E1)
         P(3)=JCONN(1,-E1)
         ENDIF
C
        IF (E2.GT.0) THEN
         P(1)=JCONN(2,E2)
          ELSE
         P(1)=JCONN(1,-E2)
         ENDIF
C
        DO 2002 I=1,3
        DO 2001 J=1,3
         V(J,I)=CDATNOD(J,P(I))
2001    CONTINUE
2002    CONTINUE
C
        RETURN
        END
C
C this routine returns the vertices of face F on the coating
C v(i,j) = vertex opposite jth edge; i=1=x, i=2=y, i=3=z
C
        SUBROUTINE VTXCRD2(F,V)
C
        INTEGER I,J,F,E1,E2,E3,P(3),KCONN(2,1)
        REAL V(3,3),KDATNOD(4,1)
        COMMON/KPLAT1/KDATNOD
        COMMON/KPLAT2/KCONN
C
        CALL FACEDG2(F,E1,E2,E3)
C
```

```
      IF (E1.GT.0) THEN
       P(2)=KCONN(1,E1)
       P(3)=KCONN(2,E1)
        ELSE
       P(2)=KCONN(2,-E1)
       P(3)=KCONN(1,-E1)
       ENDIF
C
      IF (E2.GT.0) THEN
       P(1)=KCONN(2,E2)
        ELSE
       P(1)=KCONN(1,-E2)
       ENDIF
C
      DO 2002 I=1,3
      DO 2001 J=1,3
       V(J,I)=KDATNOD(J,P(I))
2001   CONTINUE
2002   CONTINUE
C
      RETURN
      END
C
C this routine returns the endpoints of segment I on perfect conductor
C  vtx(i,1) is the lower numbered endpoint
C
      SUBROUTINE ENDPTS(I,VTX)
      REAL VTX(3,3),WR(4,1)
      INTEGER I,J,K,SEG(4,1)
      COMMON/RWIRE/WR
      COMMON/SWIRE/SEG
       DO 2002 J=1,2
       DO 2001 K=1,3
        VTX(K,J)=WR(K,SEG(J,I))
2001    CONTINUE
2002    CONTINUE
      RETURN
      END
C
C this routine returns the endpoints of segment I on coating
C  vtx(i,1) is the lower numbered endpoint
C
      SUBROUTINE ENDPTS1(I,VTX)
      REAL VTX(3,3),CWR(4,1)
      INTEGER I,J,K,SEGJ(4,1)
      COMMON/CRWIRE/CWR
      COMMON/CSWIRE/SEGJ
       DO 2002 J=1,2
       DO 2001 K=1,3
        VTX(K,J)=CWR(K,SEGJ(J,I))
2001    CONTINUE
2002    CONTINUE
```

```
      RETURN
      END
C
C this routine returns the endpoints of segment I on coating
C  vtx(i,1) is the lower numbered endpoint
C
      SUBROUTINE ENDPTS2(I,VTX)
      REAL VTX(3,3),KWR(4,1)
      INTEGER I,J,K,SEGK(4,1)
      COMMON/KRWIRE/KWR
      COMMON/KSWIRE/SEGK
       DO 2002 J=1,2
       DO 2001 K=1,3
        VTX(K,J)=KWR(K,SEGK(J,I))
2001    CONTINUE
2002    CONTINUE
      RETURN
      END
C
      REAL FUNCTION GETRAD(I,CASE)
      REAL WR(4,1)
      INTEGER I,CASE,SEG(4,1)
      COMMON/RWIRE/WR
      COMMON/SWIRE/SEG
       IF (CASE.EQ.2) THEN
        GETRAD=( WR(4,SEG(1,I)) + WR(4,SEG(2,I)) ) / 2
       ELSE IF (CASE.EQ.3) THEN
        GETRAD=0
       ENDIF
      RETURN
      END
C
      REAL FUNCTION GETRAD1(I,CASE)
      REAL CWR(4,1)
      INTEGER I,CASE,SEGJ(4,1)
      COMMON/CRWIRE/CWR
      COMMON/CSWIRE/SEGJ
       IF (CASE.EQ.2) THEN
        GETRAD1=( CWR(4,SEGJ(1,I)) + CWR(4,SEGJ(2,I)) ) / 2
       ELSE IF (CASE.EQ.3) THEN
        GETRAD1=0
       ENDIF
      RETURN
      END
C
      REAL FUNCTION GETRAD2(I,CASE)
      REAL KWR(4,1)
      INTEGER I,CASE,SEGK(4,1)
      COMMON/KRWIRE/KWR
      COMMON/KSWIRE/SEGK
       IF (CASE.EQ.2) THEN
        GETRAD2=( KWR(4,SEGK(1,I)) + KWR(4,SEGK(2,I)) ) / 2
```

```
        ELSE IF (CASE.EQ.3) THEN
          GETRAD2=0
        ENDIF
      RETURN
      END
C
C sign function
C
      INTEGER FUNCTION ISGN(C)
      INTEGER C
      IF (C.NE.0) THEN
        ISGN=C/ABS(C)
        ELSE
       ISGN=0
       ENDIF
      RETURN
      END
C
C sign function
C
      INTEGER FUNCTION RSGN(C)
      REAL C
      IF (C.NE.0) THEN
       RSGN=C/ABS(C)
         ELSE
       RSGN=0
       ENDIF
      RETURN
      END
C
Cthis routine employs a 7-point numerical integration rule and
Canalytical integration to evaluate the vector and scalar potential
Cintegrals over a triangular region.
C
      SUBROUTINE NINT7(VX,V1,CVEC,CXSI,CETA,POT,CPHI,P1,RC1,AREA,DIST)
C
C VX(3,3) are the vertices of the source triangle
C V1(3) are the coordinates of the observation centroid
C
      COMPLEX JI,CF,CFX,CFN,CF1,CVEC,CXSI,CETA,CPHI
      REAL XSI(7),ETA(7),WGHT(7)
      REAL PI,KN,R1(3),P1(3),RC1(3)
      REAL DR,MAGNI,ALIMIT,POT,AREA,DIST
      REAL VX(3,3),V1(3)
      INTEGER I,J
C
      COMMON/CONST/PI,KN,JI
      COMMON/NUMINT/XSI,ETA,WGHT
      EXTERNAL MAGNI
C
      PARAMETER (ALIMIT=1D-10)
C
```

```
      DATA XSI/ 0.3333333333, 0.05971587, 0.47014206,
     + 0.47014206, 0.79742699, 0.10128651,0.10128651/
      DATA ETA/ 0.3333333333, 0.47014206, 0.05971587,
     + 0.47014206, 0.10128651, 0.79742699,0.10128651/
      DATA WGHT/ 0.225, 0.13239415, 0.13239415,
     + 0.13239415, 0.12593918, 0.12593918,0.12593918/
      CF=0
      CFX=0
      CFN=0
      DIST = 0
      DO 2002 I=1,7
       DO 2001 J=1,3
        R1(J) = (V1(J)-VX(J,1)) - (VX(J,2)-VX(J,1))*XSI(I) -
     +   (VX(J,3)-VX(J,1))*ETA(I)
2001    CONTINUE
       DR=MAGNI(R1)
       IF (I.EQ.1) THEN
         DIST = DR
       ELSE IF (DR.LT.DIST) THEN
         DIST = DR
       ENDIF
       IF (DR.LE.ALIMIT) THEN
        CF1=-JI*KN
         ELSE
        CF1=(EXP(-JI*KN*DR)-1)/DR
        ENDIF
       CF=CF+CF1*WGHT(I)
       CFX=CFX+CF1*WGHT(I)*XSI(I)
       CFN=CFN+CF1*WGHT(I)*ETA(I)
2002   CONTINUE
C
      CVEC = CF * AREA
      CXSI = CFX * AREA
      CETA = CFN * AREA
C
      CALL INTGRL(VX,V1,POT,P1,RC1,AREA)
      CPHI=CVEC+POT
      RETURN
      END
C
Cthis routine employs a 7-point numerical integration rule and
Canalytical integration to evaluate the vector and scalar potential
Cintegrals over a triangular region.
C
      SUBROUTINE NINT7A(VX,V1,CVEC1,CXSI1,CETA1,POT,CPHI1,P1,RC1,
     +                          AREA,DIST)
C
C VX(3,3) are the vertices of the source triangle
C V1(3) are the coordinates of the observation centroid
C
      COMPLEX JI,CF,CFX,CFN,CF1,CVEC1,CXSI1,CETA1,CPHI1,KN1
      REAL XSI(7),ETA(7),WGHT(7)
```

```
      REAL PI,KN,R1(3),P1(3),RC1(3)
      REAL DR,MAGNI,ALIMIT,POT,AREA,DIST
      REAL VX(3,3),V1(3)
      INTEGER I,J
C
      COMMON/CONST/PI,KN,JI
      COMMON/CONST1/KN1
      COMMON/NUMINT/XSI,ETA,WGHT
      EXTERNAL MAGNI
C
      PARAMETER (ALIMIT=1D-10)
C
      CF=0
      CFX=0
      CFN=0
      DIST = 0
      DO 2002 I=1,7
       DO 2001 J=1,3
        R1(J) = (V1(J)-VX(J,1)) - (VX(J,2)-VX(J,1))*XSI(I) -
     +   (VX(J,3)-VX(J,1))*ETA(I)
2001    CONTINUE
       DR=MAGNI(R1)
       IF (I.EQ.1) THEN
         DIST = DR
       ELSE IF (DR.LT.DIST) THEN
         DIST = DR
       ENDIF
       IF (DR.LE.ALIMIT) THEN
        CF1=-JI*KN1
         ELSE
        CF1=(EXP(-JI*KN1*DR)-1)/DR
        ENDIF
       CF=CF+CF1*WGHT(I)
       CFX=CFX+CF1*WGHT(I)*XSI(I)
       CFN=CFN+CF1*WGHT(I)*ETA(I)
2002   CONTINUE
C
      CVEC1 = CF * AREA
      CXSI1 = CFX * AREA
      CETA1 = CFN * AREA
C
      CALL INTGRL(VX,V1,POT,P1,RC1,AREA)
      CPHI1 = CVEC1 + POT
      RETURN
      END
C
Cthis routine employs a 7-point numerical integration rule and
Canalytical integration to evaluate the vector and scalar potential
Cintegrals over a triangular region.
C
      SUBROUTINE NINT7B(VX,V1,CVECK0,CXSIK0,CETAK0,AREA,DIST)
C
```

```
C VX(3,3) are the vertices of the source triangle
C V1(3) are the coordinates of the observation centroid
C
      COMPLEX JI,CF,CFX,CFN,CF1,CVECK0,CXSIK0,CETAK0
      REAL XSI(7),ETA(7),WGHT(7)
      REAL PI,KN,R1(3)
      REAL DR,MAGNI,AREA,DIST
      REAL VX(3,3),V1(3)
      INTEGER I,J
C
      COMMON/CONST/PI,KN,JI
      COMMON/NUMINT/XSI,ETA,WGHT
      EXTERNAL MAGNI
C
      CF=0
      CFX=0
      CFN=0
      DIST = 0
      DO 2002 I=1,7
       DO 2001 J=1,3
        R1(J) = (V1(J)-VX(J,1)) - (VX(J,2)-VX(J,1))*XSI(I) -
     +   (VX(J,3)-VX(J,1))*ETA(I)
2001    CONTINUE
       DR=MAGNI(R1)
       IF (I.EQ.1) THEN
         DIST = DR
       ELSE IF (DR.LT.DIST) THEN
         DIST = DR
       ENDIF
       CF1=(1+JI*KN*DR)*(EXP(-JI*KN*DR))/(DR*DR*DR)
       CF = CF + CF1 * WGHT(I)
       CFX= CFX + CF1 * WGHT(I) * XSI(I)
       CFN= CFN + CF1 * WGHT(I) * ETA(I)
2002   CONTINUE
C
      CVECK0 = CF * AREA
      CXSIK0 = CFX * AREA
      CETAK0 = CFN * AREA
C
      RETURN
      END
C
Cthis routine employs a 7-point numerical integration rule and
Canalytical integration to evaluate the vector and scalar potential
Cintegrals over a triangular region.
C
      SUBROUTINE NINT7C(VX,V1,CVECK1,CXSIK1,CETAK1,AREA,DIST)
C
C VX(3,3) are the vertices of the source triangle
C V1(3) are the coordinates of the observation centroid
C
      COMPLEX JI,CF,CFX,CFN,CF1,CVECK1,CXSIK1,CETAK1,KN1
```

```
      REAL XSI(7),ETA(7),WGHT(7)
      REAL PI,KN,R1(3)
      REAL DR,MAGNI,AREA,DIST
      REAL VX(3,3),V1(3)
      INTEGER I,J
C
      COMMON/CONST/PI,KN,JI
      COMMON/CONST1/KN1
      COMMON/NUMINT/XSI,ETA,WGHT
      EXTERNAL MAGNI
C
      CF=0
      CFX=0
      CFN=0
      DIST = 0
      DO 2002 I=1,7
       DO 2001 J=1,3
        R1(J) = (V1(J)-VX(J,1)) - (VX(J,2)-VX(J,1))*XSI(I) -
     +   (VX(J,3)-VX(J,1))*ETA(I)
2001    CONTINUE
       DR=MAGNI(R1)
       IF (I.EQ.1) THEN
         DIST = DR
       ELSE IF (DR.LT.DIST) THEN
         DIST = DR
       ENDIF
       CF1=(1+JI*KN1*DR)*(EXP(-JI*KN1*DR))/(DR*DR*DR)
       CF = CF + CF1 * WGHT(I)
       CFX= CFX + CF1 * WGHT(I) * XSI(I)
       CFN= CFN + CF1 * WGHT(I) * ETA(I)
2002   CONTINUE
C
      CVECK1 = CF * AREA
      CXSIK1 = CFX * AREA
      CETAK1 = CFN * AREA
C
      RETURN
      END
C
C this subroutine, with the help of subroutine ca, evaluates
C the 1/r integral over a triangular region and the line integral
C of (r times the normal to the triangle boundary) over the
C triangle boundary.
C
      SUBROUTINE INTGRL(VX,V1,POT,P1,RC1,AREA)
      REAL PI,VDOT,ALP,ALM,ZNOT,P0,POT,VAL1,VAL2,AREA
      REAL VX(3,3),V1(3),UN1(3),UL1(3),UU1(3),T1(3),P1(3),RC1(3)
      INTEGER I,J,K,SGN,RSGN
      COMMON/CONST/PI
      EXTERNAL RSGN,VDOT
C
C init
```

```
C
      POT=0
C
C calculate unit normal = UN1
C
      CALL CROSS1(VX,UN1)
      DO 2001 I=1,3
       UN1(I)=UN1(I)/(2*AREA)
2001   CONTINUE
C
C ZNOT is the perpendicular (to the source triangle) distance
C between the source (vertex 1) and observation triangles
C
C RC1 is the nonperpendicular ("coplanar" according to source tri)
C vector from source (vertex 1) to observation triangles
C
C  NOT USED call centroid(vtx,t1)
      DO 2002 K=1,3
       T1(K)=V1(K)-VX(K,1)
2002   CONTINUE
      ZNOT=VDOT(T1,UN1)
C
      DO 2003 I=1,3
       RC1(I)=V1(I)-ZNOT*UN1(I)
       P1(I)=0
2003   CONTINUE
      ZNOT = ABS(ZNOT)
C
C integrate over each edge
C UL1 is unit edge
C
      DO 2009 I=1,3
C
       J=MOD(I,3)+1
       DO 2004 K=1,3
        UL1(K)=VX(K,J)-VX(K,I)
2004    CONTINUE
       CALL UNIT(UL1,UL1)
C
       CALL CROSS2(UL1,UN1,UU1)
       DO 2005 K=1,3
        T1(K)=VX(K,I)-RC1(K)
2005    CONTINUE
       P0=VDOT(T1,UU1)
       SGN=RSGN(P0)
       P0=ABS(P0)
       DO 2006 K=1,3
        T1(K)=VX(K,J)-V1(K)
2006    CONTINUE
        ALP=VDOT(T1,UL1)
       DO 2007 K=1,3
        T1(K)=VX(K,I)-V1(K)
```

```
2007     CONTINUE
         ALM=VDOT(T1,UL1)
        CALL CA(P0,ZNOT,ALP,ALM,VAL1,VAL2)
        POT=POT+VAL1*SGN
        DO 2008 K=1,3
         P1(K)=P1(K)+UU1(K)*VAL2
2008     CONTINUE
2009    CONTINUE
C
       RETURN
       END
C
C-------------------------------------------------
C
       SUBROUTINE CA(P0,D,ALP,ALM,VALA,VALL)
       REAL P0,D,R0,RP,RM,ALP,ALM,MIN,TOP,BOT
       REAL LP,LM,VALA,VALL,ALGTRM,ARGTNP,ARGTNM
C
C MIN depends on machine precision
C  --use 1D-5 for 32 bit reals
C  --can use 1D-8 for 64 bit reals
C
       PARAMETER (MIN=1D-5)
C
       R0 = D**2 + P0**2
       RP = SQRT( R0 + ALP**2)
       RM = SQRT( R0 + ALM**2)
       TOP = RP+ALP
       BOT = RM+ALM
       IF (ALP.LT.0.AND.TOP.LT.MIN) TOP = R0/ABS(ALP)/2
       IF (ALM.LT.0.AND.BOT.LT.MIN) BOT = R0/ABS(ALM)/2
       IF (ALP.LT.0.AND.ALM.LT.0.AND.TOP.LT.MIN.AND.BOT.LT.MIN) THEN
        ALGTRM = LOG(ALM/ALP)
        ELSE
        ALGTRM = LOG(TOP/BOT)
        ENDIF
       IF (D.GT.0) THEN
        ARGTNP=P0*ALP/(R0+D*RP)
        ARGTNM=P0*ALM/(R0+D*RM)
        VALA=P0*ALGTRM-D*(ATAN(ARGTNP)-ATAN(ARGTNM))
       ELSE
        VALA=P0*ALGTRM
        ENDIF
       VALL=(R0*ALGTRM+ALP*RP-ALM*RM)/2
C
       RETURN
       END
C
C save matrix
C
       SUBROUTINE SAFE(CZ,JUNKNS,KUNKNS,NUNKNS,P)
       INTEGER JUNKNS,KUNKNS,NUNKNS,P
```

```
      COMPLEX CZ(2*JUNKNS+KUNKNS+NUNKNS)
      IF (P.EQ.1) THEN
       REWIND(22)
       REWIND(26)
       DO 10 J=1,JUNKNS
        READ(22) (CZ(I),I=1,JUNKNS)
        READ(26) (CZ(I),I=JUNKNS+1,JUNKNS+J)
        WRITE(57) (CZ(I),I=1,JUNKNS+J)
10     CONTINUE
       CLOSE(22)
       CLOSE(26)
      ELSE IF (P.EQ.2) THEN
       REWIND(23)
       REWIND(27)
       REWIND(31)
       DO 11 J=1,KUNKNS
        READ(23) (CZ(I),I=1,JUNKNS)
        READ(27) (CZ(I),I=JUNKNS+1,2*JUNKNS)
        READ(31) (CZ(I),I=2*JUNKNS+1,2*JUNKNS+J)
        WRITE(57) (CZ(I),I=1,2*JUNKNS+J)
11     CONTINUE
       CLOSE(23)
       CLOSE(27)
       CLOSE(31)
      ELSE
       REWIND(24)
       REWIND(28)
       REWIND(36)
       DO 12 J=1,NUNKNS
        READ(24) (CZ(I),I=1,JUNKNS)
        READ(28) (CZ(I),I=JUNKNS+1,2*JUNKNS)
        DO 20 L=1,KUNKNS
          CZ(2*JUNKNS+L) = 0
20      CONTINUE
        READ(36) (CZ(I),I=2*JUNKNS+KUNKNS+1,2*JUNKNS+KUNKNS+J)
        WRITE(57) (CZ(I),I=1,2*JUNKNS+KUNKNS+J)
12     CONTINUE
       CLOSE(24)
       CLOSE(28)
       CLOSE(36)
      ENDIF
C
      RETURN
      END
```

Appendix E

RADAR CROSS SECTION MEASUREMENTS AND PREDICTIONS

E.1 Introduction

This appendix contains the radar cross section (RCS) plots discussed in Chapter 5. The graphs of the experimental RCS data generated from the experimental RCS measurements performed at the MIT Lincoln Laboratory Group 95 RCS Measurement Facility are contained in Section E.2. The graphs of the theoretical RCS predictions generated from the EFIE series of computer programs discussed in Chapter 3 are contained in Section 3.3.

E.2 Experimental Radar Cross Section Measurements

This section contains the graphs of the experimental RCS data generated from the experimental RCS measurements performed at the MIT Lincoln Laboratory Group 95 RCS Measurement Facility. Each figure contains two RCS plots. The top plot in each figure is the horizontally transmitted and horizontally received monostatic far-field RCS (σ_{hh}) versus angle. Horizontally transmitted means the electric field of the incident wave is polarized parallel to the edge of the square aluminum plate when the incident wave is travelling in the plane of the plate and normal to an edge. The bottom plot in each figure is the vertically transmitted and vertically received monostatic far-field RCS (σ_{vv}) versus angle. Therefore, each figure contains the co-polarized RCS plots for two orthogonally polarized incident electric fields.

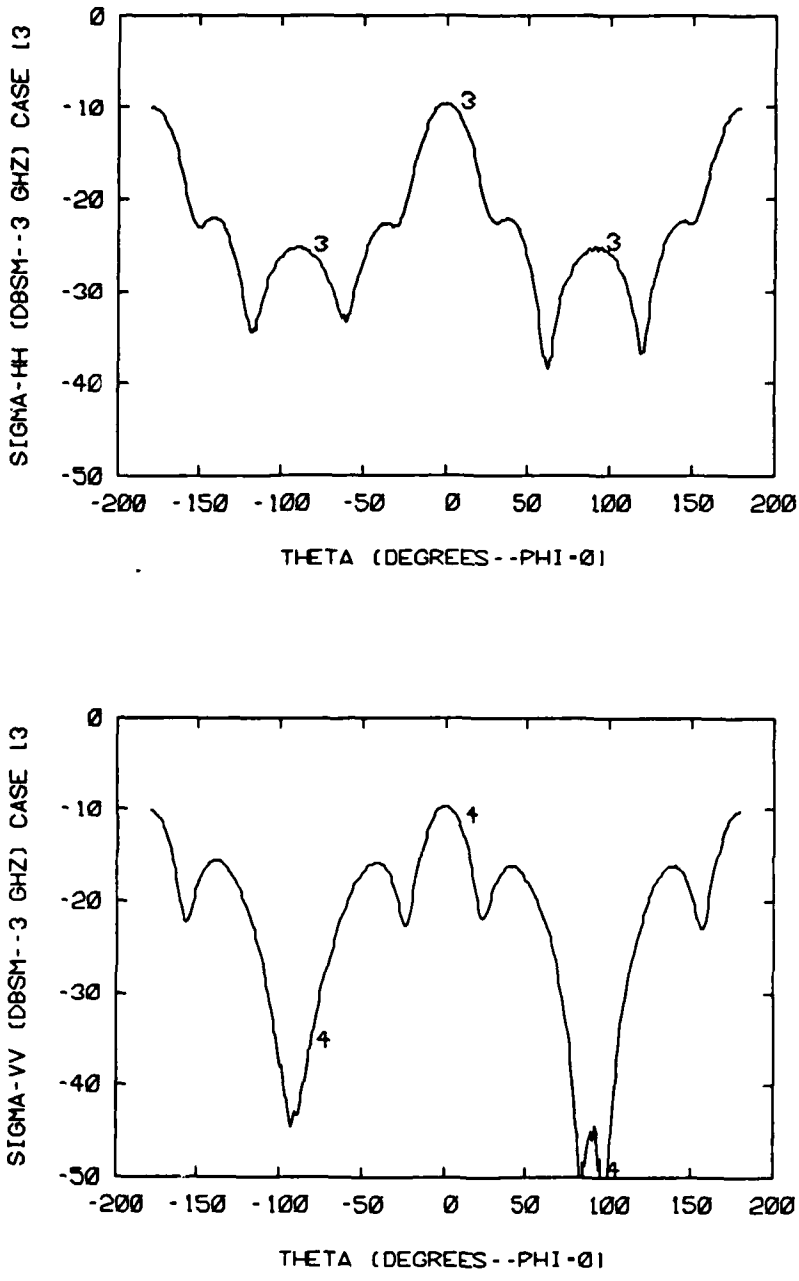

Figure E.1. Experimental monostatic 3.0 GHz RCS plots for uncoated 10cm by 10cm square aluminum plate: (top) σ_{hh} versus angle and (bottom) σ_{vv} versus angle

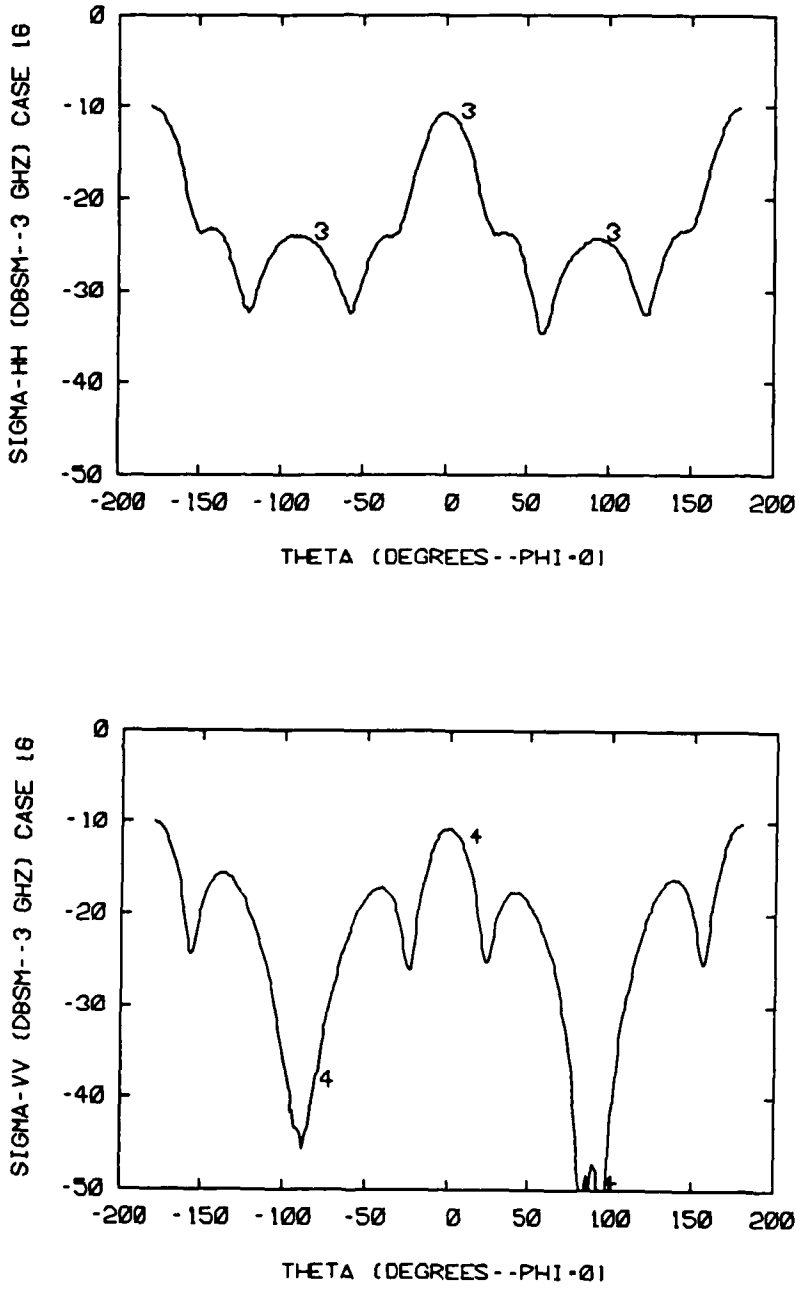

Figure E.2. Experimental monostatic 3.0 GHz RCS plots for Eccosorb FDS coated 10cm by 10cm square aluminum plate: (top) σ_{hh} versus angle and (bottom) σ_{vv} versus angle

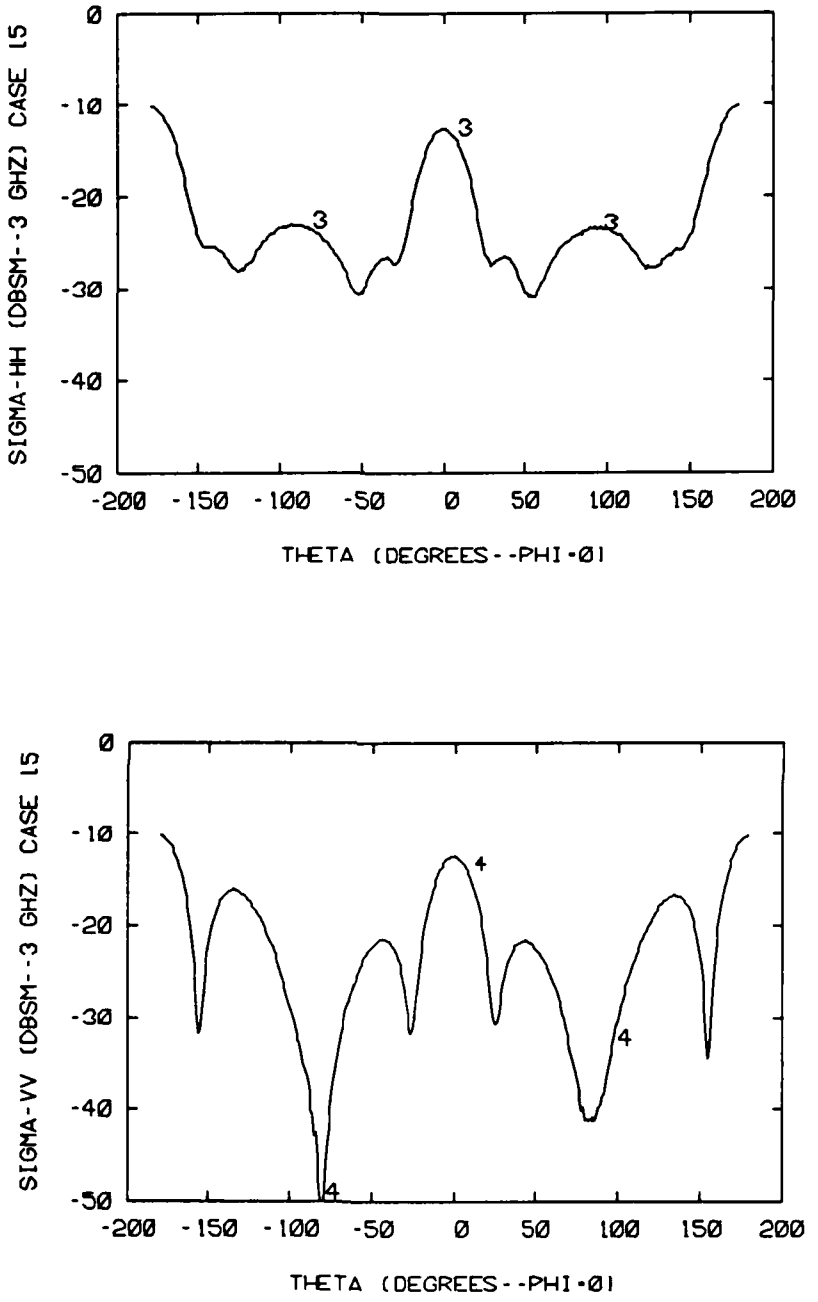

Figure E.3. Experimental monostatic 3.0 GHz RCS plots for Eccosorb SF 6.0 coated 10cm by 10cm square aluminum plate: (top) σ_{hh} versus angle and (bottom) σ_{vv} versus angle

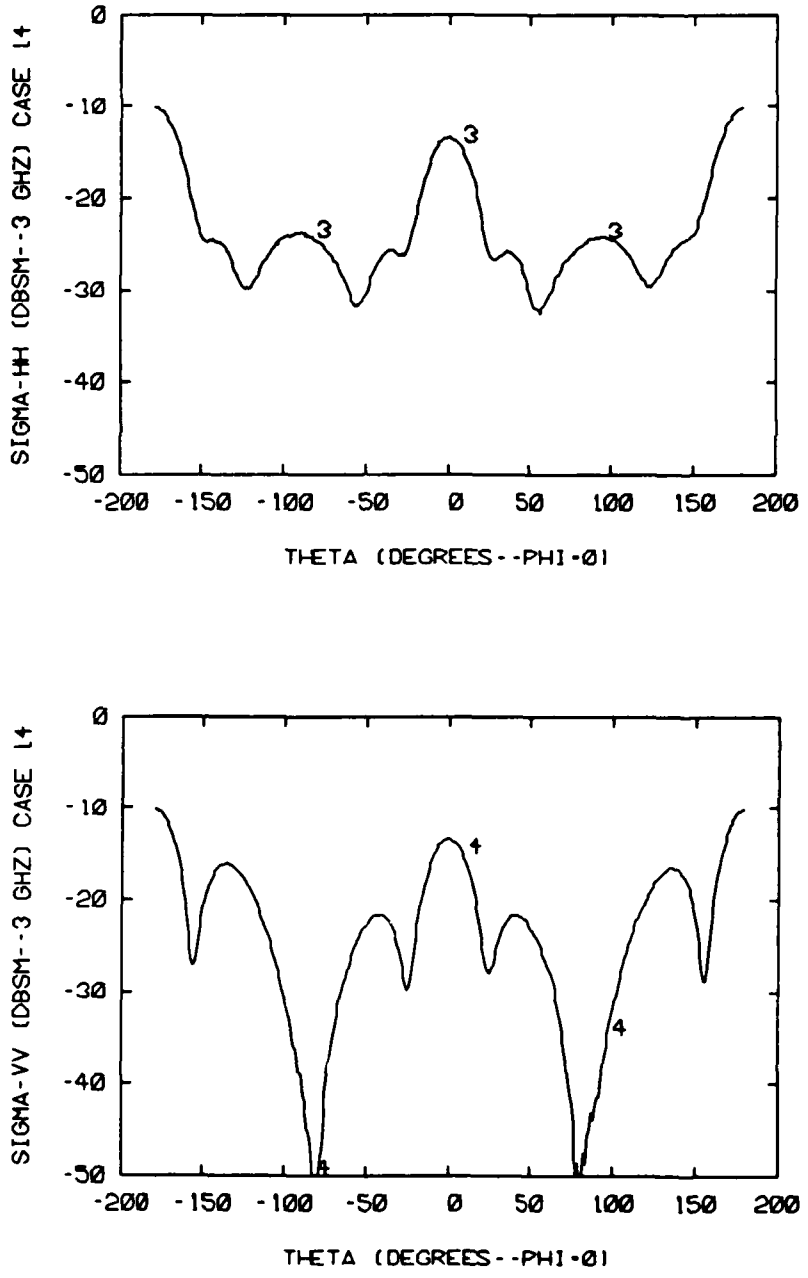

Figure E.4. Experimental monostatic 3.0 GHz RCS plots for Eccosorb FGM 40 coated 10cm by 10cm square aluminum plate: (top) σ_{hh} versus angle and (bottom) σ_{vv} versus angle

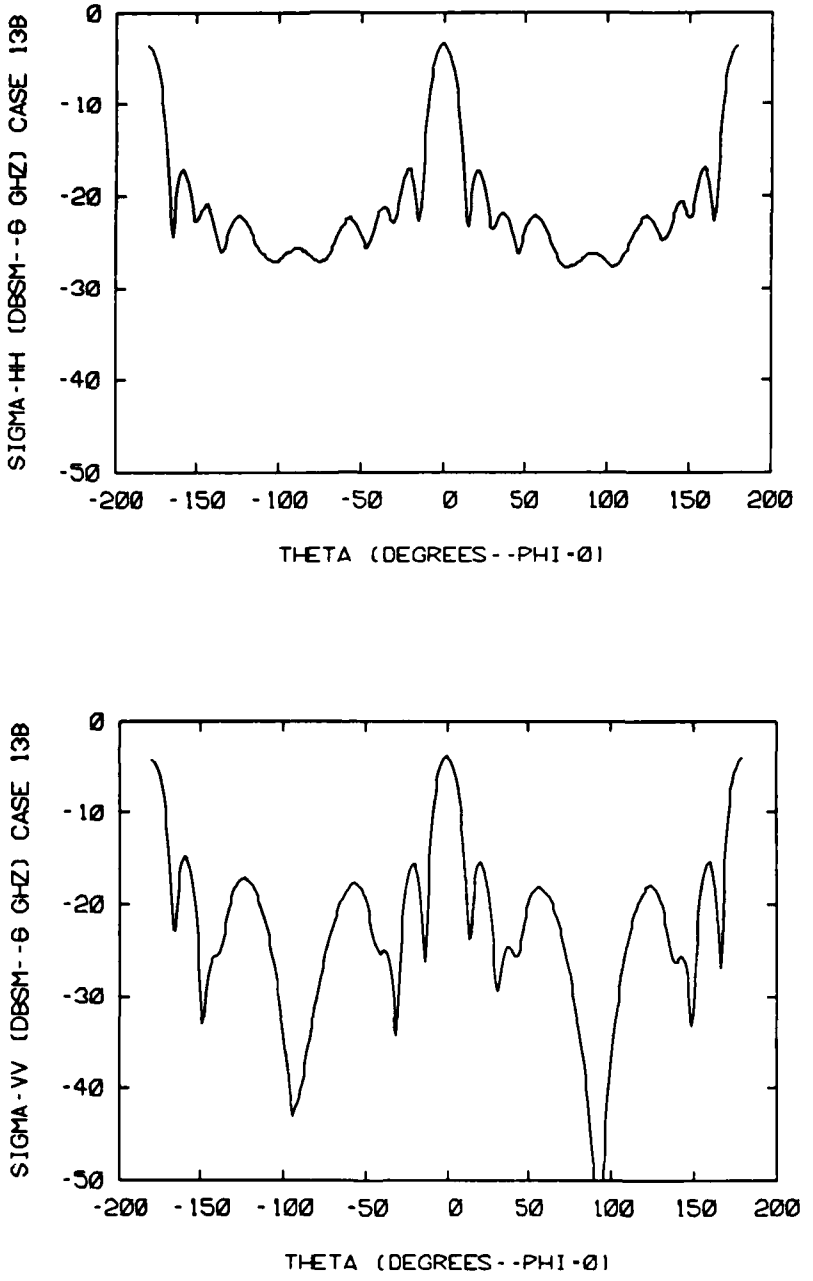

Figure E.5. Experimental monostatic 6.0 GHz RCS plots for uncoated 10cm by 10cm square aluminum plate: (top) σ_{hh} versus angle and (bottom) σ_{vv} versus angle

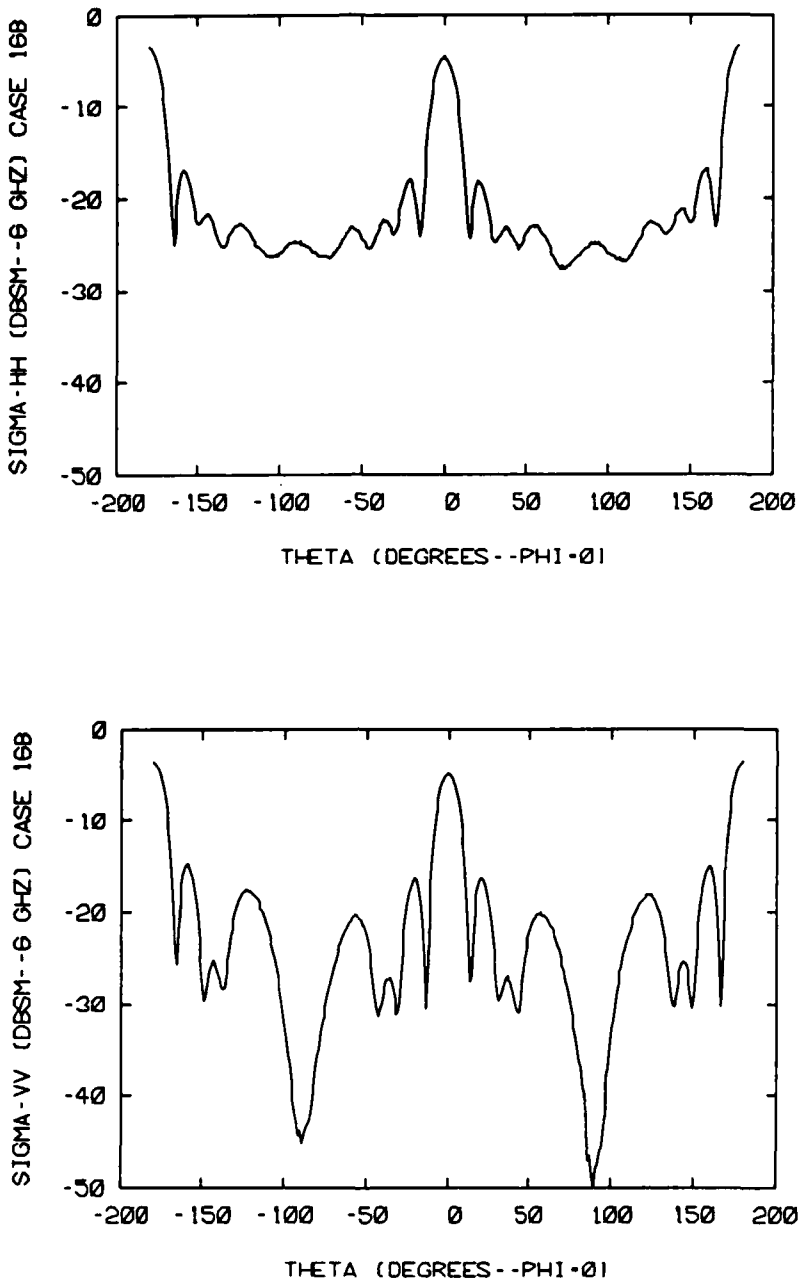

Figure E.6. Experimental monostatic 6.0 GHz RCS plots for Eccosorb FDS coated 10cm by 10cm square aluminum plate: (top) σ_{hh} versus angle and (bottom) σ_{vv} versus angle

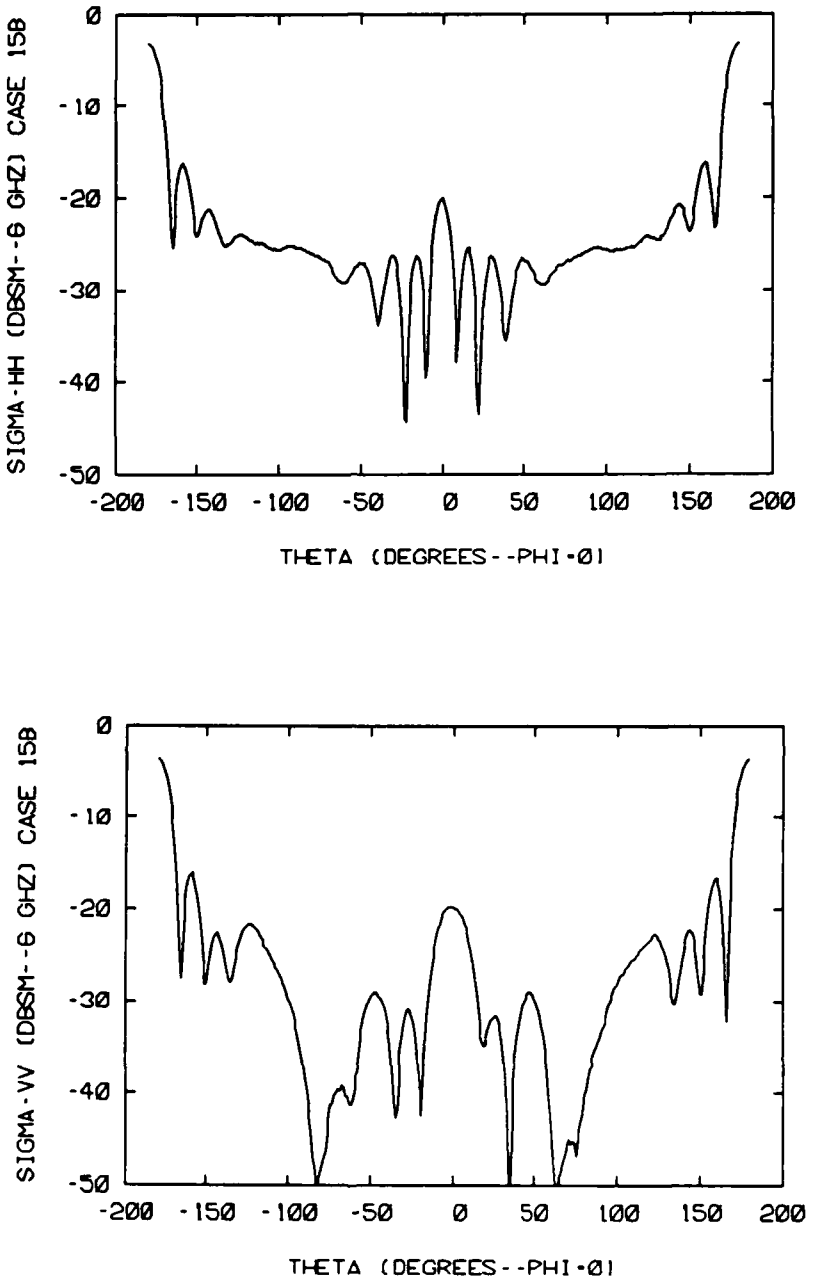

Figure E.7. Experimental monostatic 6.0 GHz RCS plots for Eccosorb SF 6.0 coated 10cm by 10cm square aluminum plate: (top) σ_{hh} versus angle and (bottom) σ_{vv} versus angle

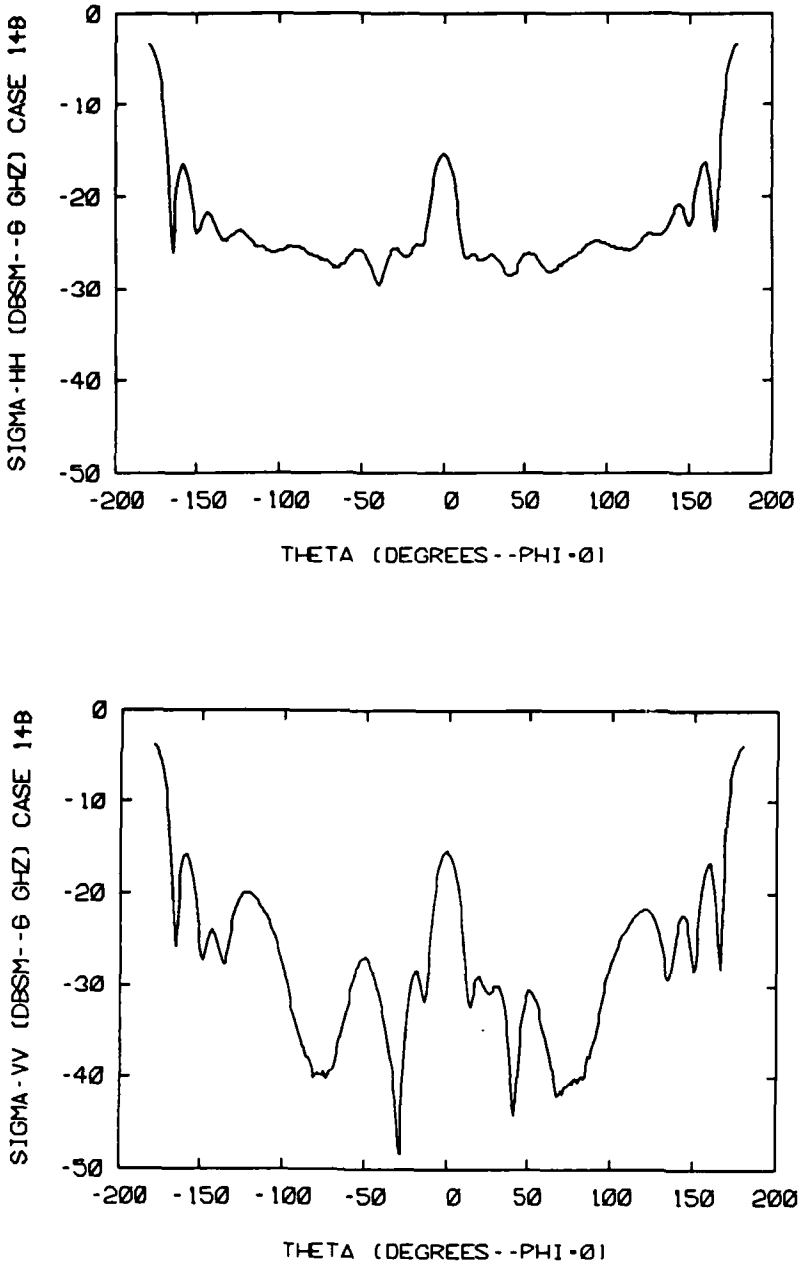

Figure E.8. Experimental monostatic 6.0 GHz RCS plots for Eccosorb FGM 40 coated 10cm by 10cm square aluminum plate: (top) σ_{hh} versus angle and (bottom) σ_{vv} versus angle

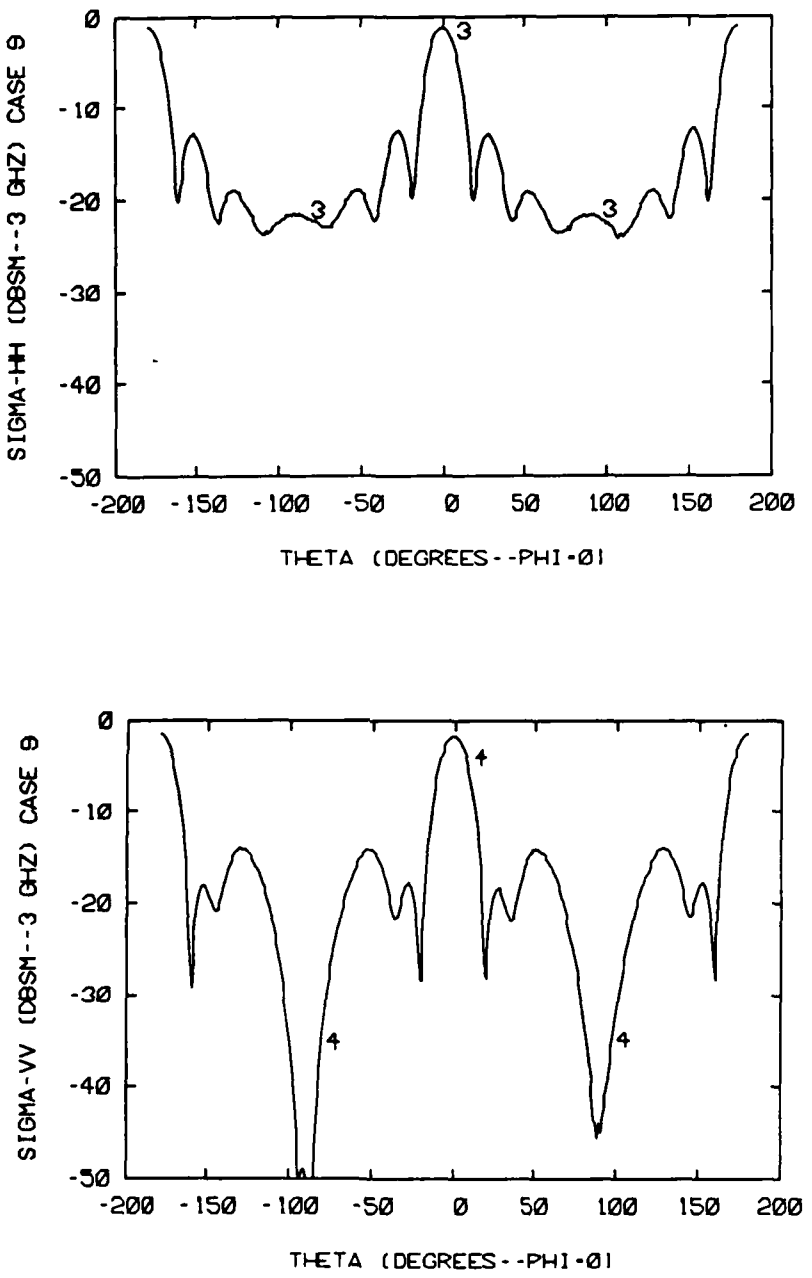

Figure E.9. Experimental monostatic 3.0 GHz RCS plots for uncoated 15cm by 15cm square aluminum plate: (top) σ_{hh} versus angle and (bottom) σ_{vv} versus angle

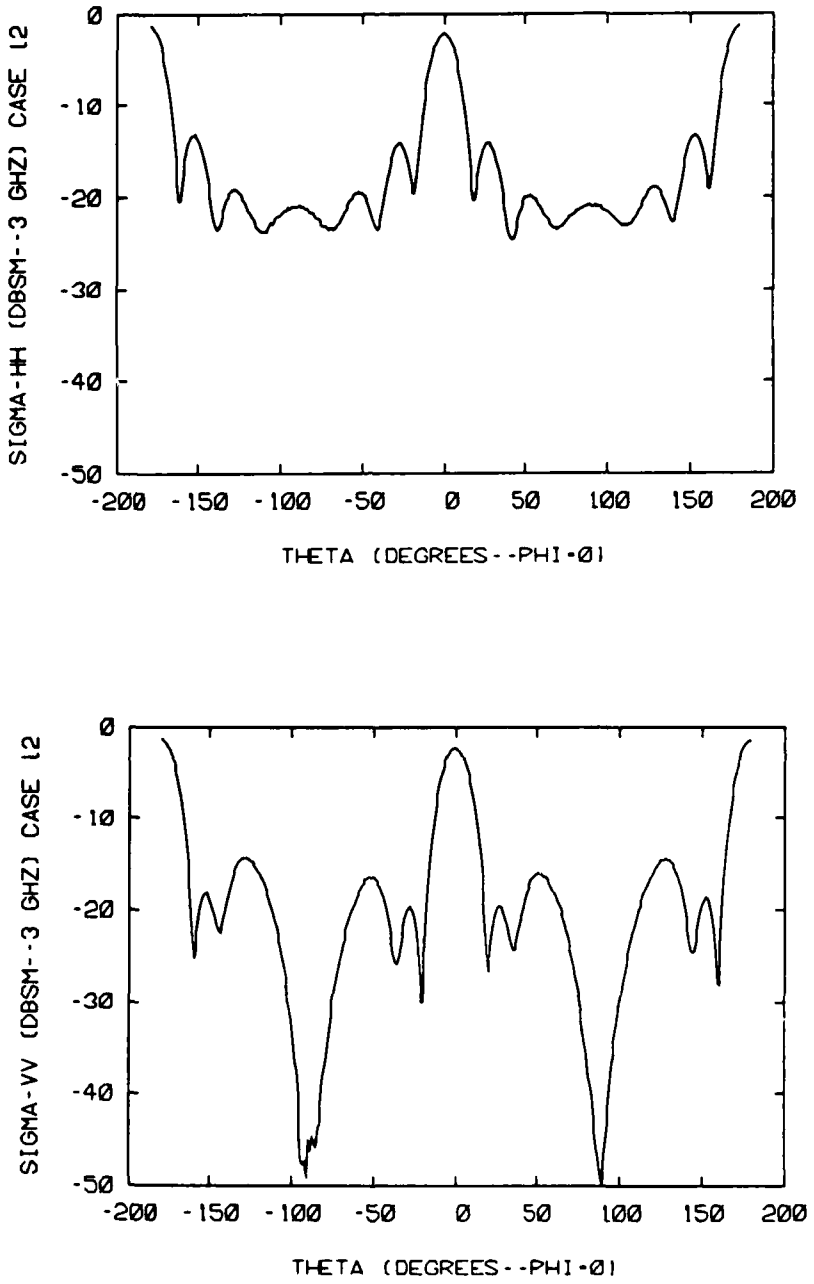

Figure E.10. Experimental monostatic 3.0 GHz RCS plots for Eccosorb FDS coated 15cm by 15cm square aluminum plate: (top) σ_{hh} versus angle and (bottom) σ_{vv} versus angle

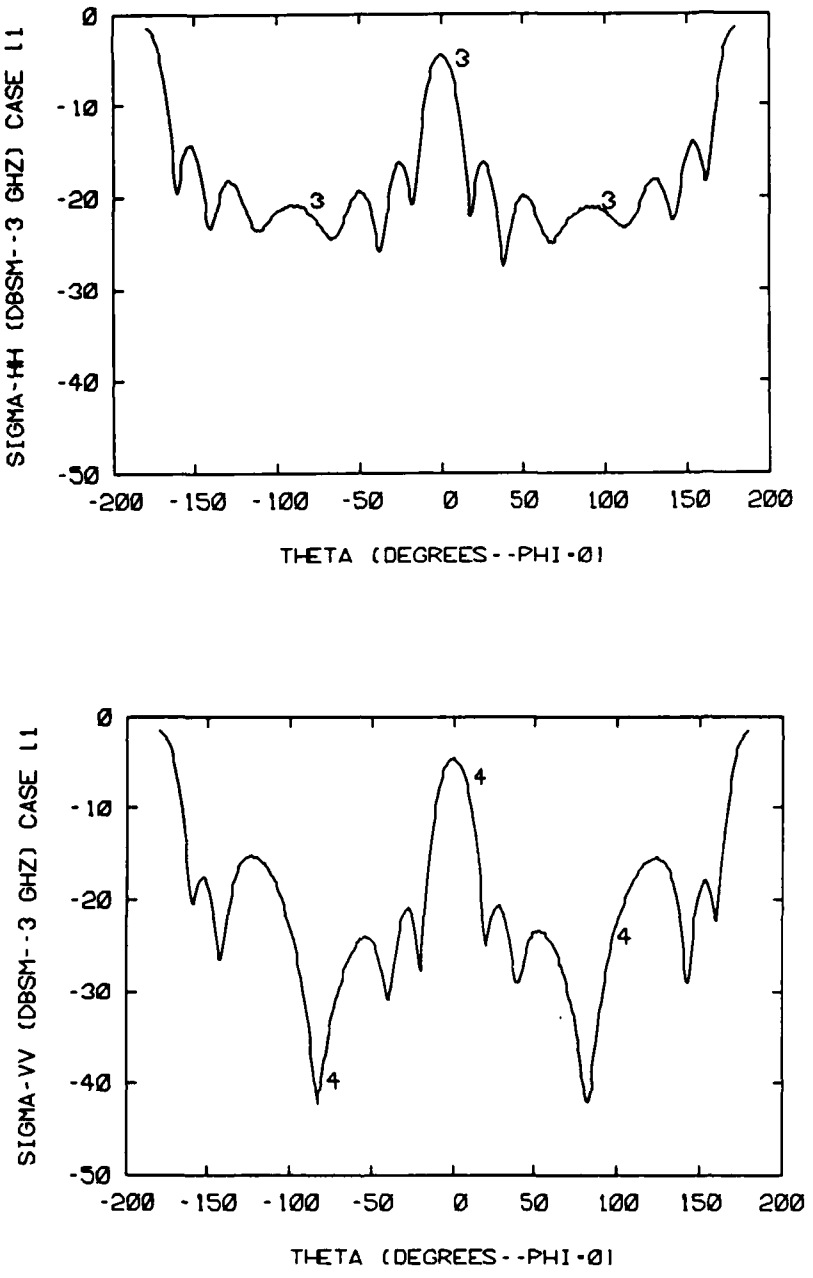

Figure E.11. Experimental monostatic 3.0 GHz RCS plots for Eccosorb SF 6.0 coated 15cm by 15cm square aluminum plate: (top) σ_{hh} versus angle and (bottom) σ_{vv} versus angle

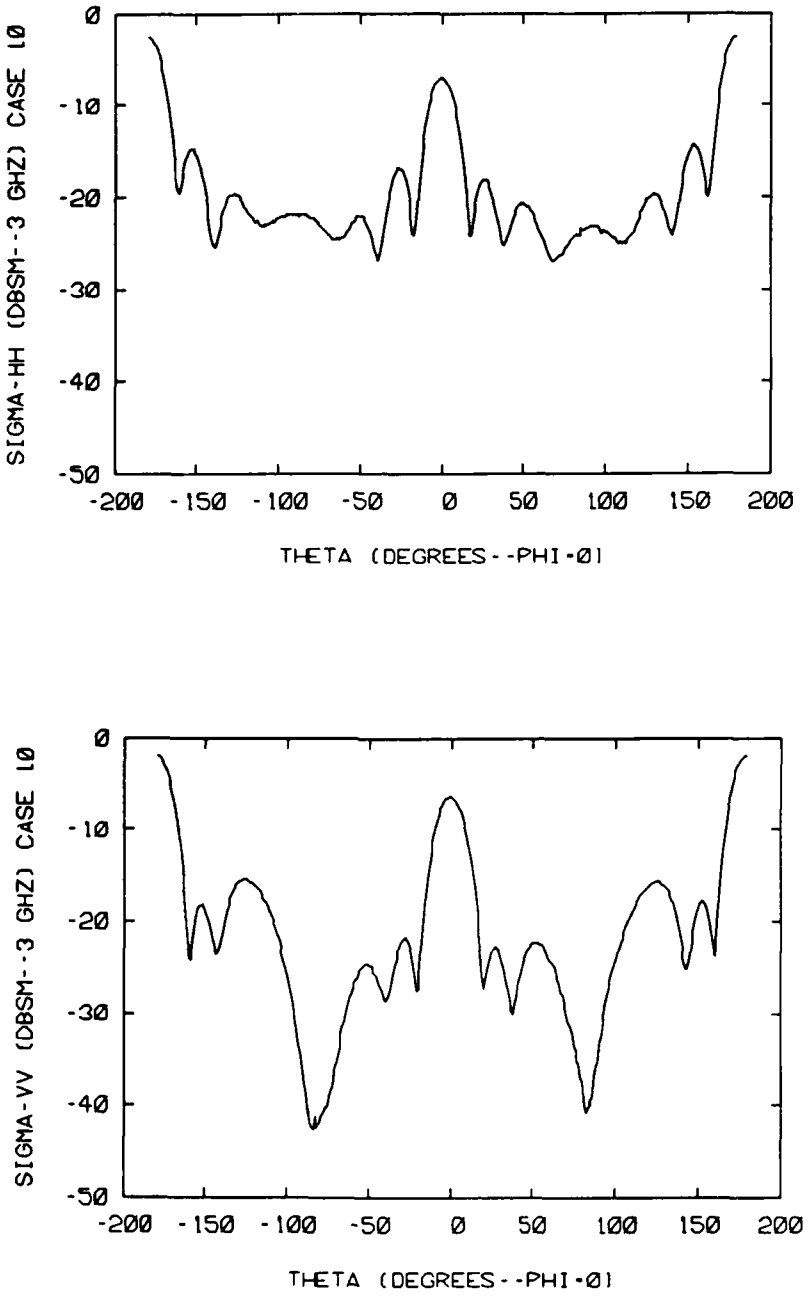

Figure E.12. Experimental monostatic 3.0 GHz RCS plots for Eccosorb FGM 40 coated 15cm by 15cm square aluminum plate: (top) σ_{hh} versus angle and (bottom) σ_{vv} versus angle

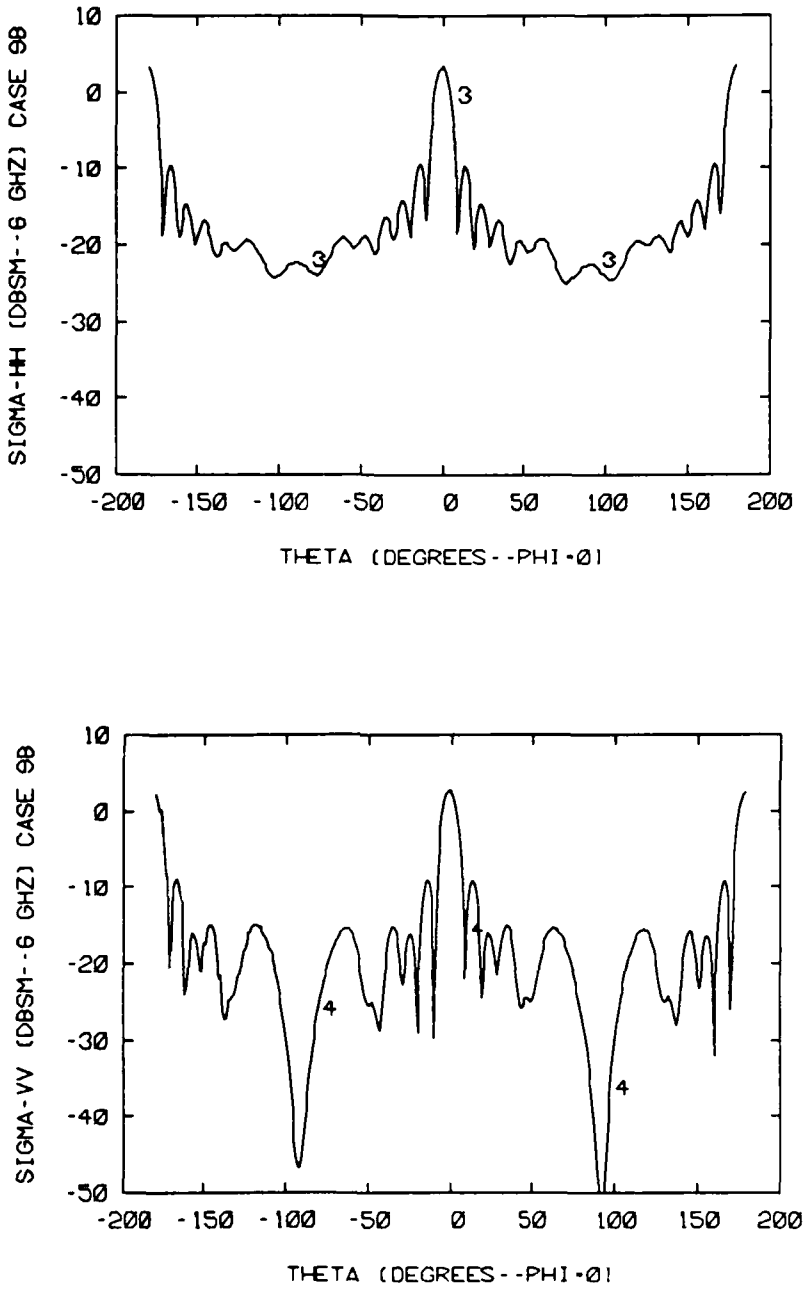

Figure E.13. Experimental monostatic 6.0 GHz RCS plots for uncoated 15cm by 15cm square aluminum plate: (top) σ_{hh} versus angle and (bottom) σ_{vv} versus angle

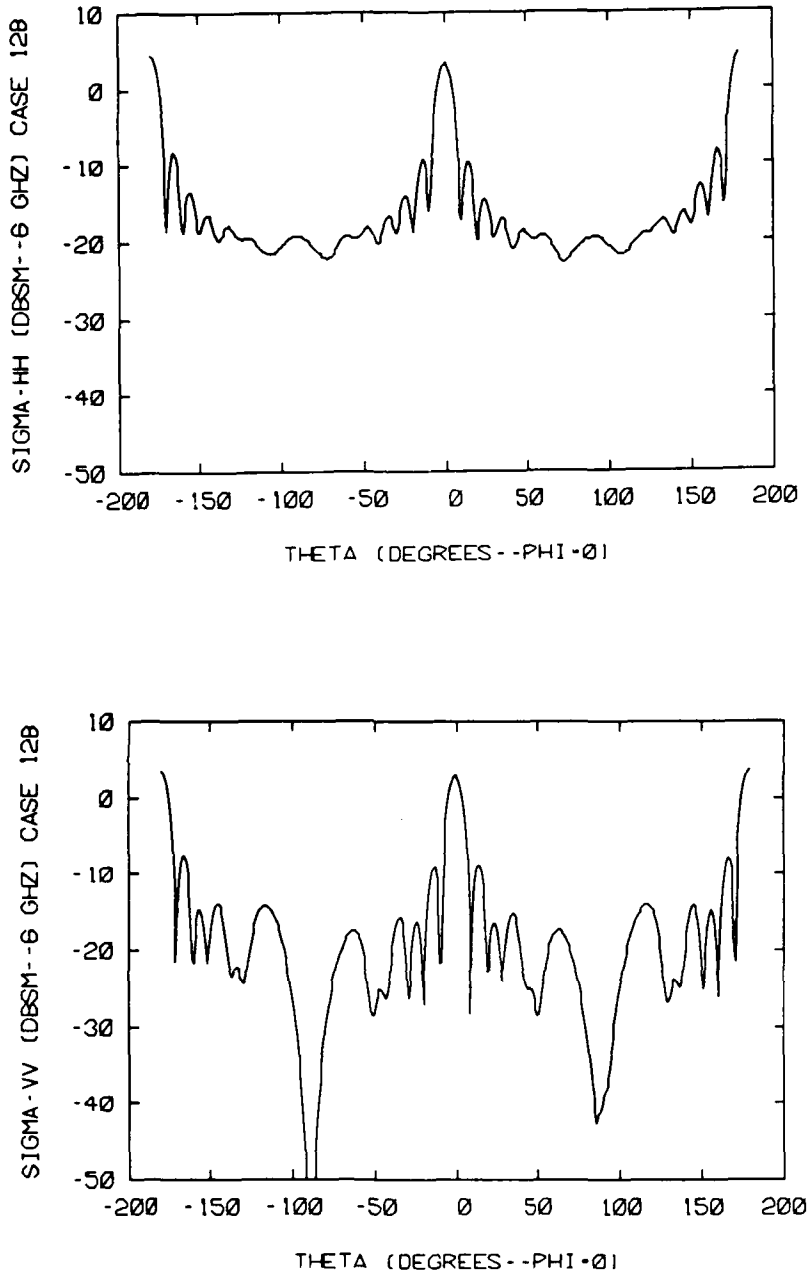

Figure E.14. Experimental monostatic 6.0 GHz RCS plots for Eccosorb FDS coated 15cm by 15cm square aluminum plate: (top) σ_{hh} versus angle and (bottom) σ_{vv} versus angle

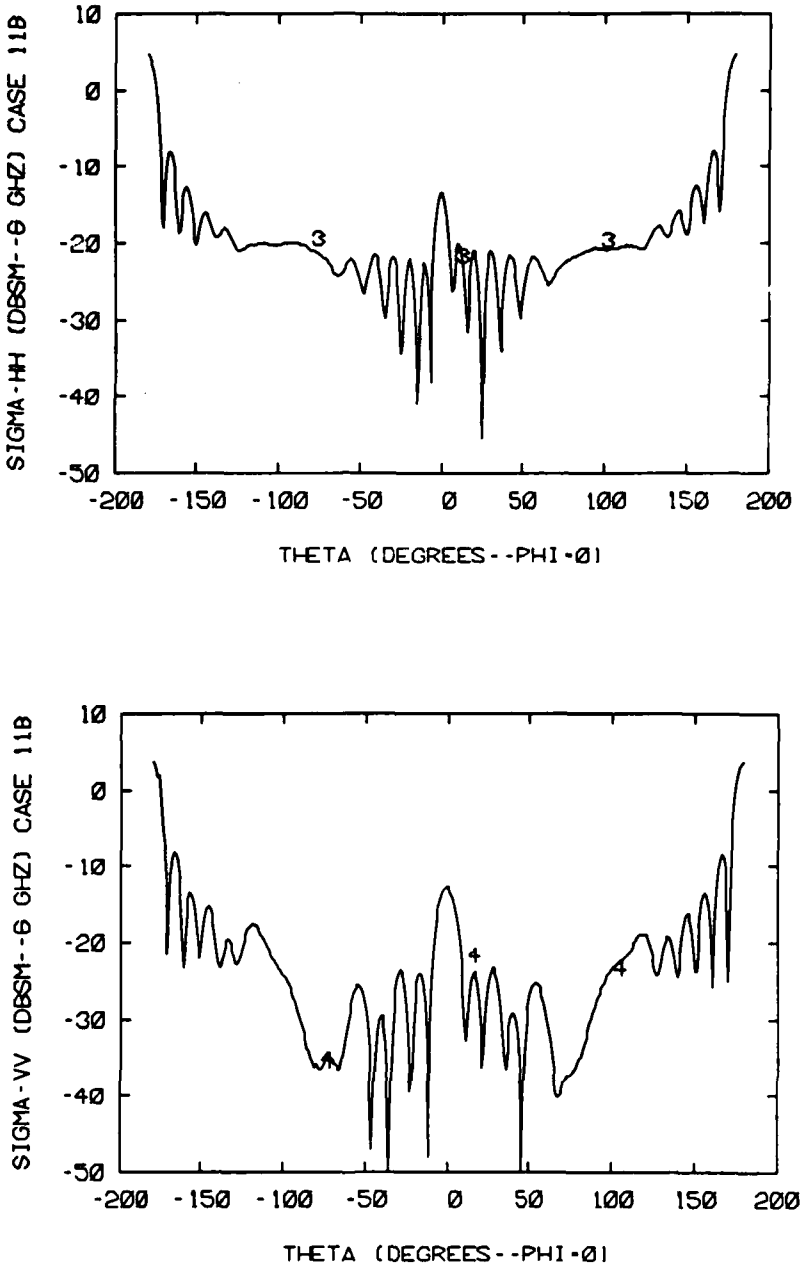

Figure E.15. Experimental monostatic 6.0 GHz RCS plots for Eccosorb SF 6.0 coated 15cm by 15cm square aluminum plate: (top) σ_{hh} versus angle and (bottom) σ_{vv} versus angle

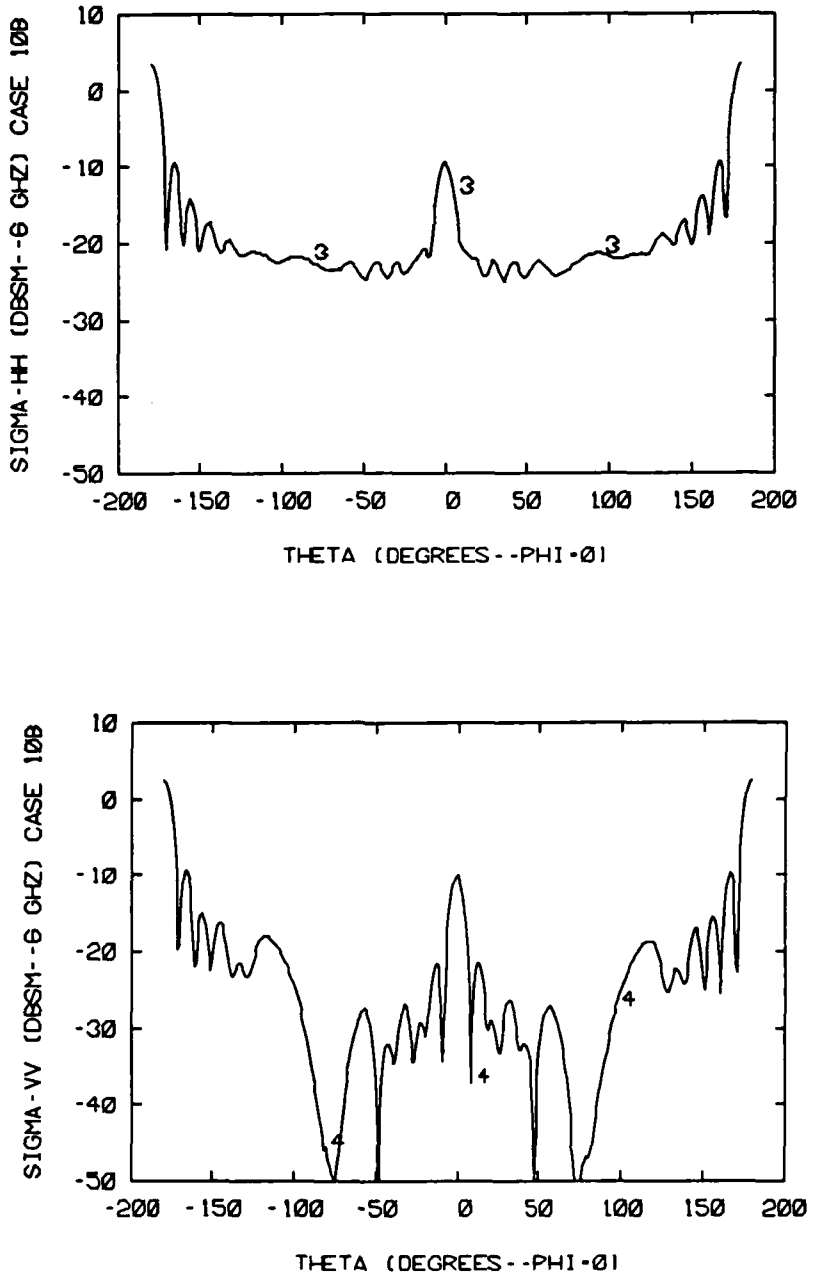

Figure E.16. Experimental monostatic 6.0 GHz RCS plots for Eccosorb FGM 40 coated 15cm by 15cm square aluminum plate: (top) σ_{hh} versus angle and (bottom) σ_{vv} versus angle

E.3 Theoretical Radar Cross Section Predictions

This section contains the graphs of the theoretical RCS predictions discussed in Chapters 3 and 5. They were generated from the EFIE series of computer programs. Each figure contains two RCS plots. The top plot in each figure is the horizontally transmitted and horizontally received monostatic far-field RCS (σ_{hh}) versus angle. Horizontally transmitted means the electric field of the incident wave is polarized parallel to the edge of the square plate when the incident wave is travelling in the plane of the plate and normal to an edge. The bottom plot in each figure is the vertically transmitted and vertically received monostatic far-field RCS (σ_{vv}) versus angle. Therefore, each figure contains the co-polarized RCS plots for two orthogonally polarized incident electric fields.

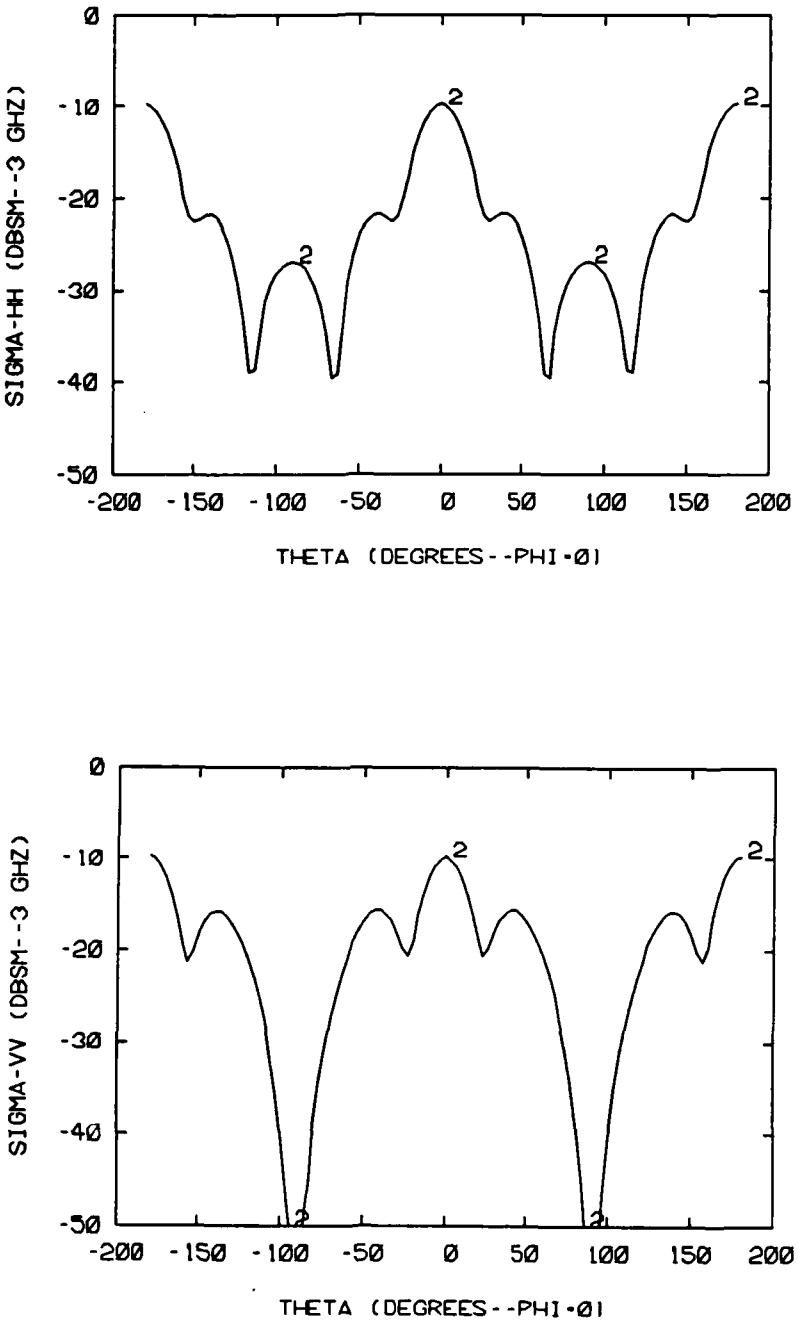

Figure E.17. Theoretical monostatic 3.0 GHz RCS plots for uncoated 10cm by 10cm square plate: (top) σ_{hh} versus angle and (bottom) σ_{vv} versus angle

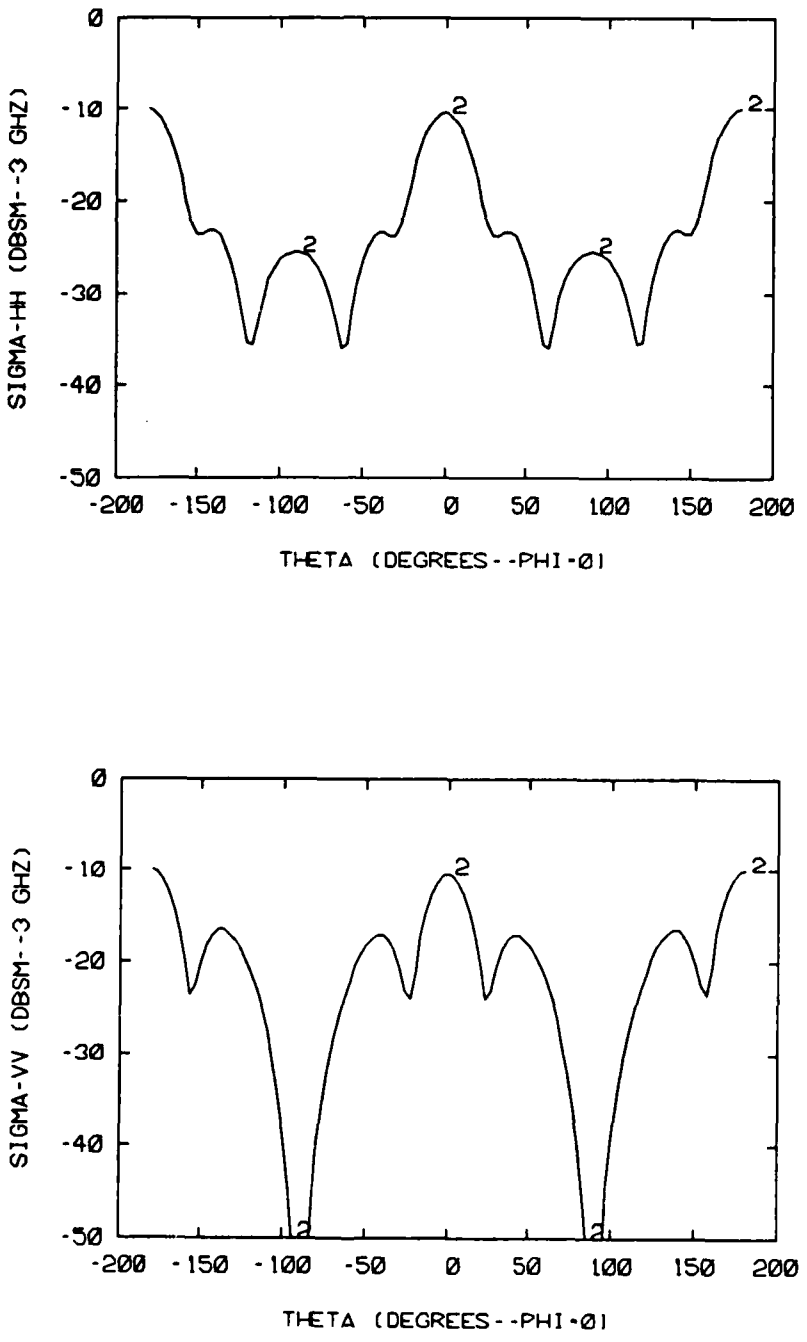

Figure E.18. Theoretical monostatic 3.0 GHz RCS plots for Eccosorb FDS coated 10cm by 10cm square plate: (top) σ_{hh} versus angle and (bottom) σ_{vv} versus angle

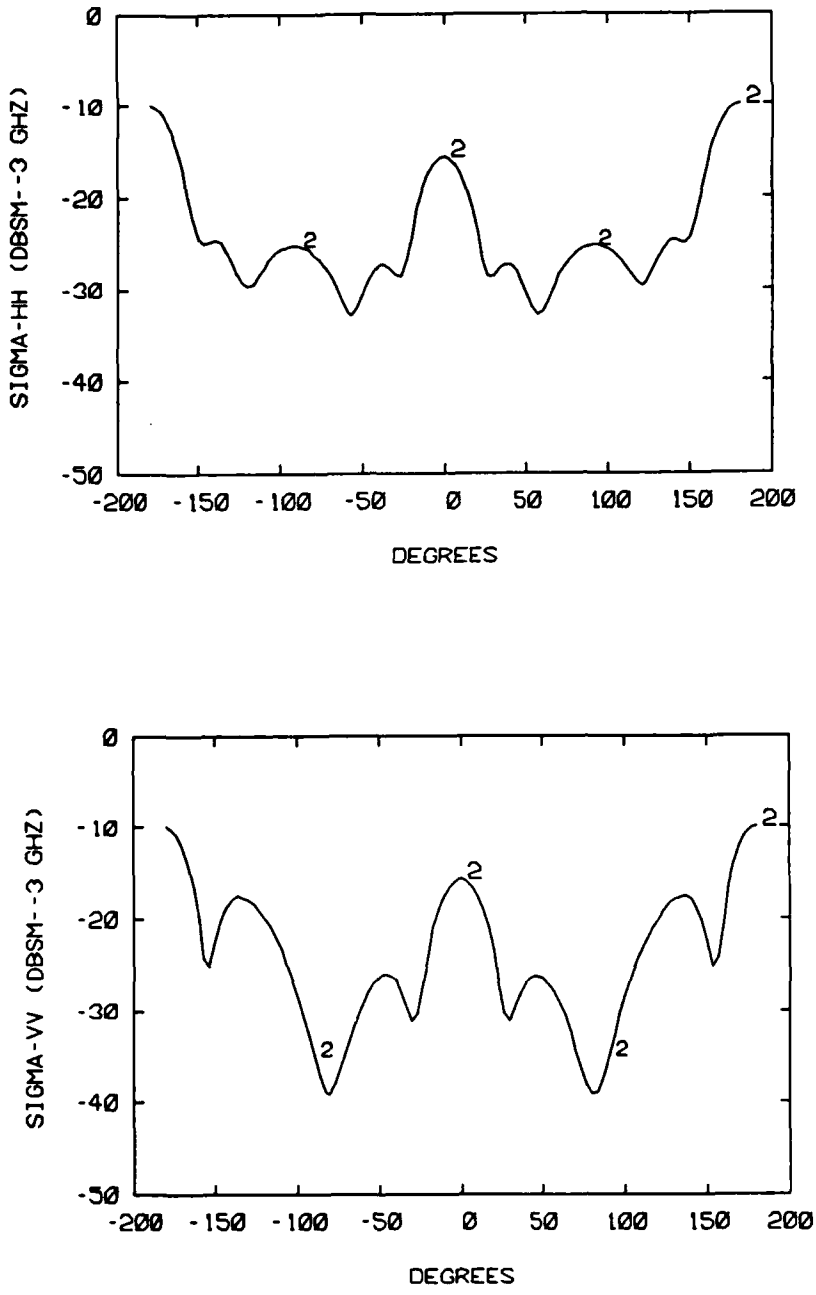

Figure E.19. Theoretical monostatic 3.0 GHz RCS plots for Eccosorb SF 6.0 coated 10cm by 10cm square plate: (top) σ_{hh} versus angle and (bottom) σ_{vv} versus angle (1 of 5)

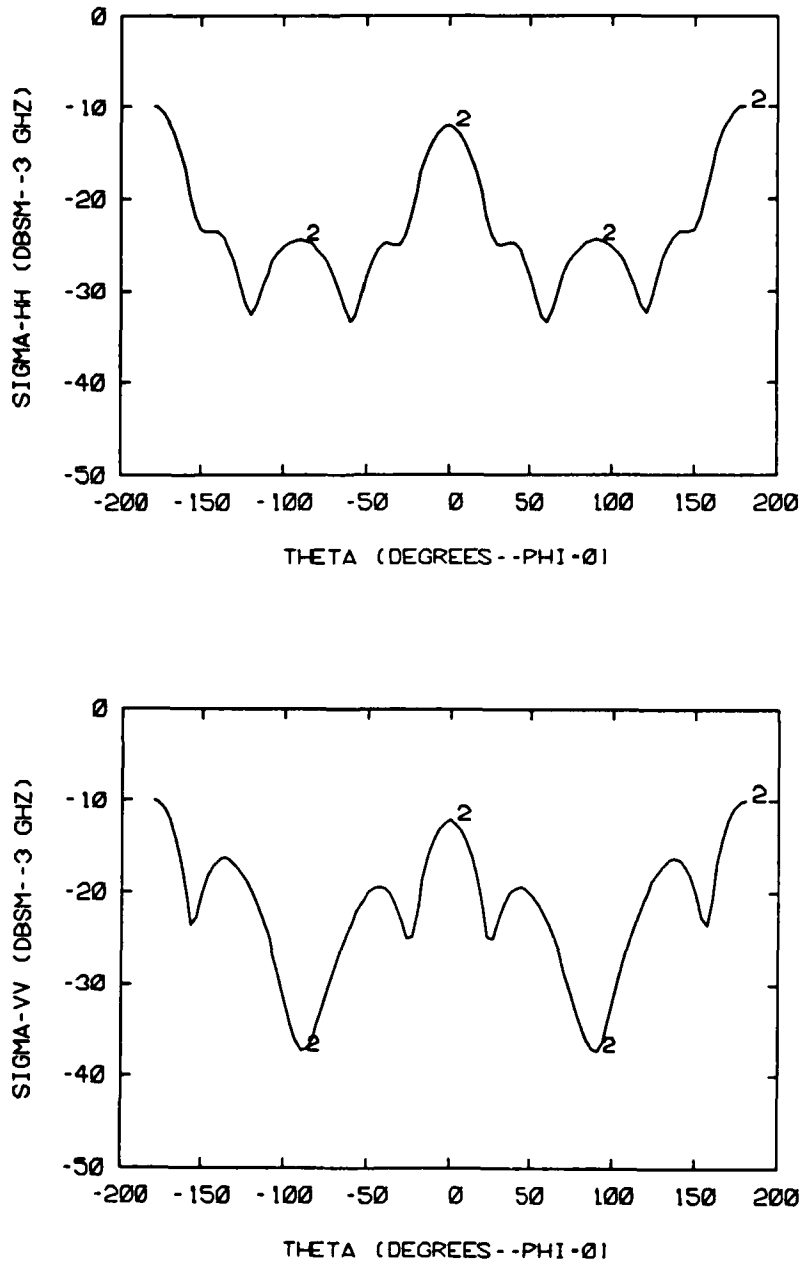

Figure E.20. Theoretical monostatic 3.0 GHz RCS plots for Eccosorb SF 6.0 coated 10cm by 10cm square plate: (top) σ_{hh} versus angle and (bottom) σ_{vv} versus angle (2 of 5)

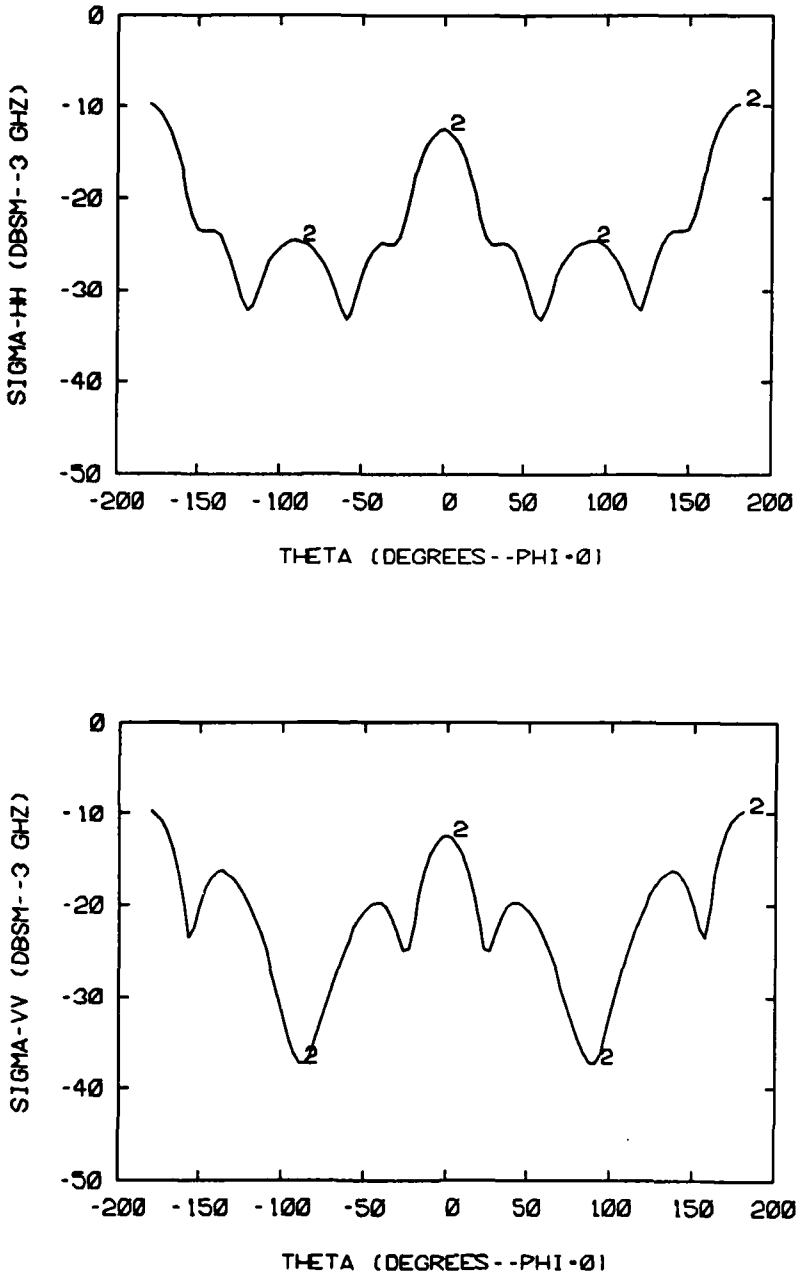

Figure E.21. Theoretical monostatic 3.0 GHz RCS plots for Eccosorb SF 6.0 coated 10cm by 10cm square plate: (top) σ_{hh} versus angle and (bottom) σ_{vv} versus angle (3 of 5)

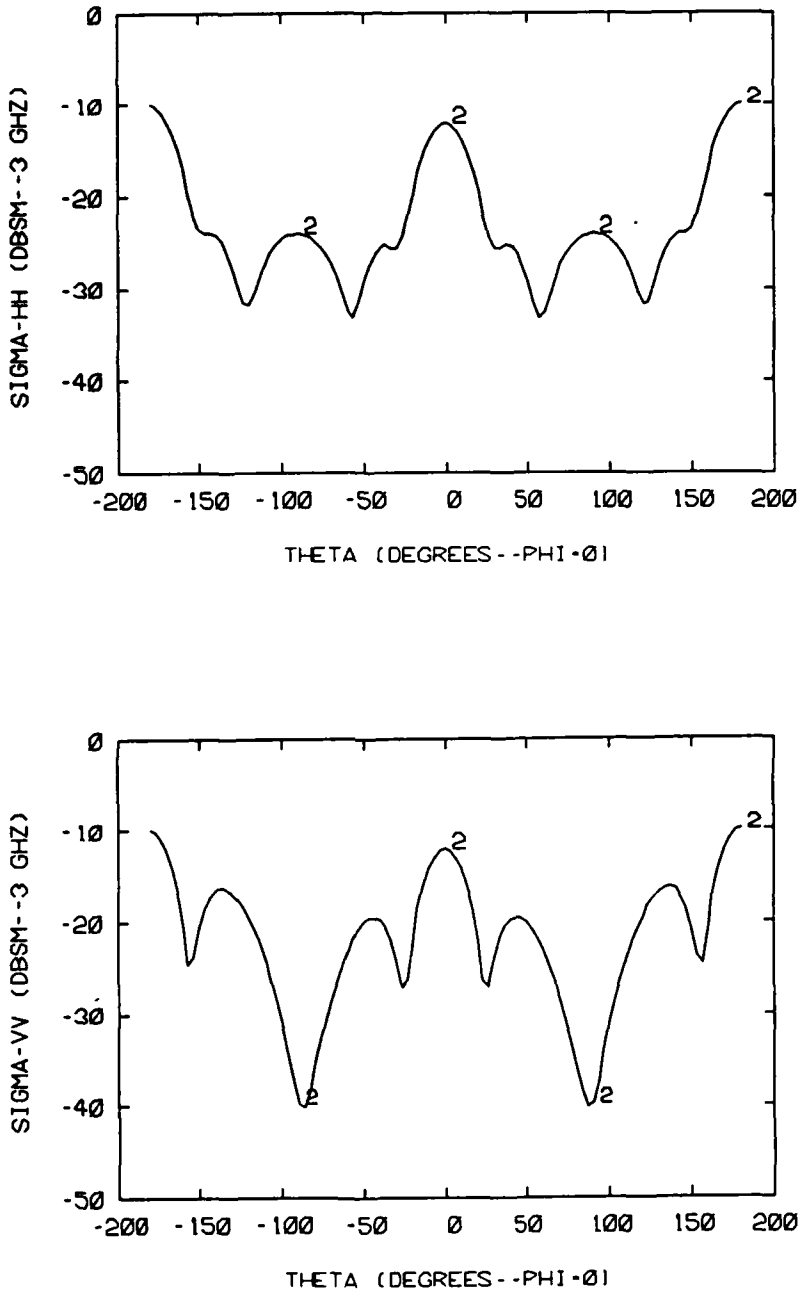

Figure E.22. Theoretical monostatic 3.0 GHz RCS plots for Eccosorb SF 6.0 coated 10cm by 10cm square plate: (top) σ_{hh} versus angle and (bottom) σ_{vv} versus angle (4 of 5)

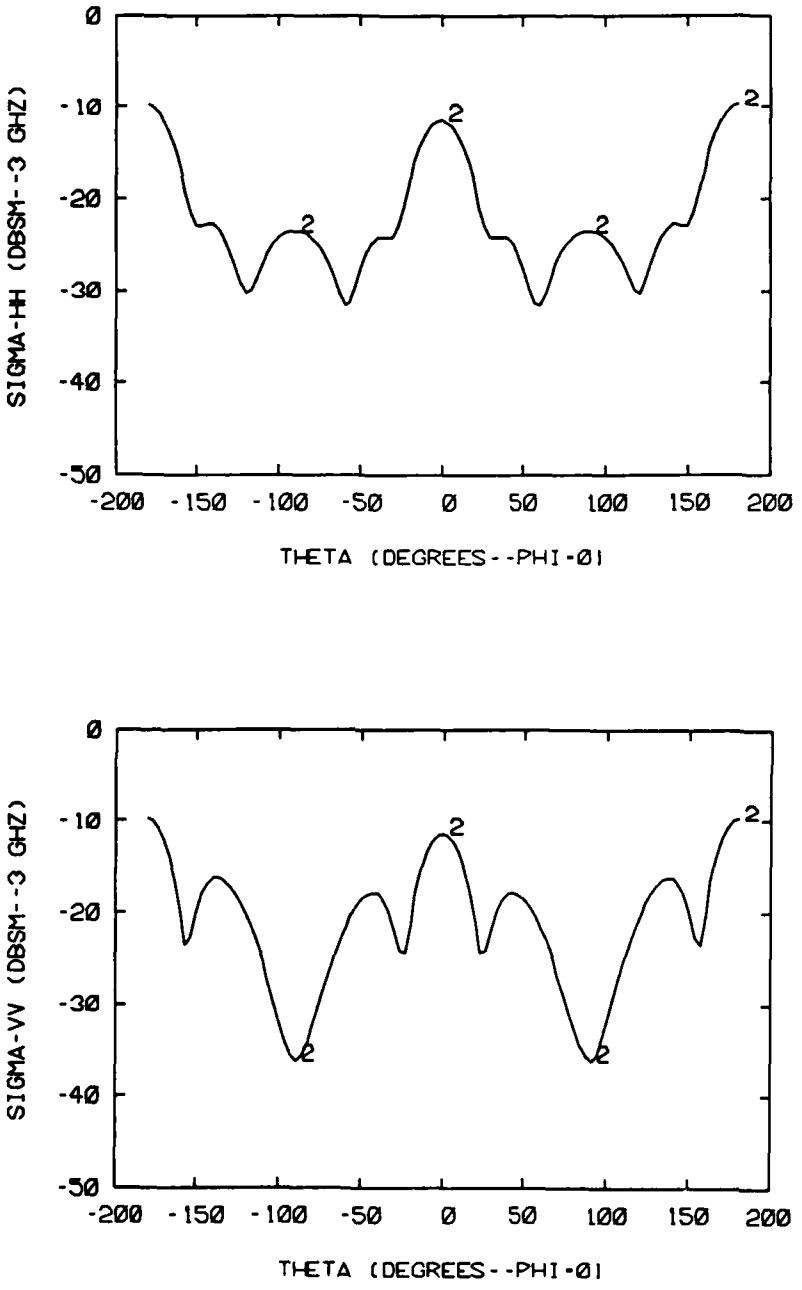

Figure E.23. Theoretical monostatic 3.0 GHz RCS plots for Eccosorb SF 6.0 coated 10cm by 10cm square plate: (top) σ_{hh} versus angle and (bottom) σ_{vv} versus angle (5 of 5)

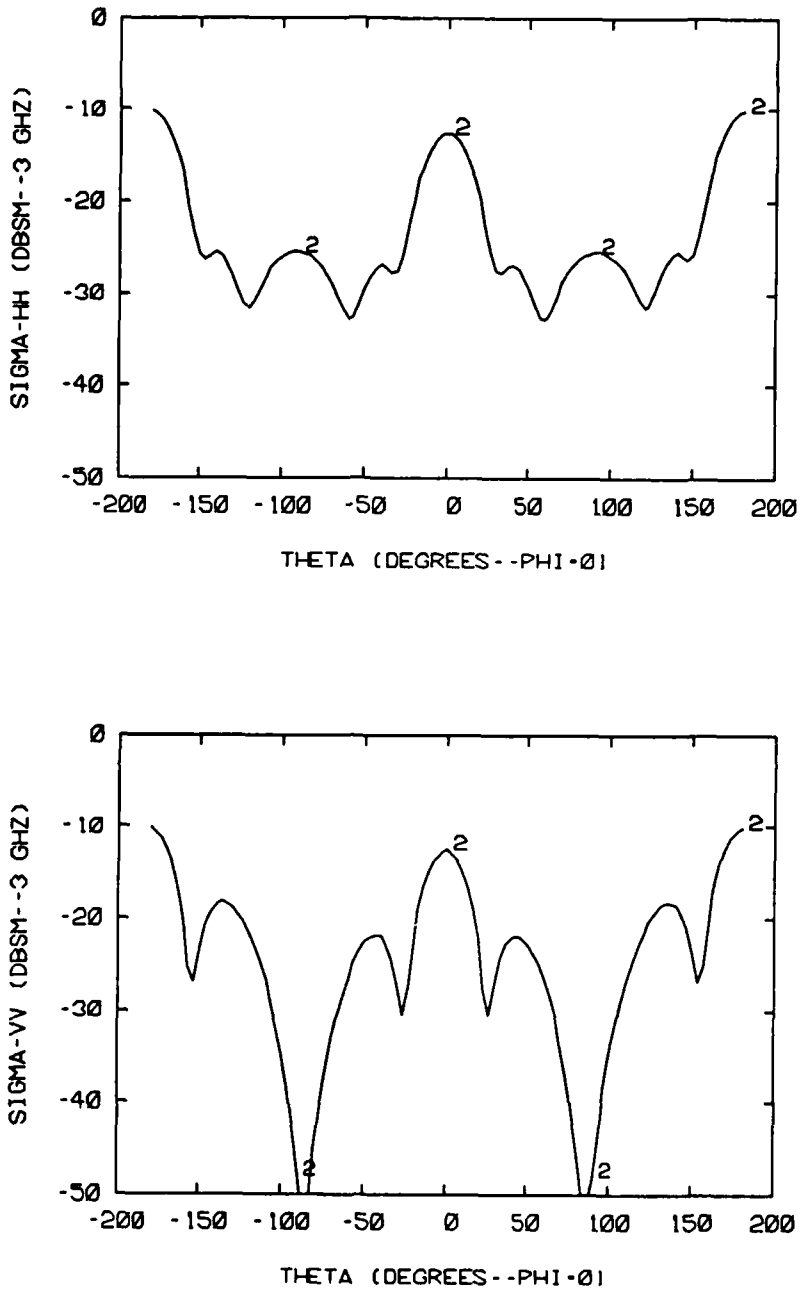

Figure E.24. Theoretical monostatic 3.0 GHz RCS plots for Eccosorb FGM 40 coated 10cm by 10cm square plate: (top) σ_{hh} versus angle and (bottom) σ_{vv} versus angle (1 of 5)

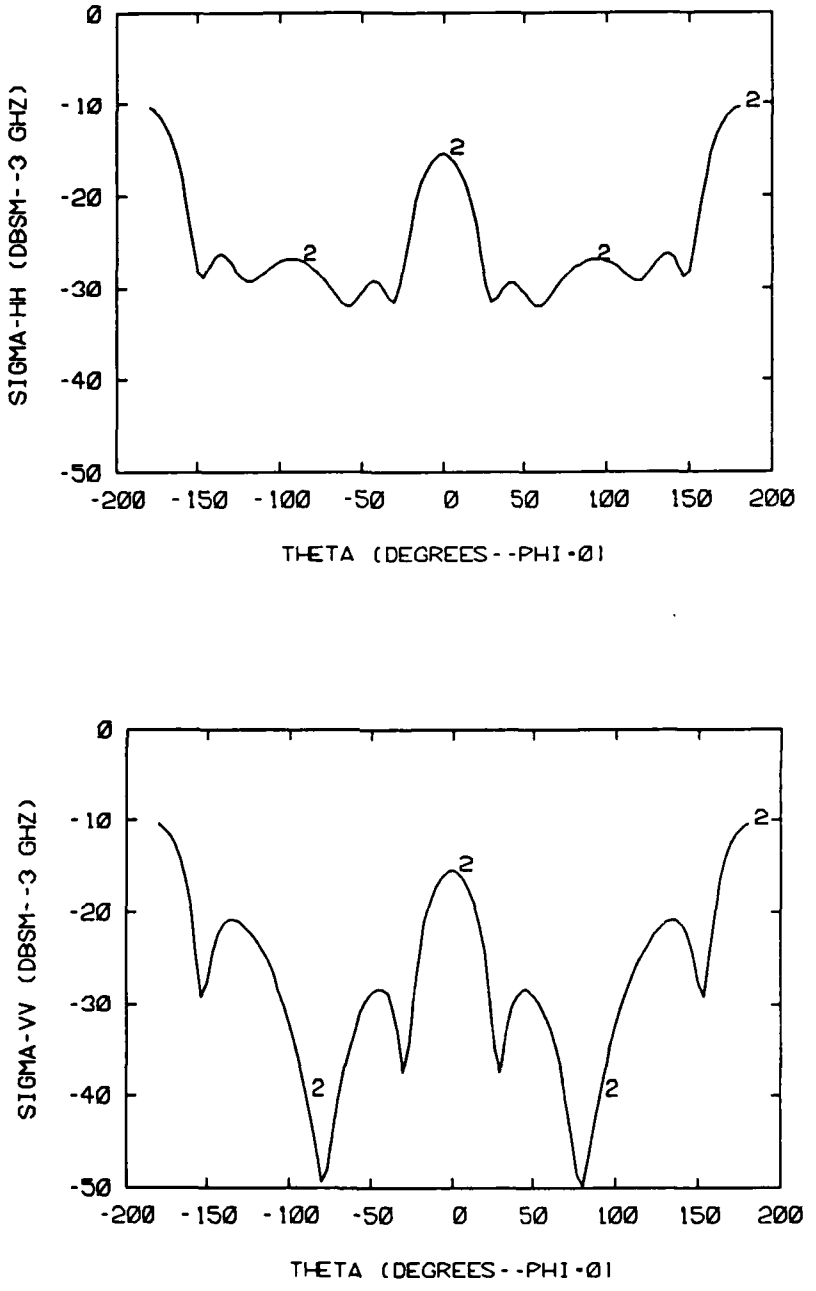

Figure E.25. Theoretical monostatic 3.0 GHz RCS plots for Eccosorb FGM 40 coated 10cm by 10cm square plate: (top) σ_{hh} versus angle and (bottom) σ_{vv} versus angle (2 of 5)

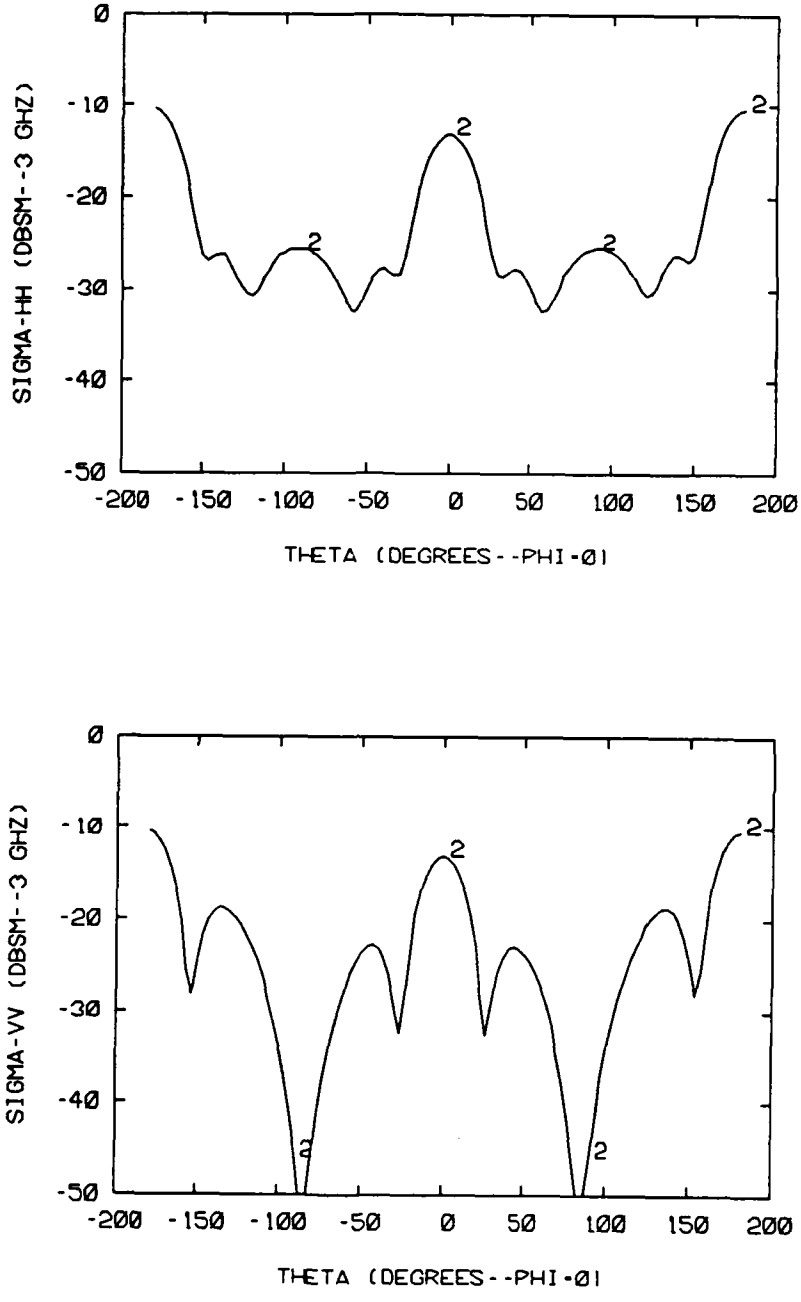

Figure E.26. Theoretical monostatic 3.0 GHz RCS plots for Eccosorb FGM 40 coated 10cm by 10cm square plate: (top) σ_{hh} versus angle and (bottom) σ_{vv} versus angle (3 of 5)

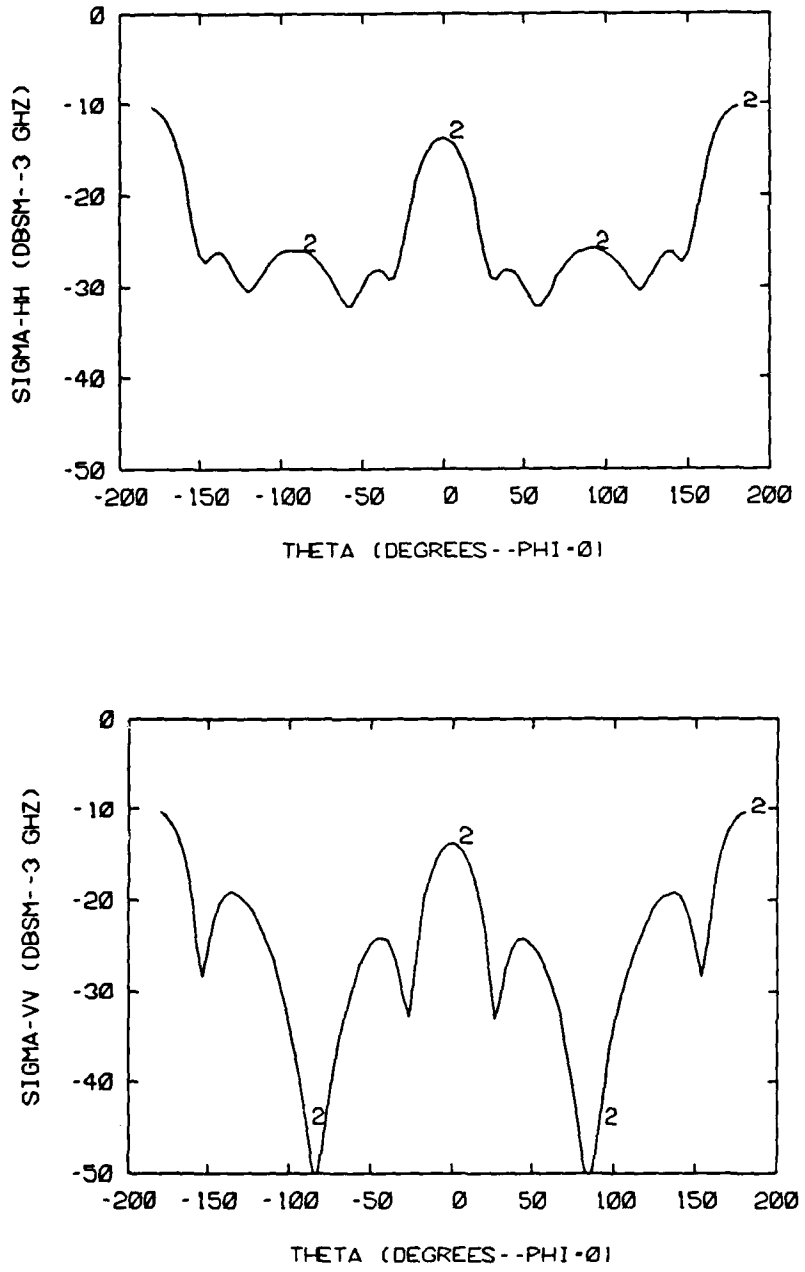

Figure E.27. Theoretical monostatic 3.0 GHz RCS plots for Eccosorb FGM 40 coated 10cm by 10cm square plate: (top) σ_{hh} versus angle and (bottom) σ_{vv} versus angle (4 of 5)

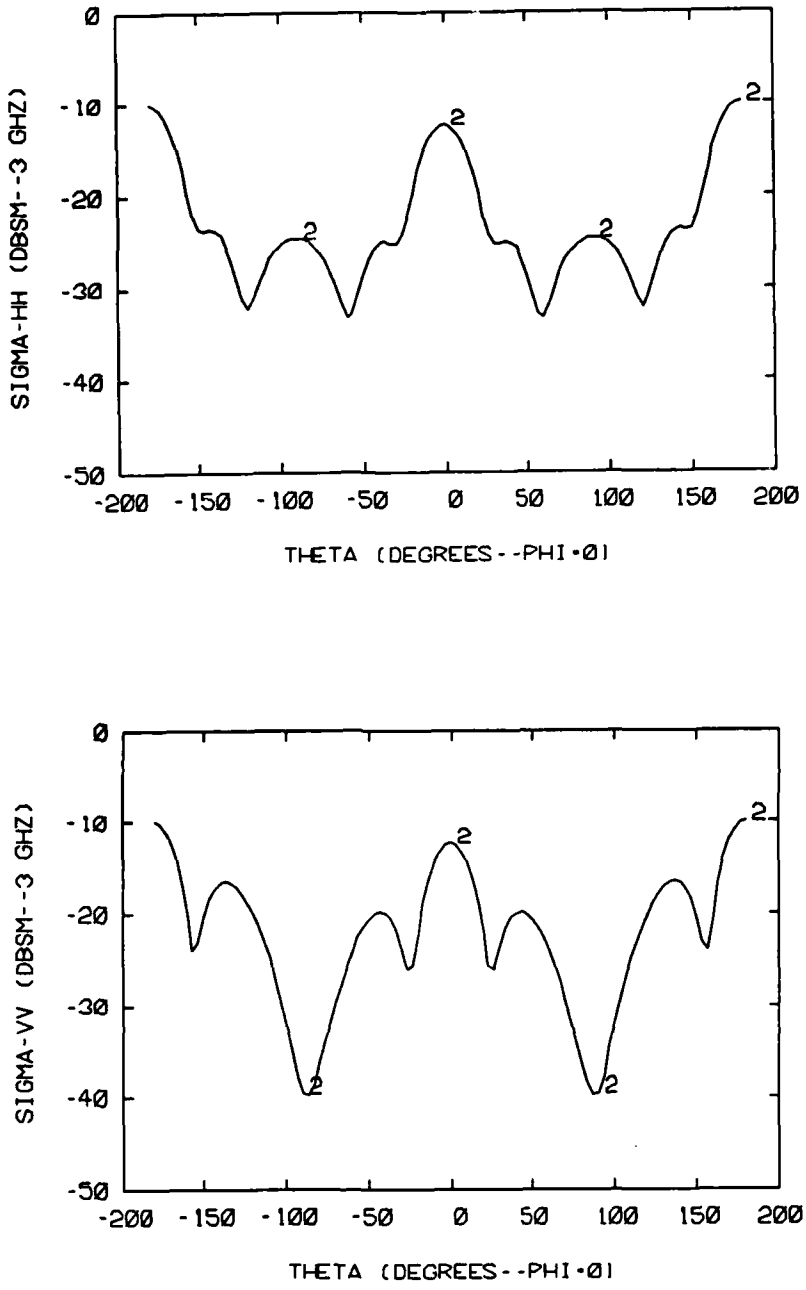

Figure E.28. Theoretical monostatic 3.0 GHz RCS plots for Eccosorb FGM 40 coated 10cm by 10cm square plate: (top) σ_{hh} versus angle and (bottom) σ_{vv} versus angle (5 of 5)

END

DTIC

9-86